Krylov Subspace Based Direct Projection Techniques for Low Frequency, Fully Coupled, Structural Acoustic Analysis and Optimization.

R. Srinivasan Puri

A thesis submitted in partial fulfillment of the

requirements of Oxford Brookes University

for the degree of Doctor of Philosophy.

13th March 2008

I dedicate this very small piece of work to my dearest Ms. Maruxa M. R.

Abstract

Noise, Vibration and Harshness (NVH) is a critical consideration in the design of automotive and aerospace vehicles for comfort, and fatigue of components arising from interior structural and acoustic pressure fluctuations due to external structural or acoustic loading. In the low to mid frequency range, current NVH models, obtained by direct, unsymmetric, coupled Eulerian Finite Element discretization (often known as the *Cragg's u/p* unsymmetric formulation) cannot provide a highly accurate and computationally efficient lower order model suitable for iterative structural and acoustic design modifications, or for example control applications via state-space techniques. The task of generating an accurate and a computationally efficient lower order model is further complicated due to the addition of non-trivial trim details such as frequency dependent damping resulting in an explicit participation of the damping matrix in the coupled higher dimensional system. In this thesis, lower order, fully coupled, structural-acoustic models are developed using a systematic dimension reduction procedure from the higher dimensional coupled structural-acoustic system to enable efficient, fully-coupled, undamped and damped structural-acoustic analysis and optimization.

The proposed dimension reduction techniques do not require the solution of the traditional coupled or uncoupled eigenvalue problems; but instead are based on *im-*

plicit, low frequency moment matching of the coupled higher dimensional system matrices via Krylov subspaces. This method matches the input to output characteristic of the higher dimensional structural-acoustic model and constructs a reduced order model by removing the uncontrollable, unobservable and weakly controllable, observable parts without affecting the transfer function of the coupled system. The new approaches for interior, fully coupled, structural-acoustic analysis are based on the computation of Arnoldi vectors using one of the several available Arnoldi variants; which essentially compute orthogonal vectors belonging to the induced Krylov subspaces. As a consequence, it turns out that a single projection framework is suitable for all the three possible damping formulations arising in interior structural acoustics: undamped, constantly damped and linearly damped material models.

To achieve the projected form, either second-order or state-space, five different approaches based on the Arnoldi process are proposed. The proposed reduction techniques are applied to six different test cases, ranging from a two dimensional fluid filled Benchmark problem to a realistic scaled vehicle cabin incorporating adhesively bonded joints. In the numerical test cases, both air and water are considered for the fluid medium to test the accuracy and computational efficiency of moment-matching Arnoldi formulations for *weakly* and *strongly* coupled problems. The structural and acoustic quantities of interest are compared with the direct and uncoupled modal formulations, where available. Structural-Acoustic reciprocity is considered as a validation tool for coupled models with acoustic excitation. It is shown that the moment matching reduced order models preserves the underlying second order form and the solution state accuracy whilst saving computational times of at least 1-2 orders in magnitude.

Further, a fast and efficient optimization framework is developed to optimize the lamination angles of a composite structure for reduced interior noise at a representa-

tive location in the fluid domain. In this vibro-acoustic optimization framework, the primary cost functions are derived based on the reduced order structural-acoustic models obtained via the Arnoldi based projection formulation to save computational time whilst maintaining the desired accuracy of required states. The optimization method in itself is a tailored version of the derivative-free Mesh Adaptive Direct Search algorithm which allows for both local and global exploration of the design space at any given iteration of the optimization process. An adaptation to this method, incorporating the Latin Hypercube Sampling technique is investigated as a part of the global search step to increase computational efficiency and avoiding being trapped at local minima. It is numerically demonstrated that by varying the lamination angles of a composite structure, it is possible to reduce interior noise levels.

Acknowledgements

Many people have contributed so much to this very small piece of work that it is very difficult to know where to make a start. Therefore, I have simply drawn up a list of people along with their affiliation who have provided me with immense support - in some form or the other, throughout my studies at Oxford Brookes.

... to my friends: Abhaya Vartak-Shetty aka *Abs*, Guido Fessel, Yeshwanth, Subash, Murugan (the lucky flight chap), Deepu, Pavika, Nikhil, Popo, and Alyson Smith for all their support; and the *maths* kids at Alyson's place: Aaron, Alex Pigache, Maraid Folan, Kirsty, Stephanie, Asif, Rana, Ibrahim[2], Tasmia and Yasmeen who gave me the break and the fun I needed - I really did learn quite a lot from them!

A big thanks to my mum, who has been really patient with me - and has supported me both morally and financially through out my life. I certainly cannot thank her enough for everything she has done for me.

Happy Reading!

Contents

List of Figures

List of Tables

List of Symbols and Abbreviations

Abbreviations

AMLS   Automated Multi-Level Substructuring.

AWE   Asymptotic Waveform Evaluation.

BEM   Boundary Element Method.

BIW   Body-in-White.

CL   Coupled Lanczos procedure.

CLF   Coupling Loss Factor.

DLF   Damping Loss Factor.

DMTA   Dynamic Mechanical Thermal Analysis.

$DOFs$ Degrees of Freedom (FEM).

EMA   Experimental Modal Analysis.

FEM   Finite Element Method.

FEM/FEM   Coupled FEM/FEM solution for structure and fluid.

FEM/BEM   Coupled FEM/BEM solution for structure and fluid.

FSI   Fluid Structure Interaction (Flag).

GPS   Generalized Pattern Search.

LHS   Latin Hypercube Sampling.

LTI   Linear Time Invariant.

LIN-OSA	Linearization of a second order system followed by dimension reduction through the One-Sided Arnoldi process.
MADS	Mesh Adaptive Direct Search.
MEMS	Micro Electro Mechanical System.
MIMO	Multiple Input Multiple Output.
MOF	Modal Overlap Factor.
MOR	Model Order Reduction.
NTF	Noise Transfer Function.
NVH	Noise, Vibration and Harshness.
OSA	One-Sided Arnoldi process.
POD	Proper Orthogonal Decomposition.
PP	Polypropylene.
RMS	Root Mean Square.
ROM	Reduced order model.
SISO	Single Input Single Output.
SICO	Single Input Complete Output.
SOAR	Second Order Arnoldi Reduction.
SPL	Sound Pressure Level.
SVD	Singular Value Decomposition.
pSEA	Predictive Statistical Energy Analysis.
eSEA	Experimental Statistical Energy Analysis.
hSEA	Hybrid Statistical Energy Analysis.
TBR	Truncated Balanced Realization.
TSA	Two-Sided Arnoldi process.
TS-SOAR	Two-Sided, Second Order Arnoldi Reduction process.

Symbols

u	Unknown coupled displacement component (states) for the coupled structural-acoustic model.
p	Unknown coupled pressure component (states) for the coupled structural-acoustic model.
ω	Frequency in rad/s.
f_{exp}	Expansion point frequency in Hz.
s_0	Complex frequency $i\omega$ for expansion.
$s_1 \ldots s_n$	Multiple expansion points for factorization.
q	Number of Arnoldi vectors and order for the reduced structural-acoustic system (Dimension of ROM).
K_s	Structural stiffness matrix.
M_s	Structural mass matrix.
C_s	Structural damping matrix.
K_a	Acoustic stiffness matrix.
M_a	Acoustic mass matrix.
C_a	Acoustic damping matrix.
K_{fs}	Coupled structural-acoustic Stiffness matrix.
M_{fs}	Coupled structural-acoustic mass matrix.
K_{sa}	Block Coupled structural-acoustic Stiffness matrix.
M_{sa}	Block Coupled structural-acoustic mass matrix.
C_{sa}	Block structural-acoustic Damping matrix.
L^T	Structural-Acoustic output scattering Matrix/Vector for undamped systems.
$\mathbf{l}^T$	Structural-Acoustic output scattering vector for damped systems.
$\tilde{K}_{sa}$	Modified bock Coupled structural-acoustic stiffness matrix.
$\tilde{C}_{sa}$	Modified block Coupled structural-acoustic damping matrix.
$y(t)$	Higher dimensional output state vector in the time domain.

$\mathbf{f}_{sa}$ SISO forcing vector for Structural-Acoustic coupled model.

K_{rsa} Reduced order block Coupled structural-acoustic stiffness matrix.

M_{rsa} Reduced order block Coupled structural-acoustic mass matrix.

C_{rsa} Reduced order block structural-acoustic damping matrix.

F_{rsa} Reduced order block structural-acoustic forcing vector.

L_{rsa} Reduced order structural-acoustic output scattering Matrix/Vector.

$y(\omega)_{rsa}$ Reduced order output state vector in the frequency domain.

z generalized co-ordinates for Krylov Subspace based projection techniques.

V Projection matrix for one-sided reduction methods.

W Projection matrix for two-sided reduction methods.

ζ Damping Ratio.

η Loss Factor.

β_{ac} Acoustic admittance coefficient.

$H(s)$ Structural-Acoustic transfer function without damping.

$H(s)_{rsa}$ Reduced order Structural-Acoustic transfer function without damping.

$h(s)_{sa}$ Structural-Acoustic transfer function with damping.

$h(s)_{rsa}$ Reduced order structural-acoustic transfer function with damping.

$h(s)_{LIN}$ Structural-Acoustic transfer function for the equivalent linearized, first order system with damping.

H_q Upper Hessenberg matrix of order q.

R_q residue matrix from Arnoldi process of order q.

m_i Moments of the second order, undamped/damped (complex stiffness), structural-acoustic system.

m_z Moments of the second order, damped, structural-acoustic system: C_{sa} participation .

$\mathcal{K}_q^r(A, g)$ Right, single block, input standard Krylov subspace.

$\mathcal{K}_q^l(A^T, \bar{l})$ Left, single block, output standard Krylov subspace.

$\mathcal{K}_q^{ri}(A, B, g)$ Second order, right, single block, input Krylov subspace.

$\mathcal{K}_q^{le}(A^T, B^T, l)$ Second order, left, single block, output right Krylov subspace.

$K_q(A_1, g_1, g_2)$ Multiple block Krylov subspace.

E_s Youngs modulus.

G Shear modulus.

D_{sa}, G_{sa} First order transformed coupled structural-acoustic system matrices.

$\hbar$ First order transformed unknown *structural-acoustic* states.

ϵ_{sa} Error resulting from transformation to state co-ordinates via projection matrices.

$\breve{\hbar}_{rsa}(s)$ Local error in the frequency domain between direct inversion and Arnoldi based projection formulation.

$\vartheta_{rsa}(s)$ True error in the frequency domain between direct inversion and Arnoldi based projection formulation.

$\hat{\vartheta}_{rsa}(s)$ Relative error in the frequency domain between direct inversion and Arnoldi based projection formulation.

ρ_s Structural mass density.

ρ_c Fluid mass density.

κ_f Bulk modulus of the fluid.

1. Preliminaries

1.1. Background

NVH stands for Noise Vibration and Harshness and is an industry term associated with the prediction and active/passive treatment of vibration and audible sounds. Findings show that NVH not only causes annoyance and fatigue, but also affects the efficiency and health of people (Leslie and Doelle 1972). NVH is very important from an engineering and customer satisfaction point of view and thus a very significant issue in automobile and aerospace cabin interior design. The concerns have primarily been those of speech interference, crew fatigue, and passenger comfort, the latter arising primarily in for example private/business jets and first class accommodations on commercial airlines (Fernholz and Robinson 1998). Though there are currently no regulations on interior noise levels, airline operators require guarantees from manufacturers on these noise levels. In automobile design, during earlier years, NVH was primarily investigated at the end of the production line and additional damping (vibration absorbing) materials were added to reduce noise and vibration based on user tests on road conditions. However, today, in a passenger car, the NVH performance is one of the most important parameters that determine the quality of passenger comfort in manufactured car. In fact, NVH is rated as among the top five priorities by automobile manufacturers. Due to the nature of the current automotive business, where competition is very high, manufacturers are today striving to bring NVH levels down as low as possible.

Typically, the parameter of interest used to judge the NVH performance of an automotive/aerospace interiors is the pressure or velocity response at a given location inside the fluid filled cabin or the enclosing structure to a known excitation. This relationship between the response and excitation is often called *Noise Transfer Function* (NTFs) or simply *Frequency response Functions* (FRFs). In aerospace and defence applications, such as an aircraft, launch vehicle or submarine design, predicting acoustic pressure response of cabin interiors is almost inevitable, since these also have a critical influence on aircraft satellite communications and fatigue of components due to acoustic loading (Crane et al. 1997; Pirk et al. 2002). For example, around 40 % of the mass of a satellite is present just to survive the harsh launch environments (Henderson et al. 2003). With the advent of modern computers and powerful instrumentation, it is now become common practice for design engineers to pay much attention to the NVH performance of cabin interiors at the design stage of the product development process.

Over the last twenty five years, a large amount of work has been published addressing the vibration and acoustic characteristics of vehicle interiors. This has included both numerical and experimental techniques or a combination of them. Today, the NVH behavior of a typical automotive body is typically classified into three distinct descriptors, based primarily on their transmission phenomenon and frequency range. This is tabulated in Table:[1.1]. This distinction can be attributed to the fact that the vibro-acoustic behavior of the vehicle structure under investigation tends to be different in all three frequency ranges. As a result, there does not exist a single prediction technique which can be applied to a complex structure such as a *trimmed* automotive vehicle to predict the vibro-acoustic behavior in all three frequency ranges. In fact, this is true for most real life problems.

Descriptor	Phenomenon	Frequency Range
Low Frequency	Structure borne	0 - 100Hz.
Mid Frequency	Structure and Air borne	100 - 250Hz.
High Frequency	Air borne	>250Hz.

Table 1.1.: NVH description based on Phenomenon and Frequency Range

At low frequencies, an *exact* solution is sought for a set of governing equations arising from the discretization of the structural and acoustic fields into mass, stiffness and damping matrices in space, subject to a number of boundary conditions including enforcement of coupling between the fluid and structural domains. This is often achieved using well known coupled element based deterministic techniques such as the Finite Element Method (FEM), Boundary Element method (BEM) or a combination of them leading to coupled FEM/FEM or coupled FEM/BEM based procedures. Common to these methods, the response is described in terms of a large number of trial functions over various local elements in the computational domain. These trial functions, also known as *shape functions* are chosen to interpolate between the nodal values of response. The *shape functions* for the elements are chosen such that they have a unit value at each node (In the FEM, a *node* is described by its degree's of freedom), and zero at all others. Since the structural and acoustic behavior at low frequencies is characterized by long wavelengths ($\lambda = c/f$, where λ is the wavelength, c the speed of sound in the fluid and f is the frequency in Hz.), the use of lower order polynomials as shape functions often yields acceptable levels of response solution accuracy. This is often the case, when in addition to FEM/BEM based techniques, model updating techniques (Mottershead and Friswell 1993) based on experimental modal models are applied to the structural modal problem.

However, as the excitation frequency is increased, it can be observed that the response becomes increasingly sensitive to minor structural modifications (Estorff

2003). Such a behavior is often associated with shorter fluid/structural wavelengths and very irregular (and higher) modal density (*modal density* is defined as the number of modes in a given frequency band) resulting in highly complex mode shapes at higher frequencies. This in turn results in a large spatial variation in response across the frequency domain. In order to adequately capture the dynamic behavior at such higher frequencies, a large number of elements accompanied by a fine frequency resolution is often employed to compute the response via the coupled FEM/FEM or FEM/BEM based procedures, assuming the computational feasibility within available resources. For large scale scale systems such as an automotive or an aerospace interior cabin, beyond a certain frequency band, the use of such deterministic techniques often become questionable due to the huge computational time required to solve the discretized matrix equations and the validity of such computed results (Shorter 1998).

To counter the problem at very high frequencies[1], researchers have developed energy based methods, based on the principle of conservation of energy, to predict the statistically time/frequency averaged response, on the fluid or the structural domain. One popular method among the energy based methods is the *predictive* Statistical Energy Analysis (*p*SEA). In this method, the structural and the fluid domains are discretized into a number of subsystems, and the response is described in terms of time averaged energy contained within each of the subsystems (Lyon and DeJong 1995). On the other hand, the excitation is described in terms of time average input power applied to the subsystems. The two important parameters in SEA, namely, the Coupling Loss Factors (CLFs) - which describes the energy transfer between different subsystems, and Damping Loss Factors (DLFs) - which describes the energy loss and their interactions between different subsystems. The computation of these parameters for a complex structure such as an automotive/aerospace cabin structure

---

[1]This is typically between 250Hz. to 5KHz. for automotive NVH applications.

involves either solving discretized structural equations via the FEM , calculation of radiation/transmission efficiencies (e.g. the *wave approach* for CLF) or measuring them using Experimental SEA (*e*SEA).

In the mid-frequency range, none of these above mentioned techniques alone have alone been found to be adequate enough predict the response accurately. This has often been attributed to the fact that the response is a combination of longer and shorter wavelengths, making them *fuzzy*, rendering both the FEM and SEA impractical. Although the use of deterministic techniques are theoretically feasible to be applied in this frequency range, the computational time required to solve the discretized matrix equations, prohibit its subsequent use. In addition to this, since the response becomes increasingly sensitive to minor structural modifications (*e.g.* material properties), model updating is often employed, requiring re-running of the updated deterministic models to predict structural/acoustic response. In the past, two approaches have been used to tackle this problem: (a) Decrease element size and *extend* the use of deterministic techniques to the mid-frequency range and average the response (b) Derive SEA parameters from deterministic or experimental techniques and use them in SEA models or model stiff parts of the structure as a global system and the rest as the local system (based on wavelengths), leading to *hybrid* FEA-SEA methods (*h*SEA) (Langley and Bremner 1999; Jayachandran and Bonilha 2003).

In general, the following qualitative definitions hold for low, mid and high frequency dynamic response analysis (Soize et al. 1992; Rabbiolo et al. 2004):

(a) *Low frequency*: The response spectra exhibits strong modal behavior.

(b) *Mid frequency*: The response spectra exhibits high irregularities, indicating irregular modal density. Boundary conditions, geometry and materials play

an important role.

(c) *High frequency*: The response spectra are smooth (as a consequence of cancelations), indicating high modal density. Boundary conditions, geometry, and material are no longer important.

Once the response is computed, intelligent strategies such as active control and passive damping can be employed to modify parts of the transfer function for better acoustic response in the audible frequency range. Typically, the steps involved can be summarized as shown in Figure:[1.1].

At this point, it is worth reminding the reader that, manufacturing variability is also a significant variable which dictates the choice of prediction methods for structural-acoustic analysis. In general, the experimental noise transfer function (Force/Pressure) variability increases with increasing frequency (Wood and Joachim 1984; Kompella and Bernhard 1993). Therefore, care must be taken to identify limits of the involved frequency range; which in turn depends on the characteristics of the coupled problem (such as dimensions, fluid mass, thickness of the structural panels) and prediction methodologies.
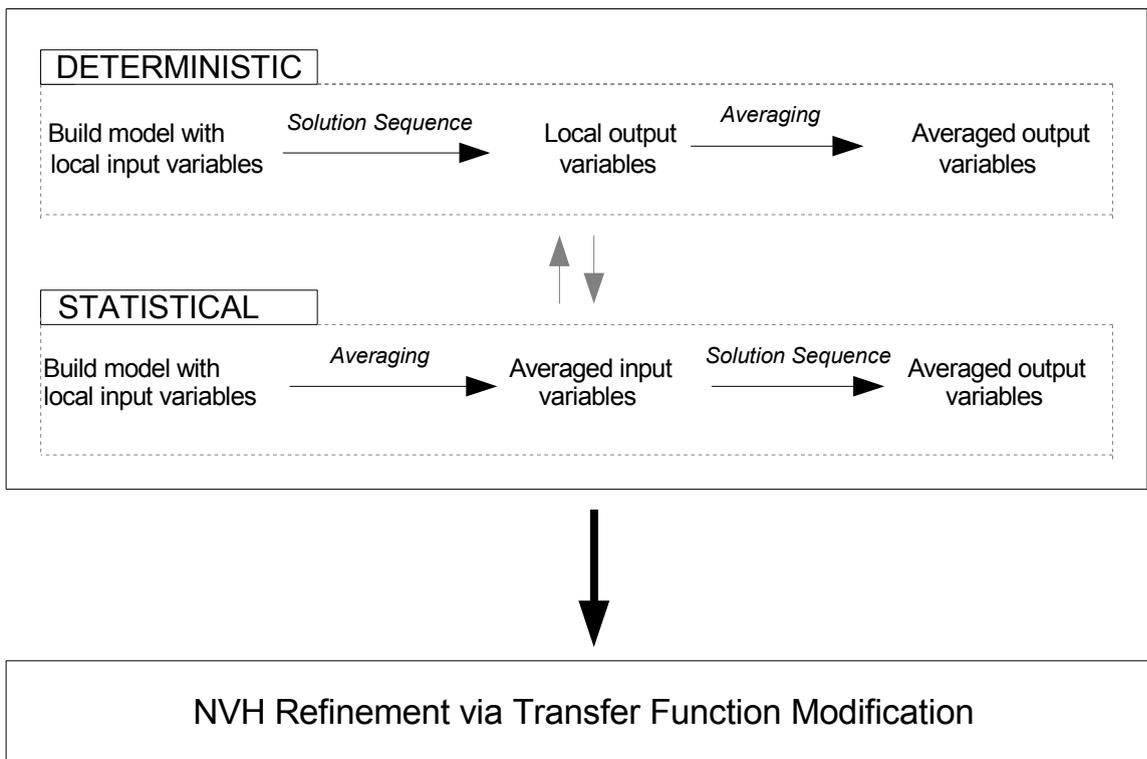
Figure 1.1.: Methodology for predictive NVH refinement.

1.2. The need for fast structural acoustic analysis

Even with the advent of modern computers and cheaper computational power, the simulation of a complex structure such as a vehicle/aerospace cabin often involves tedious and time consuming modeling procedures leading to higher dimensional models. Today, it is common practice to investigate NVH behavior using models which range up 50,000 to 1Million Degrees of freedom (DOFs), often requiring a solution to a set of linear equations $[\mathbf{A}] \, . \, \{x\} = \{b\}$, for every a single frequency evaluation (when a solution is required for an entire frequency range, a *frequency sweep* is executed). Here,$[\mathbf{A}]$ arises from the discretization of the coupled formulation and of an order equal to the number of DOFs, $\{x\}$ is a vector of states to be found and $\{b\}$ arising from the forcing function of the coupled formulation. The simulation of such higher dimensional models in many cases is prohibitive or even impossible. This is often the case when repeated analysis is required to calculate the *best* design parameters for good NVH characteristics over the entire applicable frequency range.

Typically, in automotive and aerospace applications, design engineers are interested in the 0 - 5KHz frequency range. Since there does not exists a single prediction tool to predict the NVH behavior in all three frequency ranges, design engineers are often forced to resort to a combination of prediction techniques, involving both deterministic and statistical methods. Although active research in the mid-frequency range is giving rise to hybrid techniques such as hSEA, it has now become more common practice to investigate the mid-frequency range, by *extending* the analysis frequency range of deterministic and statistical energy based methods in order to cover the mid-frequency gap. An illustration of techniques for interior NVH behavior prediction based on frequency range is shown in Figure:[1.2].

In deterministic techniques, the analysis range is increased by introducing more
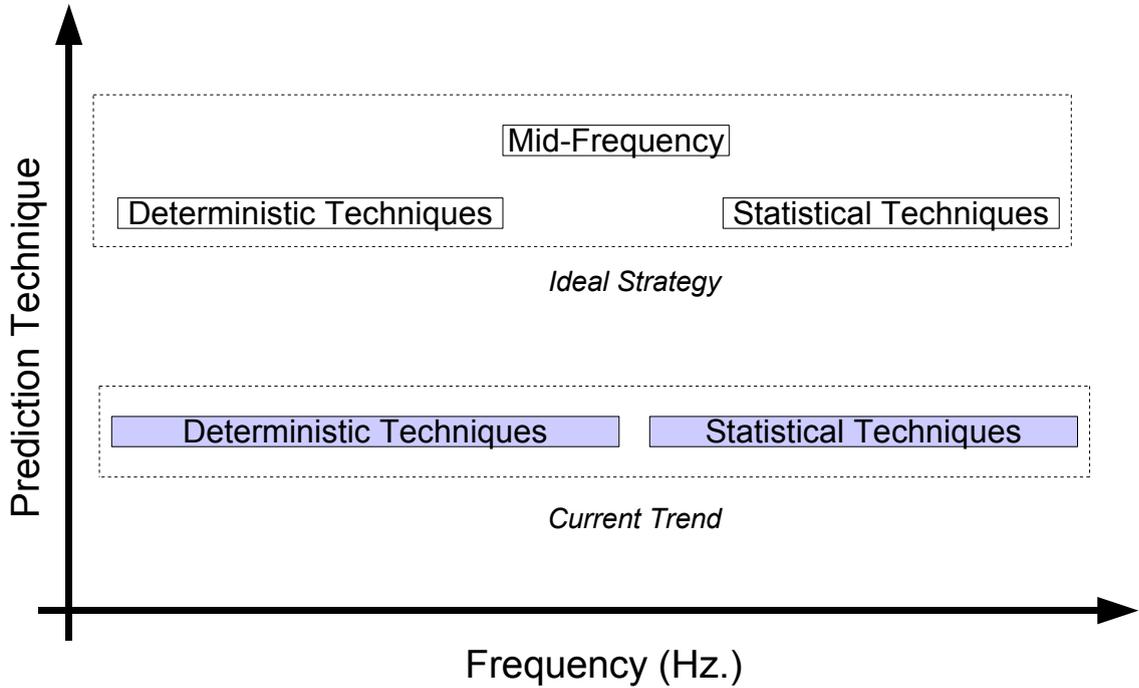
Figure 1.2.: Ideal and current trend for NVH prediction

elements (In FEM, an element is characterized by its associated nodes) to balance the element to wavelength ratio at higher frequencies (Wolf 1977; Atalla and Bernhard 1994; Desmet 1998), leading to models of much higher dimension than required to investigate the low-frequency band by itself. In energy based methods, the parameter Modal Overlap Factor (MOF) is used to determine if a particular coupled system *qualifies* for analysis via SEA. Essentially, MOF is the ratio of the bandwidth individual resonance peaks to the average spacing of adjacent resonances. In some sense, MOF measures the *smoothness* of the FRF. A MOF value greater than one, indicates that several modes make a significant contribution at any given frequency and the total response can be governed by a summation of these contributions. It is worth pointing out that a high modal overlap factor implies either high damping or high modal density[2] or both (Yap and Woodhouse 1996; Hopkins 2002). In general, it is well accepted that the uncertainty of SEA predictions may be unacceptably

---

[2]Note that in the pSEA method the modal densities are often obtained using analytical expressions (as opposed to numerical e.g. the FEM) for simple structures. These expressions are incorrect, since they do not take into account the boundary conditions.

high when the modal overlap factors of the uncoupled subsystems are much lower than unity[3](Fahy and Mohammed 1992). However, more recently, it has also been experimentally demonstrated that SEA based methods could be applicable to coupled structural-acoustic system with a MOF value less than unity - implying useful SEA/hybrid SEA based predictions at the mid frequency range e.g. see Marberg and Miasa (2002), Lalor and Priebsch (2007). Ideally, power-balance equations are derived for coupled structural-acoustic models utilizing information from the input power, CLF's, DLF's and the response is written in terms of energy parameters - which are later converted to averaged velocity or pressure response on the structural or fluid domains respectively. For a detailed discussion on the fundamentals of the SEA method, the reader is referred to Lyon and DeJong (1995), Keane and Price (1997).

In short, although SEA predictions are computationally very cheap compared to solving coupled fluid-structure equations via deterministic techniques, SEA's underlying assumptions regarding modal density render predictions that are invalid in the low frequency range. The reader is referred to (Plunt 1993) for a short review on use and misuse of the SEA method. As mentioned earlier, a sufficiently refined deterministic coupled model would make response predictions possible up to 100-500 Hz thereby providing a very useful supplement in the low to mid frequency range. Therefore, techniques to enhance computational efficiency (in terms of solution time and computational resources required) of the deterministic techniques whilst preserving the desired solution accuracy would save both time as a result of fast broadband NVH analysis.

The tremendous growth in both active and passive damping technologies, involving novel materials such as multi-layered composite or piezoelectric materials has

---

[3]From current literatures, it is not clear by how much this empirical value should be lower (than unity) to render SEA predictions impractical.

Figure 1.3.: Launch vehicle fairing structure (NASA 1996).

Figure 1.4.: Noise control of fairing by using acoustic heavy blankets.

made the design of complex structures with ideal NVH criterion ever more complicated. Figures:[1.3,1.4] illustrate the use of passive damping technology (in this case heavy blankets) for a launch vehicle fairing structure. Firstly, tremendous effort is required to identify the right modeling methodology associated with the incorporation of such damped structures on vehicle or a satellite. Often, such modeling techniques involve the use of higher order solid elements thereby further increasing computational burden. Secondly, the number of design parameters (such as stacking sequences on a composite structure) available to tailor the NVH performance is far greater than traditionally used isotropic materials such as mild steel. Lastly, since passively damped materials inherently exhibit viscoelasticity, both in the temperature and frequency domain, the analysis of structures incorporating damped materials need to carried out for different temperatures and solving updated matrices in the frequency domain.

This means that, repeated simulation is inevitable in order to identify the best design parameters in the case of actively or passively damped structures. This often forms the basis for optimization or a sensitivity analysis to determine the important parameters which significantly alter the NVH performance of the coupled system under investigation. For example, an optimization of a scale model of a launch vehicle

fairing carrying tuned mass dampers and Helmholtz resonators to reduce payload noise required around 18000 function evaluations (Howard et al. 2006). The steps involved in a broad band structural-acoustic optimization is shown in Figure:[1.5].

Therefore, it is often concluded that one of the big challenges in fully coupled vibro-acoustic modeling is the development of new deterministic prediction techniques and solution procedures, which provides accurate prediction results with an enhanced computational efficiency, compared with existing element based prediction procedures (Desmet 1998; Desmet and Vandepitte 2005; Desmet and Vandepitte 2002).

Precisely speaking, fast structural-acoustic coupled analysis would serve the following purposes:

(a) Assist in simulation speed up necessary to analyze NVH behavior in the low and mid frequency range, especially when a frequency sweep over a wide frequency band is required.

(b) Save computational time in the case of optimization or sensitivity analysis of structural and acoustic systems.
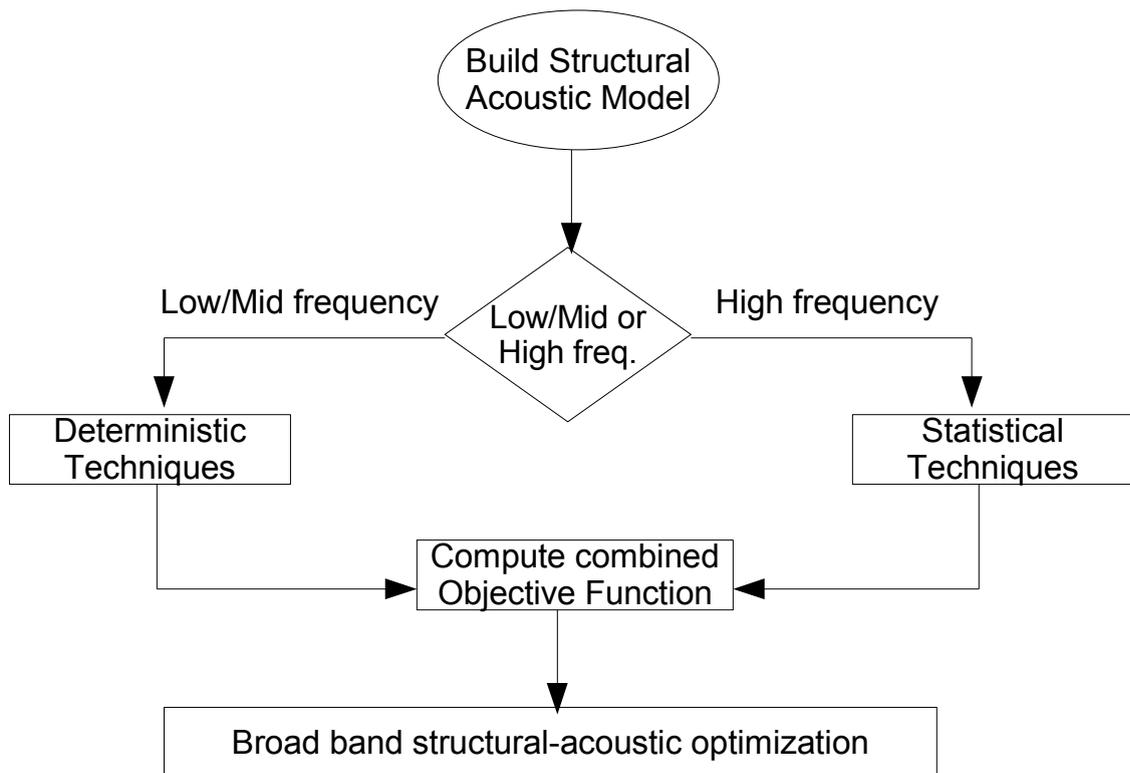
Figure 1.5.: Strategy for broadband NVH optimization.

1.3. Original Contributions of this thesis

(1) To alleviate the computational burden associated with a direct frequency resolution, the uncoupled and coupled modal formulations are often utilized to generate reduced order models. These modal methods and their drawbacks are well documented (Desmet 1998; Tournour and Atalla 2000; Ohayon 2004). More recently, however, generating reduced order models via implicit low frequency moment matching, has received considerable attention among mathematicians, circuit simulation and the control theory community (Freund 2000; Bai 2002). It has been shown in various engineering applications (Grimme 1997; Antoulas and Sorensen 2001; Willcox 2000; Willcox et al. 2002; Bechtold et al. 2005a) that the time required to solve reduced order models by matching some of the low frequency system moments is significantly reduced when compared to solving the original higher dimensional model, whilst maintaining the desired accuracy of the solution. Therefore, in this thesis, an attempt is made to exploit such moment matching based direct projection approaches, which essentially start off from an input-output problem formulation to efficiently construct a Padé or a Padé type approximant. As a result, new methods to generate accurate and efficient reduced order models for fully coupled structural-acoustic analysis via Krylov Subspace techniques are presented. In particular, the thesis focuses on *structure preserving*, moment matching transformations for dimension reduction.

(2) Four different algorithms for efficient construction of the reduced basis consisting of vectors belonging to the standard and second order Krylov subspaces are studied. The algorithms of interest are: One Sided Arnoldi (OSA), Two-Sided Arnoldi (TSA), Multi-point Arnoldi (MP-TSA) and the Two-Sided Second order Arnoldi (TS-SOAR) process. The suitability and capability of these

processes for fully coupled structural-acoustic systems, involving undamped, constantly damped and linearly damped material models are studied. It is shown how to construct a *structure preserving*, moment matching, reduced order model from a given coupled higher dimensional system under any of the above damping model scenarios. This has been achieved by identifying the specific process associated with the particular damping model. In this way, an explicit participation of the damping matrix is also made possible within the moment matching dimension reduction framework.

(3) The particular application interest of this thesis is the NVH simulation for automotive and aerospace type vehicles. Therefore, numerical test cases involving low density and high density fluid, in the form of air and water have been used to demonstrate the accuracy and computational efficiency of the new methods for the solution of interior, fully coupled, structural-acoustic analysis. In this manner, the properties of the ROMs for both weakly and strongly coupled problems are investigated. It is shown that by applying the moment matching, Arnoldi based *Galerkin* or *Petrov-Galerkin* type projections, it is possible to obtain an accurate input-output representation of the coupled problem, irrespective of the fluid medium. Further, it is also demonstrated that it is possible to generate *structure preserving* ROMs for the most commonly used damping models. Some attention has also been given to the choice of expansion points and convergence models for low frequency, structural-acoustic analysis.

(4) A new optimization framework for fast NVH simulation has been developed. This new framework involves objective function computation by intermediate ROMs generated via the One-Sided Arnoldi process. For the optimization method, the Mesh Adaptive Direct Search (MADS) is used in conjunction with

Latin Hypercube Sampling (LHS) in order to escape *local minimas.* The developed optimization framework is applied to a fully coupled structural acoustic problem, to demonstrate the computational efficiency of the optimization framework and the accuracy of the ROMs generated by moment matching.

1.4. Purpose of this thesis

The goal of this thesis is to introduce the reader to dimension reduction techniques for fully coupled, interior structural-acoustic systems based on *moment-matching* concepts via Krylov Subspaces. The key idea of constructing a reduced order model via Krylov subspaces is to remove the uncontrollable, unobservable and weakly controllable, observable parts without affecting the transfer function of the coupled system under investigation. The thesis makes use of the Arnoldi process to preserve the moment matching property in the reduced order model. Further, two extensions of the Arnoldi algorithm namely, the multi-point and two-sided algorithm are discussed with an aim to further increase the accuracy of the reduced order model. The numerical algorithms are applied to the Cragg's unsymmetric displacement/pressure formulation which is considered to be the most appropriate fully coupled structural-acoustic formulation in the NVH community. Simple extensions of the projection based formulation are made to accommodate various types of damping models (constant and frequency dependent) via first order transformation and Second Order Arnoldi (SOAR) process. Results are compared using direct results obtained via the ANSYS FEM program, Closed form solutions (where available) and the principle of *vibro-acoustic reciprocity.* For the test cases investigated in this thesis, it is shown that the reduced order modelling technique results in a very significant reduction in simulation time, while maintaining the desired accuracy of the state variables (displacements and pressures) under investigation.

The work also forms a small part of the EPSRC Low NVH Vehicle Structure project (EPSRC - Faraday Advance 2003) which seeks to investigate the use of light weight composite materials in production vehicle environment. In particular, the roof panel of a Ford model is subject to investigation. To this end, *moment-matching* based optimization framework is proposed and applied to a scale model to gain fundamental understanding on the NVH behavior of such composite light-weight designs. The optimization is carried out using a hybrid strategy involving Latin Hypercube Sampling (LHS) and Mesh Adaptive Direct Search (MADS) algorithm to counter the problem of *local minima*. In particular, the influence of stacking sequences of a laminated composite structure on the interior sound pressure level (SPL) are of particular interest. The optimization results indicate that by tailoring the stacking sequence to shift the first natural frequency produces reduced SPL levels in the fluid domain. Further, it is shown that by incorporating moment matching approaches for vibro-acoustic optimization, the computational burden can be significantly reduced whilst maintaining the accuracy of the objective function for the optimization.

1.5. Thesis Outline

Chapter 2 reviews the literature focusing on current state of art techniques for modeling interior acoustic noise. Both numerical and experimental work is included. FEM and BEM techniques, their formulations, advantages, disadvantages are reviewed. This chapter also reviews some of the most commonly used model order reduction techniques for structural-acoustics, methodologies for modeling passive noise control treatments via novel materials and modeling strategies for fully coupled structural acoustic optimization.

Chapter 3 is dedicated to the study of the governing equations for fully coupled structural acoustic systems. The FEM/FEM fully coupled structural-acoustic discretization, based on. Particularly, the Eulerian unsymmetric displacement/pressure formulation is derived. The fully coupled and uncoupled modal formulations are also briefly reviewed.

Chapter 4 introduces Krylov Subspace based projection techniques for fuly coupled structural acoustics utilizing the *Eulerian (u/p)* formulation for the underlying problem. The concepts of system representation, state-space modeling and the so called *leading co-efficients* of the transfer function are introduced. Four algorithms based on the classical Arnoldi process, to generate vectors belonging to the Krylov Subspace and their connection to the *leading co-efficients* of the transfer function are described. Dimension reduction techniques to deal with undamped, constantly damped and frequency dependent, linearly varying damping are presented. Finally, some convergence models and error parameters applicable to Krylov Subspace based direct projection techniques are discussed from a stopping criterion viewpoint.

Chapter 5 describes the application of dimension reduction methodologies to six different fully coupled structural-acoustic test cases. The test cases range from a 2-D, water filled, benchmark structural-acoustic models to real-life, adhesively bonded vehicle type structures. Structural excitation, in the form of point force, and acoustic excitation, in the form of volume acceleration are considered to demonstrate computational accuracy and efficiency of the proposed dimension reduction techniques. Throughout this section, the examples are extended to constant structural/acoustic and frequency dependent damping models.

Chapter 6 applies the concept of *moment matching* to perform goal oriented fully coupled structural-acoustic optimization. In this chapter, a new optimization framework is proposed, which exploits the structure preserving, moment matching con-

cepts to enable efficient structural-acoustic optimization. A simple optimization test case, a constrained plate-rectangular prism cavity structural-acoustic system is considered. The stacking sequence of the clamped plate structure enclosed by the rigid walled acoustic cavity are considered as design variables for the optimization. The optimization is carried out using the Mesh Adaptive Direct Search (MADS) algorithm, incorporating a Latin Hypercube Sampling (LHS) technique at the start of the optimization process. Results for four parameter and eight parameter stacking sequences for two different composite materials are presented.

Chapter 7 draws some general conclusions on ROM*s* via Krylov Subspace based projection techniques and suggests possible directions for future research.

2. Literature Review

This chapter focuses on the techniques for the analysis of interior structure-acoustic systems, consisting of a flexible structure in contact with an enclosed acoustic cavity. A short literature review is presented here which focuses on the purpose of the coupled analysis and the current NVH industry standard methods available to predict structural and acoustic behavior. The literature review addresses the following topics: Analytical methods for prediction, Finite element and Boundary element techniques, hybrid experimental-numerical approaches and vibro-acoustic optimization. In the sections following, the governing equations of the structure-acoustic problem are given and the finite element formulation of this problem are discussed.

2.1. Low Frequency Analysis: Structure Borne Noise

Structure borne noises (low frequency) are primarily caused due to the road (wheel rotation), engines and power train excitations, which transmits to the vehicle body (structural panels), to result in noise being radiated inside the interior cabin (Jha and Priede 1972). In order to numerically predict the coupled behavior of a passenger cabin-structure, the displacements of the structure and the acoustic pressure fields inside the cabin are considered individually or simultaneously - depending on the nature of the mutual coupling between the structural and acoustic systems. This nature of this mutual coupling behavior is often categorized as *weakly coupled*

or *strongly coupled* systems. When the influence of the fluid loading has a significant effect on the vibration of the enclosing structure, the problem of analysis of the coupled behavior of the resulting system is said to be *strongly coupled*. When this influence is low, the system is described as a *weakly coupled* system. In weakly coupled systems, the mutual vibro-acoustic coupling interaction between the structural and the fluid components is very weak and therefore can be omitted in the analysis of the dynamic behavior of such systems. This considerably simplifies the solutions procedures for the prediction of the dynamic quantities under study. In strongly coupled systems, the mutual vibro-acoustic coupling interaction is no longer negligible and all components must be treated as parts of a single coupled system, resulting in a complex prediction procedures. Therefore, it is often desirable to know before hand whether a system is weakly or strongly coupled. Atalla and Bernhard (1994) put forward a dimensionless quantity (λ_c) to classify if a vibro-acoustic system is weakly or strongly coupled:

$$\lambda_c = \frac{\rho_0 \ c}{\rho_s \ t \ \omega} \tag{2.1}$$

where, ω is the circular frequency of a time-harmonic structural or acoustic excitation of the system, t is a characteristic thickness of the structure, ρ_s is the mass density of the structure, ρ_0 and c are the mass density and sound speed of the fluid. The authors state that a value of $\lambda_c > 1$ indicates strong coupling and a value of $\lambda_c < 1$ indicates weak coupling. Equation:[2.1] indicates that a heavy fluid (e.g. water) would indeed have a significant influence on the coupling measure. Unfortunately, this measure is not fully comprehensive, since it does not take into account the dimensions of the structural or fluid subsystems[1]. Due to this difficulty in generally classifying vibro-acoustic systems for their coupling behavior, industrial studies relating to for example, for the interaction between the vibrations of the double wall aircraft fuselage structure or the structural and fluid domains of an automotive

---

[1]For example, the dynamic behavior of an elastic structure enclosing a very small acoustic cavity can be strongly coupled due to the fluid back pressure, even when the cavity is filled with a low-density fluid such as air (Desmet 1998)

structure are often modeled as fully coupled systems.

Weak coupling allows the *in vacuo* modal response of the structure and the response of a rigidly enclosed space to be used to determine the coupled system response. Lyon and Maidanik (1962), Pretlove (1966) both considered the theoretical coupling of a single flexible rectangular panel backed by a rigid walled acoustic cavity. The study was performed via a space average energy approach. It was assumed that the fluid loading is small (weak coupling) relative to the panel stiffness and that the fundamental *in vacuo* panel natural frequency is lower than the natural frequency of the first cavity mode. The frequency range was classified into three distinct bands: *low frequencies* below the fundamental panel resonance where both the panel and interior volume are stiffness controlled; *intermediate frequencies*, where the panel is resonant and the cavity is stiffness controlled; and *high frequencies* in which the both the panel and the interior volume display resonant behavior.

Fahy (1969) studied the vibration of a rectangular flexible panel backed by an air filled rigid rectangular box using the modal coupling approach. A weak coupling assumption was made for the analysis. The author further describes that the weak coupling assumption does not necessarily hold for low-order acoustic modes and small volumes or very light panels. Pope (1971) utilized the modal coupling theory and experimentally verified the predictions for a closed cylinder and a rectangular parallelepiped enclosure with a single flexible panel. The authors demonstrate that the experimental results are in good agreement with modal coupling predictions. Dowell et al. (1977) presented the theory of *acoustoelasticity* to analyze the coupled behavior of a plate backed by an acoustic enclosure. Detailed analytical formulations of the harmonic solution to the resonant transmission of sound through a structure into a rigid walled acoustic space based upon a modal interaction model are presented. The predictions were successfully verified via experimental vibro-acoustic

analysis.

If the geometry of the vibro-acoustic system and the boundary conditions are simple, then, in general, it is possible to derive analytical expressions for the terms in the series solutions to the governing differential equations. However, for a majority of real life vibro-acoustic systems, it is not possible to obtain analytical solutions to the model equations because of the geometric or dynamic loading complexity of the coupled system. Deterministic techniques based on FEM and BEM are often utilized to counter this problem. Craggs (1969), Craggs (1971) studied a transient coupled system using a displacement and pressure FE/FE formulation. In such Vibro-acoustic FE models, the fluid is described in terms of acoustic pressure, and the structure in terms of structural displacements. The formulation can also be found in Zienkiewicz and Newton (1969). Due to the formulation of the coupled problem by employing displacement and pressure as state variables, the resulting set of coupled stiffness and mass matrices become unsymmetric. A description of modal methods for acoustics using the pressure formulation can be found in Craggs (1972). The idea of using these methods, is to find an exact solution for a set of governing equations. To achieve this, the coupled domain is first discretized into a number of elements. Within these elements, the dynamic response variables, in this case the structural displacements or the acoustic pressures, are described in terms of simple, polynomial shape functions.

In order to describe the spatial variation in the dynamic response with a certain level of accuracy, often the *rule of thumb* is applied, which states that at least 6 to 10 linear finite elements should be used per wavelength (Atalla and Bernhard 1994; Desmet 1998; Desmet and Vandepitte 2005). For quadratic finite elements, about 4 elements per wavelength are required (Pluymers 2006). These criterions are mainly due to the upper bound limit for the relative *prediction error* of the FE

method, which is given by (Ihlenburg and Babuska 1995; Ihlenburg and Babuska 1997; Bouillard and Ihlenburg 1999; Desmet and Vandepitte 2002):

$$\epsilon_{FEM} \leq C_1 \; \left(\frac{k\,h}{p}\right)^p \; + \; C_2 \; k \; L \; \left(\frac{k\,h}{p}\right)^{2p} \tag{2.2}$$

where, k is the wavenumber, C_1 and C_2 are constants, where h is the finite element size, p is the order of the polynomial shape functions and L is a characteristic length of the problem domain.The first term in this prediction error is related to the approximation error or the so called *prediction error* and the second term is the *pollution error.* The prediction error[2] results from the description of a dynamic response field by the application of simple polynomials in the FEM. On the other hand, the pollution error[3] results from the difference in wave numbers for the FE discretization and the exact problem. This phenomenon is referred to as *numerical dispersion.*

In order to keep the errors at acceptable levels (by keeping $k\,h$ constant), leads to huge model sizes (as a consequence of smaller mesh size) for increasing frequency and hence a significant increase of computational time and expense. In some sense, the *rule of thumb* is used to control the approximation error well for low frequencies or small wave numbers, where the approximation error is governed primarily by the interpolation error of the employed FE scheme. Note that another possible approach to limit the prediction error is to employ higher-order finite elements (Harari and Avraham 1997). A notable disadvantage of this method, however, is the increase in the matrix bandwidth, which results in increased computational effort. Therefore, it can be concluded that if a higher degree of accuracy is required, quadratic elements should be employed at an increased computational cost. On the other hand,

---

[2]This is dominant at low frequencies.

[3]This is dominant at higher frequency. For specific discretization criterions used to control this type of error, the reader is referred to Ihlenburg and Babuska (1995), Ihlenburg and Babuska (1997), Bouillard and Ihlenburg (1999).

if a lower degree of accuracy is sufficient, linear elements could be employed. As a general trend, it is common practice to use linear elements and is employed by most commercial FE packages for fully coupled structural-acoustic analysis.

On the other hand, the BEM is also a well established alternative method for the FEM for various engineering problems (Brebbia et al. 1984). In this approach, the application of boundary integral formulations forms the basis of the BEM. These boundary integral formulations relate the field variables inside the problem domain to boundary variables at the boundary surface. In general, the BEM approach consists of a two-step procedure: In the first step, the distributions of the boundary variables are determined. In the second step, the field variables in any point in inside the acoustic domain are obtained from the boundary integral formulation, using the boundary surface results of the first step. The two most popular BEM approaches are the *direct* (Schenck 1968) and *indirect* BEM. When compared to the finite element method, since only the boundary surface of the acoustic domain is discretized into elements, the size of direct and indirect boundary element models are substantially smaller. From an industrial viewpoint, significant saving in man hours is achieved, since only the boundary of the acoustic domain is discretized. However, due to the fact that the Green's kernel function used in the BEM is a complex function, the matrix coefficients in boundary element models are complex. Additionally, the resulting matrix coefficients are also frequency dependent. This means that, a BEM model does not lead to a natural eigenvalue problem as encountered in an FEM model. To counter this drawback, a decomposition method is proposed (Ali et al. 1995; Coyette and Fyfe 1990), which leads to an algebraic non-symmetric eigenvalue problem for the computation of natural frequencies and mode shapes of an interior acoustic system. Therefore, when the BEM is utilized for fully coupled analysis, the computational effort becomes much larger when compared to solving the sparsely populated, frequency independent FEM based methods (Desmet 1998).

To alleviate the computational difficulties encountered with the Eulerian u/p formulation, alternative FE/FE formulations leading to positive-definite, symmetric matrices have been proposed. In such studies, the structural field, the primary variable considered is displacement. For the fluid field, the unknown variables have taken the form of velocity potential (Everstine 1981; Olson and Bathe 1985), a combination of velocity potential and sound pressure level (Morand and Ohayon 1979), displacements in the fluid (Feng and Kiefling 1976) and a combination of displacements and pressures (Wang and Bathe 1997). For an application of the mode superposition method utilizing the velocity potential and pressure formulation for the acoustic field and displacement formulation for the structure, the reader is referred to Wang (1998). However, these formulations encounter new problems such as spurious rotational modes (for a treatment of this problem via the *vorticity moment* formulation, the reader is referred to Bathe et al. (1995)), increase in dimension of the problem size, rendering the coupled system gyroscopic or involves solving a complex matrix even for an undamped coupled structural-acoustic problem (thus requiring complex eigen value routines to determine real eigen values). Such problems with these other formulations have resulted in the *Eulerian (u/p)* formulation (Craggs 1969; Zienkiewicz and Newton 1969; Craggs 1971; Craggs 1973) being adopted as the most appropriate prediction technique (Desmet and Vandepitte 2005), and being widely employed in commercially available FE codes such as ANSYS, MSC/Nastran, DSS ABAQUS, LMS SYSNOISE.

Irrespective of the structural-acoustic formulation employed, it is clear the dimension reduction reductions are required to reduce the system matrices such that computationally efficient analysis and sensitivity analysis is feasible. The two most popular approaches to reduce the computational time of such coupled fluid-structure formulations are the coupled mode superposition and the uncoupled modal synthesis

methods (Desmet 1998). Both these methods, perform a change of base (through a set of eigenvectors), resulting in a lower dimensional model. The former method uses the dominant natural frequencies and mode shapes, extracted from a coupled modal analysis (i.e. the coupled eigenvalue problem) and the response is assumed to be a linear combination of these modes. However, the standard mode superposition method, suffers from four major drawbacks: (a) The computation of coupled modes using a non-symmetric eigen-solver tends to be computationally very demanding (Pirk et al. 2002); (b) The second drawback is the treatment of damping. For well damped structures, a spatially distributed damping - often varying with frequency, has to be utilized (Marburg 2002a); (c) If a structural-acoustic optimization problem in a particular frequency band is considered, there exists the problem of only the higher order modes being truncated, leading to unwanted estimation of lower order modes repeatedly (Pal and Hagiwara 1993); and (d) The number of modes required to represent the frequency band under investigation is often an approximate guess of between $1.5\omega_E$ to $2\omega_E$ where ω_E is the upper frequency range.

In the uncoupled modal synthesis type approach, the system is divided into distinct natural components[4] (structure and fluid), and the uncoupled modes from a symmetric eigenvalue problem are calculated. This set can then be treated as vectors for projection in the standard modal superposition model. However, the efficiency of the uncoupled modal formulation for coupled structural-acoustic problems in reducing model size is poor, since a large number of acoustic modes are required to enforce displacement continuity along the fluid-structure interface. This is mainly due to the fact that the modes of the uncoupled acoustic model have a zero normal fluid displacement along the fluid-structure coupling interface. Therefore, for an accurate representation of the near-field effects in the vicinity of the fluid-structure

---

[4]In some sense, this approach can also be referred to as a *global* component modes approach, since the coupled problem is now partitioned into different uncoupled natural components - namely the structure and the fluid.

coupling interface a large number of high-order modes in the acoustic modal basis is required, resulting in slow convergence of the coupled problem. This has been numerically demonstrated for a 1-D tube example (Desmet 1998). Further, the effect of the kept (retained) *dry* modes is critical to the convergence in the uncoupled modal basis method, especially for *strongly coupled* problems (Ohayon and Soize 1998; Boily and Charron 1999; Tournour and Atalla 2000; Ohayon 2004) e.g. presence of heavy fluid. Davidson (2004), proposed a selection criterion which identifies the coupling influence of the uncoupled modes based on the coupled stiffness matrix (starting from the u/p formulation) and the resulting natural frequencies and mode shapes from an uncoupled modal approach. This coupling expression allows a quantification of the coupling between the structural domain and the fluid domain to be determined creating the possibility of choosing the most important uncoupled modes to include in the reduced coupled problem. In this way, the *important* modes of the subsystems are retained for the modal type projection. The approach has been successfully utilized for regular air filled cavities and cavities including porous media.

The restriction of these two primary modal type reduction methods has left NVH engineers with a very limited number of tools for the numerical analysis of vehicle/aerospace interior noise prediction problems, and hence they are often forced to resort to mixed experimental-numerical approaches (Kim et al. 1999). Other approaches to reduce computational time for structural-acoustic problems include the use of symmetrization techniques (Morand and Ohayon 1995; Ohayon and Soize 1998; Ohayon 2004; ABAQUS 2005), geometric mesh skinning and the use of non-matching fluid and structural meshes (Coyette and Dubois-Perlerin 1994), computation of eigenvectors of the original system by using eigenvectors of a reduced eigenvalue problem and local substructure modes via the Automated Multi-level Substructuring method (Bennighof 1999; ABAQUS 2005), the recently developed,

modified AMLS method for non-symmetric eigenvalue problems (Stammberger and Voss 2007), the component modes approach (Magahlaes and Ferguson 2003; Magahlaes and Ferguson 2005), generation of Ritz vectors (Seybert et al. 1993; Morand and Ohayon 1995), use of acoustic influence co-efficients from BE models (Marburg et al. 1997), truncated FE/FE analysis (Pal and Hagiwara 1993), the patented Acoustic Transfer Vector (ATV) method (Sysnoise 2004), the wave based prediction technique (Desmet 1998) and the use of banded Lanczos process for symmetric matrices arising from exterior acoustic problems (Malhotra and Pinsky 2000; Wagner et al. 2003), to name a few. For interior structural-acoustic problems, the AMLS method offers significant speed up in simulation time, without user intervention for partitioning the components (Kroop and Heiserer 2003; Stryczek et al. 2004; Gao et al. 2005). In this method, an automatic partitioning of the FE model into sub-structures is performed on a number of levels, based on the sparsity structure of the system matrices for eigenvalue and eigenvector computations. In practice, the substructure partitioning is normally achieved utilizing efficient graph partitioner such as METIS (METIS 2005). The response is then represented in terms of the substructure eigenvectors. The reader is referred to the reviews by Atalla and Bernhard (1994), Ohayon and Soize (1998), Marburg (2002a), Desmet and Vandepitte (2002), Thompson (2006), ABAQUS (2005) for a description of some of the above mentioned modal and model type dimension reduction approaches.

It is worth reminding the reader that the reduction techniques based on uncoupled modal synthesis do suffer from accuracy problems in terms of the number of *kept modes* for strongly coupled problems and computational efficiency for weakly coupled systems. In some sense, the AMLS method alleviates this problem for coupled structural acoustic analysis by employing an efficient procedure to compute a large number of eigenvectors[5]. For a general review on CMS type approaches for

---

[5]This is later demonstrated in Chapter:5.1 of this thesis.

structural dynamic analysis, the reader is referred to Craig (2000). In what follows, a short review of the interior structural-acoustic modeling methodology, with a focus on its application to automotive and aerospace type cabin interiors is presented.

2.1.1. Low Frequency NVH: Prediction Methodologies

Petyt et al. (1976) were probably the first to utilize finite element technique for acoustic analysis. In this work, the authors developed a 20 node acoustic finite element to compute the natural frequencies and mode shapes for applications involving irregular enclosures. Experimental modal analysis were carried out on a one twelfth, scale model van type enclosure, using 10mm perplex sheets to introduce *rigid walled* boundary conditions. The authors report excellent agreement between numerical and experimental natural frequencies. Nefske et al. (1982) described the development of coupled structural-acoustic analysis, including structural forcing vectors, utilizing the coupled FEM for the study of vehicle interior noise. A comprehensive review of the formulation of FEM in both physical (*direct*) and modal co-ordinates to investigate the structural-acoustic behavior of passenger car cavity is presented. Resonant frequencies and noise transfer functions calculations for a vehicle body are presented. The effect of the contributions of each panel to the total sound pressure level (SPL) has also been investigated. This analysis was performed by re-running the analysis, each time with a single panel. In a similar study, Nefske and Sung (1985), Sung and Nefske (1986) demonstrated the use of the FEM to compute natural frequencies, mode shapes and interior SPL of a van type structure. Due to the computer limitations at that time, for the coupled analysis (in the frequency range of 0-100Hz), the authors diagonalized the resulting fluid-structure matrices to save computational time. In general, the noise transfer function values were within ± 5dB agreement (in comparison with experiment) at peaks but significant deviations were observed at troughs. The authors point out that this discrepancy could be a result

of inaccurate modeling of damping or the fact that too few modes were included in the uncoupled modal basis technique (Lalor and Priebsch 2007).

Campbell (1993) suggested the form of body acoustic sensitivities to study the vibro-acoustic behavior. Finite Element models of the car body and the cavity were generated using commercial software SDRC-IDEAS. The uncoupled modal *(u/p)* approach has been utilized. A unit force was applied to the front control attachment arm, and the acoustic response computed. An empirical model to include seats, by increasing the mass density of the fluid elements by a factor of 10 in the acoustic FE model is also suggested. Side doors were modeled as lumped masses to simplify the coupled analysis. The author reported that the trends predicted by the model were generally found in good agreement with experimental test data. Design modifications were then introduced in the form of beam and panel section modifications to reduce interior noise. Sung and Nefske (1999) utilized the coupled FE/FE formulation, within the framework of MSC/NASTRAN finite element code. The uncoupled modal superposition method was used to compute the coupled response. Computed response quantities were compared with experimental results of a trimmed passenger car in the 0-200Hz frequency range. Techniques to deal with symmetric and unsymmetrical structures have also been highlighted. Modal damping was assumed. The structural and acoustic damping used in the coupled analysis were 3% and 6% respectively. The structural response functions showed a mixture of under-predicted peaks and major differences in the 40-70Hz and 125-175Hz frequency range. One of the reasons put forward by the authors of the paper for under-predicted peaks was identified as inaccuracies in representing damping. The measured interior noise levels above 150Hz. had significant discrepancies, which could not be resolved. The authors of the paper suggest that these discrepancies could be resolved by improving modeling of joints and structural, acoustic damping factors.

To study the geometric effects of acoustic cavities, an uncoupled analysis is preferred. Compared to a fully coupled analysis, an uncoupled analysis based on the FE/FE methods leads to symmetric and sparse matrices. At this point, it is worth mentioning that the natural frequencies and modes of a coupled system are different from those of the individual uncoupled systems (Dowell et al. 1977; Fahy 2000). Kopuz and Lalor (1995) carried out a series of numerical investigations (FEM and BEM) on simple box shaped structures and then extended the idea to study the effects of a car boot (luggage compartment) on the interior acoustics of the passenger car cabin (box shaped structure). The work utilized the SYSNOISE finite element and boundary element codes. The use of the direct approach, which requires an inversion of the stiffness matrix and the modal superposition approach, in which the problem is formulated and solved in the modal co-ordinates have been compared. It was found that both yield similar results and no significant difference were observed. The direct and indirect BEM approaches have also been compared with each other in terms of solution state accuracy.

Kim and Lee (1995), put forward a hybrid Finite element- Experimental Structural Modal Analysis (ESMA) based method for noise reduction in a vehicle passenger compartment. In this study, the coupled response of the cavity is described in terms of structural and acoustic modal co-efficients and modal parameters of the vehicle. The variables of pressure and displacement were described using the rigid wall cavity modes and the structural modes. Using these results, an expression for the coupling coefficients has been formulated. These co-efficients were used to analyze the coupling behavior between the structural and acoustic modes. The structural modes were obtained using ESMA. The developed method has been validated on a fabricated half scale passenger car model. Structural modifications, in the form of damped structures were introduced to reduce overall SPL inside the cabin. The work was extended in Kim et al. (1999) by applying the method to a real life pas-

senger vehicle. The acoustic modes were computed using the ANSYS finite element code. The structural modes (obtained by ESMA) were used as boundary conditions for the coupled model. The authors conclude that the method is particularly suited to trouble-shoot noise problems on production vehicles.

Lee et al. (2000) proposed a similar hybrid approach, but using the FEM for the structure and the BEM for the fluid to analyze the booming noise encountered in the low frequency range. In addition to this, experimental data acquired from ESMA, Transfer path analysis (TPA), and Running Mode Analysis (RMA) were introduced into the computational model. Running mode data, in the form of accelerations, were introduced into the acoustic model to study the response. Measured impedance, from impedance tube tests, were imported into the FE model. Similar response patterns were observed from FE models and experiments. Panel Contribution Analysis (PCA), which used the running mode data to generate velocity boundary conditions in the BE model, showed that the contributions from vehicle roof and rear windshield were dominant. These were then reduced by reinforcing the cross member of the roof rail.

For fully trimmed structures, structural or acoustic damping (energy dissipation) mechanisms are commonly modeled using constant/frequency dependent damping or by specifying an impedance value at the boundary of the acoustic domain[6]. Morrey and Whear (1996) studied the NVH behavior of an interior car cavity, where, the frequency response functions of the vehicle structure (utilizing element based techniques) were applied as a forcing function to the acoustic boundary and a PCA analysis performed using the BEM. In this study, experimentally obtained boundary impedance values were also included in the deterministic model to represent the presence of carpet and seats. The experimentally obtained noise transfer functions

---

[6]Such computations are predominantly carried out assuming harmonic excitation - resulting in damping formulations in the frequency domain.

were in good agreement with predicted values. Wentzel and Green (1997) specifically addressed the importance of choice of roof assembly and head liners on the development of quieter vehicles. A review of techniques for obtaining material properties of an acoustical product (like sound transmission loss, absorption co-efficient) is included. It has been reported that, higher the head liner thickness, the better were the acoustical properties. Typically, such acoustical properties (impedance, absorbtion coefficients) can be extracted using an impedance tube (see e.g. (Peng et al. 1996). Kang et al. (2000) studied the interaction between roof, air-gap, trim and floor. To simplify the *coupled* analysis procedures, the authors proposed a one dimensional impedance model. The theoretical model was then compared with the FEM using the MSC/NASTRAN code. The developed method was applied on a fabricated passenger car compartment to study the effects of variables such as trim mass, air gap thickness and the roof and floor. As one would expect, a higher trim mass has shown to reduce the amplitude of the response. Similarly, higher air gap thickness has also shown to reduce the amplitude of the resonance peaks, but tends to induce another resonance peak with a significantly low magnitude. It has been identified that the air gap thickness and the trim mass can be effectively utilized to reduce the resonance peaks of the up/down acoustic mode (parallel to roof). Proper choices of adhesive systems have also been proven to have a significant effect in the NVH behavior of vehicle structures (Krois et al. 2003).

The majority of the current materials used in the automotive industry are made up of thin sheets of metals, which in general have very low internal damping (energy dissipation) mechanisms. Due to this, high resonant vibration levels are observed when such structures are excited. To tackle this problem, engineers often resort to active or passive noise control. Active noise control (ANC) involves the use of electronic devices such as speakers, microprocessors or actuators (Lane and Griffin 2001; Oliveira et al. 2006) to produce an out of phase signal to cancel the distur-

bance. The use of electronic devices to achieve reduced NVH causes an inevitable increase in cost, which manufacturers often strive to minimize. On the other hand, passive noise control involves the use of high damping materials, which tend to reduce the amplitudes of vibrations, thus reducing noise levels, while maintaining or reducing the component weight. In general, the passive control techniques works well in middle to high frequencies while the active control methodology provides noise cancelation at low frequencies (Mathur et al. 2001). By combining active and passive concepts, hybrid noise control methodologies are obtained, which allows the control of noise over a wide frequency bandwidth. Such hybrid noise control techniques are often deployed in aerospace and space craft type vehicle structures.

Niyogi et al. (2000) utilized a coupled FE/BE formulation to study the coupled effects of folded laminated composite structure backed by an acoustic cavity. The authors note that no results were available (at that time) in the open literature that addresses the problem of interaction between a composite structure and an interior acoustic domain. First order Shear Deformation Theory (FSDT) has been used for the structural analysis. An impedance relationship has been used to derive the normal forces which act on the fluid- structure interaction zone. Using this method, the effect of stacking sequence, wall thickness and damping ratio's on the variation in pressure level inside a rectangular enclosure were studied in detail. This is shown in Figures:[2.1,2.2]. It can be observed that for the same stacking sequence, wall thickness is a significant variable which dictates the SPL pattern.

The pattern of the variation in pressure level has been attributed to the fundamental natural frequencies of the composite folded plate. Similar structural frequencies have generated similar pressure level response pattern. As one would expect, a higher damping ratio of the composite structure, resulted in a decrease in the magnitude of the pressure response. These results clearly indicate that the material properties
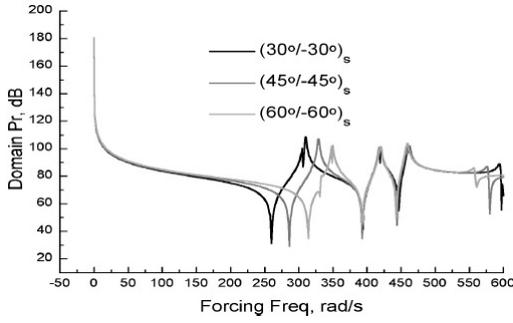
Figure 2.1.: Pressure variation with stacking sequence (Niyogi et al. 2000).
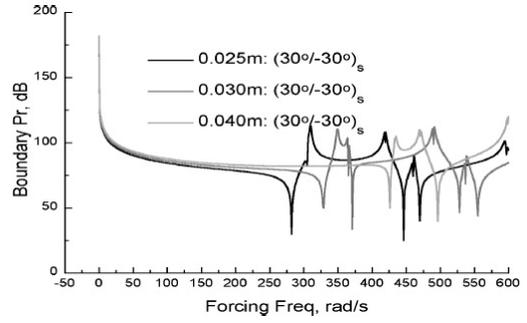
Figure 2.2.: Pressure variation with stacking sequence and wall thickness (Niyogi et al. 2000).

of the structure play an important role in the structural-acoustic NVH behavior. In automotive applications, passive damping in the form different material models such as sandwich structures are often used to reduce noise and vibration, with an aim to improve the interior sound quality. The study also confirms the use of deterministic techniques to study the effect of composite materials on low frequency, interior, structural-acoustic behavior.

An uncoupled acoustic computation often forms the start point for fully coupled structural-acoustic analysis. Whear and Morrey (1996) put forward an experimental *side-by-side* microphone probe technique for acoustic modal analysis using a commercial structural modal analysis software and an analogue differential amplifier. The developed technique was verified by measuring the natural frequencies and mode shapes of a bare rectangular office along with analytical calculations and uncoupled acoustic finite element results. The authors demonstrated that there was very good agreement for all modes in the considered frequency range (0-100Hz). The authors have utilized the developed acoustic modal analysis technique in Morrey and Whear (1995), Morrey and Whear (1996), to study the structural-acoustic behavior of a Rover Metro R-6 Body-in-White (BIW). A finite difference principle was used in conjunction with three microphone probes technique to obtain the second derivative of partial pressures. The pressure measurements were taken using the

microphones, while a developed electronic circuit was used to carry out the finite difference calculations. Experimentally obtained natural frequencies and mode shapes were compared with numerical (element based) predictions. The authors note that estimates of natural frequencies compared well with numerical results, but the mode shapes did not match well. This can be attributed to the fact that, while testing on a real-life vehicle, the so-called *rigid wall* condition were not satisfied. Indeed, the authors find a ($\frac{1}{2}$,0,0) acoustic mode. This is likely due to the presence of a coupled fluid/structure mode(s) i.e. coincident fluid and structural natural frequencies. Further, the authors also demonstrate that the boundary impedance has little effect of the natural frequency, but significantly affects the mode shapes, due to the displacements of the structure.

Cornish (2000) proposed an experimental based approach to study the interior noise of a commercial vehicle in the low frequency range. The technique is based on the well-known principle of Structural-Acoustic Reciprocity (Fahy 2000; Fahy 2003). The approach was applied on a commercial production vehicle. A monopole sound source was used near the driver's head, which generated a random noise. Accelerometers were then mounted on the front right engine mount, to obtain the acceleration data. Noise paths were quantified using this method. When computational modeling is a constraint, or where manufacturing variability is a significant issue, this method seems to be particularly attractive to quantify noise paths and apply appropriate structural/body modifications to reduce overall SPL. Maruyama et al. (1999) analyzed the interior acoustic behavior of a passenger car by making use of the structural-acoustic reciprocity technique. The author explains why the concept of reciprocity should be applied to the study of low-frequency structure-borne sound and also discusses some of the common causes of structure borne noise associated with passenger cars. Desmet (1998) extensively utilized the vibro-acoustic reciprocity relationship for the computational validation of the wave based prediction

technique. In this way, two computational dynamical transfer functions, resulting from unit structural and acoustic excitations were compared for accuracy. This study also indicates that the reciprocity relationship could be used to validate new computational techniques for fully coupled structural- acoustic systems.

Priebsch et al. (2001) proposed methodologies to study the structural-acoustic behavior in a sequential manner. In this study a coupled FE/FE formulation has been employed using commercially available finite element codes NASTRAN and LMS SYSNOISE. The car body is tested in four steps: (a) Stripped BIW (b) BIW with windshield and bulkhead fitted (c) Closed BIW (All doors added) (d) Fully trimmed vehicle. Using this four-step methodology, the effects of seats, varnishing, paint, internal damping of structures have been studied. Precise modeling of gaps and joints, which has shown to significantly affect the interior noise have also been studied using this method. Figure:[2.3] show the effect of accurate modeling of gaps and uncovered openings on interior SPL.
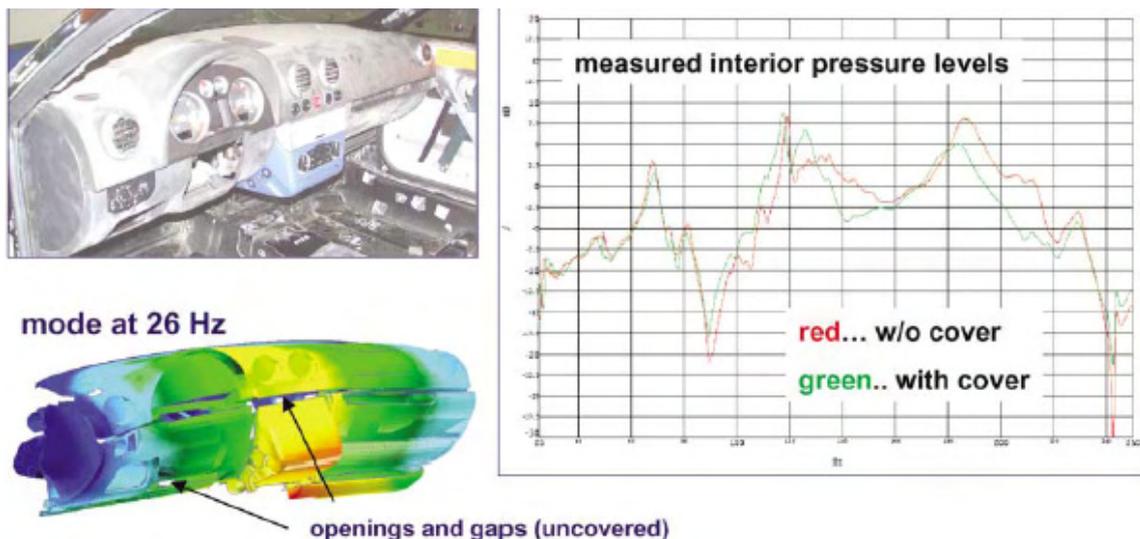
Figure 2.3.: Effects of gaps and openings on interior SPL (Priebsch et al. 2001).

Pirk et al. (2002) described the vibro-acoustic analysis of a launch vehicle fairing. The analysis has been carried out using a coupled FE/FE formulation in the low fre-

quency range, and Statistical energy Analysis (SEA) in the higher frequency range. In some sense, the authors have performed a broad band vibro-acoustic analysis on the launch vehicle fairing. Special considerations were given to modeling the fairing structure, which is a detailed model. The fairing structure is meshed using 4 noded shell elements, while the acoustic domain is meshed using 8 noded brick elements. An uniform exterior pressure (simulating lift off) loading is specified by applying a normal point force on all nodes of the external fairing shell elements. The force value is defined such that the total load is equivalent to a uniform pressure loading of 160dB. In this instance, the structural mesh is very much different from the acoustic mesh. To tackle this problem, a geometric interpolation algorithm has been used to project the structural modes on a coarser mesh, representing the structure. The uncoupled FE/FE method was compared with the FE/BE method in the low frequency range. It was shown that the results were accurate till 150Hz. The computational efficiency of the uncoupled FE/FE method, compared to the uncoupled FE/BE method has also been demonstrated.

Buehrle et al. (2001) utilized the FEM/BEM method to predict sound transmission loss of CFRP honeycomb panels. The structural response of the curved panels due to point force excitation was predicted using MSC/NASTRAN and the radiated sound was computed with COMET/Acoustics. The predicted velocities from the FEM, was projected on the BEM mesh for acoustic analysis. The core of the honeycomb panel has been modeled by 8 noded solid elements, while the face sheets were modeled using 4 noded shell elements. To test the solid modeling methodology, modal analysis tests of the honecomb panel were carried out under free-free conditions. These modal parameters were then verified by FE simulations. Experimental verification of the acoustical numerical analysis approach to predict radiated sound power have also been provided. In a similar study, Buehrle et al. (2003) used the FEM/BEM technique to predict sound transmission loss of damped plexiglass win-

dows. The construction of the material was similar to that of a constrained layer damping (CLD) treatment. A viscoelastic material was used for the core, in two and three layer configurations as shown in Figure:[2.4]. The mode superposition, with frequency dependent properties constant at 100Hz. was used for the structural FEM study. The core was modeled by 8 noded solid elements, while the face sheets were modeled using 4 noded shell elements with node offset. The computed velocities were then projected on the BEM mesh to compute the acoustic response. These results show that it is most advantageous to place all of the damping material at the mid-plane where the shear strains are the largest. In terms of FEM modeling of the CLD treatment, it was observed that using a solid-solid-solid layered model yielded better response predictions when compared to the solid-shell offset method.

Figure 2.4.: Two layer (left) and three layer damped plexiglass windows for aircraft interior noise control (Buehrle et al. 2003).

2.2. Structural Acoustic Optimization

In order to improve the acoustic characteristics of a vehicle interior, numerical optimization is often employed. Such a multi disciplinary optimization approach requires the coupled fluid and structural equations (assuming only a few design variables), causing an inevitable increase of computational time and expense. Since there exists two forms of solution (coupled and uncoupled), it is often left to the engineer to decide which one of them would best suit the problem under investigation. From a design point of view, it would be worth while to note that an uncoupled analysis would often be well suited. This is because, the acoustic modes of the cavity arise from the geometric dimensions of the cavities themselves, and the coupling effect can

be observed only when the structural and the acoustic frequencies are closer to each other. Such a *one-way interaction model* (uncoupled) assumes that the structural changes are very small when compared to the fluid wavelength. This is a reasonable assumption, from a materials stand point, since we do not seek to alter the geometric shape of the panel/structure under investigation, but to study the effects of material properties and material orientation on the acoustic behavior of such panels.

Marburg (2002a) has provided a detailed review of the current practices in structural-acoustic optimization with focus towards passive noise control for automotive type structures. The author has focused on the following aspects: Optimization methodologies, objective function formulations, design variable choices, *speed-up* techniques for NVH simulation, results from objective functions and design modifications and numerical algorithms. From currently existing literatures, it can be concluded that there are three different optimization approaches for interior acoustic NVH optimization. They are: (1) Structure only (2) Uncoupled Fluid-Structure and (3) Fully Coupled Fluid-Structure. One of the main aims of all the above optimization formulations is to avoid re-computing the fluid domain for every iteration (except 3). In what follows, a brief description of these optimization methodologies and their subsequent applications for interior acoustic NVH modifications are reviewed. For a complete review of low frequency, structural-acoustic optimization, the reader is referred to Marburg (2002a).

Lamancusa and Eschenauer (1994) used a combination of the finite element method and the CONMIN optimizer code to optimize the radiated sound power of simple plates. In the first step, the structural normal velocities are calculated from displacements from a finite element harmonic analysis. To compute a related acoustic quantity (usually the radiation efficiency), the Rayleigh Integral (Fahy 1985; Fahy 2000) is employed. According to the Rayleigh Integral, the sound pressure at

any point r is evaluated by:

$$p(r) = \frac{j\omega\rho}{2\pi} \int_s \frac{\breve{v}(r_s)e^{-jkR}}{R} dS \qquad (2.3)$$

where, $p(r)$ is the complex sound pressure at r, r is the position vector of the observation point, r_s is the position vector of the elemental surface δS, $R = \mid r - r_s \mid$, $\breve{v}$ is the normal velocity of the elemental surface area δS, k is the acoustic wave number, ρ is the mean density of the fluid and $j = \sqrt{-1}$. In the second step the integral (Equation:2.3) is numerically evaluated by discretizing the structure into a set number of finite elements. Accordingly, the sound pressure at the centroid of each element is computed by summing the contributions of each element and then by integrating the acoustic intensity over the surface of the structure to calculate the radiated sound power. Once the radiation efficiency of the structure is determined (from the radiated sound power), it is then used as an objective function for the optimization problem. The authors carried out optimizations using the CONMIN optimization code which in turn employed the method of feasible directions. Results report around 6.7dB improvement in radiated power in certain cases. It was further concluded that using sound power as the objective function produced consistent results. It is worth pointing out that for simple plates with isotropic material properties, the radiation efficiency can be calculated from closed form solutions (Wallace 1972).

Naghshineh et al. (2002) reported significant reductions in sound power level by tailoring the material properties of a beam in a rigid baffle. A distribution of Young's modulus and density is found for the structure such that it exhibits the weak radiator velocity profile as one of its mode shapes. The *weak radiator profile* is found using the surface velocity distribution that produces a minimum radiation condition. Belegundu et al. (1994) presented a general approach to optimize struc-

tures for sound power minimization. Rayleigh Integral is used in conjunction with design sensitivity analysis and optimization is carried out using the method of feasible directions. The methodology is first validated on a flat plate and then applied on an engine cover. Results report reduction of sound power by around 30dB in certain frequency ranges.

Pierre and Koopmann (1995) used a similar method to modify the mode shapes of the structure, forcing the structure under investigation to radiate sound inefficiently (*weak radiator* modes). Common to such studies, the discretized form of Raleigh integral was used to calculate the radiated sound power. Analytical sensitivities of sound power with respect to the design variables were used for optimization. Small masses on the structure were used as design variables. Results report around 30dB improvement in sound power (reduced sound power) in certain cases. Experimental investigation using sound intensity measurements compares well with predicted optimization results, but the authors report differences of up to 7dB in some cases. The authors of the paper report that this could be due to the assumption of perfect clamped boundary conditions in the finite element model.

Wodtke and Lamancusa (1998) applied the Rayleigh Integral to compute sound power and optimize a circular, unconstrained damping layer plate. Frequency dependent loss factors and modulus values were employed in the structural harmonic response analysis[7]. Note that for sound power computation via the Rayleigh Integral, only a structural harmonic simulation is required, which results in banded, symmetric matrices. The thickness of the damping layer was used as the design variable. Different damping materials were used to study the effects of frequency dependent modulus on the radiated sound power. Reduced sound power levels have been reported by using softer damping material. The authors further demonstrate

---

[7]The direct inversion method is required to take into account frequency dependent loss factor values for multiple materials in a structural harmonic response analysis.

that starting from a uniform damping layer distribution, substantial reduction in radiated sound power can be achieved through the redistribution of the damping layers. Patil and Crocker (2000) conducted further studies using the Rayleigh integral formulation to predict radiation efficiencies and radiated sound power os simple plates. Shell thicknesses of individual elements of a rectangular 1mm flat plate were used as design variables. In certain cases, the mass of the plate was used as a state variable to search for the best design while maintaining the original mass. The ANSYS FE code was employed to carry out the mode superposition harmonic analysis under diffuse field excitation and optimization using the sub-problem optimization algorithm. A constant damping ratio of 1% has been used. Results report decrease in frequency averages sound power of 0.0013 Watt. The paper concludes by suggesting this method for designing vibrating body panels in automobiles and aircrafts.

Orzechowski and Landmann (1994) utilized the combined finite element / Rayleigh integral approach to predict far field radiated mean square pressure in the 350-1000Hz frequency range. The structure under investigation was a section of an aircraft fuselage which comprised of damping tiles (made of viscoelastic material) in between stringers. The modal strain energy approach was used to calculate damping of the constrained layer structure and further used these damping values in a mode superposition harmonic analysis. The modulus of the damping material was varied, and the effect of such variation on the acoustic behavior (here sound pressure level) is studied. The authors conclude that the sound reduction increases when the modulus of the viscoelastic material is high. The results were reported in terms of space averaged mean square velocity and sound pressure level obtained from Rayleigh formulation. The calculation and use of sound pressure level using the Rayleigh Integral is not appropriate and it has been shown that the Rayleigh formulation can lead to inaccurate results for sound pressure level estimation, but accurate enough for sound power computation (Seybert and Herrin 1999; Herrin

et al. 2003). This is the reason most authors employ the Rayleigh Integral to compute sound power from sound pressure. Comparing this method to the FE/FE or FE/BE coupled analysis, the Rayleigh Integral formulation is much efficient in terms of computational time and expense, but this method has not been used specifically for interior acoustics. In fact, Marburg (2002a), in his review paper, seems to classifies the Rayleigh Integral formulation for exterior acoustics and no application of this technique is yet found for interior acoustics.

This second type of vibro-acoustic optimization approach is considered as the *purely acoustic* approach. Often, the structural normal velocity is assumed to excite the fluid boundary. The fluid *back pressure* is neglected in this type of analysis and subsequent optimization. Engelstad et al. (1995) designed a computational tool combining FE and BE, for the structure and the fluid respectively. The structural harmonic velocities were obtained using the FE code MSC/NASTRAN. These velocities were then used as boundary conditions on the COMET acoustic BE model to predict SPL at desired locations. Sensitivities to changes in velocity boundary conditions were then obtained using the COMET BE program. The computed sensitivities were then combined with FE generated structural sensitivities, to produce complete, global structural- acoustic sensitivities. This information on sensitivities were then combined with feasible directions algorithm to search for the best design.

Crane et al. (1997) extended this concept, by analyzing a vibrating cylinder under tonal excitation (monopole model). Cylinder thicknesses were used as design variables subject to maximum weight constraints. In this work, four different acoustic objective functions (sum of acoustic pressure squared at points inside the cylinder, weight and summed pressures, sum of acoustic pressures with constraint on weight, weight of the structure with constraint on sum of acoustic pressures) have been studied. It was reported that other than setting weight of the cylinder as the objective

function and sum of acoustic pressure as a constraint, all the other three formulations yielded similar results.

Marburg et al. (1997) developed numerical models to optimize a vehicle roof based on acoustic influence coefficients. The acoustic influence coefficients have been obtained from the fluid BE formulation. Results from a harmonic analysis of a structure using the modal superposition technique were used as velocity boundary conditions in the acoustic BE model. These methods have also been extended to study properties of other specific subsystems like the roof and floor of a passenger car. The influence coefficients, computed from a boundary element analysis of the cavity acts as a transfer relation between the normal structural velocity and the sound pressure level at a particular node/field point. Since the influence coefficients obtained are nothing but the solution to the fluid's boundary value problem, they are dependent only on the fluid properties, frequency, geometry of the fluid domain, the position of the node (e.g. drivers ear location) and the boundary admittance. Due to this, the influence coefficients have to be computed only once for the cavity. For every subsequent iteration, the normal structural velocity requires a simple scalar multiplication with the influence coefficients to obtain the SPL at that location.

Marburg et al. (2002) extended the concept of influence co-efficients and applied it to a box like structure made of simple beams and panels. The panel thicknesses varied from about 1.2mm to 3mm. A sine sweep signal was used to excite the structure. The structural part of the analysis (Modal analysis and response calculation using mode superposition method) was carried out using FE code ANSYS. The influence co-efficients were then extracted from a fluid boundary value problem and these co-efficients were multiplied with the structural normal velocity. The structural normal velocity was varied by varying the shell thicknesses (design variables) and performing a harmonic analysis on the structure for each iteration. Some guidelines

for modeling welds and junctions are also highlighted. Optimization was carried out using the random iteration method available within the FE package ANSYS (ANSYS 2005). A total of about 500 computations of the objective function provided the optimized design. Additionally, masses were added close to the front panel to investigate their effects on the sound pressure level. As expected, a decrease in SPL levels were noticed when the mass was added. Results of the optimization report decrease in noise levels up to 6.2dB at certain locations. The optimized simulation model was then tested in reality to validate and confirm the improvements. Experimental results indicated a maximum decrease of 6.7dB. The reliable end frequency range for the structural model (6577 linear shell elements) was found to be around 60Hz. Above this frequency, the stiffness of the modeled structure is too high, which the authors conclude might be due to the inaccuracies in modeling edges and welded connections.

Further, Marburg and Hardtke (2002) applied a direct modification technique on shell meshes to optimize the floor panel of a sedan vehicle. Although there was no scope for shape optimization (since the floor panel is connected to a number of other structural components), the thickness of the shell meshes was optimized. 33 design variables took the form of local and global modification functions, which are described by polynomial functions. A Component Mode Synthesis (CMS) technique, by which the floor panel is represented as a detailed structural finite element model, is coupled with a super element, which represents the rest of the sedan body structure, has been used in the study. A BE model is used for the fluid. The concept of computing noise transfer functions, however, remains the same as described above. The optimized structure proved to reduce the SPL by 3.8dB in certain frequency range.

Marburg et al. (2003) investigated the effect of spare wheel on the noise trans-

fer function inside a sedan vehicle. Excitations, in the form of unit forces were applied on two locations, and response computed. Only the part of the structure needing modification (assuming this modification is very small with respect to the fluid wavelength) was modeled, while the rest of the structure was represented by a super element. Material property (by artificially increasing the Young's modulus by a factor of 106 in this case) modifications were then suggested to stiffen the wheel well portion of the structure. Around 1.2dB reduction in noise transfer functions have been observed. Experimental validation of the optimization results has also been presented.

The sequential adjoint variable method employing a reverse solution process was developed in Kim et al. (2003) for uncoupled structural-acoustic optimization problems. Basically, in this approach, the adjoint load is obtained from boundary element re-analysis, and the adjoint variable is calculated from structural dynamic re-analysis. The deployment of the adjoint variable method offers significant savings in computational time for design sensitivity calculations. As a starting point, the structural normal velocities were generated using the mode superposition method. The computed normal structural velocity is then projected to a fluid BE mesh to compute the response. Then, the reverse solution process is employed for the design sensitivity calculation using the adjoint variable method. Finally, a function call is made to a sequential quadratic programming algorithm to search for a global minimum. The structural and acoustic responses were obtained using commercially available FE packages MSC NASTRAN and LMS SYSNOISE. The authors have successfully applied this approach in Dong and Kim (2003), Kim et al. (2004) to optimize a large number of design variables. The shell thicknesses and even the material costs have been used as objective functions, subject to structural weight as the side constraint. Results report decrease in sound pressure level up to about 6dB in certain cases.

Fernholz and Robinson (1998) studied the influence of lamination angles of composite materials on the interior noise levels in an aircraft. To demonstrate the feasibility of the approach, the authors carried out investigations on two computational models: (a) Scale cylinder model and (b) Coupled FE/FE model of an eight to ten passenger twin turboprop aircraft. The primary approach used by the authors, was to compute the response quantities of a *Eulerian (u/p)* formulation using the uncoupled modal superposition approach. The authors acknowledged the fact that the method has a particular disadvantage in the formulation of modal damping. At various stages of this work (analytical-numerical sensitivity comparisons, modal truncation assessment), the direct inversion method has been chosen to compare the accuracy of other approximation methods. 500 structural modes (up to 650.4Hz) and 200 fluid modes (up to 480.94Hz.) were used to model the behavior of the aircraft fuselage and cabin interior over an excitation frequency range of 50 to 250Hz. 3 percent structural damping was specified for the elements with composite material properties. The optimization problem involved minimizing pressure levels at ten fluid grid locations, chosen to represent the approximate listening locations of the passengers in the cabin. Design variables took the form of 8 graphite epoxy face sheets of a honeycomb sandwich construction. In terms of optimization algorithm, a combination of the method of steepest descent and feasible directions was applied. Through the proposed optimization framework, the peak acoustic response in the aircraft interior cabin was reduced by 4.03 dB.

3. Finite Element Theory

The starting point for a computational investigation is a statement of the governing equations for the phenomena under study. In this chapter, the governing equations and subsequently, the FE/FE discretization for fully coupled fluid-structure interaction is presented. The advantages and drawbacks of different formulations briefly reviewed. This presentation, for the purposes of consistency and coupled formulation comparisons, follows the notation given by Desmet (1998), Desmet and Vandepitte (2005).

3.1. Fully Coupled Structural-Acoustic Discretization

For an interior, fully coupled structural-acoustic case and considering the enclosed acoustic fluid domain, D_V, the boundary surface D_a ($D_a = D_s \cup D_{ve} \cup D_p \cup D_z$) contains an elastic surface D_s as shown in Figure:[3.1]. Considering the boundary surface, four different types of boundary conditions can be applied on D_a of the bounded fluid domain D_V:

(a) Applied normal velocity on D_{ve}: $v_n = (j/\rho_0\omega).(\partial p/\partial n)$

(b) Normal velocity continuity on D_s: $v_n = (j/\rho_0\omega).(\partial p/\partial n) = j\omega u_n = \bar{v}_n$

(c) Applied pressure on D_p: $p = \bar{p}$

(d) Applied normal impedance on $D_z : p = \bar{Z}.v_n$

where, $\bar{p}$ is a prescribed pressure function, $\bar{v}$ is the prescribed normal velocity function, $\bar{Z}$ is the prescribed normal impedance function, u_n is the normal structural displacement and n denotes the normal to the boundary surface of D_a. The normal velocity continuity condition enforces the *two-way* fluid-structure coupling such that the normal fluid velocity equals the normal structural velocity at the coupling interface, often referred to as the *wetted surface.*
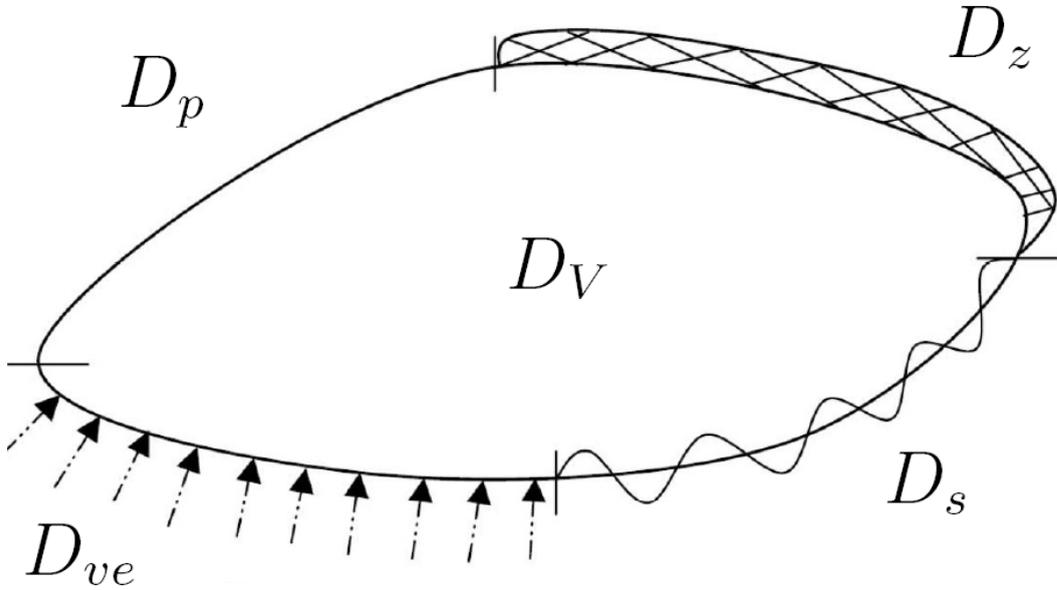
Figure 3.1.: Interior Coupled Structural-Acoustic System.

The steady-state pressure p (changes to reference pressure) at any point, r, in a homogeneous, inviscid, irrotational fluid in domain D_V is governed by the linear Helmholtz wave equation:

$$\nabla^2 p + k^2 p = 0 \tag{3.1}$$

where, ∇^2 is the Laplacian operator, p is the acoustic pressure, and k is the wave number $(k = \omega/c)$, ω is the circular frequency, and c is the speed of sound in the acoustic medium. Taking into account a purely acoustic excitation, q, located within the fluid domain D_V and by confining the acoustic field variables to their steady-state

values for a time-harmonic excitation , the wave equation can be written as:

$$\nabla^2 p(r) + k^2 p(r) = -j\rho_f \omega q(r) \tag{3.2}$$

where, r is any point in the fluid domain, ρ_f is the fluid density and $q(r)$ is a distribution of acoustically applied forces, in this case the volume velocity per unit volume in domain D_V.

An equivalent weighted residual formulation of the above Helmholtz equation (Equation:3.3) is given by:

$$\int_{D_V} \breve{p}(\nabla^2 p(r) + k^2 p(r) + j\rho_f \omega q(r)) \, dD_V = 0 \tag{3.3}$$

$$\int_{D_V} \left[\frac{\partial}{\partial x}(\breve{p}\frac{\partial}{\partial x}) + \frac{\partial}{\partial y}(\breve{p}\frac{\partial}{\partial y}) + \frac{\partial}{\partial z}(\breve{p}\frac{\partial}{\partial z}) \right] dD_V - \int_{D_V} \left(\frac{\partial \breve{p}}{\partial x}\frac{\partial p}{\partial x} + \frac{\partial \breve{p}}{\partial y}\frac{\partial p}{\partial y} + \frac{\partial \breve{p}}{\partial z}\frac{\partial p}{\partial z} \right) dD_V$$

$$+ \int_{D_V} k^2 \breve{p}p \, dD_V + \int_{D_V} j\rho_f \omega \breve{p}q \, dD_V = 0 \tag{3.4}$$

where, $\breve{p}$ is the weighting function which is uniquely defined within the defined volume D_V and on the boundary surface of the acoustic domain D_a.

According to Gauss divergence theorem, the integral of the normal component of a vector field $\overrightarrow{\phi}$, taken over a closed surface D_a, is equal to the integral of the divergence of the vector field, taken over the volume D_V, enclosed by the surface D_a. This can be written as:

$$\int_{D_V} \left(\overrightarrow{\nabla}.\overrightarrow{\phi} \right) dD_V = \int_{D_a} \left(\overrightarrow{\phi}.\overrightarrow{n} \right) dD_a \tag{3.5}$$

where, $\overrightarrow{n}$ is the unit normal vector. Using this theorem, and applying this on the first integral term Equation:[3.3] yields:

$$\int_{D_V} \left(\overrightarrow{\nabla} \breve{p} . \overrightarrow{\nabla} p \right) \, dD_V \; - \; \omega^2 \int_{D_V} \left(\frac{1}{c^2} \breve{p} p \right) \, dD_V$$

$$= \int_{D_V} (j\rho_f \omega \breve{p} q) \, dD_V \; - \; \int_{D_a} (j\rho_f \omega \breve{p} \overrightarrow{v} . \overrightarrow{n}) \, dD_a \tag{3.6}$$

Note that the transformation of the momentum equation yields the desired relationship between the steady-state fluid velocity vector field and the steady-state pressure field, given by:

$$\overrightarrow{v} = \frac{j}{\rho_f \omega} \overrightarrow{\nabla} p \tag{3.7}$$

Now, the boundary conditions for an uncoupled acoustic problem[1] are as follows:

(a) Applied normal velocity *(Neumann Boundary Condition)* on D_{ve}: $\overrightarrow{v} . \overrightarrow{n} = \bar{v}$

(b) Applied pressure *(Dirichlet Boundary Condition)* on D_p: $p = \bar{p}$

(c) Applied normal impedance *(Robin Boundary Condition)* on $D_z = \overrightarrow{v} . \overrightarrow{n} = p/\bar{Z}$

Using the finite element method, the fluid domain D_V is discretized into a number of finite elements, and a number of nodes, n_e, are defined at some particular locations (usually in the corner of each element face) in each element. On each element, the distribution of the pressure p, is approximated as a pressure expansion $\hat{p}$ in terms prescribed shape functions, N_i^{el}. Note that for the commonly used linear tetrahedral and linear hexahedral pressure fluid elements the number of element shape functions is equal to the number of nodes. Each shape function N_i^{el} is defined, such that it has a value of unity at node i of the element and that it is zero at all other element nodes. This can be verified in the model by substituting nodal coordinate values in the prescribed pressure expansion. Therefore, each pressure approximation, $\hat{p}$,

---

[1]Note that for an uncoupled problem (i.e. purely acoustic), the boundary surface $D_a = D_{ve} \cup D_p \cup D_z$.

directly represents the pressure approximation p_i at node i of the element. This is written as:

$$p(x, y, z) \approx \hat{p}(x, y, z) = \sum_{i=1}^{n_p} N_i^{el}(x, y, z) \; \hat{p}_i \tag{3.8}$$

where, n_p is the number of shape functions N_i^{el}, and $\hat{p}$ are the desired pressure approximations. In the next step, based on the local shape functions, N_i^{el}, global shape functions, N_i, are constructed. Here, the global shape function N_i is identical to the corresponding element shape function N_i^{el}, while it is zero in all other element domains. In this way, a global pressure expansion can be written as:

$$p(x, y, z) \approx \hat{p}(x, y, z) = \sum_{i=1}^{n_f} N_i(x, y, z) \; \hat{p}_i = [N] \; \hat{p}_i \tag{3.9}$$

where, $[N]$ is the vector of global shape functions and $\hat{p}_i$ is the vector of unknown nodal pressure values and n_f is the total number of nodes.

In the weighted residual formulation approach, the weighting function for weighted residual is expanded in the same as the shape function as in Equation:[3.8]. This gives:

$$\breve{p}(x, y, z) = \sum_{i=1}^{n_f} N_i(x, y, z) \; \breve{p}_i = [N] \; \breve{p}_i \tag{3.10a}$$

$$\overrightarrow{\nabla} \; \breve{p} = [B] \; \breve{p}_i \tag{3.10b}$$

since,

$$\overrightarrow{\nabla} \; \hat{p} = \left[\frac{\partial \hat{p}}{\partial x} \; \frac{\partial \hat{p}}{\partial y} \; \frac{\partial \hat{p}}{\partial z} \right]^T = [\partial] \, . [N] \; \hat{p}_i = [B] \; \hat{p}_i \tag{3.10c}$$

Substituting the Equations:[3.10a,3.10b,3.10c] into the first term of the weighted residual formulation in Equation:[3.6] yields:

$$\int_{D_V} \left(\overrightarrow{\nabla} \breve{p} . \overrightarrow{\nabla} p \right) \; dD_V = \int_{D_V} \left(\overrightarrow{\nabla} \breve{p} . \overrightarrow{\nabla} \hat{p} \right) \; dD_V = \int_{D_V} \left(([B] . \{\breve{p}_i\})^T \, . \, ([B] . \{\hat{p}_i\}) \right) \; dD_V$$
$$\tag{3.11}$$

This directly yields the *inverse mass* or the so called acoustic stiffness matrix as follows:

$$\int_{D_V} \left(\vec{\nabla} \breve{p} \; \vec{\nabla} \hat{p} \right) \; dD_V = \{\breve{p}_i\}^T \overbrace{\left(\int_{D_V} \left([B]^T \; [B] \right) \; dD_V \right)}^{[K_a]} \{\hat{p}_i\} \tag{3.12a}$$

$$= \{\breve{p}_i\}^T \; [K_a] \; \{\hat{p}_i\} \tag{3.12b}$$

Each entry of the acoustic stiffness matrix, taking into account common nodes (due to the fact that the global shape functions have only non-zero entries for elements to which the node i and node j belong) yields:

$$K_{i,j} = \int_{D_V} \left(\frac{\partial N_i}{\partial x} \frac{\partial N_j}{\partial x} + \frac{\partial N_i}{\partial y} \frac{\partial N_j}{\partial y} + \frac{\partial N_i}{\partial z} \frac{\partial N_j}{\partial z} \right) \; dD_V \tag{3.13a}$$

$$= \sum_{el=1}^{z_{i,j}} \left[\int_{D_{V_{el}}} \left(\frac{\partial N_i^{el}}{\partial x} \frac{\partial N_j^{el}}{\partial x} + \frac{\partial N_i^{el}}{\partial y} \frac{\partial N_j^{el}}{\partial y} + \frac{\partial N_i^{el}}{\partial z} \frac{\partial N_j^{el}}{\partial z} \right) \; dD_V \right] \tag{3.13b}$$

where, $z_{i,j}$ are the number of common elements to which both node i and j belongs. This means that most of the entries in the Equation:[3.13b] are zero, since each element shares nodes with common adjacent nodes. This means that, the acoustic stiffness matrix is a *sparse* matrix.

Therefore, one can observe that the global computation of the acoustic stiffness matrix, can be obtained by a two-step procedure:

(a) First, all individual element stiffness matrices are computed.

(b) Now, the non-zero entries of the global element stiffness matrix are obtained by addition of the corresponding entries[2]. This results in the non-zero entries

---

[2]This can be obtained by the addition of entries belonging to each element:

$$K_{i,j}^{el} = \int_{D_{V_{el}}} \left(\frac{\partial N_i^{el}}{\partial x} \frac{\partial N_j^{el}}{\partial x} + \frac{\partial N_i^{el}}{\partial y} \frac{\partial N_j^{el}}{\partial y} + \frac{\partial N_i^{el}}{\partial z} \frac{\partial N_j^{el}}{\partial z} \right) \; dD_V$$

where, ^{el} represents a single element domain.

in the stiffness matrix appearing in a narrow band around the matrix diagonal, yielding a sparsely populated, banded stiffness matrix. In this work, in Section:[5], sparsity plots of the resulting matrices are illustrated.

Returning to the equivalent Helmholtz weighted residual formulation, the acoustic mass matrix can be computed as follows:

$$-\omega^2 \int_{D_V} \left(\frac{1}{c^2} \breve{p}\hat{p} \right) \, dD_V = -\omega^2 \{\breve{p}_i\}^T \overbrace{\left[\int_{D_V} \left(\frac{1}{c^2} [N]^T [N] \right) dD_V \right]}^{M_a} \{\hat{p}_i\} \tag{3.14a}$$

$$= -\omega^2 \{\breve{p}_i\}^T \cdot [M_a] \cdot \{\hat{p}_i\} \tag{3.14b}$$

Similar to the acoustic stiffness matrix, the acoustic mass matrix can be computed via a two-step procedure based on the computation of individual element mass matrices given by:

$$M_{i,j} = \int_{D_V} \left(\frac{1}{c^2} [N_i] [N_j] \right) \, dD_V \tag{3.15a}$$

$$= \sum_{el=1}^{z_{i,j}} \left[\int_{D_{V_{el}}} \left(\frac{1}{c^2} [N_i^{el}] [N_j^{el}] \right) \, dD_V \right] \tag{3.15b}$$

By using the relationship given in Equation:[3.10a], for $\breve{p}$, the acoustic source term in Equation:[3.6], can be written as:

$$\int_{D_V} (j \, \rho_f \, \omega \, \breve{p} \, q) \, dD_V = \{\breve{p}_i\}^T \cdot \overbrace{\left[\int_{D_V} (j \, \rho f \, \omega \, [N]^T \, q) \, dD_V \right]}^{Q_i} \tag{3.16a}$$

$$= \{\breve{p}_i\}^T \cdot \{Q_i\} \tag{3.16b}$$

It is worth noting that for an acoustic point source of magnitude $\acute{q}_i$, located at any point in the fluid domain (other than the boundary surface), the source vector

in Equation:[3.16b] becomes:

$$\{Q_i\} = j \; \rho_f \; \omega \; \left[\int_{D_V} \left(\acute{q}_i . [N]^T . \delta \right) \; dD_V \right]$$

(3.17)

where, δ is the Dirac delta function at the specified node of acoustic excitation[3].

Returning to the boundary conditions for the uncoupled acoustic problem, the velocity and the impedance boundary condition can be incorporated by substitutions into the second term on the right hand side of Equation:[3.6]. Indeed, the boundary conditions can be written as split integral terms as follows:

$$-\int_{D_a} \left(j \; \rho_f \; \omega \; \breve{p} \; \overrightarrow{v}.\overrightarrow{n} \right) .dD_a = -\int_{D_{ve}} \left(j \; \rho_f \; \omega \; \breve{p} \; \bar{v}_n \right) \; dD_a - \int_{D_z} \left(j \; \rho_f \; \omega \; \breve{p} \; \bar{A} \; \hat{p} \right) \; dD_a$$

$$-\int_{D_p} \left(j \; \rho_f \; \omega \; \breve{p} \; \overrightarrow{v}.\overrightarrow{n} \right) \; dD_a$$

(3.18)

where, $\bar{A} = 1/\bar{Z}$. Now, the first term on the right hand side of Equation:[3.18], can be re-written as:

$$-\int_{D_{ve}} \left(j \; \rho_f \; \omega \; \breve{p} \; \bar{v}_n \right) \; dD_a = \{\breve{p}_i\}^T . \overbrace{\left[\int_{D_{ve}} \left(-j \; \rho_f \; \omega \; [N]^T \; \bar{v}_n \right) \; dD_a \right]}^{V_i}$$

(3.19a)

$$= \{\breve{p}_i\}^T . \{V_i\}$$

(3.19b)

For a single specified velocity input on node i, the velocity vector can be written as:

$$\{V_i\} = \left[\int_{D_{ve}} \left(-j \; \rho_f \; \omega \; [N_i] \; \bar{v}_n \right) \; dD_a \right]$$

(3.20)

However, it can be noted that the velocity input is only specified on the faces of an acoustic element (f_{mi}^{el}, D_{el}^f which form a part of the velocity boundary condition surface) since the boundary surface of any given element type is an explicit union of

---

[3]The finite element program ANSYS requires an input of $\rho_f.\omega.\acute{q}_i$ resulting in volume acceleration and has units of $mass/time^2$

the faces. Therefore, the global shape functions specified in Equation:[3.20], $[N_i]$ and $\{V_i\}$, has a non-zero value for nodes located on the boundary surface of an element subject to input velocity. This can be written as:

$$\{V_i\} = -j \; \rho_f \; \omega \; \sum_{e=1}^{z_{mi}} \; \sum_{f=1}^{f_{mi}^{el}} \left[\int_{D_{el}^f} \left(\left[N_i^{el} \right] . \bar{v}_n \right) \; dD_a \right] \tag{3.21}$$

where, z_{mi} are the number of elements for which the node i is on the respective element face f_{mi}^{el} on the given boundary surface of the volume D_V. This form of excitation is often specified in an uncoupled force response analysis or the so called *chained approach*, where the structural displacements from a forced response are used as excitations in an uncoupled acoustic model. For a complete description of this process, the reader is referred to Desmet (1998), Desmet and Vandepitte (2005) and Marburg (2002a).

It is now possible to observe that Equation:[3.18] also allows the formulation of the acoustic damping matrix. The second term in Equation:[3.18], can be written in terms of the shape function matrix as follows:

$$-\int_{D_z} \left(j \; \rho_f \; \omega \; \breve{p} \; \bar{A}\hat{p} \right) \; dD_a = j \; \omega \; \{\breve{p}_i\}^T . \overbrace{\left[\int_{D_z} \left(\rho_f \; \bar{A}[N]^T . [N] \right) \; dD_a \right]}^{[C_a]} . \{\hat{p}_i\} \tag{3.22a}$$

$$= j \; \omega \; \{\breve{p}_i\}^T . [C_a] . \{\hat{p}_i\} \tag{3.22b}$$

where, $[C_a]$ is the acoustic dissipation or the damping matrix. Similar to the velocity input, the admittance, or the so called *acoustic damping* value is specified on the faces of the acoustic element and therefore the elements of $[C_a]$ can be compactly

written as:

$$[C_{i,j}] = \int_{D_z} \left(\rho_f \ \bar{A} \ [N_i] \ [N_j] \right) \ dD_a \qquad (3.23a)$$

$$= \sum_{f=1}^{z_{A:i,j}} \left[\int_{D_{fz}} \left(\rho_f \ \bar{A} \ [N_i^{el}] \ [N_j^{el}] \right) \ dD_a \right] \qquad (3.23b)$$

Finally, the third term in Equation:[3.18], can be written as:

$$- \int_{D_p} \left(j \ \rho_f \ \omega \ \breve{p} \overrightarrow{v}.\overrightarrow{n} \right) \ dD_a = \{\breve{p}_i\}^T . \overbrace{\left[\int_{D_V} \left(-j \ \rho_f \ \omega \ [N]^T \overrightarrow{v}.\overrightarrow{n} \right) \ dD_a \right]}^{P_i} \qquad (3.24a)$$

$$= \{\breve{p}_i\}^T . \{P_i\} \qquad (3.24b)$$

which is non-zero only if the node i is on the boundary surface of dD_p. It is worth noting that applied pressure is a Dirichlet boundary condition and enters the global acoustic finite element by the elimination of constraint equations and shifting the mass, stiffness and damping (if present) terms to obtain a well conditioned set of equations (ANSYS 2005).

Substituting the expressions given in Equations:[3.12b, 3.14b, 3.16b, 3.19b, 3.22b, 3.24b] into the so called *weak-form* of the weighted residual formulation given by Equation:[3.6], yields:

$$\{\breve{p}_i\}^T . \left([K_a] + j \ \omega \ [C_a] - \omega^2 [M_a] \right) . \{\hat{p}_i\} = \{\breve{p}_i\}^T . \left(\{Q_i\} + \{V_i\} + \{P_i\} \right) \qquad (3.25)$$

Performing the required cancelations, a set of N_a equations with N_a unknown pressure values can be obtained as follows:

$$\left([K_a] + j \ \omega \ [C_a] - \omega^2 [M_a] \right) . \{\hat{p}_i\} = \overbrace{\left(\{Q_i\} + \{V_i\} + \{P_i\} \right)}^{\tilde{F}_a} \qquad (3.26)$$

A finite element discretization of Equation:[3.1] for the acoustic discretization, in terms of global shape functions for the nodal pressure p, results in :

$$\left(-\omega^2[M_a] + j\omega[C_a] + [K_a]\right).\{p\} = \{\tilde{F}_a\} \tag{3.27}$$

where the subscript a denotes the matrix terms belonging to the acoustic medium.

Turning then to the enclosing structure, and considering the uncoupled structural domain, the steady state displacements $\hat{u}_x, \hat{u}_y, \hat{u}_z$, along the middle surface of an elastic shell in the x, y, z co-ordinates are given by (Desmet and Vandepitte 2005; Desmet 1998):

$$\left\{ \begin{array}{c} \hat{u}_x(x,y,z) \\ \hat{u}_y(x,y,z) \\ \hat{u}_z(x,y,z) \end{array} \right\} = [N_s].\{u_i\} + [N_w].\{\bar{u}_i\} \tag{3.28}$$

where, $[N_s]$ and $[N_w]$ are the structural global shape functions related to the unconstrained and constrained degrees of freedom given by $\{u_i\}$ and $\{\bar{u}_i\}$ respectively. A forced response analysis of the uncoupled structure in the frequency domain is quite straightforward (Bathe 1995), resulting in the uncoupled finite element model for the set of unconstrained degrees of freedom as follows:

$$\left(-\omega^2[M_s] + j\omega[C_s] + [K_s]\right).\{u\} = \{\tilde{F}_s\} \tag{3.29}$$

where, $[M_s]$ is the structural mass matrix, $[C_s]$ is the structural damping matrix[4], $[K_s]$ is the structural stiffness matrix and $\{\tilde{F}_s\}$ is the structural excitation vector, which in this case consists of forces and moments applied on the part of the shell boundary, the external load f_s applied normal to the discretized shell surface and the terms resulting from the constraint degrees of freedom from the structural model.

---

[4]This later becomes a part of the global structural-acoustic damping matrix, representing damping in the structural domain.

Assuming only the external load f_s applied normal to the discretized shell surface as the prescribed load, $\{\tilde{F}_s\}$ can be written as:

$$\{\tilde{F}_s\} = \sum_{el=1}^{n_{se}} \left[\int_{D_{se}} \left([N_s]^T.\{n^{el}\}.f_s\right) \, dD_a \right] \tag{3.30}$$

where, n_{se} is the number of elements in the shell discretization D_{se} and $\{n^{el}\}$ is the unit normal vector.

Throughout this work, the structural damping matrix $[C_s]$, is written as:

$$[C_s] = \alpha[M_s] + (\beta + \beta_c)[K_s] + \sum_{j=1}^{N_m} \left[\left(\beta_j^m + \frac{2}{\omega}\beta_j^\xi\right)[K_s]_j \right] \tag{3.31}$$

where, α is the mass matrix multiplier, β is the stiffness matrix multiplier, β_c is the variable stiffness matrix multiplier, N_m are the number of materials, β_j^m stiffness matrix multiplier for material j, β_j^ξ is the constant, frequency-independent stiffness matrix coefficient for material j, $[K_s]_j$ is the part of the structural stiffness matrix belonging to the material j.

Therefore, it can be observed that an explicit participation of $[C_s]$ can be avoided by using the structural damping model, in which the damping effect is modeled by defining a complex stiffness[5]. The finite element software, ANSYS formulates constant damping via the command DMPRAT and MP, DMPR which adds imaginary terms to the stiffness matrix according to the relationship (ANSYS 2005):

$$\beta_c = \frac{2}{\Omega}\zeta \tag{3.32}$$

---

[5]It is worth reminding the reader that the complex stiffness approach does not have an equivalent time domain representation.

where, β_c is the constant multiplier applied to the structural parts of the coupled stiffness matrix, and Ω is the frequency in rad/s and ζ is the constant damping ratio. Note the constant damping is frequency independent by definition. This implies that $[K_s]$ is complex valued. In other words, the damping is included at a constitutive level in the structural domain using the complex stiffness approach (also known as *structural* or *hysteresis* damping) as follows (Meirovitch 1980; Boily and Charron 1999; Davidson 2004; ANSYS 2005):

$$\hat{K}_s = K_s(1 + j2\zeta_s) \tag{3.33}$$

where, K_s is the structural stiffness matrix and ζ_s is the constant damping ratio for the structural domain. Note that a similar approach can also be adapted for the acoustic domain, relating to the bulk modulus of the fluid, given by (Boily and Charron 1999; Davidson 2004):

$$\hat{B}_f = B_f(1 + j2\zeta_f) \tag{3.34}$$

where, B_f is the bulk modulus of the fluid and ζ_f is the constant damping ratio for the fluid domain. At this point, it is worth mentioning that, for complex arithmetic, when direct solvers like the LU decomposition (Meyer 2000) are employed to solve the set of linear equation*s*:

$$[A] \cdot \{x\} \;=\; \{b\} \tag{3.35}$$

operation counts are increased by a factor of four, and storage by a factor of two (Harari and Hughes 1992). Another approach to include acoustic damping effects in the fluid can be achieved by specifying a *boundary admittance coefficient*, defined as follows (ANSYS 2005):

$$\beta_{ac} = \frac{\rho_f \; c}{Re|\tilde{w}|} \tag{3.36}$$

where, $\tilde{w}$ is the *specific acoustic impedance* per unit area. For interior, structural-acoustic NVH applications, the values for β_{ac} ideally range from 0 to 1[6]. In this manner, the acoustic loss effects are directly modeled by inserting terms into the acoustic damping matrix, C_a, in the uncoupled acoustic Equation:[3.27].

Returning to the fully coupled boundary conditions, it is possible to observe that two additional loads must be considered for a completely coupled formulation. They are:

(1) The *additional* force loading of the acoustic pressure on the elastic shell structure along the fluid-structure coupling interface.

(b) The continuity of the normal shell velocities and the normal fluid velocities at the fluid-structure coupling interface.

The *additional* force loading of the acoustic pressure on the structure can be considered as an additional normal load in the uncoupled structural model. This modifies the uncoupled structural equation (Equation:3.29) as follows:

$$\left(-\omega^2[M_s] + j\omega[C_s] + [K_s]\right).\{u\} \ + \ [K_{fs}].\{p\} = \{F_s\} \qquad (3.37)$$

where, the *cross coupling* stiffness matrix $[K_{fs}]$ and the loading vector $\{F_s\}$ are given by:

$$[K_{fs}] = -\sum_{el=1}^{n_{se}} \left[\int_{D_{se}} \left([N_s]^T.\{n^{el}\}.[N_a]\right) \ dD_a \right] \qquad (3.38a)$$

$$\{F_s\} = \{\tilde{F}_s\} \ + \ \sum_{el=1}^{n_{se}} \left[\int_{D_{se}} \left([N_s]^T.\{n^{el}\}.[N_p]\{\bar{p}_i\}\right) \ dD_a \right] \qquad (3.38b)$$

where, $[N_s]$, $[N_a]$ are the structural and acoustic shape functions associated with the unconstrained degrees of freedom, $[N_p]$ are the shape functions associated with the

---

[6]β_{ac}=0.0 represents no sound absorption and β_{ac}= 1.0 represents full sound absorption along the acoustic boundary with or without the fluid-structure coupling interface.

specified pressure values $\{\bar{p}_i\}$ at node i belonging to the acoustic boundary surface.

The continuity of the normal shell velocities and the normal fluid velocities can be considered as an *additional* velocity input on the boundary surface of the acoustic domain. This results in a modified acoustic equation (from Equation:3.27) as follows:

$$\left(-\omega^2[M_a] + j\omega[C_a] + [K_a]\right).\{p\} \; - \; \omega^2[M_{fs}].\{u\} = \{F_a\} \tag{3.39}$$

where, the *cross coupling* mass matrix $[M_{fs}]$ and the loading vector $\{F_a\}$ are given by:

$$[M_{fs}] = \sum_{el=1}^{n_{se}} \left[\int_{D_{se}} \left(\rho_f \, [N_a]^T.\{n^{el}\}^T.[N_s]\right) \, dD_a \right] \tag{3.40a}$$

$$\{F_a\} = \{\tilde{F}_a\} \; + \; \sum_{el=1}^{n_{se}} \left[\int_{D_{se}} \rho_f \, \omega^2 \left([N_a]^T.\{n^{el}\}^T.[N_w]\{\bar{u}_i\}\right) \, dD_a \right] \tag{3.40b}$$

Note that a comparison between Equations:[3.38a,3.40a] indicates that the mass and stiffness coupling matrices are related as follows:

$$[M_{fs}] = -\rho_f[K_{fs}]^T \tag{3.41}$$

Combining the modified structural and acoustic equations given in Equations:[3.37,3.39] leads to the well known combined *Eulerian* displacement - pressure (u/p) formulation for the structural-acoustic model as a whole (Zienkiewicz and Newton 1969; Craggs 1971; Craggs 1973):

$$\left(-\omega^2 \begin{bmatrix} M_s & 0 \\ M_{fs} & M_a \end{bmatrix} + j\omega \begin{bmatrix} C_s & 0 \\ 0 & C_a \end{bmatrix} + \begin{bmatrix} K_s & K_{fs} \\ 0 & K_a \end{bmatrix}\right) \left\{ \begin{array}{c} u \\ p \end{array} \right\} = \left\{ \begin{array}{c} F_s \\ F_a \end{array} \right\} \tag{3.42}$$

Equivalently, the fully coupled model can be written in the time domain as follows:

$$
\begin{bmatrix} M_s & 0 \\ M_{fs} & M_a \end{bmatrix} \begin{Bmatrix} \ddot{u} \\ \ddot{p} \end{Bmatrix} + \begin{bmatrix} C_s & 0 \\ 0 & C_a \end{bmatrix} \begin{Bmatrix} \dot{u} \\ \dot{p} \end{Bmatrix} + \begin{bmatrix} K_s & K_{fs} \\ 0 & K_a \end{bmatrix} \begin{Bmatrix} u \\ p \end{Bmatrix} = \mathbf{F}_{MIsa} \, \mu(t)
$$

(3.43a)

and,

$$
y(t) = L^T \begin{Bmatrix} u(t) \\ p(t) \end{Bmatrix}
$$

(3.43b)

where, M_s is the structural mass matrix, M_a is the acoustic mass matrix (acoustic *compressibility* matrix); K_s is the structural stiffness matrix, K_a is the acoustic stiffness matrix (acoustic *inverse mass/mobility* matrix); M_{fs} is the coupling mass matrix, and K_{fs} is the coupling stiffness matrix; u denotes the structural displacements, p denotes the nodal pressures in the fluid domain, $\mu(t)$ is the input force vector and $\mathbf{F}_{MIsa}$ is the multiple-input structural-acoustic input distribution matrix consisting of F_s and F_a which denote the input distribution force(s) on the structural domain and constrained acoustic pressure degrees of freedom (DOF's) or purely acoustic excitation, in the form of volume acceleration belonging to the fluid domain respectively. The matrix L^T is the output scattering matrix (or the so called *field point* matrix), of dimension $N \times N$, which is a square identity matrix to restore a complete output of states, which in this case the displacements and pressures corresponding to the structural and fluid domain respectively. It is worth noting that, in the case where fewer outputs are required, the matrix L^T is permuted to form $1's$ only at required output DOF's. Thus, if an average value of the desired states are sought, the diagonal entries of the square matrix L^T would be $1/N$, where, N is the dimension of the original higher dimensional model.

Comparing Equation:[3.43a] to a one-way coupled analysis, the coupled formulation results in unsymmetric stiffness and mass matrices given by the terms K_{fs} and

M_{fs} respectively. It is worth mentioning that Equation:[3.43a] is unsymmetric due to the fact that the force loading of the fluid on the structure is proportional to the pressure, given by the term K_{fs} in the coupled stiffness matrix, and the force loading of the structure on the fluid is proportional to acceleration, given by the term M_{fs} in the coupled mass matrix (Desmet 1998; Desmet and Vandepitte 2005).

The two most common methods for modal reduction of the Eulerian *(u/p)* formulation are the standard coupled mode superposition technique and the modal synthesis via the uncoupled modes approach. Both these methods utilize eigenvectors obtained from an undamped modal analysis of the fully coupled or uncoupled systems. Suppressing any damping terms, the fluid and or the structural forcing, and any terms associated with a reactive surface, the non symmetric eigenvalue problem for the coupled formulation can be written as:

$$
\left(-\omega^2 \begin{bmatrix} M_s & 0 \\ M_{fs} & M_a \end{bmatrix} + \begin{bmatrix} K_s & K_{fs} \\ 0 & K_a \end{bmatrix} \right) \begin{Bmatrix} u \\ p \end{Bmatrix} = 0 \tag{3.44}
$$

Application of the the coupled modal superposition to Equation:[3.44] to form a reduced system must be done with some caution, since this unsymmetric system has distinct left and right eigenvector sets. At this point, it is worth reminding the reader that the undamped, fully coupled, unsymmetric eigenvalue problem is known to have real eigenvalues (Ma and Hagiwara 1991; Stammberger and Voss 2007). The modal parameters (eigenvalues and eigenvectors) of the coupled system result from the following right eigenvalue problem (Desmet 1998):

$$
\begin{bmatrix} K_s & K_{fs} \\ 0 & \rho_f^{-1} K_a \end{bmatrix} \{ \Psi_c \} = \omega_c^2 \begin{bmatrix} M_s & 0 \\ -K_{fs}^T & \rho_f^{-1} M_a \end{bmatrix} \{ \Psi_c \} \tag{3.45}
$$

where, $c = 1 \dots n_s + n_a$, $\{\Psi_c\}$ is the eigenvector and ω_c is the coupled natural frequency of that mode. However, the left eigenvectors $\{\widehat{\Psi}_c\}$ of the left eigenvalue problem differ from the right eigenvectors $\{\Psi_c\}$. Note that the left eigenvalue problem is given by:

$$\{\widehat{\Psi}_c\}^T \begin{bmatrix} K_s & K_{fs} \\ 0 & \rho_f^{-1} K_a \end{bmatrix} = \omega_c^2 \{\widehat{\Psi}_c\}^T \begin{bmatrix} M_s & 0 \\ -K_{fs}^T & \rho_f^{-1} M_a \end{bmatrix} \tag{3.46}$$

Although the right and left eigenvectors are distinct, it is possible to retrieve the left eigenvectors (from the right eigenvectors) to build the complete modal model for a reduced modal superposition analysis. Following the works by Luo and Gea (1997), Desmet (1998), Sysnoise (2004), the structural and acoustic components of the eigenvectors corresponding to the n_a acoustic DOF in each pair of associated left and right eigenvectors, are identical and that the components, which correspond with the n_s structural degrees of freedom in the left eigenvector are given by:

$$\{\widehat{\Psi}_c\} = \left\{ \begin{array}{c} \widehat{\Psi}_{sc} \\ \widehat{\Psi}_{ac} \end{array} \right\} = \left\{ \begin{array}{c} \omega_c^2 \Psi_{sc} \\ \Psi_{ac} \end{array} \right\} \tag{3.47}$$

where the subscripts *sc* and *ac* correspond to the structural and acoustic components[7] of the respective eigenvectors. Now, the *Eulerian (u/p)* formulation can be transformed to a modal model by expanding the nodal DOFs in terms of m_c coupled modes of the system as follows:

$$\left\{ \begin{array}{c} u \\ p \end{array} \right\} = \sum_{c=1}^{m_c} \Phi_c \left\{ \begin{array}{c} \Psi_{sc} \\ \Psi_{ac} \end{array} \right\} = [\Psi]\{\Phi_c\} \tag{3.48}$$

where, $[\Psi]$ is the matrix of right eigenvectors and $\{\Phi_c\}$ is the vector of modal participation factors. A projection using Equation:[3.48] on Equation:[3.42], yields the

---

[7]This result is achieved by imposing the *M-orthonormal* condition on the transformed modal co-ordinate model. A detailed derivation can be found in Luo and Gea (1997).

required modal modal as follows:

$$[-\omega^2[\widehat{M}] + j\omega[\widehat{C}] + [\widehat{K}]]\{\Phi_c\} = \{\widehat{F}\} \tag{3.49}$$

where, the modal stiffness, mass matrices are given by:

$$[\widehat{K}] = [\widehat{\Psi}]^T \begin{bmatrix} K_s & K_{fs} \\ 0 & \rho_f^{-1} K_a \end{bmatrix} [\Psi]; \quad [\widehat{M}] = [\widehat{\Psi}]^T \begin{bmatrix} M_s & 0 \\ -K_{fs}^T & \rho_f^{-1} M_a \end{bmatrix} [\Psi] \tag{3.50}$$

and the modal damping matrix and the forcing function are given by:

$$[\widehat{C}] = [\widehat{\Psi}]^T \begin{bmatrix} C_s & 0 \\ 0 & \rho_f^{-1} C_a \end{bmatrix} [\Psi]; \quad [\widehat{F}] = [\widehat{\Psi}]^T \begin{Bmatrix} F_s \\ \rho_f^{-1} F_a \end{Bmatrix} \tag{3.51}$$

The orthogonality of the left and right eigenvectors with respect to the mass matrix means that the resulting modal matrices: $[\widehat{K}], [\widehat{M}], [\widehat{C}]$ are diagonal matrices. Thus, the use of eigenvectors of modal reduction is often referred to as the *diagonalization* method. Further, by normalizations of the eigenvectors to the mass matrix, the modal mass matrix becomes the unity matrix, and the modal stiffness matrix becomes a matrix where the diagonal entries are the squared of the eigenfrequency value.

An alternate approach, adopted by ABAQUS (2005), is the symmetric formulation following the works of Morand and Ohayon (1995), Ohayon and Soize (1998). In this method, an auxiliary variable is introduced $[\tau = p/\omega^2]$, and the system of equations are augmented $[K_a\, p = \omega^2\, K_a\, \tau]$, yielding the following symmetric coupled

formulation:

$$\left(-\omega^2 \begin{bmatrix} M_s & 0 & 0 \\ 0 & 0 & 0 \\ 0 & 0 & K_a \end{bmatrix} + \begin{bmatrix} K_s & K_{fs} & K_{fs} \\ -M_{fs} & -M_a & K_a \\ 0 & K_a^T & 0 \end{bmatrix} \right) \left\{ \begin{matrix} u \\ p \\ \tau \end{matrix} \right\} = 0 \qquad (3.52)$$

This above formulation now allows for the construction of the left and right eigenvectors of Equation:[3.44] via a Lanczos based eigenvalue extraction routine. However, note that the size of the symmetric matrix is now $[N_s + (2 \times N_f)]$, where, N_s and N_f are the dimensions of the individual structural and fluid matrices. The remainder of the procedure consists of using the left and right eigenvector subspaces to compute the desired modal quantities such as participation factors and project the mass, stiffness, and damping matrices to obtain a reduced system of equations. The reader is referred to ABAQUS (2005) for a complete description of this procedure. An alternative symmetric method, requiring a diagonal acoustic mass matrix, can be found in MSC/NASTRAN (2005).

The second popular modal approach via the eigenvalue/eigenvector based procedure, is the uncoupled, symmetric modal formulations of the structural-acoustic problem (Wolf 1977; Fahy 1985; Tournour and Atalla 2000). In general, in this approach, the structural and acoustic expansions, are written individually as follows:

$$\{u\} = \sum_{m=1}^{m_s} \phi_{sm} \{\psi_{sm}\} = [\psi_{sm}]\{\phi_s\} \qquad (3.53a)$$

$$\{p\} = \sum_{m=1}^{m_a} \phi_{am} \{\psi_{am}\} = [\psi_{am}]\{\phi_a\} \qquad (3.53b)$$

where, m_s and m_s are the number of uncoupled structural and uncoupled acoustic modes of the system, $[\psi_{sm}]$, $[\psi_{am}]$ are matrices consisting the modal vectors $\{\psi_{sm}\}$, $\{\psi_{am}\}$ arising from the respective uncoupled eigenvalue problems and $\{\phi_s\}$ and $\{\phi_a\}$ are the structural and acoustic modal participation factors respectively.

The substitutions of the uncoupled expressions given by Equations:[3.53a,3.53b] in Equation:[3.42], yields the modal model, given by:

$$[-\omega^2[\breve{M}] + j\omega[\breve{C}] + [\breve{K}]]\{\gamma\} = \{\breve{F}\} \tag{3.54}$$

where, $\{\gamma\} = \left\{ \begin{array}{c} \{\phi_s\} \\ \{\phi_a\} \end{array} \right\}$, and the modal stiffness and mass matrices are given by:

$$[\breve{K}] = \begin{bmatrix} J_s & R \\ 0 & J_a \end{bmatrix} ; \quad [\breve{M}] = \begin{bmatrix} I_s & 0 \\ -\rho_f R^T & I_a \end{bmatrix} \tag{3.55}$$

where, diagonal sub matrices J_s and J_a are written as:

$$J_s = \begin{bmatrix} \omega_{s,1}^2 & & 0 \\ & \ddots & \\ 0 & & \omega_{s,m_s}^2 \end{bmatrix} ; \quad J_a = \begin{bmatrix} \omega_{a,1}^2 & & 0 \\ & \ddots & \\ 0 & & \omega_{a,m_a}^2 \end{bmatrix} \tag{3.56}$$

where, I_s, and I_a are the identity matrices of an order equal to the number of modes retained in the respective basis. The matrix R and the forcing vector on the right hand side of Equation:[3.54]is given by:

$$[R] = [\psi_{sm}]^T [K_{fs}] [\psi_{am}]; \quad \{\breve{F}\} = \begin{bmatrix} [\psi_{sm}]^T & 0 \\ 0 & [\psi_{am}]^T \end{bmatrix} \left\{ \begin{array}{c} F_s \\ F_a \end{array} \right\} \tag{3.57}$$

The modal damping matrix is given by:

$$[\breve{C}] = \begin{bmatrix} [\psi_{sm}]^T C_s [\psi_{sm}] & 0 \\ 0 & [\psi_{am}]^T C_a [\psi_{am}] \end{bmatrix} \tag{3.58}$$

Note that, in this procedure, the uncoupled structural and acoustic modal vectors are normalized with respect to their corresponding, individual mass matrices. This means that, along the fluid-structure interface or the so called wetted surface, the

continuity condition is violated. Therefore, a large number of modes should be retained in the acoustic modal base. The problem becomes more complicated, if the enclosed volume is filled with a higher density fluid. An illustration of the reduced efficiency of the uncoupled modal synthesis approaches (which treat fluid and structure as separate components) can be found in Desmet (1998), Desmet and Vandepitte (2005), Boily and Charron (1999), Tournour and Atalla (2000).

Finally, it is worth mentioning that an approach to the two uncoupled problems can also be made via the AMLS formulation[8] (ABAQUS 2005; Bennighof 1999; Bennighof et al. 2000). Apparently, the efficiency of the general AMLS method can be put down to two distinct factors (Gao et al. 2005):

(a) The method does not construct or maintain an orthonormal basis of the subspace into which the original eigenvalue problem is projected.

(b) The formulation of the method makes it suitable for an out-of-core implementation that requires a limited amount of input and output traffic.

On the other hand, it is also important to recognize that the AMLS gives approximate solutions that are less accurate than those computed utilizing standard techniques such as the shift and invert Lanczos methods. For structural-acoustic frequency response computations, existing literatures have based the AMLS formulation on the velocity potential approach (Everstine 1981; Olson and Bathe 1985), which renders the solution system of a gyroscopic type (Tournour and Atalla 2000). Therefore, the velocity potential approach is not very suitable for the eigen solution phase of modal reduction (Cipolla 2006). For a complete description of the distinct phases (reduction, reduced eigen solution and recovery) involved in the AMLS procedure via the velocity potential approach based on the formulation described by

---

[8]In the FE software ABAQUS, for structural-acoustic frequency extractions that use the AMLS eigensolver, the modes are computed using *traction-free* boundary conditions on the structural side of the coupling boundary and *rigid boundary* conditions on the acoustic side.

Everstine (1981), the reader is referred to ABAQUS (2005). Note that in comparison with the *diagonalization* method, in this approach, the damping and coupling matrices in modal coordinates are densely populated.

As discussed in the previous chapter, due to these drawbacks with other formulations, and the fact that the unsymmetric *(u/p)* formulation is a direct relationship to its experimental counterpart (unsymmetric formulation with displacement and pressure as field variables), this thesis only considers only the Eulerian *(u/p)* formulation of the structural-acoustic problem.

3.2. Solution Procedures

The frequency domain structural acoustic coupled system described in the previous section can be solved at each frequency of interest using a variety of well known direct and iterative methods. The structural acoustic system yields:

$$
\underbrace{\left(-\omega^2 \begin{bmatrix} M_s & 0 \\ M_{fs} & M_a \end{bmatrix} + j\omega \begin{bmatrix} C_s & 0 \\ 0 & C_a \end{bmatrix} + \begin{bmatrix} K_s & K_{fs} \\ 0 & K_a \end{bmatrix} \right)}_{[A_{sa}]} \overbrace{\begin{Bmatrix} u \\ p \end{Bmatrix}}^{\tilde{x}} = \overbrace{\begin{Bmatrix} F_s \\ F_a \end{Bmatrix}}^{b}
$$

$$
[A_{sa}(\omega)].\{\tilde{x}(\omega)\} = \{b\} \tag{3.59a}
$$

and the output measurement vector given by,

$$
y(\omega) = L^T \{\tilde{x}(\omega)\} \tag{3.59b}
$$

The basic idea of solving the set of equations by the direct method is to form $[A_{sa}]$ at each frequency of interest followed by a transformation of the system into an equivalent system having a triangular form. This is then followed by a forward and a backward substitution to yields the desired state vector.

---

[1]. *Initialization:* Form $[A_{sa}]$ for required frequencies

[2]. *[L, U] factors:* $[A_{sa}] = L_d U_d$ (L_d lower, U_d upper triangular matrix)

[2.1] Forward Substitution: $L_d \ \tilde{y} = b$

[2.2] Backward Substitution: $U_d \ \tilde{x} = \tilde{y}$

[3]. *Compute States:* $y(\omega) = L^T \{\tilde{x}(\omega)\}$

Figure 3.2.: Algorithm:1: Setup for solving linear systems via the direct method.

Note that due to the frequency dependence of the dynamic stiffness matrix, a new system of equations must be solved in each user specified sub step.

4. Dimension Reduction via Krylov Subspace Techniques

Today, one of the popular choices for the reduction of very high order systems arising in various fields of engineering (such as circuit simulation, CFD, MEMS) are based on the computation of Padé or Padé type approximants via Krylov subspace techniques. For example, it has been shown in various engineering applications (Grimme 1997; Malhotra and Pinsky 2000; Willcox 2000; Antoulas and Sorensen 2001; Bai 2002; Lassaux 2002; Willcox et al. 2002; Wagner and Malhotra 2003; Wagner et al. 2003; Bechtold et al. 2005a; Salimbahrami 2005) that the time required to solve reduced order models by implicitly matching some of the low frequency moments (and therefore constructing a Padé or Padé type approximant) is reduced significantly when compared to solving the original higher dimensional model, whilst maintaining the desired accuracy of the solution. These methods define an *orthogonal* or an *oblique* projection from the high dimensional space of the original model to a lower dimensional space and vice versa and thereby define the reduced order model with very good approximation properties. The goal of this chapter, is to discuss the reduction methods by applying a projection using bases of some particular Krylov subspaces. Reduction via linearization followed by moment matching and methods to directly preserve the second order structure of the underlying fully coupled structural-acoustic formulation are also discussed.

The reminder of the chapter is laid out as follows: Section:[4.1] describes the general framework for second order systems for moment matching based reduced order modeling. In Section:[4.2], the coupled system representation and moment expansions for the fully coupled structural-acoustic case is described. Section:[4.3] describes the reduced order modelling procedure for undamped and constantly damped structural-acoustic systems. The one sided and two-sided (and multi-point) Arnoldi processes form the main subject of this section. Section:[4.4] extends the reduction methodology to fully coupled, frequency dependent damping. Techniques such as linearization and structure preserving MOR via Two-sided Second order Arnoldi process are presented and discussed. Finally, in Section:[4.5], a description of error quantities and convergence properties are discussed.

4.1. General Framework for Reduction by Direct Projection

After discretization in space of a general mechanical system model, one obtains a system of ordinary differential equations of second order in matrix form as follows (Bathe 1995):

$$[\mathbf{M}]\ddot{x}(t) + [\mathbf{C}]\dot{x}(t) + [\mathbf{K}]x(t) = Fu(t) \tag{4.1}$$

$$y(t) = L^T x(t)$$

where, t is the time variable, $x(t)$ is a vector of state variables, $u(t)$ is the input force vector, and $y(t)$ the output measurement vector which is used to extract the desired state variable(s) $x(t)$. The matrices $\mathbf{M}$, $\mathbf{C}$ and $\mathbf{K} \in \Re^{N \times N}$ are the mass, damping and stiffness matrices respectively. N is the state-space dimension. $F \in \Re^{N \times p}$ and $L \in \Re^{N \times m}$ are the input distribution and output scattering matrix. The matrix $L^T \in \Re^{N \times N}$ is a square identity matrix in the case of a complete output of states

$x(t)$ being required.

Assuming harmonic excitation of the form $Fu(t) = Fe^{j\omega t} = \{F\}$, a response of $\{x\} = \{x_{max}e^{j\phi}\}e^{j\omega t}$, where ϕ is the phase shift and removing the time dependency term $e^{j\omega t}$ on both sides of Equation:[1] yields:

$$[-\omega^2[\mathbf{M}] + j\omega[\mathbf{C}] + [\mathbf{K}]]\{x\} = \{F\} \tag{4.2}$$

$$y(\omega) = L^T x(\omega)$$

where, ω denotes the circular frequency, and $\{x\}$ and $\{F\}$ denote complex vectors of state variables and inputs to the system respectively.

Ignoring damping, Equation:[4.2] becomes:

$$[-\omega^2[\mathbf{M}] + [\mathbf{K}]]\{x\} = \{F\} \tag{4.3}$$

$$y(\omega) = L^T x(\omega)$$

The principle of model order reduction is to find a lower dimensional subspace $[V] \in \Re^{N \times q}$, such that:

$$x \approx [V]z + \varepsilon \tag{4.4}$$

where, $z \in \Re^q$ and $q \ll N$, such that the steady state or time-dependent behavior of the original higher dimensional state vector can be well approximated by the projection matrix $[V]$ in relation to a considerably reduced vector of order q, with the exception of a small error, ε. Once the projection matrix V is found, the original Equation:[4.3] is projected onto it. The projection produces a reduced set of system equations, in second order form, as follows:

$$[-\omega^2[\mathbf{M}_r] + [\mathbf{K}_r]]\{z\} = \{F_r\} \tag{4.5}$$

$$y_r(\omega) = L_r^T z(\omega)$$

where the subscript r denotes the reduced matrix and:

$$[\mathbf{M}_r] = [V^T][\mathbf{M}][V]; [\mathbf{K}_r] = [V^T][\mathbf{K}][V]; \{F_r\} = V^T\{F\}; L_r^T = L^T V. \qquad (4.6)$$

It is worth noting that $y_r(\omega) \approx y(\omega)$, with the exception of the small error ε. Due to its low dimensionality, the solution to Equation:[4.5] is much faster than the original higher dimensional model. There exist several methods to choose $[V]$. In this work, we choose the projection matrix $[V]$ to be a Krylov subspace (Krylov 1931; Reid 1970; Saad 1981) in order to provide the *moment matching* property (Su and Craig 1991a). Given a matrix $[A]$ and a vector g, a Krylov subspace of order q is defined by:

$$K_q(A, g) = span(g, Ag, ...A^{q-1}g) \qquad (4.7)$$

where, g is called the starting vector and $Ag, ...A^{q-1}g$ are vectors which define the subspace. A straightforward application of the Krylov subspace methods for second order system with damping produces a reduced order system which is of first order. This is not so desirable because the properties of the matrices and the physical significance of the original system could be destroyed. However, for a second-order undamped system, an application of Krylov subspace methods, based on moment matching, generates a reduced order model (ROM) in second order form (Su and Craig 1991a).

In short, if the projection matrix $[V]$ is chosen from a Krylov subspace defined by:

$$\mathcal{K}_q(K^{-1}M, K^{-1}F) = span(K^{-1}F, K^{-1}MK^{-1}F, ...K^{-1}M^{q-1}K^{-1}F) \qquad (4.8)$$

then, the reduced order model matches q moments of the higher dimensional model. Loosely speaking, if the qth vector spanning the Krylov sequence is present in matrix

$[V]$, we match the qth moment of the system. The block vectors $K^{-1}F$ and $K^{-1}M$ can be interpreted as the static deflection due to the force distribution F, and the static deflection produced by the inertia forces associated with the deflection $K^{-1}F$, respectively (Su and Craig 1991a).

4.2. Coupled System Representation and Moments

Ignoring damping for the structure and fluid, the coupled equations become:

$$\left(\begin{bmatrix} K_s & K_{fs} \\ 0 & K_a \end{bmatrix} - \omega^2 \begin{bmatrix} M_s & 0 \\ M_{fs} & M_a \end{bmatrix} \right) \cdot \begin{Bmatrix} u \\ p \end{Bmatrix} = \begin{Bmatrix} F_s \\ F_a \end{Bmatrix} \tag{4.9}$$

$$y(\omega) = L^T \begin{Bmatrix} u \\ p \end{Bmatrix}$$

It can be seen that Equation:[4.9] is similar to Equation:[4.3] except that there is explicitly more than one output in the case of Equation:[4.3]. These are displacements of the structure and pressure levels at nodes inside the fluid. From a MOR point of view, this is not of any concern, since the projection matrix $[V]$ is related to the generalized co-ordinates, and is not directly related to nodal degrees of freedom. In this case, the approximation becomes:

$$\begin{Bmatrix} u \\ p \end{Bmatrix} = \begin{Bmatrix} x \end{Bmatrix} \approx [V] \{z\} + \varepsilon \tag{4.10}$$

This form is often denoted as the *change of state co-ordinates*.

Ignoring damping and rewriting Equation:[3.43a] using Laplace transforms, in terms of the input $U(s)$ and the output $Y(s)$ which are related by the *transfer*

function $H(s) = [Y(s)/U(s)]$, gives:

$$H(s) = L^T(s^2 M_{sa} + K_{sa})^{-1} F_{sa} \tag{4.11}$$

where, $(s^2 M_{sa} + K_{sa})$ is called the *characteristic polynomial matrix* and the block matrices K_{sa}, M_{sa} and the forcing vector F_{sa} are given by:

$$K_{sa} = \begin{bmatrix} K_s & K_{fs} \\ 0 & K_a \end{bmatrix}, \ M_{sa} = \begin{bmatrix} M_s & 0 \\ M_{fs} & M_a \end{bmatrix}, \ \text{and } F_{sa} = \begin{Bmatrix} F_s \\ F_a \end{Bmatrix}.$$

Expanding Equation:[4.11] using the Taylor series about $s = 0$ results in:

$$H(s) = L^T(s^2 K_{sa}^{-1} M_{sa} + I)^{-1} K_{sa}^{-1} F_{sa} \tag{4.12}$$

$$H(s) = \sum_{i=0}^{\infty} (-1)^i L^T (K_{sa}^{-1} M_{sa})^i K_{sa}^{-1} F_{sa} s^{2i} \tag{4.13}$$

$$H(s) = \sum_{i=0}^{\infty} m_i s^{2i} \tag{4.14}$$

where, $m_i = (-1)^i L^T (K_{sa}^{-1} M_{sa})^i K_{sa}^{-1} F_{sa}$ are called the moments of $H(s)$. Note that for a value of $s = s_0 \neq 0$, the series expansion can be written as follows (Grimme 1997; Bai 2002):

$$H(s) = \sum_{i=0}^{\infty} m_i^{s_0} (s - s_0)^{2i} \tag{4.15}$$

where, $m_i^{s_0} = (-1)^i L^T ([K_{sa} + s_0^2 M_{sa}]^{-1} M_{sa})^i ([K_{sa} + s_0^2 M_{sa}]^{-1} F_{sa})$ are called the *shifted low frequency moments* of $H(s)$.

The transfer function described in Equation:[4.11], can be represented as a rational function:

$$H(s) = \frac{N(s)}{D(s)} \tag{4.16}$$

where, the numerator and denominator, given by $N(s)$ and $D(s)$, are both polyno-

mials in s. A qth order Padé approximation[1] of the transfer function, can be defined as follows:

$$H_q(s) = \frac{b_{q-1}s^{q-1} + ... + b_1 s + b_0}{a_q s^q + a_{q-1}s^{q-1} + ... + a_1 s + 1} \quad (4.17)$$

Now, the $2q$ co-efficients in Equation:[4.17], namely the co-efficients of $N(s)$ and $D(s)$ can be selected to match the $2q$ terms of the Taylor series expansion of the transfer function in Equation:[4.14], denoted by:

$$H(s) = \sum m_i s^{2i} \; for \; i = 0 \; \to \infty \quad (4.18)$$

By matching some of these moments about $s = 0$, the reduced order model can be constructed, as it directly relates the input to the output of the system. One approach to construct the qth order Padé approximation, is to explicitly compute the moments m_i, using:

$$m_i = (-1)^i L^T (K_{sa}^{-1} M_{sa})^i K_{sa}^{-1} F_{sa} \quad (4.19)$$

and then generate the co-efficients of the polynomials in equation Equation:[4.17]. However, computing Padé approximants using explicit moment computations, is done using the Asymptotic Waveform Evaluation (AWE), and suffers from fundamental numerical limitations and is numerically unstable (Gallivan et al. 1994; Feldmann and Freund 1995). Each run of AWE generates only a small number of accurate poles and zeros. The main reason for the instability in AWE, is the formulation of explicit computation of moments given in Equation:[4.19].

By setting $[A] = K_{sa}^{-1} M_{sa}$, $g = K_{sa}^{-1} F_{sa}$ and $\bar{l} = K_{sa}^{-T} L$ the computation of mo-

---

[1]A Padé approximant, so called, is that rational function (of a specified order) whose power series expansion agrees with a given power series to the highest possible order (Press et al. 2002).

ments can be achieved by generating two sets of vectors (Freund 2001):

$$g, Ag, (A)^2 g, ..., (A)^{q-1} g \tag{4.20}$$

and,

$$\bar{l}, (A)^T \bar{l}, ((A)^T)^2 \bar{l}, ..., ((A)^T)^{q-1} \bar{l} \tag{4.21}$$

and computing the inner products to form the moments of the transfer function:

$$m_{2i} = ((A^T)^i \bar{l})^T \cdot (A^i g) \quad , \quad m_{2i+1} = ((A^T)^i \bar{l})^T \cdot (A^{i+1} g) \tag{4.22}$$

for $i = 0, \dots, q-1$. Starting from this moment information[2], the $2q$ co-efficients of the numerator and denominator polynomials described in Equation:[4.17] can now be computed by solving a system of linear equations with the moment information stored in a Hankel matrix. The main problem with AWE (explicit moment generation) is that the vectors described by Equation:[4.20] and Equation:[4.21] quickly converge to the right and left eigenvector corresponding to the dominant eigenvalue of A, and so contain only part of the spectrum of A, which is often not sufficient to approximate the original transfer function. The reader is referred to Pillage et al. (1989), Ratzlaff et al. (1991), Chiprout and Nakhla (1994), Cockrell and Beck (1996) for applications of AWE in other fields of engineering.

It can be also be seen however, that the vectors spanning the space in Equation:[4.20] and Equation:[4.21] are none other than the qth right and left Krylov subspaces given by:

$$\mathcal{K}_q^r(A, g) = span(g, Ag, ...A^{q-1} g) \tag{4.23}$$

---

[2]At this point, it is worth mentioning that the required moment information can also be generated by simply computing one set of $2q$ vectors: $g, Ag, (A)^2 g, ..., (A)^{2q-1} g$, the $2q$ and then by computing the inner products to form the moments: $m_i = L^T \cdot (A^i g)$ for $i = 0, \dots, 2q-1$.

which is called the qth right Krylov subspace induced by A and g, and,

$$\mathcal{K}_q^l(A^T, \bar{l}) = span(\bar{l}, A^T\bar{l}, ..., (A^T)^{q-1}\bar{l}) \tag{4.24}$$

which is called the qth left Krylov subspace induced by the matrix A and vector $\bar{l}$. The inner products of these two expressions lead to the same moments of the transfer function as given in Equation:[4.22]. However, the vectors belonging to the Krylov subspace quickly become linearly dependent and there is a rapid accumulation of rounding errors, and hence these are not suitable in general as basis vectors. Instead, a more suitable and stable set of basis vectors can be constructed using vectors v and w, given by:

$$v_1, v_2, v_3, ..., v_q \quad and \quad w_1, w_2, w_3, ..., w_q \tag{4.25}$$

where, v and w are column vectors stored in matrices $[V]$ and $[W]$, such that:

$$\mathcal{K}_q^r(A, g) = span(v_1, v_2, v_3, ..., v_q) \tag{4.26a}$$

and,

$$\mathcal{K}_q^l(A^T, \bar{l}) = span(w_1, w_2, w_3, ..., w_q) \tag{4.26b}$$

Now, the direct computation of moments via Equation:[4.20), (4.21] can be avoided, and the so-called *modified moments* can be computed as (Freund 2001):

$$w_i^T v_i \ and \ w_i^T A v_i, \ i = 1, 2, .., q. \tag{4.27}$$

It is worth mentioning that, the *modified moments* contain the same information as the moments in Equation:[4.22], and in fact for each $i = 1, 2, .., 2q - 1$, the ith moment can be expressed as a suitable linear combination of equation Equation:[4.27]. Therefore, for the coupled structural-acoustic system, if the projection matrix $[V]$ is

chosen from a Krylov subspace defined by:

$$\mathcal{K}_q(\mathbf{A}_{sa}, \mathbf{g}_{sa}) = span(\mathbf{g}_{sa}, \mathbf{A}_{sa}\mathbf{g}_{sa}, ...\mathbf{A}_{sa}^{q-1}\mathbf{g}_{sa}) \tag{4.28}$$

$$\mathcal{K}_q(K_{sa}^{-1}M_{sa}, K_{sa}^{-1}F_{sa}) = span(K_{sa}^{-1}F_{sa}, K_{sa}^{-1}M_{sa}K_{sa}^{-1}F_{sa}, ...K_{sa}^{-1}M_{sa}^{q-1}K_{sa}^{-1}F_{sa})$$
$$\tag{4.29}$$

then, the projected reduced order model would match q moments of the higher dimensional, fully coupled, undamped structural-acoustic system.

It turns out that the two main approaches to generate vectors belonging to the Krylov subspace are the Lanczos (Lanczos 1950) and the Arnoldi process (Arnoldi 1951). Mathematically speaking, both Lanczos and AWE are equivalent, but their performance differ vastly when implemented on a computer. The classical Lanczos process generates two sets of basis vectors which span the right and left Krylov subspaces defined in Equation:[4.26a,4.26b] and are bi-orthogonal to match $2q$ moments of the system matrices. However, the Lanczos process terminates prematurely due to $w_i^T v_i \approx 0$. To remedy this problem, a *look-ahead* Lanczos algorithm was proposed (Freund and Gutknecht 1994). Another disadvantage of the Lanczos process is that, although the original higher dimensional model is stable and passive, there is no guarantee that the reduced order model generated by projecting the two sets of bi-orthogonal vectors on the original system would generate a stable and passive reduced order model. i.e The stability and passivity of the higher dimensional model is not preserved. A partial Padé via Lanczos has been introduced to counter this problem (Bai et al. 1997). Additionally, to match more than one specific output state, a multiple band version of the Lanczos process is required. For this very reason, in this thesis, we consider the use of the Arnoldi iteration to generate vectors containing the low frequency moments of the fully coupled fluid-structure system matrices.

4.3. Undamped and Constantly Damped Structural-Acoustic Systems

Second order fully coupled structural-acoustic systems, where damping is not included in the analysis are called undamped systems. Systems with constant damping (irrespective of frequency) are called constantly damped systems. The goal of this section is to describe the methodology to reduce such higher dimensional *undamped* and *constantly damped* systems. It is explained how to compute a reduced order model from the higher dimensional model with superior solution accuracy and computational efficiency properties.

4.3.1. The One-Sided Arnoldi Algorithm (OSA)

The two key properties essential for generating vectors belonging to the Krylov subspace imply that (Antoulas 2003):

(a) The low frequency moments of the coupled system are matched without explicit computation of moments; and

(b) The procedure is implemented iteratively.

This ensures numerical stability while building up the Krylov subspace, and that an orthogonal basis is constructed for the given subspace $\mathcal{K}_q(A, g)$. This is done using the Arnoldi algorithm. Given a Krylov subspace , the Arnoldi algorithm finds a set of vectors with norm one, that are orthogonal to each other, given by:

$$V^T V = I \tag{4.30}$$

where, the columns of $[V]$ are the basis for the given Krylov sequence and $I \in \Re^{q \times q}$ is the identity matrix . Additionally,

$$V^T \ A \ V = H_q \tag{4.31}$$

Where $[H_q]$ is a block upper Hessenberg matrix, and is an orthogonal projection of $[A]$ onto the Krylov subspace defined in Equation:[4.23]. Figure:[4.1] gives the simplified single- input, single-output (SISO) version of the implemented Arnoldi algorithm. In comparison with the Lanczos process, it can be observed that the Arnoldi process produces only one sequence of vectors, which span the right Krylov subspace in Equation:[4.23], and are orthonormal, as given by:

$$v_i^T v_j = \left\{ \begin{array}{l} 1 \ if \ i = j \\ 0 \ if \ i \neq j \end{array} \right\} \tag{4.32}$$

for all $1 \leq i$ *and* $j \leq q$. For the fully-coupled structural-acoustic problem described, we have:

$$[A] = K_{sa}^{-1} M_{sa}, \ \{g\} = K_{sa}^{-1} F_{sa} \tag{4.33}$$

$$V^T K_{sa}^{-1} M_{sa} V = H_q \ and \ V^T V = I \tag{4.34}$$

$$Colspan(V) = \mathcal{K}_q(K_{sa}^{-1} M_{sa}, \ K_{sa}^{-1} F_{sa}) \tag{4.35}$$

The initial dimension of q is chosen such that the input-output behavior of the coupled system is well represented. The discussion of the block version of the algorithm, which is used to generate the Arnoldi vectors for a coupled structural-acoustic system with multiple-inputs and multiple-outputs (MIMO) is quite involved, and the reader is referred to (Freund 2000) for a detailed discussion. In short, the multiple block version of the Arnoldi algorithm generates orthogonal vectors belonging to the

block Krylov subspace[3]:

$$\mathcal{K}_q(A_1, g_1, g_2) = span(g_1, g_2, A_1 g_1, A_1 g_2 ... A^{q-1} g_1, A^{q-1} g_2) \tag{4.36}$$

Returning to the SISO version of the algorithm as given in Figure:[4.1], it can be seen that in each step, one vector orthogonal to all previously generated vectors is constructed and normalized. The process is numerically very similar to the modified Gram-Schmidt orthogonalization with the following properties (Antoulas 2003; Simoncini and Szyld 2007):

$$AV_q = V_q H_q + R_q \tag{4.37}$$

and,

$$A^i g = \|g\| \; V_q \; H_q^i \; e_1 \quad for \; i = 0, 1, ...q - 1 \tag{4.38}$$

where R_q is called the *residue*, generated by the Arnoldi process, and is given by:

$$R_q = h_{q+1,q} v_{q+1} e_q^T \tag{4.39}$$

where, $h_{q+1,q}$ are the co-efficients of the upper Hessenberg matrix generated at each iteration of the Arnoldi process and e_1 and e_q are the first and the qth standard unit vectors in $\Re^N$. The moments can now be computed as (Freund 2001; Freund 2000):

$$m_i = L^T A^i g \; = \; L^T (K_{sa}^{-1} M_{sa})^i (K_{sa}^{-1} F_{sa}) \tag{4.40}$$

Substituting Equation:[4.38] in Equation:[4.40], we have:

$$m_i = L^T A^i g \; = L^T \|g\| V_q H_q^i e_1 \; = \; L^T V_q H_q^i \|g\| e_1 \tag{4.41}$$

---

[3]A block Krylov subspace with say m starting vectors can be considered as a union of m Krylov subspaces defined for each starting vector (Salimbahrami 2005).

where,

$$L^T V_q = L_{rsa}^T, \ H_q^i = A_{rsa}^i \ and \ \|g\|e_1 = g_{rsa} \tag{4.42}$$

where, the subscript rsa denotes the reduced structural-acoustic matrix. In this case, since only q moments are matched, the approximation is said to be a Padé-type approximant. In some sense, the Arnoldi process trades some optimality to match only q moments of the coupled system matrices, but in turn generates a guaranteed stable and passive reduced order model. i.e. the stability and passivity of the original coupled higher dimensional model is preserved. Once the projection matrix $[V]$ is found, $[H_q]$ is discarded and a Galerkin projection $\prod = [V][V]^T$ on Equation:[4.9] generates a reduced order model in second order form, given by:

$$[-\omega^2 [M_{rsa}] + [K_{rsa}]]\{z\} = \{F_{rsa}\} \tag{4.43a}$$

$$y_{rsa}(\omega) = L_{rsa}^T z(\omega) \tag{4.43b}$$

where,

$$[M_{rsa}] = V^T M_{sa} V; \ [K_{rsa}] = V^T K_{sa} V; \ \{F_{rsa}\} = V^T \{F_{sa}\}; \ L_{rsa}^T = L^T V. \tag{4.44}$$

It is now possible to define a reduced order transfer function, as follows:

$$H_{rsa}(s) = L_{rsa}^T (s^2 M_{rsa} + K_{rsa})^{-1} F_{rsa} \tag{4.45}$$

and the associated moments, given by:

$$m_i^{rsa} = (-1)^i L_{rsa}^T A_{rsa}^i g_{rsa} \tag{4.46}$$

where, m_i^{rsa} are the moments of the reduced order model, and the space spanned by vectors $A_{rsa}^i g_{rsa}$ are the Krylov subspace vectors. It is worth mentioning that, due to the iterative property of the algorithm, it is also possible to generate a reduced order model of lower dimension than initially specified, by just discarding columns in matrix $[V]$ and subsequently the rows and columns of the reduced matrices. This property is later used to determine the number of vectors needed to accurately represent the system.

Input: Read coupled system matrices $[K_{sa}]$, $[M_{sa}]$, $\{F_{sa}\}$, L^T, q (Number of vectors) and expansion point s, in this case $s = (\omega_e + \omega_b)/2$.

Output: q Arnoldi vectors belonging to the Krylov Subspace $\mathcal{K}_q^r(A, g)$.

[0]. Set $v_1^* = g$

[1]. $^*for \; i = 1 \rightarrow q \quad ^*do :$

    [1.1] Deflation Check: $h_{i,i-1} = \|v_i^*\|$

        *if, $h_{i,i-1} = 0$, the induced subspace is exhausted.

    [1.2] Normalization: $v_i = v_i^*/h_{i,i-1}$

    [1.3] Generation of next vector: $v_{i+1}^* = Av_i$

    [1.4] Orthogonalization with old vectors $^*for \; j = 1 \rightarrow i \quad ^*do :$

        [1.4.1] $h_{j,i} = v_j^T v_{i+1}^*$

        [1.4.2] $v_{i+1}^* = v_{i+1}^* - h_{j,i} v_j$

[2]. Discard resulting H_q and project $[M_{sa}]$, $[K_{sa}]$, F_{sa}, L^T onto $[V]$ to obtain reduced system matrices $[M_{rsa}]$, $[K_{rsa}]$, $\{F_{rsa}\}$, L_{rsa}^T

Figure 4.1.: Algorithm:1: Complete set-up for SISO/SICO Arnoldi (OSA) process (Bai 2002; Freund 2000)

4.3.2. The Two-Sided Arnoldi Algorithm (TSA)

The use of Arnoldi variants in reduced order modeling serve two distinct purposes:

(a) Increase the accuracy of the approximation by matching more moments; and/or

(b) Generate candidate vectors containing minimum number of moments matched thereby further reducing computational time.

In terms of coupled structural-acoustic modeling, it is well known that the accuracy of the secondary state variables (e.g. fluid velocity or cavity potential energy), depends on the accuracy of the primary state variables e.g. fluid pressure (Desmet and Vandepitte 2005). Therefore, numerical algorithms, which preserve a higher degree of accuracy of the primary variables, whilst maintaining reasonable computational time would give NVH engineers more choices depending on the application. As a result, a two-sided version of the Arnoldi algorithm , a multi-point Arnoldi variant and its application to fully coupled structural acoustic modeling is discussed in this section.

Since the *moments of the transfer function* forms the fundamental basis for order reduction, an increase in the number of moments matched would also increase the accuracy of the solution state variables. The accuracy of the one sided Arnoldi approximation discussed in the previous section can be further improved by matching more than q moments of the higher dimensional coupled system. This process can be achieved by computing two different sets of vectors, stored in column matrices $[V]$ and $[W]$ and a subsequent *Petrov-Galerkin* projection on the higher dimensional system leads to a reduced order model matching $2q$ moments of the coupled system, there by guaranteeing a higher degree of accuracy compared to the one-sided methods. This process can also be seen as running two separate Arnoldi processes, one for the controllability subspace, and the other for the observability subspace and

then constructing an oblique projection from the two Arnoldi generated orthogonal basis sets(Antoulas and Sorensen 2001).

Returning to the one sided Arnoldi algorithm, and considering the fact that the columns of $[V]$ form the basis of the input Krylov subspace $\mathcal{K}_q^r(A, g)$, where, $A = [K_{sa}]^{-1}[M_{sa}]$ and $g = [K_{sa}]^{-1}\{F_{sa}\}$, then q moments of the higher dimensional system and the ROM match, and it can be shown that:

$$[V]\ ([K_{rsa}]^{-1}[M_{rsa}])^{i+1}\ [K_{rsa}]^{-1}\{F_{rsa}\} = ([K_{sa}]^{-1}[M_{sa}])^{i+1}\ [K_{sa}]^{-1}\{F_{sa}\} \tag{4.47}$$

for $i = 1, ...q$. Similarly, considering the fact that only the columns of $[W]$ form the basis of the output Krylov subspace $\mathcal{K}_q^l(A^T, \bar{l})$, where, $A^T = [K_{sa}]^{-T}[M_{sa}]^T$ and $\bar{l} = [K_{sa}]^{-T}\{L_{sa}\}$, then q moments of the higher dimensional system and the ROM match, and it can be shown that (Salimbahrami 2005):

$$[L_{rsa}]^T([K_{rsa}]^{-1}[M_{rsa}])^{i+1}[K_{rsa}]^{-1}[W]^T = [L_{sa}]^T([K_{sa}]^{-1}[M_{sa}])^{i+1}[K_{sa}]^{-1} \tag{4.48}$$

for $i = 1, ...q$. Indeed, it can be seen that multiplying Equation:[4.48] by $\{F_{sa}\}$ completes the proof for moment matching based only using the output Krylov subspace. Common to these one sided methods, often, a second projection matrix is not chosen, thus letting $[V] = [W]$, which, under certain conditions preserve the stability and passivity of the ROM.

Now, the columns of $[V]$ and $[W]$ can be computed to form the basis of input Krylov subspace $\mathcal{K}_q^r(A, g)$, where, $A = [K_{sa}]^{-1}[M_{sa}]$ and $g = [K_{sa}]^{-1}[F_{sa}]$ and the output Krylov subspace $\mathcal{K}_q^l(A^T, \bar{l})$, where, $A^T = [K_{sa}]^{-T}[M_{sa}]^T$ and $\bar{l} = [K_{sa}]^{-T}\{L\}$, such that each set of basis vectors thus computed satisfy:

$$V^T\ V = I\ \ and\ \ W^T\ W = I \tag{4.49}$$

a *Petrov-Galerkin* $\prod = [V][W]^T$ projection (Antoulas 2003) leads to the following ROM, in second order form:

$$[-\omega^2[M_{rsa}] + [K_{rsa}]]\{z\} = \{F_{rsa}\} \qquad (4.50\text{a})$$

$$y_{rsa}(\omega) = L_{rsa}^T z(\omega) \qquad (4.50\text{b})$$

where,

$$[M_{rsa}] = [W^T][M_{sa}][V]; [K_{rsa}] = [W^T][K_{sa}][V]; \{F_{rsa}\} = [W^T]\{F_{sa}\}; L_{rsa}^T = [L^T][V].$$
$$(4.51)$$

Subsequently, using Equations:[4.47,4.48], for $i = 0, 1, \ldots 2q-1$, the reduced order system moments match the higher dimensional system moments as follows (Grimme 1997; Salimbahrami 2005):

$$m_{2i}^{rsa} = m_{2i} = \left(\ ([K_{sa}^{-1}M_{sa}]^T)^i K_{sa}^{-1}L \ \right)^T . \left(\ ([K_{sa}^{-1}M_{sa}]^T)^i K_{sa}^{-1}F_{sa} \ \right) \qquad (4.52\text{a})$$

$$m_{2i+1}^{rsa} = m_{2i+1} = \left(\ ([K_{sa}^{-1}M_{sa}]^T)^i K_{sa}^{-1}L \ \right)^T . \left(\ ([K_{sa}^{-1}M_{sa}]^T)^{i+1} K_{sa}^{-1}F_{sa} \ \right) \qquad (4.52\text{b})$$

where, m_{2i}^{rsa} and m_{2i+1}^{rsa} are the reduced order structural-acoustic coupled system moments.

The result in Equations:[4.52a,4.52b] can be generalized to match moments around any expansion point $s_1 \neq 0$, such that the moments of the reduced order structural-acoustic transfer function matches the moments of the higher dimensional structural acoustic system as follows (Grimme 1997; Freund 2001; Salimbahrami 2005)::

$$m_{2i} = m_{2i}^{rsa} = \left(\ ([(K_{rsa} + s_1^2 M_{rsa})^{-1} M_{rsa}]^T)^i (K_{rsa} + s_1^2 M_{rsa})^{-1} L_{rsa} \ \right)^T$$

$$. \left(\ ([(K_{rsa} + s_1^2 M_{rsa})^{-1} M_{rsa}]^T)^i (K_{rsa} + s_1^2 M_{rsa})^{-1} F_{rsa} \ \right) \quad (4.53)$$

$$m_{2i+1} = m_{2i+1}^{rsa} = (\ ([(K_{rsa} + s_1^2 M_{rsa})^{-1} M_{rsa}]^T)^i (K_{rsa} + s_1^2 M_{rsa})^{-1} L_{rsa}\ )^T$$

$$.\ (\ ([(K_{rsa} + s_1^2 M_{rsa})^{-1} M_{rsa}]^T)^{i+1} (K_{rsa} + s_1^2 M_{rsa})^{-1} F_{rsa}\ ) \quad (4.54)$$

where s_1 is any user specified expansion point around which the low frequency structural-acoustic moments are desired to me matched. This means that a reduced order model could also be obtained which matches moments across different points in the frequency domain simultaneously by constructing projecting vectors belonging to subspaces:

$$\mathcal{K}_q^{s_1}([K_{sa} + s_1^2 M_{sa}]^{-1}[M_{sa}], [K_{sa} + s_1^2 M_{sa}]^{-1}\{F_{sa}\}) \quad (4.55a)$$

and,

$$\mathcal{K}_q^{s_2}([K_{sa} + s_2^2 M_{sa}]^{-T}[M_{sa}]^T, [K_{sa} + s_2^2 M_{sa}]^{-T}\{L\}) \quad (4.55b)$$

for $s_1 \neq s_2$. Now, all the unknown $2q$ co-efficients in Equations:[4.16,4.17] are now found, and the approximation is said to be a *complete* Padé approximant. Note that beyond a set of single expansion points, $J_1 = s_1, s_2$, with $s_1 = s_2$, it is also possible to generate a structural-acoustic ROM with a multiple set of n expansion points $J_1, J_2 \ldots J_n$ such that the frequency response and its derivatives are well approximated by matching the coupled system moments.

Once again, to avoid numerical problems associated with the Lanczos process, in this work, the Arnoldi algorithm is applied twice to compute projection matrices $[V]$ and $[W]$. A complete two-sided Arnoldi SISO set up is shown in Figure:[4.2]. It is worth noting that the *field-point*/output scattering matrix $[L]^T$ explicitly participates in the order reduction process (in the form of $\mathcal{K}_q^l(A^T, \bar{l})$ to yield $[W]$), and therefore the approximation is restricted to SISO, and does not automatically result in a SICO approximation. The reader is reffered to Salimbahrami et al. (2005), Salimbahrami (2005) for a discussion of the MIMO version of the two sided Arnoldi

process. Shortly speaking, in the MIMO case, $\frac{q}{m}$ moments around s_1 and $\frac{q}{p}$ moments around s_2 match, where m and p are the number of inputs and the number of outputs in the system respectively.

From the one-sided and two-sided Arnoldi processes shown in Figures:[4.1,4.2], it can be seen that the coupled system matrices $K_{sa}^{-1}M_{sa}$, $K_{sa}^{-1}F_{sa}$ are very important. One of the main aims of performing model order reduction via implicit moment matching is to increase computational efficiency, whilst matching the input to output behavior for the coupled system. However, explicit computation of K_{sa}^{-1} and then using it in the Arnoldi process would lead to a loss of computational efficiency. The remedy to this problem, is to compute the LU (lower, upper triangular) factorization of K_{sa} once, and use this in every step of the iteration, thereby solving only triangular linear equations in each iteration of the Arnoldi process.

More precisely speaking, for $s = 0$:

$$K_{sa} = L_d \, U_d \qquad (4.56)$$

and then, for each iteration of the Arnoldi process, which are given by:

$$g_1 = K_{sa}^{-1} \, F_{sa} \ and \ g_{i+1} = Ag_i = K_{sa}^{-1}M_{sa}g_i \qquad (4.57)$$

a back substitution is performed for solving Equation:[4.57] by using the following three steps:

(a) First, M_{sa} is multiplied by g_i to give $a = M_{sa} \, g_i$.

(b) The linear equation $L_d \, b = a$ is forward solved. This is fast, since L is lower triangular. This means $b = L_d^{-1}a$.

(c) The linear equations $U_d \, c = b$ is solved. This is also fast, since U is upper

---

[1]. ***Initialization:*** Read coupled structural-acoustic matrices, select appropriate Input and Output Krylov Subspaces: $\mathcal{K}_q^r(A, g)$, $\mathcal{K}_q^l(A^T, L)$ and expansion points Table:5.3.

[2]. ***Generate Projection Matrices:*** Use Arnoldi Algorithm (Figure:4.1) *for*:

   2.1 $\mathcal{K}_q^r(A, g)$: Apply $A = [K_{sa}]^{-1}[M_{sa}]$ and $g = [K_{sa}]^{-1}\{F_{sa}\}$ and compute $[V]$

   2.2 $\mathcal{K}_q^l(A^T, \bar{l})$: Apply $A^T = [K_{sa}]^{-T}[M_{sa}]^T$ and $\bar{l} = [K_{sa}]^{-T}\{L\}$ and compute $[W]$

[3]. ***Apply Projection:*** Use column matrices $[V]$ and $[W]$ and apply the *Galerkin-Petrov* projection: $\prod = [V]\,[W]^T$ to obtain *structure preserving,* ROM matrices $[M_{rsa}]$, $[K_{rsa}]$, $\{F_{rsa}\}$, L_{rsa}^T for reduced harmonic or transient simulation.

Figure 4.2.: Algorithm:3: Complete set-up for SISO Two Sided Arnoldi (TSA) Process (Grimme 1997; Salimbahrami et al. 2005).

triangular. Therefore, $c = L_d^{-1}\,U_d^{-1}\,M_{sa}\,g_i = g_{i+1}$, which is the product that is required.

Obviously, for an expansion point where $s, s_1, s_2 \ldots \neq 0$, an inverse of $[K_{sa} - \omega^2 M_{sa}]$ is sought, where $\omega = (2 \times \pi \times f_{exp})$ and f_{exp} is the user defined low frequency value around which the desired moments are to be matched. Therefore, an LU factorization of $[K_{sa} - \omega^2 M_{sa}]$ is computed and using these LU factors in the above steps (*a*) *to* (*c*), leads to triangular linear equations being solved at each iteration of the Arnoldi process. Note that a similar approach can be adopted to the compute output Krylov subspace $K_{sa}^{-T}M_{sa}^T$ and $K_{sa}^{-T}L$ for the two-sided Arnoldi variant. Throughout this thesis, it is assumed that the matrices are real or complex and that the matrix pencil $[-\omega^2 M_{sa} + K_{sa}]$ is invertible.

4.4. Explicit Participation of Damping Matrix and Linearly Damped Structural-Acoustic Systems

Second order fully coupled structural-acoustic systems, where structural damping is included in the the form of frequency dependent (linearly varying) are called *linearly damped* systems. Critical in the process of NVH refinement for trimmed structures, acoustic damping is also often introduced at boundaries of the structural acoustic model in order to represent noise absorbing materials (Marburg 2002a). In such models, the explicit participation of the damping matrix $[C_{sa}]$ cannot be avoided, and thus has to be taken into account in the solution formulations. In this chapter, by introducing the second order *damped* model and thus the second-order input and output Krylov subspaces, the desired moment matching properties are described. On this course, transformation of second-order systems with an explicit participation of the damping matrix $[C_{sa}]$ to an equivalent first order form and the resulting state space moment matching framework is also outlined. That is, it is described how to compute a moment matching, reduced order model (from the underlying higher dimensional model) by using two different dimension reduction formulations: State space linearization followed by moment matching technique and the Second order Krylov subspace based *structure-preserving* dimension reduction technique.

4.4.1. Two-Sided Second Order Arnoldi Algorithm (TS-SOAR)

For structural-acoustic system matrices involving an explicit participation of the damping matrix $[C_{sa}]$, a reduced order model could be obtained by transforming the second order system into an equivalent state-space form and applying known implicit moment matching techniques via the Arnoldi process. However, such transformed systems, although maintain the desired accuracy, suffer from two fundamental drawbacks:

(a) The cast coupled structural-acoustic, state-space system is twice in dimension (2N) compared with the standard second order system (N). Thus, an initial factorization (in this case, LU decomposition) of a system matrix of twice the initial dimension is required.

(b) The projected reduced order system thus obtained is in state-space form. Thus, the second order structure and the physical significance of the original problem is initially lost in the reduced order system.

The above disadvantages can be countered using two different approaches:

(a) Back convert the reduced order structural-acoustic state space model to second order model using transformation techniques (Salimbahrami 2005).

(b) Use of one-sided or the two-sided Second Order Arnoldi procedure (Bai and Su 2005b; Bai and Su 2005a; Salimbahrami 2005) to generate orthogonal basis for the given second order Krylov Subspace including the damping matrix.

The first approach, namely converting the reduced order structural-acoustic state space model to second order model does not essentially alleviate the factorization of the system matrix of dimension 2N, but can produce a ROM of second order model thus restoring the physical significance of the problem. It is worth noting that this back-conversion procedure can reduce computational efficiency. Additionally, if the reduced order state space model is not stable and passive, the second order model generated using this state-space system will not be stable or passive. Apparently, for engineering design and control of such a systems, it is highly desirable to have a reduced-order model preserving the second-order form and the essential properties, such as stability and passivity (Bai et al. 2005). On the other hand, the SOAR procedure, which was initially developed for solving quadratic eigen-value problems, can also be effectively used for dimension reduction of second order dynamical systems arising in different fields of engineering (Bai et al. 2005; Lampe and Voss

2005), for example, structural analysis or exterior uncoupled acoustic computations arising from discretized FE/FE or FE/BE type models . Since the SOAR procedure takes the damping matrix into account directly, no further back conversion is required. Also, an initial factorization of the coupled system matrix of dimension N is required as opposed to an LU factorization of system matrices of dimension 2N in the state-space dimension reduction methods.

In this work, first, the second order Arnoldi procedure and its relationship to the standard Krylov subspaces and state-space models are described. Next, the SOAR process is extended using the output scattering matrix resulting in a two-sided Arnoldi process (TS-SOAR). In Chapter:[6], various examples arising from interior, fully coupled, linearly damped, structural-acoustic systems are reduced using TS-SOAR and their numerical benefits demonstrated against a linearized coupled system. At this point, it is worth noting that no known reduction techniques are able to deal with coupled structural-acoustic systems incorporating frequency dependent material damping. In such situations, where spatial damping is also present, a direct inversion procedure is utilized to compute the desired states.

Starting off from the known *Eulerian* displacement - pressure *(u/p)* formulation for the structural-acoustic model as a whole (Zienkiewicz and Newton 1969; Craggs 1971; Craggs 1973):

$$\underbrace{\begin{bmatrix} M_s & 0 \\ M_{fs} & M_a \end{bmatrix}}_{M_{sa}} \overbrace{\begin{Bmatrix} \ddot{u} \\ \ddot{p} \end{Bmatrix}}^{\ddot{q}(t)} + \underbrace{\begin{bmatrix} C_s & 0 \\ 0 & C_a \end{bmatrix}}_{C_{sa}} \overbrace{\begin{Bmatrix} \dot{u} \\ \dot{p} \end{Bmatrix}}^{\dot{q}(t)} + \underbrace{\begin{bmatrix} K_s & K_{fs} \\ 0 & K_a \end{bmatrix}}_{K_{sa}} \overbrace{\begin{Bmatrix} u \\ p \end{Bmatrix}}^{q(t)} = \mathbf{F}_{MIsa}\, \mu(t)$$

$$(4.58a)$$

and,

$$y(t) = L^T \overbrace{\left\{ \begin{array}{c} u(t) \\ p(t) \end{array} \right\}}^{q(t)} \tag{4.58b}$$

For simplicity, using the definitions for the matrices and the states in the above Equations:[4.58a,4.58b] , the coupled system can simply be written as:

$$[M_{sa}] \, \ddot{q}(t) + [C_{sa}] \, \dot{q}(t) + [K_{sa}] \, q(t) = \mathbf{F}_{MIsa} \, \mu(t) \tag{4.59a}$$

$$y(t) = L^T q(t) \tag{4.59b}$$

Considering a SISO second order structural-acoustic system in the time domain, it is possible to equivalently represent the coupled system as:

$$s^2 \underbrace{\begin{bmatrix} M_s & 0 \\ M_{fs} & M_a \end{bmatrix}}_{M_{sa}} \overbrace{\left\{ \begin{array}{c} \tilde{u} \\ \tilde{p} \end{array} \right\}}^{\tilde{q}(s)} + s \underbrace{\begin{bmatrix} C_s & 0 \\ 0 & C_a \end{bmatrix}}_{C_{sa}} \overbrace{\left\{ \begin{array}{c} \tilde{u} \\ \tilde{p} \end{array} \right\}}^{\tilde{q}(s)} + \underbrace{\begin{bmatrix} K_s & K_{fs} \\ 0 & K_a \end{bmatrix}}_{K_{sa}} \overbrace{\left\{ \begin{array}{c} \tilde{u} \\ \tilde{p} \end{array} \right\}}^{\tilde{q}(s)} = \mathbf{f}_{sa} \, \mu(s) \tag{4.60a}$$

and the output measurement vector given by,

$$y(s) = \mathbf{l}^T \overbrace{\left\{ \begin{array}{c} \tilde{u} \\ \tilde{p} \end{array} \right\}}^{\tilde{q}(s)} \tag{4.60b}$$

in the frequency domain using the Laplace transformation. Here, $\tilde{q}(s)$ and hence $\tilde{u}, \tilde{p}, \mu(s), y(s)$ are the Laplace transforms of $q(t)$ and hence $u, p, \mu(t)$ and $y(t)$ respectively. $\mathbf{f}_{sa}$ is the single-input structural-acoustic input distribution vector consisting of f_s and f_a which denote the input distribution force(s) on the structural domain and constrained acoustic pressure degrees of freedom (DOF's) or purely acoustic excitation, in the form of volume acceleration belonging to the fluid domain respec-

tively. $\mathbf{l}^T$ is the output scattering vector to restore a the desired state output, which in this case the displacement or pressure corresponding to the structural and fluid domain respectively.

Again, for simplicity and convenience, using the above definitions in Equations:[4.60a,4.60b],the coupled structural-acoustic system can be written using Laplace transforms as:

$$s^2 \left[M_{sa} \right] \tilde{q}(s) + s \left[C_{sa} \right] \tilde{q}(s) + \left[K_{sa} \right] \tilde{q}(s) = \mathbf{f}_{sa} \; \mu(s) \tag{4.61a}$$

$$y(s) = \mathbf{l}^T \tilde{q}(s) \tag{4.61b}$$

Now, the input $\mu(s)$ and the output $y(s)$ of Equations:[4.61a,4.61b] in the frequency domain are related by the *transfer function* of the second order structural-acoustic system, given by:

$$h_{sa}(s) = \frac{y(s)}{\mu(s)} \tag{4.62a}$$

$$h_{sa}(s) = \mathbf{l}^T \left(s^2 \; M_{sa} + s \; C_{sa} + K_{sa} \right)^{-1} \mathbf{f}_{sa} \tag{4.62b}$$

where, $s = j\omega$, with $j = \sqrt{-1}$ and $\omega \geq 0$. In this definition, we assume that K_{sa} is nonsingular. Now, a formal power series expansion of Equation:[4.62b] is given by:

$$h_{sa}(s) = m_0 + m_1 s + m_2 s^2 + m_3 s^3 + \ldots \tag{4.63a}$$

$$h_{sa}(s) = \sum_{z=0}^{\infty} m_z \; s^z \tag{4.63b}$$

where, m_z, for all $z \geq 0$ are called the *low-frequency moments* of the second order, fully coupled structural acoustic transfer function $h_{sa}(s)$. These *low-frequency moments* are the values and their subsequent derivatives of the transfer function h_{sa} at $s = 0$. The moment m_z can in fact be expressed as an inner product between $\mathbf{l}^T$

and g_z (Bai et al. 2005):

$$m_z = \mathbf{l}^T g_z \quad for \ \ all \ \ z \geq 0 \tag{4.64}$$

where, g_z is a vector sequence, defined by the second order recurrence relationship, which can be written for the coupled structural-acoustic case as follows:

$$g_0 = K_{sa}^{-1} \mathbf{f}_{sa} \tag{4.65a}$$

$$g_1 = -K_{sa}^{-1} C_{sa} g_0 \tag{4.65b}$$

$$g_z = -K_{sa}^{-1}(C_{sa} g_{z-1} + M_{sa} g_{z-2}) \tag{4.65c}$$

for values of $z = 2, 3, \ldots$.

The vector sequence defined above is called the input second order Krylov vector sequence, which belongs to the input second order Krylov subspace, induced by two matrices A, B and starting vector g_0, written as:

$$\mathcal{K}_q^{ri}(A, B, g_0) = span(g_0, g_1, g_2, g_3, \ldots g_{q-1}) \tag{4.66}$$

where, $A = -[K_{sa}]^{-1}[C_{sa}]$, $B = -[K_{sa}]^{-1}[M_{sa}]$. A similar feat of *moment computation*, can be achieved by also computing the following set of vectors in addition to the vectors defined in Equations:[4.65a, 4.65b,4.65c]:

$$l_0 = K_{sa}^{-T} \mathbf{l} \tag{4.67a}$$

$$l_1 = -K_{sa}^{-T} C_{sa}^T l_0 \tag{4.67b}$$

$$l_z = -K_{sa}^{-T}(C_{sa}^T l_{z-1} + M_{sa}^T l_{z-2}) \tag{4.67c}$$

for values of $z = 2, 3, \ldots$. The moments can now be expressed as an inner product between $\mathbf{f}_{sa}^T$ and l_z:

$$m_z = \mathbf{f}_{sa}^T l_z \quad for \; all \; \; z \geq 0 \tag{4.68}$$

The vector sequence defined above is called the output second order Krylov vector sequence, which belongs to the output second order Krylov subspace, induced by the two matrices A^T, B^T and starting vector l_0, written as:

$$\mathcal{K}_q^{le}(A^T, B^T, l_0) = span(l_0, l_1, l_2, l_3, \ldots l_{q-1}) \tag{4.69}$$

where, $A^T = -[K_{sa}]^{-T}[C_{sa}]^T$, $B = -[K_{sa}]^{-T}[M_{sa}]^T$.

It can now be observed that the vector sequence defined in Equations:[4.65a,4.65b, 4.65c,4.67a,4.67b, 4.67c] in fact form the moments of the second order, structural acoustic transfer function. In order to show the *moment matching* parameters, let us consider an equivalent system for Equations:[4.59a,4.59b] in first order form as follows (see for *e.g.* Meirovitch (1980), Su and Craig (1991b), Freund (2001), Bai (2002)):

$$\mathbf{D}_{sa}\dot{\hbar}(t) + \mathbf{G}_{sa}\hbar = \hat{b}\mu(t) \tag{4.70a}$$

$$y(t) = \hat{l}^{\;T}\hbar(t) \tag{4.70b}$$

where, $\hbar(t) = [q(t)^T, \dot{q}(t)^T]^T$ and the block matrices, vectors defined as follows:

$$\mathbf{D}_{sa} = \begin{bmatrix} C_{sa} & M_{sa} \\ -I & 0 \end{bmatrix}, \mathbf{G}_{sa} = \begin{bmatrix} K_{sa} & 0 \\ 0 & I \end{bmatrix}, \hat{b} = \begin{Bmatrix} \mathbf{f}_{sa} \\ 0 \end{Bmatrix} \text{ and } \hat{l} = \begin{Bmatrix} 1 \\ 0 \end{Bmatrix}.$$

Using the Laplace transforms, the transfer function of the system defined in Equations:[4.70a, 4.70a], and its associated power series expansion are written as follows:

$$\mathbf{h}_{Lin}(s) = \hat{l}^{\;T}(\; s\, \mathbf{D}_{sa} \; + \; \mathbf{G}_{sa} \;)^{-1}\, \hat{b} \tag{4.71a}$$

$$\mathbf{h}_{Lin}(s) = \hat{l}^{\,T}(\,I \;-\; s\,\mathbf{H}\,)^{-1}\,\hat{r} \tag{4.71b}$$

$$\mathbf{h}_{Lin}(s) = \; m_0 + m_1 s + m_2 s^2 + m_3 s^3 + \ldots = \sum_{z=0}^{\infty} m_z\,(s)^z \tag{4.71c}$$

where, $\mathbf{H} = -(\mathbf{G}_{sa}^{-1}\,\mathbf{D}_{sa})$, $\hat{r} = -\mathbf{G}_{sa}^{-1}\hat{b}$, m_z are the so called *low frequency moments* of the equivalent first order system. Note that the *equivalent shifted* low frequency moments can also be formulated with any user specified value s_0 and such that the matrix pencil $\mathbf{G}_{sa} \;+\; s_0\,\mathbf{D}_{sa}$ is invertible.

The transfer function thus defined in Equations:[4.71a, 4.71b] is in fact the equivalent transfer function of the coupled higher dimensional structural-acoustic system defined in Equations:[4.59a, 4.59b]. This can be shown by the inverse identity of the 2×2 block matrices $\mathbf{G}_{sa}$ and $\mathbf{D}_{sa}$, given by (Bai and Su 2005a):

$$\mathbf{h}_{Lin}(s) = \hat{l}^{\,T}(\,s\,\mathbf{D}_{sa} \;+\; \mathbf{G}_{sa}\,)^{-1}\,\hat{b}$$

$$(\,s\,\mathbf{D}_{sa} \;+\; \mathbf{G}_{sa})^{-1} = \begin{bmatrix} s\,C_{sa} \;+\; K_{sa} & s\,M_{sa} \\[2mm] -s\,\mathbf{I} & \mathbf{I} \end{bmatrix}^{-1} \tag{4.72a}$$

$$(\,s\,\mathbf{D}_{sa} \;+\; \mathbf{G}_{sa})^{-1} = \begin{bmatrix} \aleph(s)^{-1} & \aleph(s)^{-1}\,s\,M_{sa}\,I^{-1} \\[2mm] s\,\aleph(s)^{-1} & \aleph(s)^{-1}\,(\,s\,C_{sa} \;+\; K_{sa})\,I^{-1} \end{bmatrix} \tag{4.72b}$$

where, $\aleph(s) = \; s^2\,M_{sa} \;+\; s\,C_{sa} \;+\; K_{sa}$.

Subsequently, following from Equations:[4.71b, 4.71c], the *equivalent low frequency moments* for the transfer function of the higher dimensional fully coupled structural-acoustic system described by Equations: [4.59a,4.59b] can be written as:

$$m_z = \hat{l}^{\,T}\,(\mathbf{H})^z\hat{r} = \hat{l}^{\,T}\,(-\mathbf{G}_{sa}^{-1}\,\mathbf{D}_{sa})^z\mathbf{G}_{sa}^{-1}\hat{b} \tag{4.73}$$

Therefore, it is now natural to consider the input vector sequence, none other than the *standard*, input Krylov subspace $\mathcal{K}_q^{Lin}(\mathbf{H}, \hat{r})$, given by:

$$\hat{r}, \mathbf{H}\hat{r}, \mathbf{H}^2\hat{r}, \mathbf{H}^3\hat{r} \dots \mathbf{H}^{n-1}\hat{r} \tag{4.74a}$$

$$\mathcal{K}_n^{Lin}(\mathbf{H}, \hat{r}) = span(\hat{r}, \mathbf{H}\hat{r}, \mathbf{H}^2\hat{r}, \mathbf{H}^3\hat{r} \dots \mathbf{H}^{n-1}\hat{r}) \tag{4.74b}$$

which would generate the desired moment information $m_z = \hat{l}^T(\mathbf{H})^z\hat{r}$. Alternatively, one could also consider the output vector sequence, non other than the *standard*, output Krylov subspace $\mathcal{K}_q^{Lin}(\mathbf{H}^T, \hat{l})$, given by:

$$\hat{l}, (\mathbf{H}^T)\hat{l}, (\mathbf{H}^T)^2\hat{l}, (\mathbf{H}^T)^3\hat{l} \dots (\mathbf{H}^T)^{n-1}\hat{l} \tag{4.75a}$$

$$\mathcal{K}_n^{Lin}(\mathbf{H}^T, \hat{l}) = span(\hat{l}, (\mathbf{H}^T)\hat{l}, (\mathbf{H}^T)^2\hat{l}, (\mathbf{H}^T)^3\hat{l} \dots (\mathbf{H}^T)^{n-1}\hat{l}) \tag{4.75b}$$

and then compute the inner products in order to define the *equivalent low frequency moments* as follows:

$$m_{2z} = ((\mathbf{H}^T)^z\hat{l})^T \cdot ((\mathbf{H}^T)^z\hat{r}) \ and \ m_{2z+1} = ((\mathbf{H}^T)^z\hat{l})^T \cdot ((\mathbf{H}^T)^{z+1}\hat{r}) \tag{4.76}$$

In particular, it is worth noting that:

$$\mathbf{H} = (-\mathbf{G}_{sa}^{-1}\mathbf{D}_{sa}), \ \mathbf{H}^T = (\mathbf{D}_{sa}^T \cdot (-\mathbf{G}_{sa}^{-T}))$$

$$\mathbf{H} = \begin{bmatrix} -K_{sa}^{-1} C_{sa} & -K_{sa}^{-1} M_{sa} \\ \mathbf{I} & \mathbf{0} \end{bmatrix} = \begin{bmatrix} A & B \\ \mathbf{I} & \mathbf{0} \end{bmatrix}, \ \hat{r} = \begin{Bmatrix} K_{sa}^{-1} \mathbf{f}_{sa} \\ 0 \end{Bmatrix} \tag{4.77a}$$

and,

$$
\mathbf{H}^T = \begin{bmatrix} -K_{sa}^{-T} C_{sa}^T & -K_{sa}^{-T} M_{sa}^T \\ \mathbf{I} & \mathbf{0} \end{bmatrix} = \begin{bmatrix} A^T & B^T \\ \mathbf{I} & \mathbf{0} \end{bmatrix} , \ \hat{l} = \begin{Bmatrix} K_{sa}^{-1} \mathbf{1} \\ 0 \end{Bmatrix}
$$
(4.77b)

One can now observe that the input and the output second order Krylov subspaces, span the same space as the upper half of the standard input and output Krylov subspaces. Precisely speaking, the moments can now be defined as follows:

$$
m_z = \hat{l}^{\ T} \ (\mathbf{H})^z \hat{r} = \hat{l}^{\ T} \ (-\mathbf{G}_{sa}^{-1} \ \mathbf{D}_{sa})^z \mathbf{G}_{sa}^{-1} \hat{b}
$$
(4.78a)

$$
= \{ \ (\ (\mathbf{H}^T)^z \hat{l} \ )^T \ . \ (\ (\mathbf{H}^T)^z \hat{r} \ ), \ (\ (\mathbf{H}^T)^z \hat{l} \ )^T \ . \ (\ (\mathbf{H}^T)^{z+1} \hat{r} \ ) \ \}
$$
(4.78b)

$$
= \mathbf{l}^T g_z
$$
(4.78c)

$$
= \mathbf{f}_{sa}^T l_z
$$
(4.78d)

To illustrate the moment matching properties of Equations:[4.78a⟶ 4.78d], let us consider an example.

Example:4.1: Consider the following 3×3 SISO system as given below[4]:

$$
[A] = \begin{bmatrix} -0.3933 & 0.0061 & 0.7416 \\ 0.0624 & 0.8171 & -0.2038 \\ 0.0438 & -0.9152 & 0.2342 \end{bmatrix} ,
$$

$$
[B] = \begin{bmatrix} 0.8985 & -0.5057 & 0.0222 \\ -0.7878 & 0.0610 & 0.8698 \\ -0.1830 & 0.1353 & 0.6141 \end{bmatrix} , f_{sa} = \begin{Bmatrix} 20 \\ 0 \\ 0 \end{Bmatrix} , \ l = \begin{Bmatrix} 1 \\ 0 \\ 0 \end{Bmatrix}
$$

---

[4]The matrices for this example were generated using the *randn* command in MATLAB.

The corresponding *linearized* system is given by (Equation: 4.77a):

$$
[H] =
\begin{bmatrix}
-0.3933 & 0.0061 & 0.7416 & 0.8985 & -0.5057 & 0.0222 \\
0.0624 & 0.8171 & -0.2038 & -0.7878 & 0.0610 & 0.8698 \\
0.0438 & -0.9152 & 0.2342 & -0.1830 & 0.1353 & 0.6141 \\
1 & 0 & 0 & 0 & 0 & 0 \\
1 & 1 & 0 & 0 & 0 & 0 \\
0 & 0 & 1 & 0 & 0 & 0
\end{bmatrix}
$$

$$
\hat{b} =
\begin{Bmatrix}
20 \\
0 \\
0 \\
0 \\
0 \\
0
\end{Bmatrix}
\text{ and } \hat{l} =
\begin{Bmatrix}
1 \\
0 \\
0 \\
0 \\
0 \\
0
\end{Bmatrix}
$$

The moments can now be defined using both the original system and its *equivalent linearized* system. Table:[4.1] shows the first five moment values from $m_0 \longrightarrow m_4$ for both systems. It can be observed that the computed moments are exactly the same and is irrespective of the system representation.

The use of projection techniques for dimension reduction, similar to the projection matrix V encountered in the standard Krylov subspaces, seek an orthogonal projection onto the induced right subspace $\mathcal{K}_q^{ri}(A, B, g_0)$, to construct an approximation such that:

$$
q(t) = \begin{Bmatrix} u(t) \\ p(t) \end{Bmatrix} = V_{sa}\breve{z}(t) \; + \; \varepsilon_{sa} \tag{4.79}
$$

Moments	Equation:[4.78a]	Equation:[4.78b]	Equation:[4.78c]	Equation:[4.78d]
m_0	20	20	20	20
m_1	-7.8660	-7.8660	-7.8660	-7.8660
m_2	21.7210	21.7210	21.7210	21.7210
m_3	-19.9807	-19.9807	-19.9807	-19.9807
m_4	46.9311	46.9311	46.9311	46.9311

Table 4.1.: Computation of moment values (Example:4.1) for the original and equivalent linearized system

where, $\breve{z}(t)$ are the generalized co-ordinates and ε_{sa} is the small approximation error introduced due to the projection to generalized co-ordinates. Indeed, from Equations:[4.90], one can observe that the vector sequence g_z, of length N which is used to generate the projection matrix V_{sa}, is related to the standard Krylov vectors sequence of length $2N$ as follows:

$$\begin{bmatrix} g_z \\ g_{z-1} \end{bmatrix} = (\mathbf{H})^z \hat{r} \tag{4.80}$$

As mentioned before, such a projection to generalized co-ordinates is often referred to as *change of state co-ordinates*.

However, for dimension reduction in practice, one is often interested in approximating the higher dimensional coupled system at $s_0 \neq 0$ or possibly even multiple values of $s_0 \neq 0$ (leading to second order, rational Krylov methods) . In such a case,

the transfer function of the coupled system can be re-written as:

$$h_{sa}(s) = \mathbf{l}^T \ (\ s^2 \ M_{sa} \ + \ s \ C_{sa} \ + \ K_{sa})^{-1} \ \mathbf{f}_{sa}$$

$$h_{sa}(s) = \mathbf{l}^T \ (\ (s - s_0)^2 \ M_{sa} \ + \ (s - s_0) \ \tilde{C}_{sa} \ + \ \tilde{K}_{sa})^{-1} \ \mathbf{f}_{sa} \tag{4.81}$$

where, the block fully coupled, structural-acoustic matrices $[\tilde{K}_{sa}]$ and $[\tilde{C}_{sa}]$ are defined as:

$$[\tilde{K}_{sa}] = s_0^2 M_{sa} + s_0 C_{sa} + K_{sa} \tag{4.82a}$$

$$[\tilde{C}_{sa}] = 2s_0 M_{sa} + C_{sa} \tag{4.82b}$$

It can be seen that $[\tilde{C}_{sa}]$ is simply the first derivative of $[\tilde{K}_{sa}]$. Here, s_0 can be any user specified value, such that that matrix $[\tilde{K}_{sa}]$ is nonsingular. Now, the low frequency moments, and thus the recurrence scheme specified in Equations:[4.65a,4.65b, 4.65c,4.67a,4.67b, 4.67c] are modified as follows:

$$h_{sa}(s) = \sum_{z=0}^{\infty} \tilde{m}_z \ (s - s_0)^z \tag{4.83}$$

where, $\tilde{m}_z$, for all $z \geq 0$ are called the *shifted low-frequency moments* of the second order, fully coupled structural acoustic system defined in Equations:[4.60a,4.60b]. The *shifted* moments can be computed as follows:

$$\tilde{m}_z = \mathbf{l}^T \tilde{g}_z, \quad \tilde{m}_z = \mathbf{f}_{sa}^T \tilde{l}_z \quad for \ all \ z \geq 0 \tag{4.84}$$

with the following recurrence schemes for $\tilde{g}_z$ and $\tilde{l}_z$:

$$\tilde{g}_0 = \tilde{K}_{sa}^{-1} \mathbf{f}_{sa} \tag{4.85a}$$

$$\tilde{g}_1 = -\tilde{K}_{sa}^{-1} \tilde{C}_{sa} \tilde{g}_0 \tag{4.85b}$$

$$\tilde{g}_z = -\tilde{K}_{sa}^{-1}(\tilde{C}_{sa} \tilde{g}_{z-1} + M_{sa} \tilde{g}_{z-2}) \tag{4.85c}$$

for values of $z = 2, 3, \ldots$.

$$\tilde{l}_0 = \tilde{K}_{sa}^{-T} \mathbf{l} \tag{4.86a}$$

$$\tilde{l}_1 = -\tilde{K}_{sa}^{-T} \tilde{C}_{sa}^{T} \tilde{l}_0 \tag{4.86b}$$

$$\tilde{l}_z = -\tilde{K}_{sa}^{-T} (\tilde{C}_{sa}^{T} \tilde{l}_{z-1} + M_{sa}^{T} \tilde{l}_{z-2}) \tag{4.86c}$$

for values of $z = 2, 3, \ldots$.

The *shifted* moments defined in Equation:[4.84] thus serve as an important observation to define the goal for dimension reduction.

Since any form of explicit moment matching is known to suffer with numerical difficulties, in this work, implicit moment matching is performed via a two-sided, second order Arnoldi based direct projection technique. For this purpose, consider the orthonormal projection matrices, V_{sa} and W_{sa} for *Galerkin* or *Petrov-Galerkin* type projections, which span the input and output Krylov subspaces defined in Equations:[4.66, 4.69], i.e:

$$\mathcal{K}_q^{ri}(A, B, g_0) = span(V_{sa}) \quad and \quad V_{sa}^{T} V_{sa} = I \tag{4.87a}$$

$$\mathcal{K}_q^{le}(A, B, l_0) = span(W_{sa}) \quad and \quad W_{sa}^{T} W_{sa} = I \tag{4.87b}$$

By setting $[A]$, $[B]$, it is now possible to extend the *standard* Arnoldi iterations (Figures:4.1,4.2) to find a basis for the given Second Order Krylov Subspace. The resulting one sided SOAR procedure (which in this work is utilized to compute TS-SOAR column matrices i.e. both V_{sa}, W_{sa})), was first proposed by Su and Craig (1991b) and later improved and extended by Bai et al. (2005), Bai and Su (2005a), Salimbahrami (2005). The iterative process given below finds two sets of orthonormal basis vectors for the induced input and output subspace, i.e. $V_{sa}^{T} V_{sa} = I$ and $W_{sa}^{T} W_{sa} = I$, and therefore the columns of the matrix V_{sa} and W_{sa} form a basis for

the induced subspace. For simplicity, it SISO is assumed i.e. k_{st}, l have one entry each. In some sense, the parameter $k_{st} = 1$ is utilized to describe the process in a more efficient manner.

Comparing TS-SOAR to the TSA, it can be observed that the TS-SOAR procedure is quite similar with modifications to the orthogonalization and normalization steps to enforce orthonormality of the vectors stored in column matrices of V_{sa} and W_{sa}. The reader is made aware that there are two potential situations in the SOAR process (Bai et al. 2005; Bai and Su 2005a): *deflation* and *complete breakdown*. The former results due to the fact that the vector $\hat{v}_i$ for $i = 0 \longrightarrow j-1$ which is computed in Step:1.2: becomes linearly dependent but the double length vector sequence defined by $[\hat{v}_i^T, \hat{v}_{i-1}^T]^T$ for $i = 0 \longrightarrow j-1$ is linearly independent. In such a situation, *deflation* occurs. As shown in the SOAR process, in this case, one temporarily sets $\bar{v}_i = 0$, which is then deleted at the end. In the case when $\hat{v}_i$, $\hat{p}_i$ are both linearly dependent (and so are $\hat{v}_i$, $[\hat{v}_i^T, \hat{v}_{i-1}^T]^T$ for $i = 0 \longrightarrow j-1$), then one sets $\hat{v}_i = 0$, $p_i = 0$ both of which are deleted at the end of the process. Considering a SISO system, this defines *complete breakdown*. For real life applications, it is however not possible to check for zero vectors in finite precision arithmetic. Instead, the norm of the vectors are computed and checked against a very small number. i.e $\|\hat{v}_i\|_2 < \varphi$ and $\|\hat{p}_i\|_2 < \varphi$, where φ is the small number. Throughout this work the value of φ is set to 1.0E-12. It is worth pointing out that at the breakdown of SOAR, it is possible to prove that the transfer function of the ordinal and the reduced order model are identical (Bai and Su 2005a).

Upon completion of the TS-SOAR process, a reduced order model can now be defined by applying the *Petrov-Galerkin* projection on the coupled higher dimensional

Input: Read coupled system Matrices $[K_{sa}]$, $[M_{sa}]$, $[C_{sa}]$, $\{\mathbf{f}_{sa}\}$, $\mathbf{l}^T$, q (Number of vectors) and expansion point s_0, in this case $s_0 = (\omega_e + \omega_b)/2$; or ω_e.

Form and Set: $[\tilde{K}_{sa}] = s_0^2 M_{sa} + s_0 C_{sa} + K_{sa}$ and $[\tilde{C}_{sa}] = 2s_0 M_{sa} + C_{sa}$.

Output: q Arnoldi vectors belonging to the Second order Krylov Subspace.

$\mathcal{K}_q^{ri}(A, B, g_0)$. In this case, $\mathcal{K}_q^r(-\tilde{K}_{sa}^{-1}\tilde{C}_{sa}, -\tilde{K}_{sa}^{-1}M_{sa}, \tilde{K}_{sa}^{-1}\mathbf{f}_{sa})$.

[0]. Delete all linearly dependent starting vectors (if multiple) to obtain k_{st} linearly independent starting vectors. Set $\bar{v}_1 = \frac{g_0}{\|g_0\|}$ and $p_1 = 0$ for $p_1 \in \Re^n$.

[1]. $^*for\ i = 2, 3, .. \rightarrow q\ \ ^*do$:

   [1.1] Generate next vector: $^*if\ i \leq k_{st}$, set $\hat{v}_i$ (below) as the ith starting vector and $\hat{p}_i = 0$. $^*else$, set $\hat{v}_i = A\bar{v}_{i-k_{st}} + Bp_{i-k_{st}}$ and $\hat{p}_i = \bar{v}_{i-k_{st}}$

   [1.2] Orthogonalization: $^*for\ j = 1 \rightarrow i\ \text{-}\ 1$, $^*do$:

   $h = \hat{v}_i^T \bar{v}_j$, $\hat{v}_i = \hat{v}_i - h\bar{v}_j$, $\hat{p}_i = \hat{p}_i - hp_j$

   [1.3] Normalization and Deflation check: $^*if\ \hat{v}_i \neq 0$ (normal case), then,

   $^*do : \bar{v}_i = \frac{\hat{v}_i}{\|\hat{v}_i\|}$, $p_i = \frac{\hat{p}_i}{\|\hat{v}_i\|}$.

   $^*else\ if\ \hat{p}_i \neq 0$, $\bar{v}_i = 0$.

   $^*else$, $k_{st} = k_{st}\ -\ 1$. Go to step: [1.1]. $^*if\ \ k_{st} = 0$, delete zero columns.

   [1.4] Increase i and go to step: [1.1].

[2]. Delete zero columns from deflation, discard resulting H_q and project higher dimensional system $[M_{sa}]$, $[K_{sa}]$, $[C_{sa}]$, $\{\mathbf{f}_{sa}\}$, $\mathbf{l}^T$ onto $[V_{sa}]$ to obtain reduced system matrices $[M_{rsa}]$, $[K_{rsa}]$, $[C_{rsa}]$, $\{\mathbf{f}_{rsa}\}$, $\mathbf{l}_{rsa}^T$ for harmonic simulation.

Figure 4.3.: Algorithm:4: Set-up for SISO/SICO Second Order Arnoldi (SOAR) Process with multiple starting vectors (Bai et al. 2005; Bai and Su 2005a; Bai and Su 2005b).

[**1**]. ***Initialization:*** Read coupled structural-acoustic matrices, select appropriate Input and Output Krylov Subspaces: $\mathcal{K}_q^r(A, B, g_0)$, $\mathcal{K}_q^l(A^T, B^T, l_0)$ and expansion points. Form and Set: $[\tilde{K}_{sa}]$, $[\tilde{C}_{sa}]$ as in Figure:4.3.

[**2**]. ***Generate Projection Matrices:*** Use the SOAR Algorithm (Figure:4.3) *do:

[2.1] $\mathcal{K}_q^{ri}(A, B, g_0)$: Apply $A = [-\tilde{K}_{sa}^{-1}\tilde{C}_{sa}]$, $B = [-\tilde{K}_{sa}^{-1}M_{sa}]$ and $g_0 = [\tilde{K}_{sa}^{-1}]\{\mathbf{f}_{sa}\}$ to compute $[V]$.

[2.2] $\mathcal{K}_q^{le}(A^T, B^T, l_0)$: Apply $A^T = [-\tilde{K}_{sa}^{-T}]\,[\tilde{C}_{sa}^T]$, $B^T = [-\tilde{K}_{sa}^{-T}]\,[M_{sa}^T]$ and $l_0 = [\tilde{K}_{sa}^{-T}]\{\mathbf{l}\}$ to compute $[W]$.

[**3**]. ***Apply Projection:*** Use generated column matrices: $[V_{sa}]$ and $[W_{sa}]$ and apply the *Galerkin-Petrov* projection: $\prod = [V_{sa}]\,[W_{sa}]^T$ to obtain the *structure preserving* ROM matrices: $[M_{rsa}]$, $[C_{rsa}]$, $[K_{rsa}]$,$\{\mathbf{f}_{rsa}\}$ and $\mathbf{l}_{rsa}^T$ for reduced harmonic or transient simulation.

Figure 4.4.: Algorithm:5: Higher-level, complete set-up for SISO Two Sided Second Order Arnoldi (TS-SOAR) Process (Salimbahrami 2005).

system matrices as follows:

$$[M_{rsa}] = [W_{sa}^T]\,[M_{sa}]\,[V_{sa}], \ [K_{rsa}] = [W_{sa}^T]\,[K_{sa}]\,[V_{sa}] \tag{4.88a}$$

$$[C_{rsa}] = [W_{sa}^T]\,[C_{sa}]\,[V_{sa}], \ \mathbf{f}_{rsa} = [W_{sa}^T]\,\mathbf{f}_{sa}, \ \mathbf{l}_{rsa}^T = \mathbf{l}^T\,[V_{sa}] \tag{4.88b}$$

$$[M_{rsa}]\,\ddot{z}(t) + [C_{rsa}]\,\dot{z}(t) + [K_{rsa}]\,z(t) = \mathbf{f}_{rsa}\,\mu(t) \tag{4.88c}$$

$$y_{rsa}(t) = \mathbf{l}_{rsa}^T z(t) \tag{4.88d}$$

where, *rsa* denote the reduced structural-acoustic matrices. It is worth noting that the goal of dimension reduction i.e. reduction of the system matrices from $N \times N \longrightarrow q \times q$ is now achieved, and the system described in Equations:[4.88c,4.88d] is now ready for reduced harmonic or transient simulation. Continuing from the transfer function description about any specified expansion point s_0, a reduced order transfer

function can now be defined as (Bai et al. 2005):

$$h_{rsa}(s) = \mathbf{l}_{rsa}^T \left((s - s_0)^2 \, M_{rsa} + (s - s_0) \, \tilde{C}_{rsa} + \tilde{K}_{rsa} \right)^{-1} \mathbf{f}_{rsa} \qquad (4.89)$$

where, the shifted reduced order matrices are defined as follows: $[M_{rsa}] = [W_{sa}^T] \, [M_{sa}] \, [V_{sa}]$, $[\tilde{K}_{rsa}] = [W_{sa}^T] \, [\tilde{K}_{sa}] \, [V_{sa}]$, $[\tilde{C}_{rsa}] = [W_{sa}^T] \, [\tilde{C}_{sa}] \, [V_{sa}]$.

Indeed, it can be seen that by carrying out simple manipulations on Equation:[4.89], the reduced transfer function can be written as:

$$
\begin{aligned}
h_{rsa}(s) &= \mathbf{l}_{rsa}^T \left((s - s_0)^2 \, M_{rsa} + (s - s_0) \, \tilde{C}_{rsa} + \tilde{K}_{rsa} \right)^{-1} \mathbf{f}_{rsa} \\
&= \mathbf{l}_{rsa}^T \left((s - s_0)^2 \, M_{rsa} + (s - s_0) \, [2 s_0 M_{rsa} + C_{rsa}] \right. \\
&\quad + [s_0^2 M_{rsa} + s_0 C_{rsa} + K_{rsa}] \left. \right)^{-1} \mathbf{f}_{rsa} \\
&= \mathbf{l}_{rsa}^T \left([\, s^2 M_{rsa} + s_0^2 M_{rsa} - 2 s s_0 M_{rsa} \,] \right. \\
&\quad + [2 s s_0 M_{rsa} + s C_{rsa} - 2 s_0^2 M_{rsa} - s_0 C_{rsa}] \\
&\quad + [s_0^2 M_{rsa} + s_0 C_{rsa} + K_{rsa}] \left. \right)^{-1} \mathbf{f}_{rsa}
\end{aligned}
$$

Following from the above expanded equations and performing the required algebraic cancelations, it is now possible to define the reduced transfer function as follows:

$$h_{rsa}(s) = \mathbf{l}_{rsa}^T \left(s^2 \, M_{rsa} + s \, C_{rsa} + K_{rsa} \right)^{-1} \mathbf{f}_{rsa} \qquad (4.90)$$

with the same definitions of the reduced coupled structural-acoustic system matrices and vectors as in Equations: [4.88a,4.88b]. Subsequently, the first q low frequency shifted moments[5] about any given expansion point s_0 of the original (h_{sa}) and reduced order transfer function (h_{rsa}) are the same. More compactly, this can be

---

[5]Note that there are z and $2z$ moments defined in the case of explicit damping matrix participation. For consistency with the Arnoldi processes described in this work, a Padé approximant of qth order is assumed for the rest of the discussion.

written as:

$$\tilde{m}_z^{sa} = \tilde{m}_z^{rsa} \quad for \ \ all \ \ z \geq 0 \tag{4.91}$$

Recall that a Padé approximant, so called, is that rational function (of a specified order) whose power series expansion agrees with a given power series to the highest possible order. This implies that h_{rsa} is a qth order Padé approximation of h_{sa} about any given expansion point s_0.

Further, it can be observed from the above reduction process, that although the shifted matrix triple $(M_{sa}, \ \tilde{C}_{sa}, \ \tilde{K}_{sa})$ is used to generate the projection matrices V_{sa}, W_{sa}, the reduced order model is computed by projection onto the original higher dimensional system matrices $(M_{sa}, \ C_{sa}, \ K_{sa})$. The use of such a modified system matrices in dimension reduction is called *structure preserving dimension reduction*, since it essentially preserves the original second order structure of the problem.

In terms of computational flops and memory, the cost of carrying out the standard SOAR process (assuming no deflation), is $(3/2)Nq(q + 4/3)$ with a memory requirement of $(2 + q)N$ (Bai et al. 2005). The cost for a subsequent TS-SOAR process is dominated by the formation and the initial LU factorization of $\tilde{K}_{sa}$ and the explicit computation of $\tilde{C}_{sa}$. The remaining costs are for the orthogonalization of the old vector sets generated. It is worth pointing out that $\tilde{K}_{sa}^{-T}$ can simply be computed using the original LU factors of $\tilde{K}_{sa}$. Precisely speaking, it is possible to exploit the matrix relationship:

$$L_d^T U_d^T = (\ s_0^2 \ M_{sa} \ + \ s_0 \ C_{sa} \ + \ K_{sa})^T \tag{4.92}$$

and then perform a subsequent forward and backward solves to compute the required $\tilde{K}_{sa}^{-T}\mathbf{1}$.

In comparison to the linearization approach, one can observe that the cost of forming $\tilde{K}_{sa}$ and $\tilde{C}_{sa}$ is an additional overhead. However, since the linearization approach essentially doubles the dimension of the system, an initial LU factorization is carried out at an increased cost and memory (this is approximately a factor of 8). In some situations, this factorization might not be even possible on a standard stand alone computer. More appealing to the NVH community, is the fact that the reduced order model is in second order form - this preserves the original structure of the problem and outweighs the small additional cost of forming the required system matrices. In fact, in Chapter:[5], it will be numerically demonstrated that this cost is indeed very small.

Shortly speaking, this new method for fully coupled, interior, structural-acoustic systems is computationally efficient, preserves the second order structure of the underlying original system, does not sacrifice any information from the damping formulation, uses both input and output subspaces (if needed), and is valid over a wide range of low frequencies.

4.5. Error Quantities

In this section, a method to compute the error estimates, general to Arnoldi or Lanczos based reduced order modeling approaches and thus the convergence properties of the model is presented. The convergence models are similar to the method mentioned in (Bechtold et al. 2005b). The method is general, in the sense that any Arnoldi variant described in the previous sections, can be utilized and the desired error/convergence parameters computed. First, a *local error* for individual states is defined as:

$$\breve{\hbar}_{rsa}(s) = \frac{|H(s) - H_{rsa}(s)|}{|H(s)|} \tag{4.93}$$

for all values of s used for the higher dimensional and the ROM[6]. In the first convergence model, a straightforward *true error* and *relative error* between two models for all states considered for the ROM is computed as follows:

$$\vartheta_{rsa}(s) = \frac{\| H(s) - H_{rsa}(s) \|}{\| H(s) \|} \tag{4.94a}$$

for any user-defined value of s and any number of desired outputs, for the higher dimensional and the ROM. Here, $H(s)$ corresponds to the original transfer function, given by, $H(s) = L^T(s^2 M_{sa} + K_{sa})^{-1} F_{sa}$ where, the definitions of M_{sa}, K_{sa} and F_{sa} remain the same as in Equation:[4.11] and $H_{rsa}(s)$ is the reduced order transfer function. Further, a *relative error* between two successive reduced order models q and $q + 1$ can be defined as:

$$\hat{\vartheta}_{rsa}(s) = \frac{\| H_{rsa}(s) - H_{rsa+1}(s) \|}{\| H_{rsa}(s) \|} \tag{4.94b}$$

for any user-defined value of s and any number of desired outputs, for the higher dimensional and the ROM.

---

[6]Throughout this thesis, the absolute values for the numerator and denominator are utilized for the error computations.

5. Direct Projection via Krylov Subspaces: Numerical Test Cases.

In order to illustrate the applicability and suitability of the reduction methods proposed in the previous section of this dissertation, in this chapter, the proposed methods are applied to different fully coupled structural-acoustic systems. Four different methods form the main focus of this chapter: One Sided Arnoldi (OSA), Two-sided (and multi-point) Arnoldi (TSA, MP-TSA), Two-sided Second order Arnoldi (TS-SOAR). A description of the test cases to be considered in this section is shown in Table:[5.1]. Both air and water are considered as fluid medium in order to test the accuracy and computational efficiency for both *weakly* and *strongly* coupled problems. A short description, comparison methodologies and the induced Arnoldi variants for the test cases is shown in Table:[5.1].

The error estimates and convergence models described in Chapter:[4], Section:[4.5], are used to compute the true (*local* in frequency domain) and relative error to evaluate a stopping criterion for the fully coupled models in the frequency domain. The computational times required for the test cases are calculated using MATLAB. Unfortunately, it was not possible to run all simulations for the test cases on the same machine. Indeed, four different machines (with different specifications) have been used throughout the dissertation. The *bench* timings for the machines generated from MATLAB for the four machines are shown in Appendix:(A).

Table 5.1.: A description of selected test cases, comparison methodology and induced Arnoldi variants to demonstrate the accuracy and efficiency of Krylov Subspace based direct projection techniques.

Test Case No.	Description	Fluid Medium	Comparison Method	ROM via Arnoldi Variants
1	2-D ABAQUS Benchmark Model (The Acid Test)	Water	Direct, Uncoupled modes, Coupled Lanczos, AMLS.	OSA, TSA, MP-TSA, TS-SOAR
2	3-D Plate Backed Cavity	Air	Direct	OSA
2.1	Reciprocity Check	Air	Direct, Uncoupled modes	OSA
3	3-D Rectangular Cavity	Water	Direct	OSA, TS-SOAR, LIN-OSA
	3-D Rectangular Cavity	Air	Direct	TSA, TS-SOAR
4	3-D Cylindrical Cavity	Air	Direct	OSA, TS-SOAR, LIN-OSA
5	3-D Demonstrator Structure	Air	Direct	OSA
6	3-D Adhesively Bonded Structure	Air	Direct	TSA, TS-SOAR

5.1. Test Case: 1: 2D ABAQUS Benchmark Model: The Acid-Test.

The model is a semicircular shell and fluid mesh of radius 2.286 m. A point load on the symmetry axis of magnitude 1.0 N is applied to the shell. The shells are 0.0254 m in thickness and have a Young's modulus of 206.8 GPa, a Poisson's ratio of 0.3, and a mass density,ρ_s, of 7800.0 kg/m^3. The acoustic fluid has a density,ρ_f, of 1000 kg/m^3 and a bulk modulus,κ_f, of 2.25 GPa. The response of the coupled system is calculated for frequencies ranging from 100 to 1000Hz in 1Hz increments. The driving point displacement amplitude and the fluid pressure at the center of the acoustic domain are state variables of interest. A description of the problem can also be found in the ABAQUS Benchmark manual (ABAQUS 2005; Stepanishen and Cox 2000). It is worth mentioning that the solutions presented in Stepanishen and Cox (2000) compares analytical solutions with coupled and uncoupled modal expansion solutions obtained utilizing ABAQUS implemented modal type reduction procedures - Coupled Lanczos (CL) procedure, and the popular automated component mode method: Automated Multi-Level Substructuring (AMLS)[1]. It has been demonstrated that in comparison to the analytical results, the ABAQUS modal solutions (CL and AMLS) are in good agreement over the entire frequency range (100-1000Hz).

This undamped benchmark problem is known as the *acid-test* within the structural-acoustic community. The point load is a more challenging problem physically in the modal projection, because the single entry in the FE load vector maps to a full vector in the reduced problem, but this representation is truncated at the number of vectors. Analogy is to the Fourier transformation of a Dirac distribution (Cipolla 2006). Also, the absence of damping makes the errors more apparent, be-

---

[1]Currently, the finite element software ABAQUS, relies on AMLS for significant speed-up of fully coupled, structural-acoustic problems.

cause the response is not smoothed. Therefore, the undamped model is considered as the first test case to illustrate the accuracy, efficiency and convergence properties of Krylov subspace via Arnoldi based direct projection techniques. An extension of the undamped test case is then made to frequency dependent structural damping. This leads to an explicit participation of $[C_{sa}]$. For the test case, three Arnoldi variants form the main focus: One Sided Arnoldi (OSA), Two-Sided Arnoldi (TSA) and Two-Sided Second order Arnoldi (TS-SOAR) process.

As as first step to solve the problem using Krylov Subspace based projection techniques, the described model is modelled using the ANSYS FE package (AN-SYS 2005). The distribution of the elements in the coupled FE model is as follows: 400 2D, 4 noded, 2 DOF (UX,UY) axis-symmetric structural elements (PLANE42), 21107 2D, 4 noded, 1 DOF (Pressure) axis-symmetric fluid elements not in contact with the structure (FLUID29) and 400 2D, 4 noded, 3 DOF (UX, UY, Pressure) structural-acoustic interface elements in contact with the structure (FLUID29). For a detailed description of element formulations, the reader is referred to (ANSYS 2005). The structural and coupled FE mesh are shown in Figures:[5.1,5.2]. First, the driving point displacement obtained using the ANSYS Direct frequency sweep technique is compared with results presented in ABAQUS (2005), Stepanishen and Cox (2000). The comparison of the transfer functions is shown in Figure:[5.7]. It can be observed that there is a very good match between ANSYS direct prediction and the analytical solution for the driving point displacement amplitude. This means that, the ANSYS solution obtained by Direct inversion technique is also in very good agreement with ABAQUS implemented modal type reduction procedures (CL and AMLS). Therefore, the ANSYS fully coupled model and the solution is now considered validated and will be used as a reference solution for the remainder of the thesis.

Figure 5.1.: Test Case No. 1: Benchmark structural model.
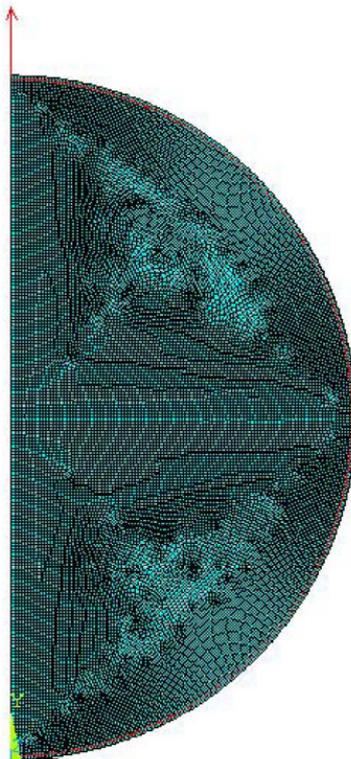

Figure 5.2.: Test Case No. 1: Benchmark coupled structural-acoustic model.

For the Arnoldi based ROM approach, 100 vectors are used for the Galerkin or Galerkin-Petrov projection. The expansion points along with the input and output Krylov Subspaces considered for the test case is shown in Table:[5.3]. For the OSA method, the expansion point, f_{exp}, is kept constant at 750Hz whilst specifying the driving point displacement and nodal pressure at the centre of the fluid domain as outputs for the coupled analysis. Since, the TSA method takes the output measurement vector (for SISO) in the order reduction process, we specify the nodal driving point displacement as the output for analysis involving TSA methods.

Table 5.2.: Structural Damping values and Expansion point for TS-SOAR for Acid-
Test, benchmark problem.

Damped Test Cases	**Damping Value**	**Expansion Point**
Low Damping [T_{ld}]	β_j^m=5.0E-06	900Hz / 900Hz
Medium Damping [T_{md}]	β_j^m=1.0E-05	1000Hz / 1000Hz
High Damping [T_{hd}]	β_j^m=2.0E-05	750Hz / 750Hz

For the frequency dependent structural damping case, three different values of β_j^m are considered for the analysis. This is shown in Table:[5.2]. These models results in an explicit participation of $[C_{sa}]$ and the *direct-inversion* technique cannot be avoided. For dimension reduction, the TS-SOAR process is chosen for the resulting coupled higher dimensional system. The aim of using different expansion points for each of the damped test cases is to observe the effects of moment matching and its resulting accuracy at different frequencies for different damping values. Theoretically speaking, since the frequency sweep is requested for a wide frequency range (101Hz to 1000Hz at 1Hz increments), the expansion points are chosen in the higher frequency range. An initial comparison between the driving point displacements for undamped and frequency dependent, linearly damped model is shown in

121
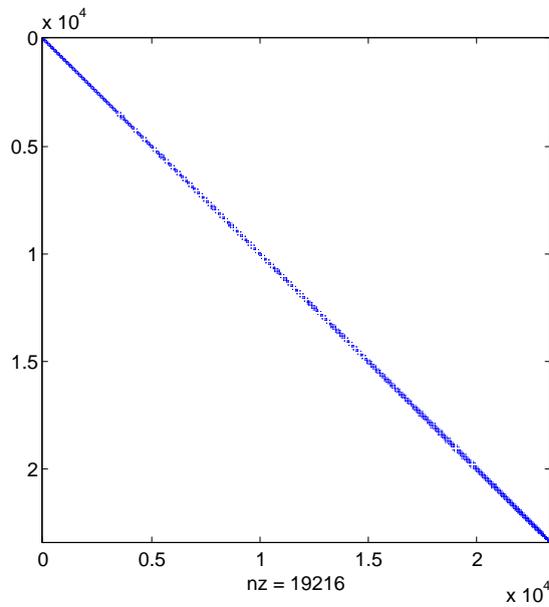
Figure 5.3.: Test Case No. 1: Structural-acoustic damping matrix sparsity plot for T_{ld} damping model.

Figure:[5.6]. It can be observed that the amplitude of displacements decrease with increasing frequency. This is as expected, since the frequency dependent damping specified, increases linearly with increasing frequency.

The sparsity plot of the stiffness and the mass matrix obtained by reading the matrices using MATLAB (Matlab 2006) for coupled structural-acoustic problem is shown in Figures:[5.4,5.5][2]. Here nz represents the number of non-zero elements present in the matrix. The sparsity plot for the coupled higher dimensional damping matrix is shown in Figure:[5.3] for T_{ld} damping model. It can also be clearly observed that the number of entries in the damping matrix is much lower than the mass matrix or the stiffness matrix.

---

[2]In MATLAB, the command *spy(X)* plots the sparsity pattern of the given matrix X.
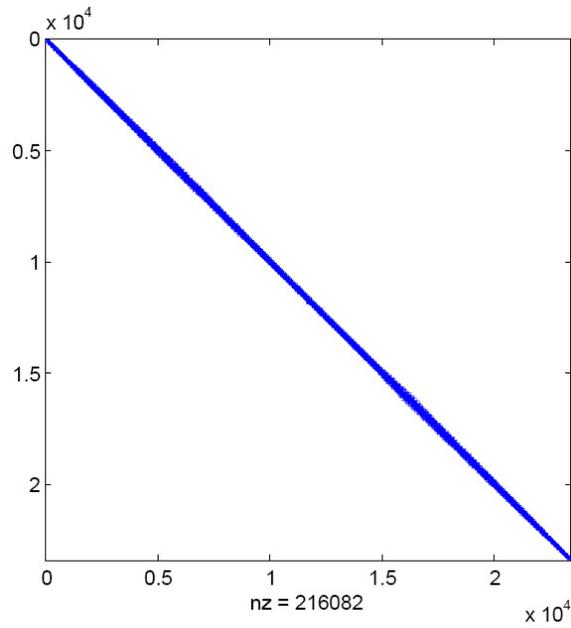
Figure 5.4.: Test Case No. 1: Coupled structural-acoustic stiffness matrix sparsity plot.
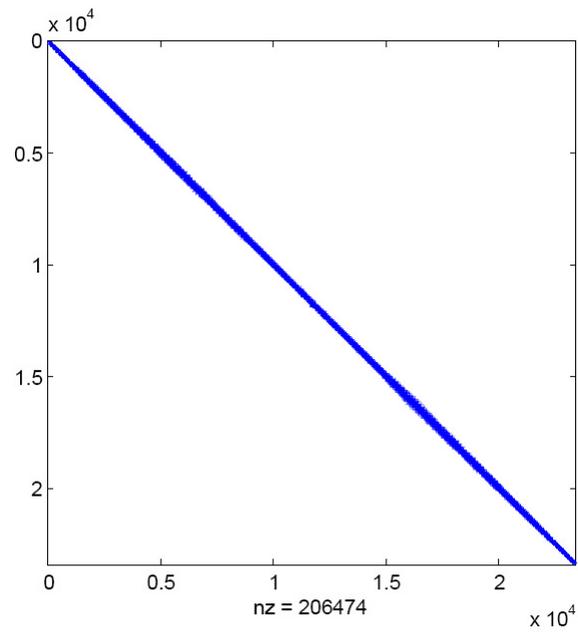

Figure 5.5.: Test Case No. 1: Coupled structural-acoustic mass matrix sparsity plot.
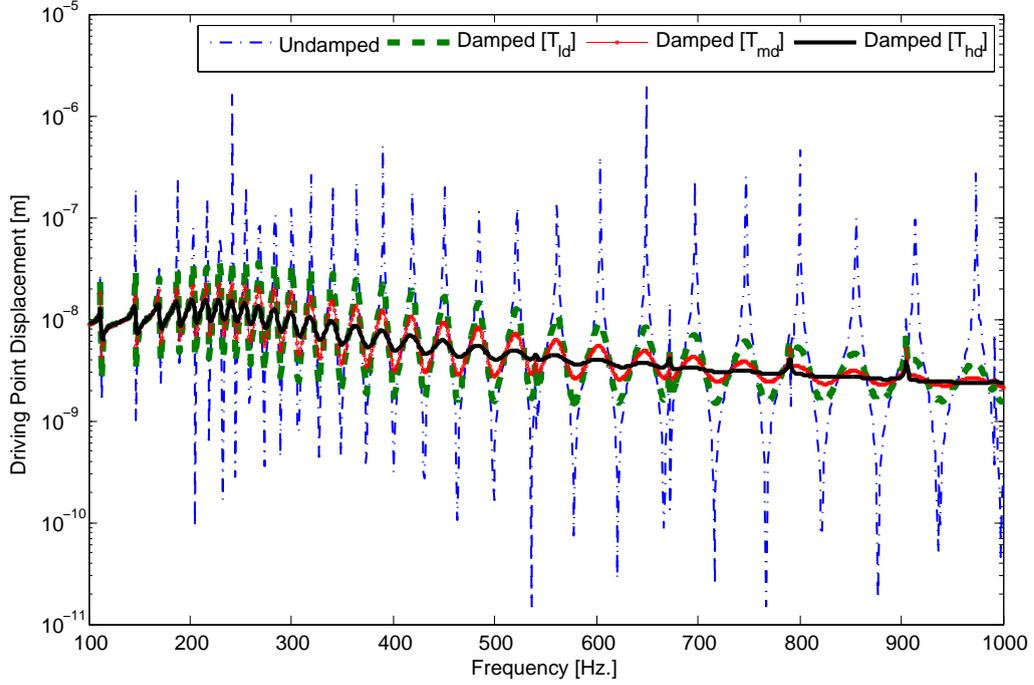
Figure 5.6.: Test Case No. 1: A comparison between ANSYS predicted driving point displacements for damped models described in Table:(5.2).

5.1.1. Computational Results and Discussion

The receptance transfer function (normal structural displacement over input structural force) and the acoustic transfer function (cavity pressure over input structural force) at the centre of the fluid domain predicted by ANSYS Direct and One-Sided Arnoldi projection are shown in Figures:[5.8,5.9][3]. A comparison of local error quantities defined by Equation:[4.93], for the OSA and TSA projection for nodal pressure and driving point displacement amplitudes are shown in Figures:[5.10,5.11]. Further, the respective error quantities for models expanded using different expansion points is shown in Figure:[5.12]. For the convergence models presented in Equations:[4.94a,4.94b], the start frequency (101Hz) and end frequency (1000Hz) are considered as inputs. Figures:[5.13,5.14] show the convergence pattern for ROMs via OSA and TSA based projection framework.

---

[3]Throughout this thesis, the displacement (receptance) and pressure (noise) transfer functions (NTFs) are illustrated using log to the base 10.

The computational times required to solve the coupled model via ANSYS direct method for all defined substeps and by employing order reduction via the Arnoldi process is shown in Table:[5.4]. The generation of the reduced order model (ROM), consisted of four different steps. First, the higher dimensional model was generated in ANSYS, and an ANSYS Static solution , combined with partial solve (ANSYS 2005) is issued to write out the relevant structural-acoustic database files. Next, an open source C++ code *dumpmatrices* (Rudnyi and Korvink 2006) was used to extract the higher dimensional mass and stiffness matrices. The higher dimensional model was then read using Mathematica (Wolfram 2003), and order reduction and projection performed via the Arnoldi process. The harmonic analysis and the error parameter computations (and therefore the convergence models) of the reduced system was performed using LU decomposition in Mathematica/Matlab (Matlab 2006) environment. The split computational times are shown in Table:[5.5].

The undamped computations described in this thesis were performed on a Windows XP, Pentium 4, 3GHz, 2GB RAM machine [Me1]. The linearly damped computations described in this thesis were performed on a Windows XP, Pentium 4, 3.2GHz, 2GB RAM machine [Me2]. Note that the computational times in the tables may slightly change according to the condition of the computer and hardware parameters such as the reading and writing rates of the hard disk drives and the number of processes running during the analysis.The *bench*[4] calculation for all three machines [Me1, Me2, Me3] used for this test case are shown in Table:[A.1], Appendix:(A).

The computational times for the projections and forced response analysis via AMLS and CL algorithms performed using [Me3] are shown in Table:[5.6]. It can be

---

[4]For comparison of performance between different machines, the thesis makes use of the MATLAB command **bench (Y)** which solves a stack of standard problems (such as LU, FFT, Sparse) *Y* times to determine the machine speed. Throughout out this work, *bench(10)* is used - values of which are later averaged.

observed that if one ignores the time required for matrix extraction and model construction from the OSA computation (which can be easily achieved in a commercial FE environment), the time required for the OSA computation is in fact smaller (82 s) than the AMLS method (131 s)[5]. It can also be seen that the Two-sided methods are also competitive in terms of computational time when compared to the AMLS method. The efficiency of the AMLS method seems to be nullified by the extraction of extremely higher number of acoustic modes (up to 4500Hz. - 58 structural and 110 fluid modes) to achieve acceptable solution state convergence. Note that this structural-acoustic test case is *strongly coupled* due to the presence of a heavy density fluid. It can also be observed (simply by visual comparison of the transfer functions) that the AMLS, CL procedures generates solution states (ABAQUS 2005) which are far less accurate than the Arnoldi based projection formulations.

The performance of the AMLS method depends on a number of factors (Yang 2005): the number of partitioning levels, the number of modes selected from each substructure, the choice of method for solving the final projected problem. Among these, the number of modes selected from each substructure is very important. In many cases, it could also turn out that most of the sub structure modes do not make a significant contribution to the approximation of the desired eigenvector. In order to increase the accuracy of the approximation, one naturally tends to compute more number of eigenvectors for modal projections. However, due to the inherent formulations of the AMLS method, the accuracy improvement would be negligible whilst the cost of solving the projected eigenvalue problem becomes significantly higher (Yang et al. 2005; Gao et al. 2005). This could possibly explain the reason for the higher computational time required by the AMLS method for this benchmark problem.

---

[5]Note that the CL, AMLS computations were performed using a compiled Fortran/C++ code and the OSA, TSA Arnoldi computations were performed in a Mathematica/Matlab environment.

Table 5.3.: Arnoldi expansion and input parameters for the undamped benchmark test case.

Method	Expansion Point(s)	Input Subspace	Output Subspace
OSA	750Hz	$\mathcal{K}_q^r(A, g)$	–
TSA[1]	750Hz/750Hz	$\mathcal{K}_q^r(A, g)$	$\mathcal{K}_q^l(A, L)$
TSA[2]	250Hz/750Hz	$\mathcal{K}_q^r(A, g)$	$\mathcal{K}_q^l(A, L)$
TSA[3]	500Hz/1000Hz	$\mathcal{K}_q^r(A, g)$	$\mathcal{K}_q^l(A, L)$
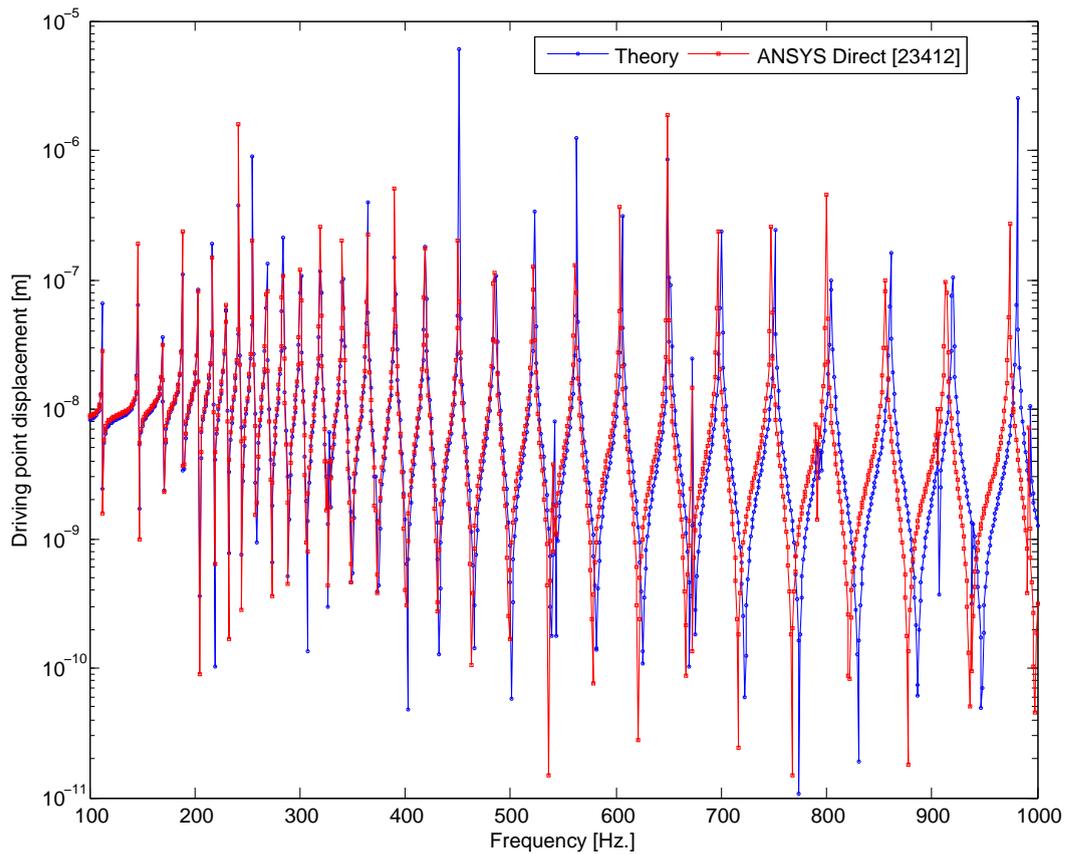
Figure 5.7.: A comparison of ANSYS direct inversion and analytical solution (Stepanishen and Cox 2000; ABAQUS 2005) for the prediction of driving point displacement.
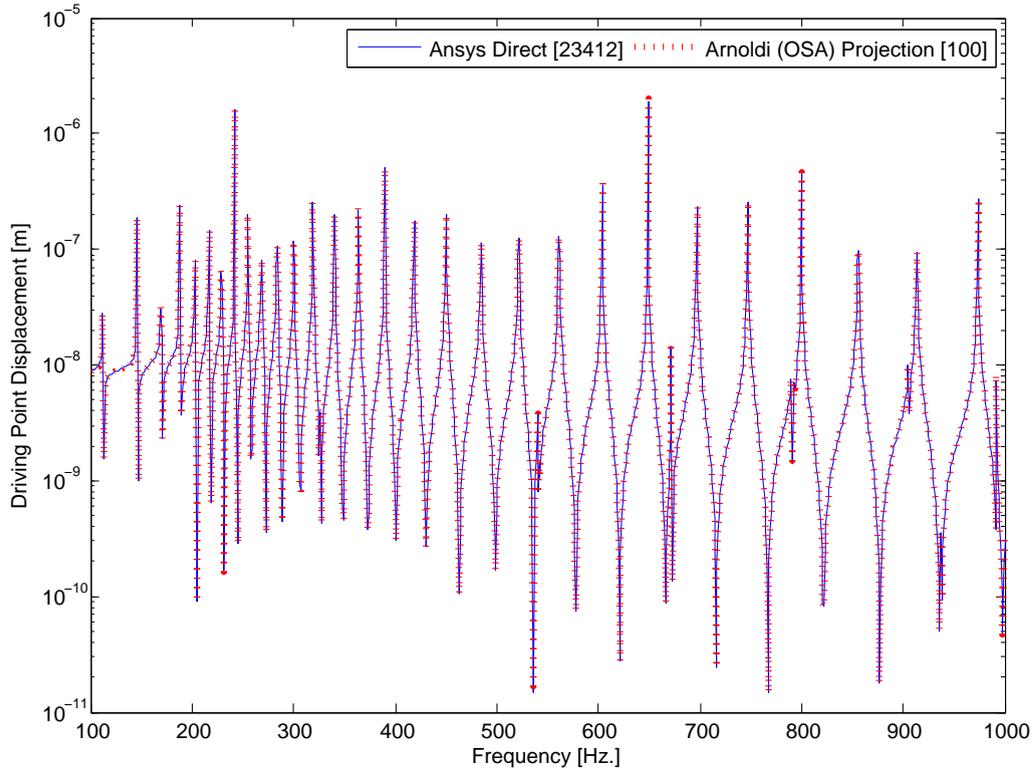
Figure 5.8.: A comparison of ANSYS direct inversion and One-Sided Arnoldi (OSA) prediction of driving point displacement.

Table 5.4.: A comparison of computational times for undamped Benchmark test case.

Test Case	ANSYS Direct	ROM via Arnoldi	Time Reduction
OSA	12413 s	286 s	97.6%
TSA[1]	12413 s	431 s	96.5%
TSA[2]	12413 s	464 s	96.2%
TSA[3]	12413 s	498 s	95.9%

Table 5.5.: A breakdown of computational times for undamped benchmark test case via One Sided and Two-Sided Arnoldi variants.

| Computational Steps: ROM via Arnoldi	Time
ANSYS Static Solution (ANSYS)	10 s
Extract Matrices (ANSYS/*dumpmatrices*)	190 s
Read Matrices (Mathematica)	04 s
Vector Computation and Projection (Mathematica)	70 s
Harmonic Analysis and Convergence (Mathematica/MATLAB)	12 s
Total: ROM via One-Sided Arnoldi	**286 s**
Read Matrices (Mathematica)	05 s
Vector Computation and Projection (Mathematica)	156 s
Harmonic Analysis and Convergence (Mathematica/MATLAB)	70 s
Total: ROM via Two-Sided Arnoldi	**431 s**
Read Matrices (Mathematica)	04 s
Vector Computation and Projection (Mathematica)	230 s
Harmonic Analysis and Convergence (Mathematica/MATLAB)	30 s
Total: ROM via Two-Sided Arnoldi	**464 s**
Read Matrices (Mathematica)	04 s
Vector Computation and Projection (Mathematica)	252 s
Harmonic Analysis and Convergence (Mathematica/MATLAB)	42 s
Total: ROM via Two-Sided Arnoldi	**498 s**
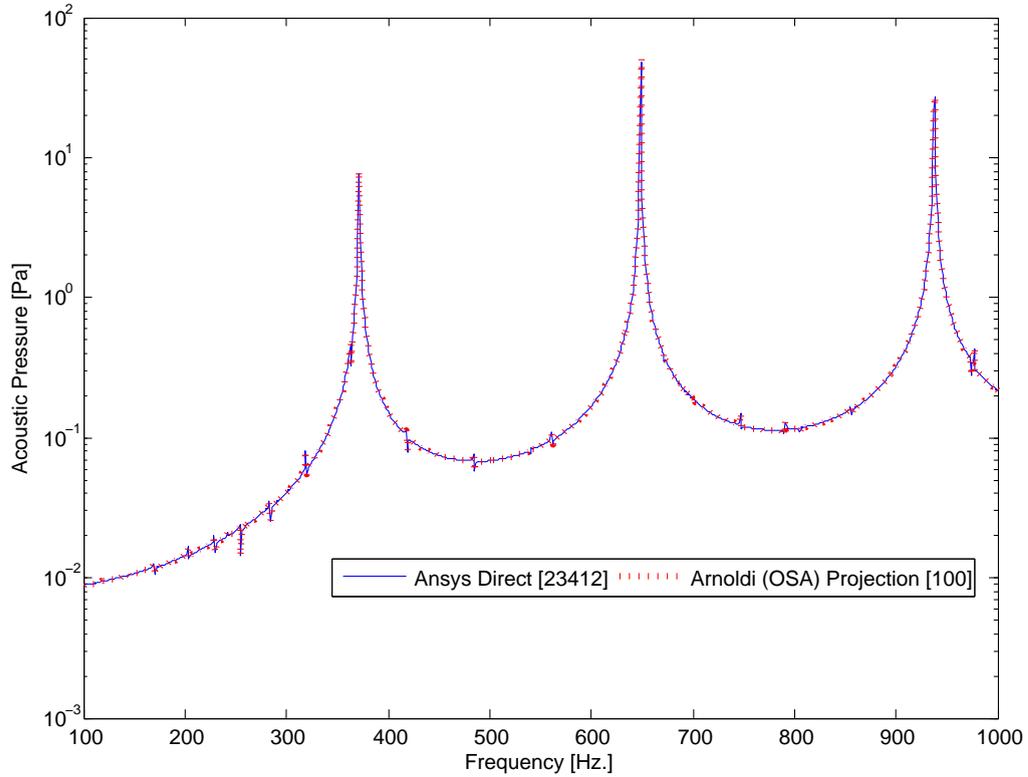
Figure 5.9.: A comparison of ANSYS direct inversion and One-Sided Arnoldi (OSA) prediction of pressure at the center of the acoustic domain.

Table 5.6.: A comparison of computational times with ABAQUS implemented (compiled Fortran/C++ code) AMLS and CL algorithms.

Method	Uncoupled AMLS	Coupled Lanczos (CL)
Pre-processing	4 s	4 s
Eigen Solution	82 s (4500Hz)	28 s (50 modes)
Forced Response	45 s	5 s
Total	131 s	33 s
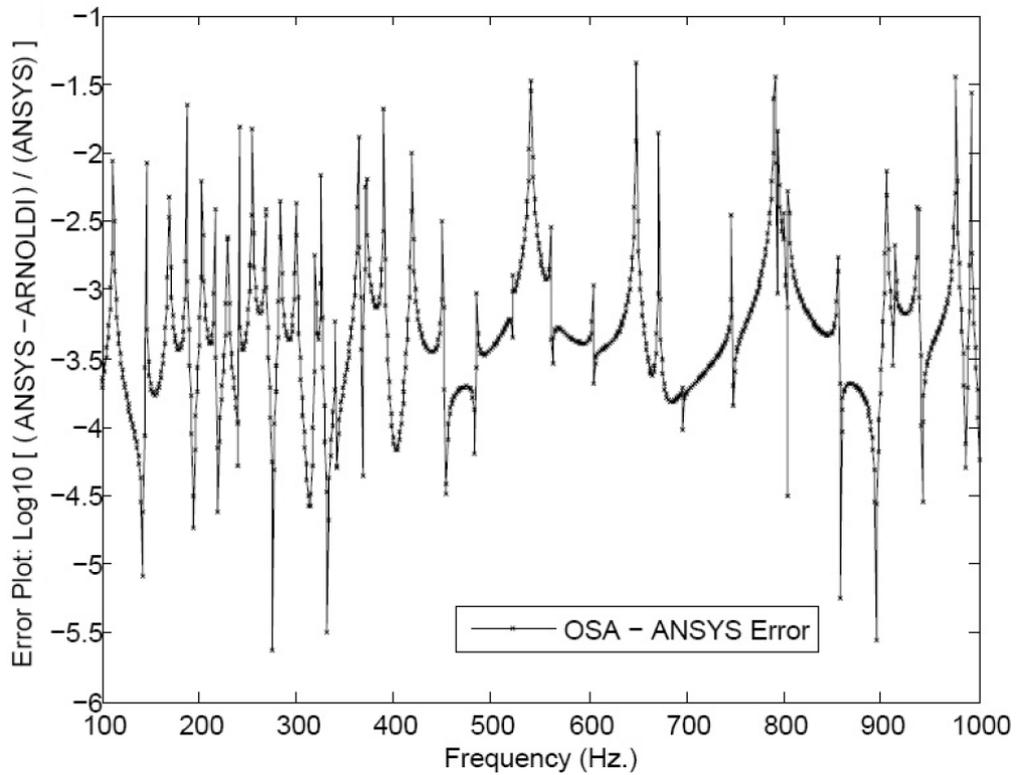
Figure 5.10.: Error Plot: ANSYS direct inversion and Arnoldi (OSA) predictions for
fluid nodal pressure at the center of the acoustic domain.
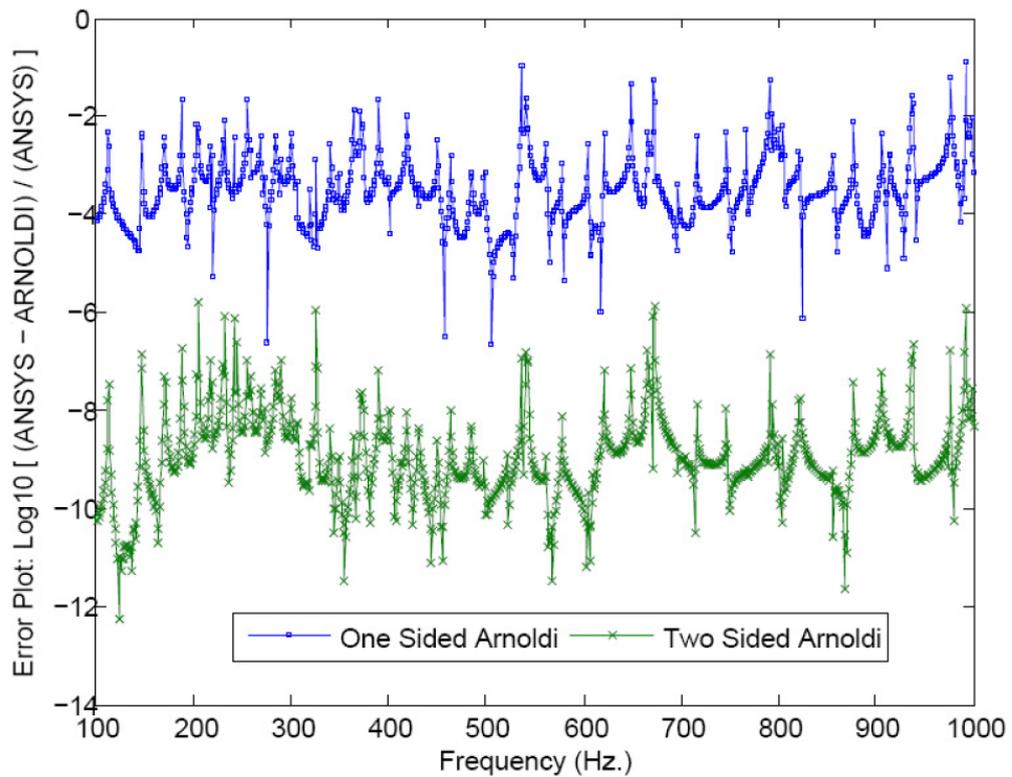
Figure 5.11.: Error Plot: ANSYS direct inversion, OSA and TSA predictions for
structural driving point displacement.

131
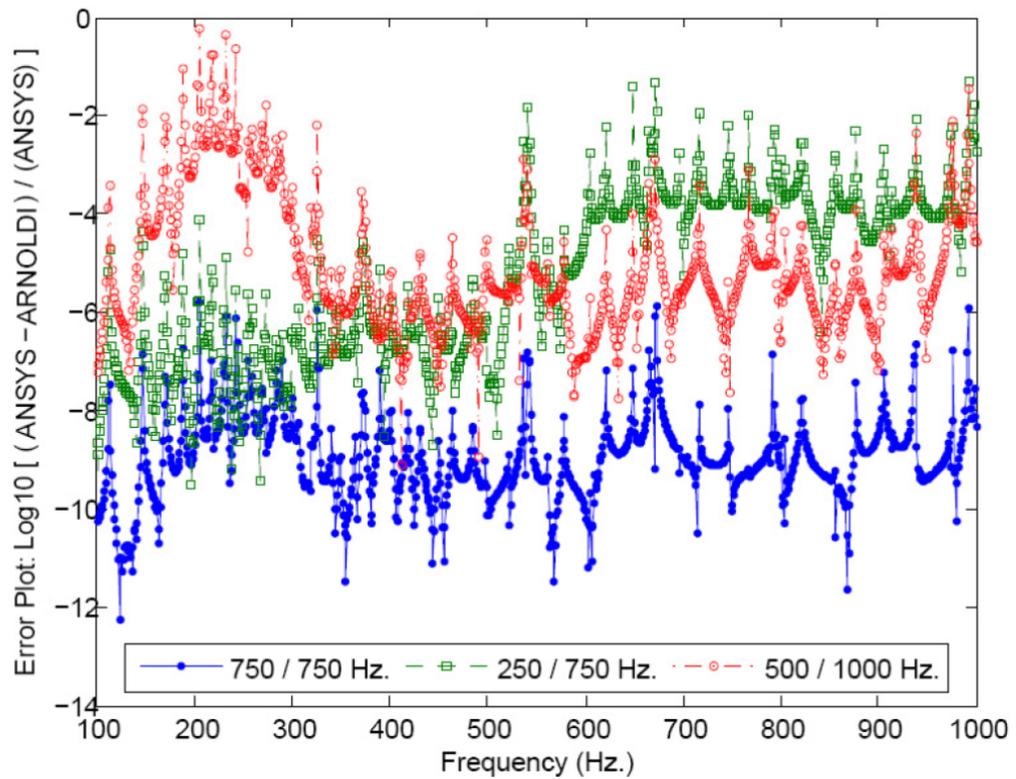
Figure 5.12.: Error Plot: ANSYS direct inversion, TSA predictions for f_{exp}=750/750Hz, f_{exp}=250/750Hz and f_{exp}=500/1000Hz for structural driving point displacement.
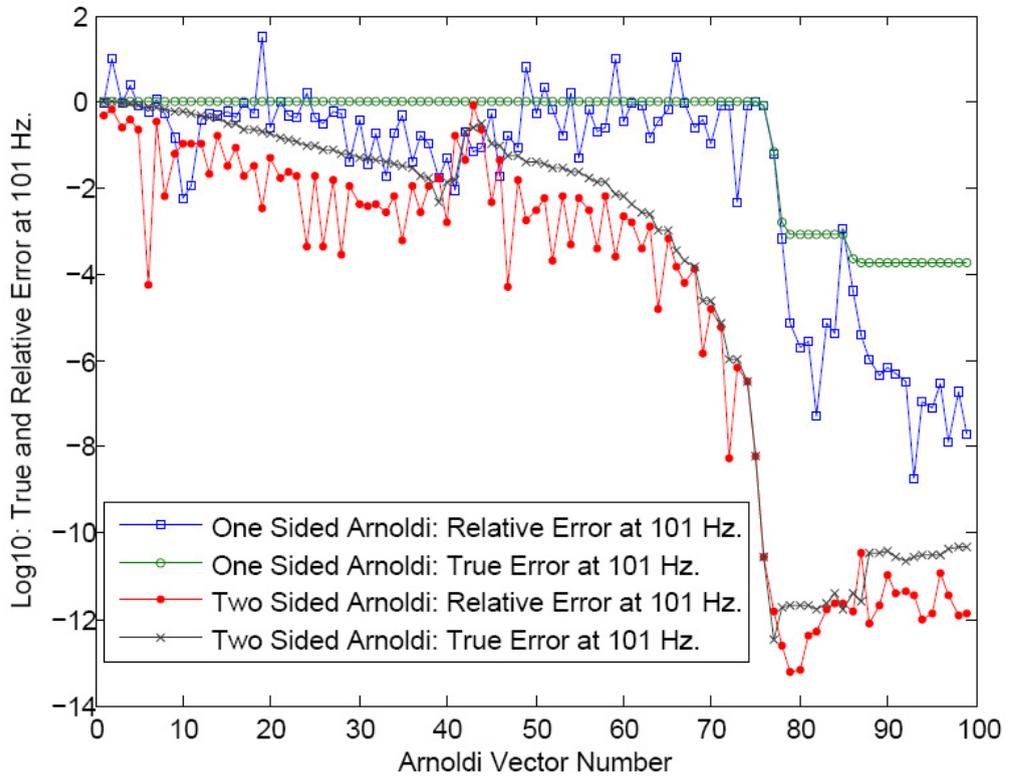
Figure 5.13.: Test Case No. 1: Convergence Plot: OSA, TSA convergence at 101Hz.
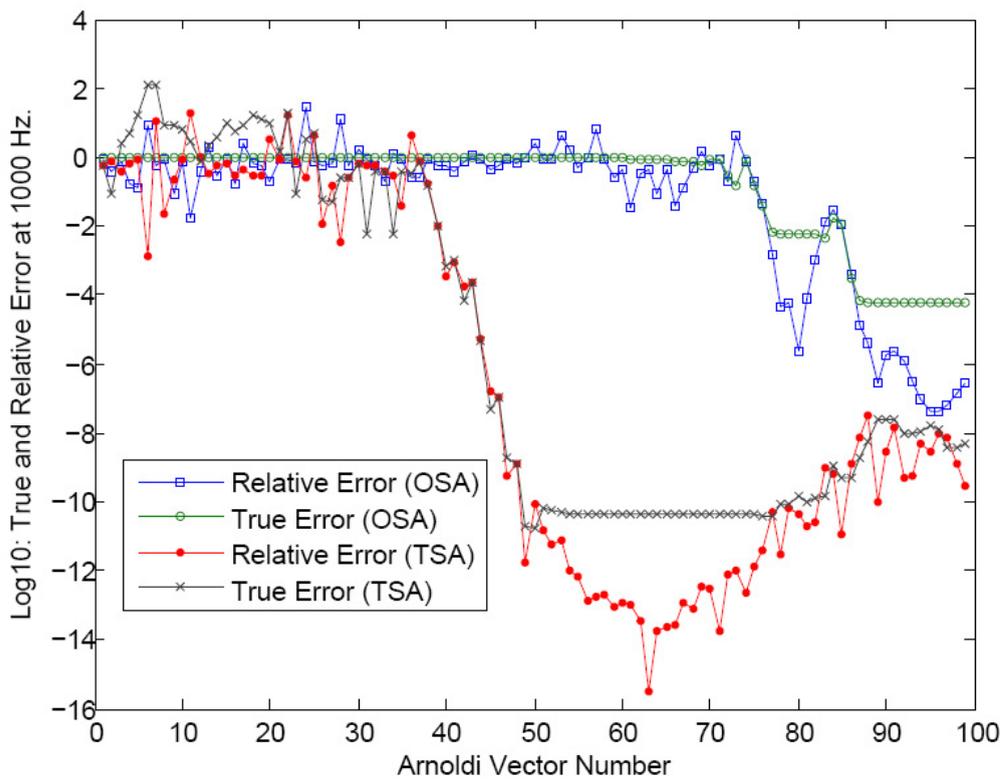
Figure 5.14.: Test Case No. 1: Convergence Plot: OSA, TSA convergence at 1000Hz.
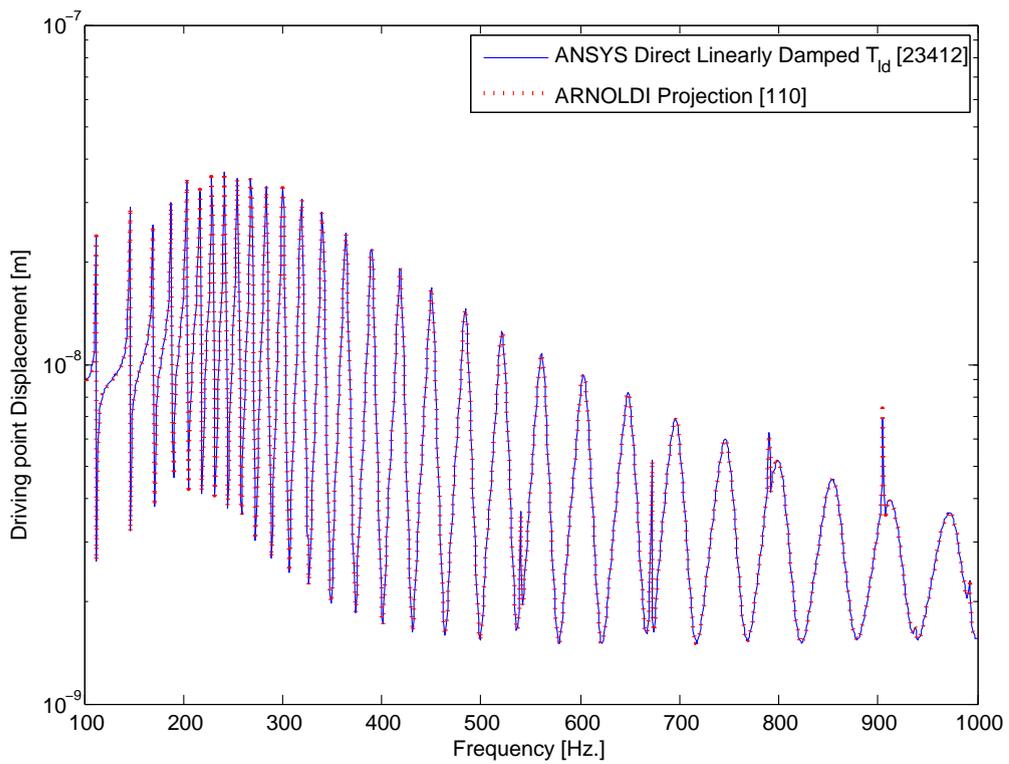
Figure 5.15.: A comparison between ANSYS direct inversion and Two-Sided Second order Arnoldi (TS-SOAR) predictions of driving point displacement for linearly damped, T_{ld} damping model.
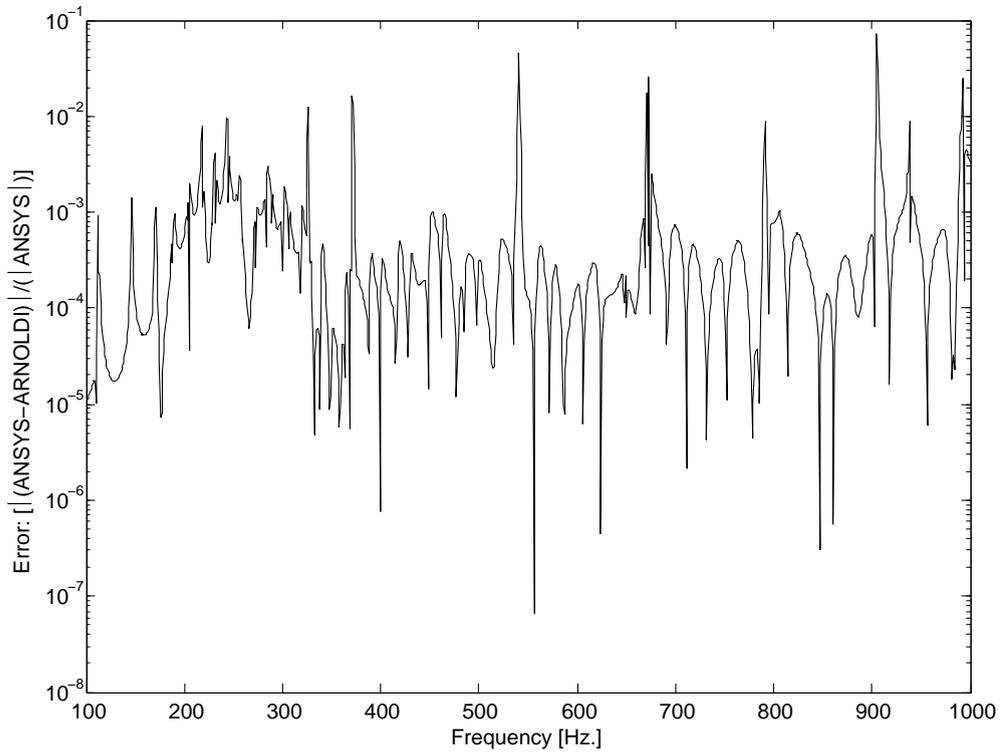
Figure 5.16.: Error Plot: ANSYS direct inversion and Two-Sided Second order Arnoldi (TS-SOAR) predictions for structural driving point displacement for T_{ld} damping model.
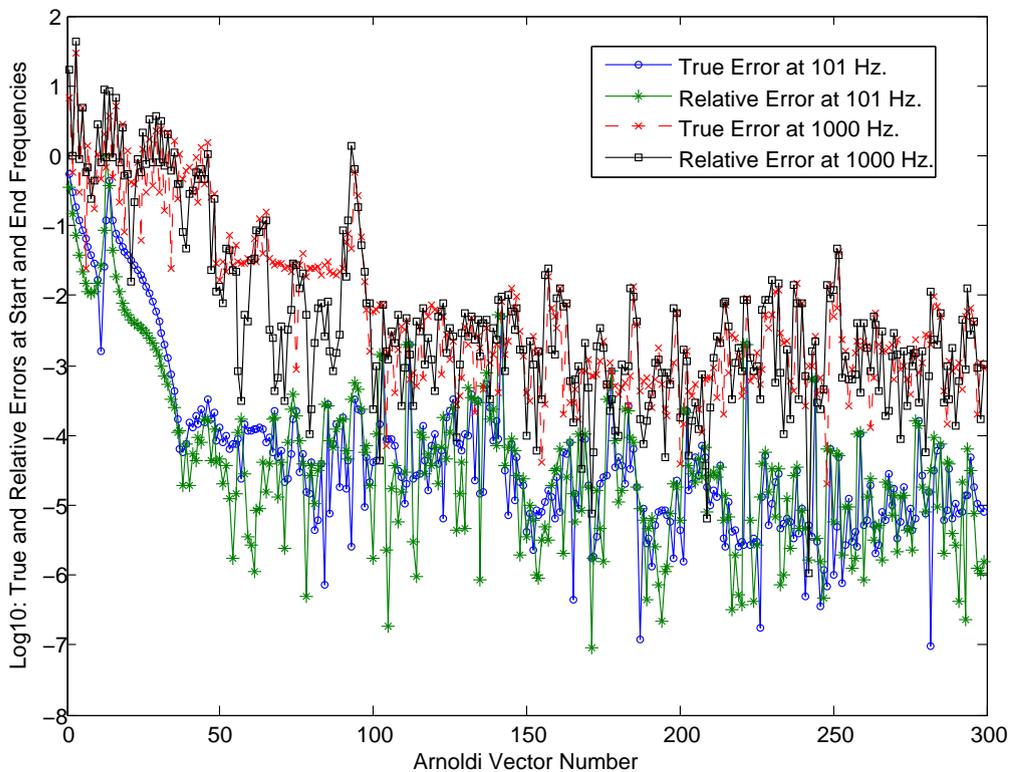

Figure 5.17.: Convergence Plot: Two-Sided Second order Arnoldi (TS-SOAR) convergence at 101Hz and 1000Hz for T_{ld} damping model.
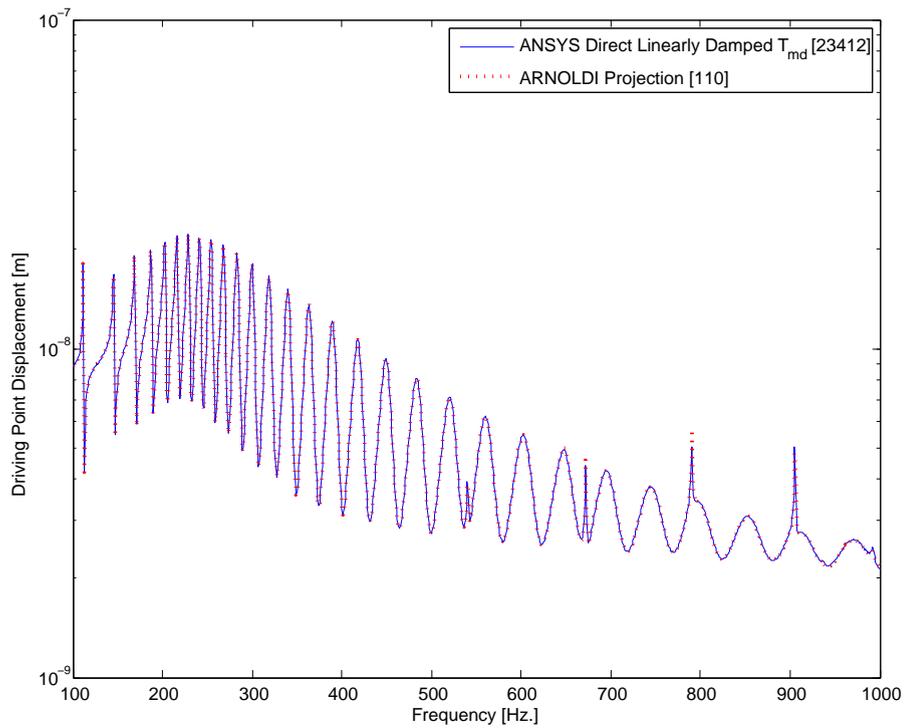
Figure 5.18.: A comparison between ANSYS direct inversion and Two-Sided Second order Arnoldi (TS-SOAR) predictions of driving point displacement for linearly damped, T_{md} damping model.
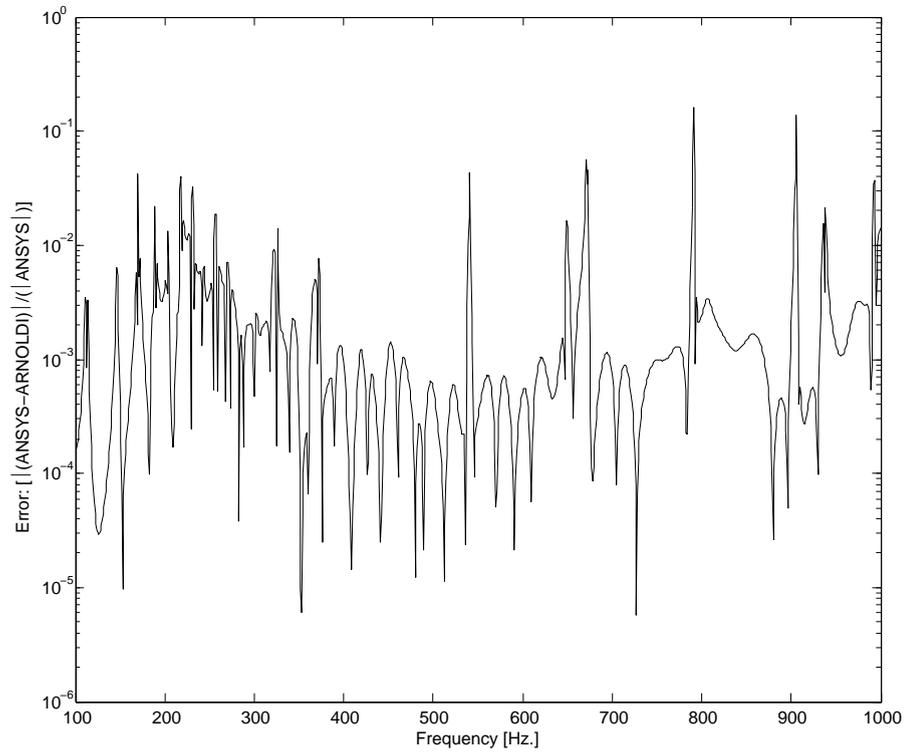
Figure 5.19.: Error Plot: ANSYS direct inversion and Two-Sided Second order Arnoldi (TS-SOAR) predictions for structural driving point displacement for T_{md} damping model.
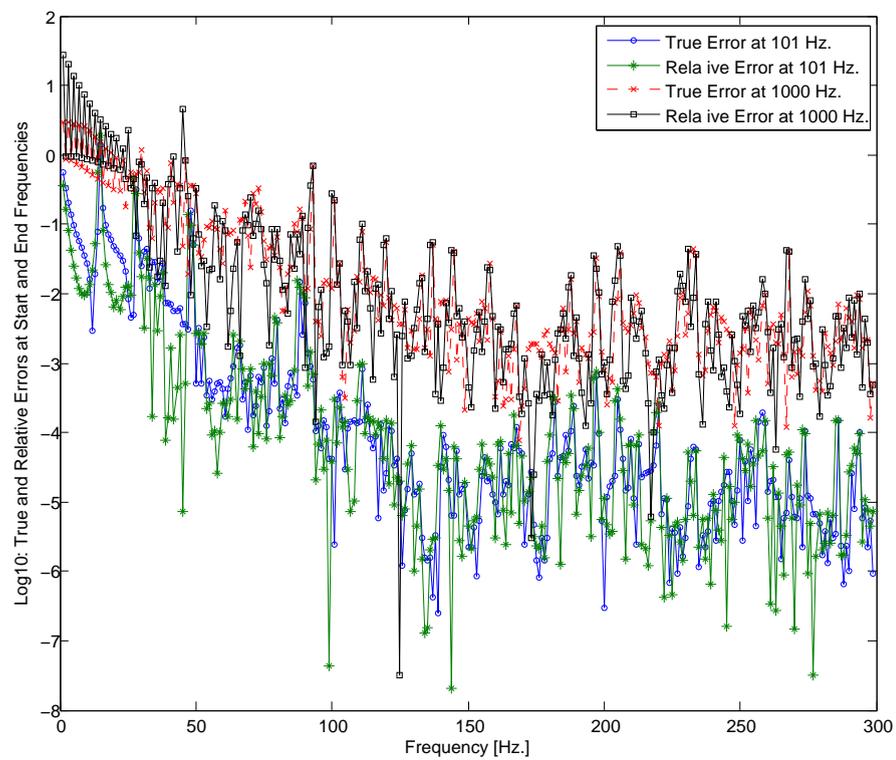

Figure 5.20.: Convergence Plot: Two-Sided Second order Arnoldi (TS-SOAR) convergence at 101Hz and 1000Hz for T_{md} damping model.
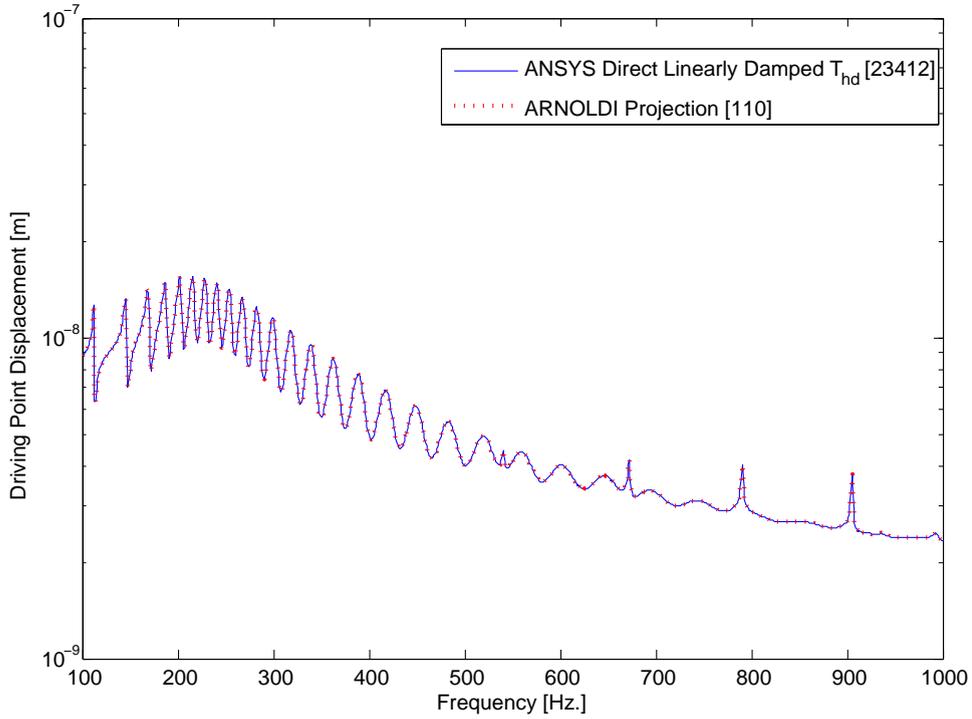
Figure 5.21.: A comparison between ANSYS direct inversion and Two-Sided Second order Arnoldi (TS-SOAR) predictions of driving point displacement for linearly damped, T_{hd} damping model.

Table 5.7.: A comparison of computational times for damped test cases.

Test Case	ANSYS Direct	ROM via TS-SOAR	Time Reduction
T_{ld}	6413 s	75 s	98.83%
T_{md}	6004 s	75 s	98.75%
T_{hd}	6319 s	176 s	97.21%

The basis vectors for matching the coupled system moments are computed by applying the Arnoldi variants, which computes the projection vectors spanning the Krylov subspace, to match the minimum and maximum number of moments of the system thereby leading to Padé type and Padé approximants. The moments in the test cases shown are matched at approximately half of the analysis range. If a Taylor series expansion is considered around a higher frequency, a reduced order
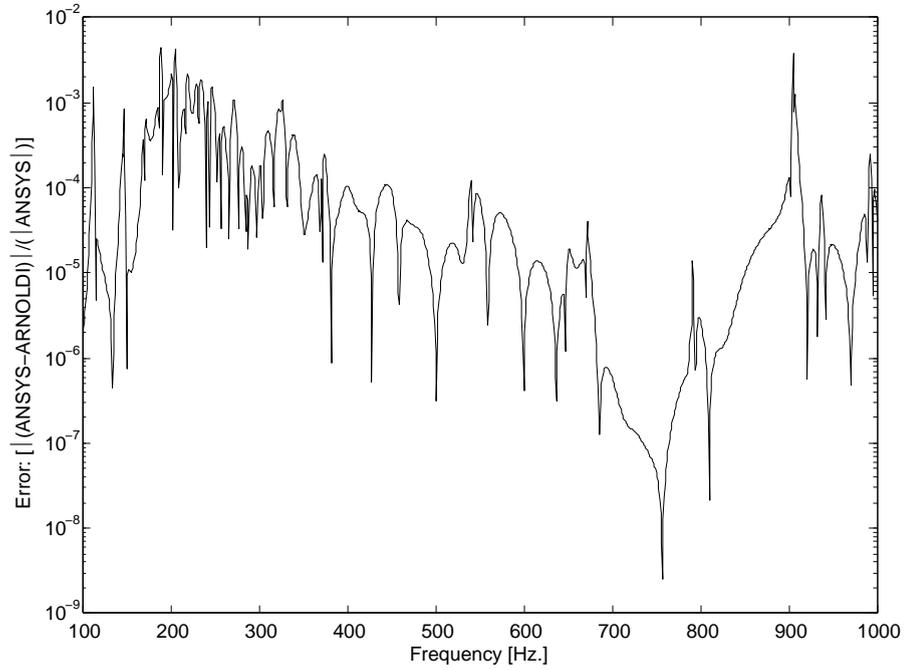
Figure 5.22.: Error Plot: ANSYS direct inversion and Two-Sided Second order Arnoldi (TS-SOAR) predictions for structural driving point displacement for T_{hd} damping model.
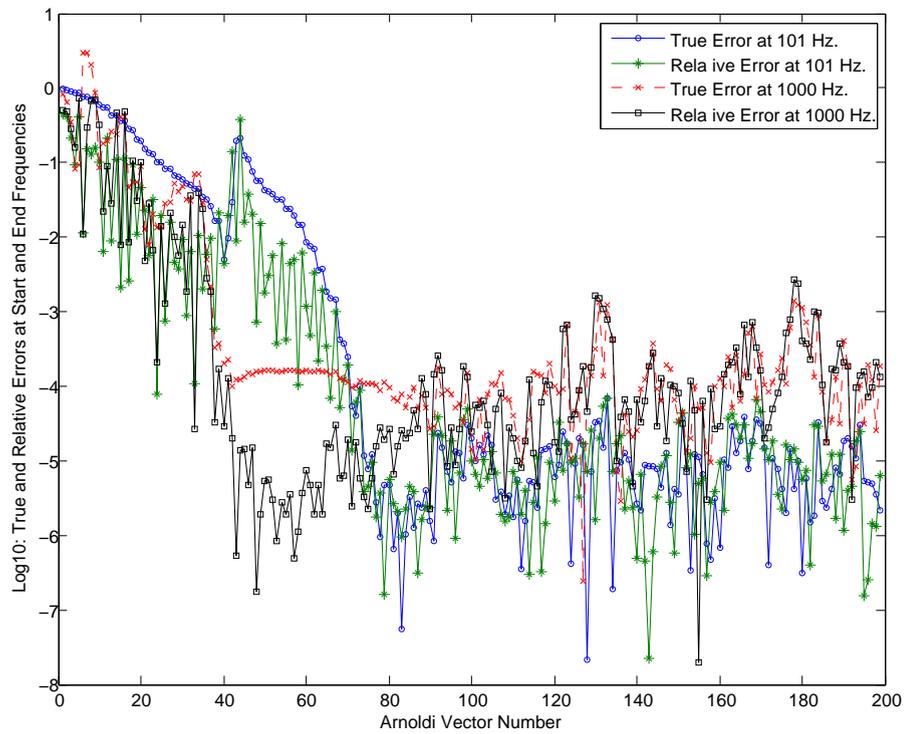

Figure 5.23.: Convergence Plot: Two-Sided Second order Arnoldi (TS-SOAR) convergence at 101Hz and 1000Hz for T_{hd} damping model.
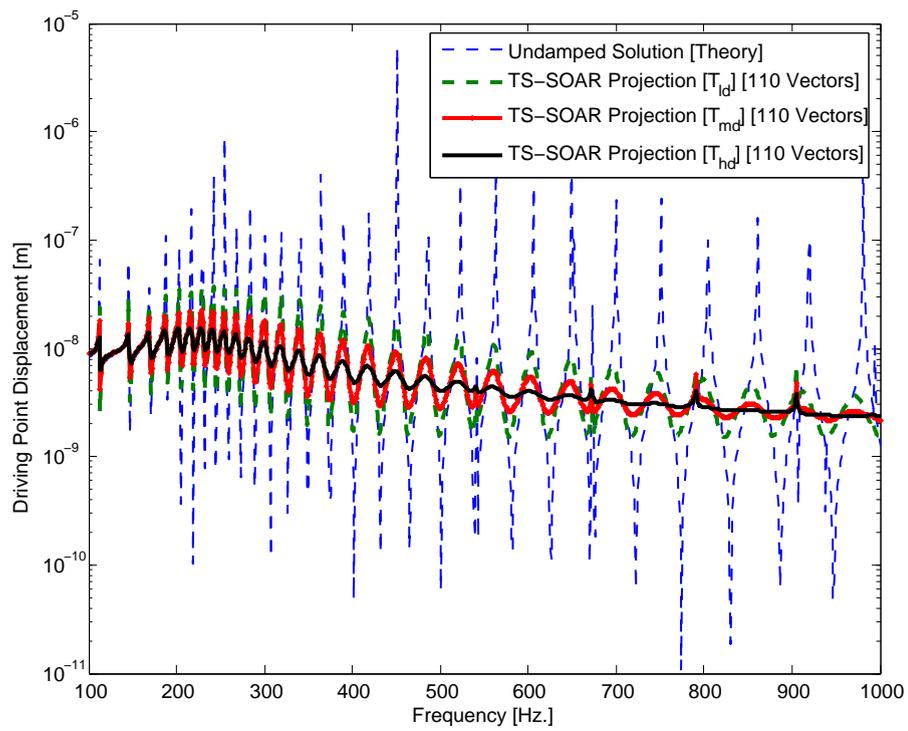
Figure 5.24.: A comparison between undamped and damped solutions obtained by analytical solution (Stepanishen and Cox 2000; ABAQUS 2005) and Two-Sided Second order Arnoldi (TS-SOAR) procedure for T_{ld}, T_{md}, T_{hd} damping models.

model could be obtained with better approximation properties around that frequency range. For the undamped test case, Figures:[5.8,5.9,5.10,5.11,5.12] indicates that very good approximation properties can be obtained by projecting the higher dimensional system to a lower dimension and matching some of the low frequency moments of the system. In the case where $2q$ moments are matched, a higher degree of accuracy is obtained at a very small additional cost. For the damped test cases, it can be observed from Figures:[5.15⟶5.23] that there is no visible difference between ANSYS predicted and Arnoldi predicted driving point displacements. A comparison between undamped (analytical modal expansion) and damped solutions obtained by and Two-Sided Second order Arnoldi (TS-SOAR) procedure for the three different linearly damped models is shown in Figure:[5.24]. Further, the convergence plots shown in Figures:[5.17, 5.20,5.23] suggest that it is not possible to increase the accuracy of the TS-SOAR approach beyond the use of 110 TS-SOAR generated vectors. This means that the reduced order system is of order 110 as opposed to the original higher dimensional model of order 23412. The computational times for the TS-SOAR process compared to the direct inversion technique in ANSYS is shown in Table:[5.7]. A significant reduction in computational time can be observed. It is worth noting that the computational time presented for this test case consists only for TS-SOAR vector generation and reduced harmonic analysis. It can be seen that in the third test case [T_{hd}], the computational time seems to be slightly more than the other two test cases. This is primarily because, different expansion points have been chosen for the analysis, and therefore, an LU decomposition depends on the expansion point used for the factorization. This means that, for this test case, an LU factorization of the higher dimensional system matrices at 750Hz is more expensive that factorization using 900Hz or 1000Hz

5.2. Test Case: 2: 3-D Plate backed air filled cavity

The second test case to be considered in this work is a simplified structure, rather than an industrial application. The test structure is a 1m × 1m × 0.01m aluminium plate, backed by a rigid walled cubic cavity of dimensions 1m × 1m × 1m. The mechanical properties of the structure are as follows: Young's Modulus E_s= 70 GPa, mass density ρ_s=2700kg/m^3 and Poisson's ratio υ=0.35. The cubic cavity is filled with air with the following properties: speed of sound $c = 343m/s$ and mass density ρ_c=1.2kg/m^3. A constant amplitude force excitation of 1N, over the frequency range from 0 - 300Hz, was applied at one of the off-center nodes of the structural FE mesh and the normal (UY) DOF's belonging to the nodes along the boundary of the aluminium plate are restrained. This is shown in Figures:[5.25,5.26]. 350 sub steps were defined for the analysis. A total of 8400 elements were used for the coupled FE model.
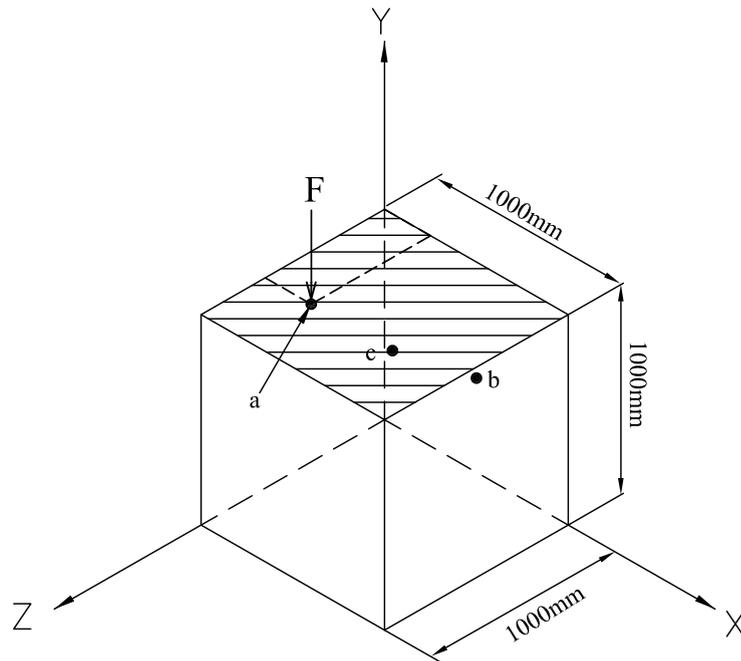

Figure 5.25.: Test Case No. 2: Plate backed cubic cavity (air filled) system. Excitation location: a=(0.25m,1m,0.65m); Measurement location(s): b=(0.75m,0.75m,0.25m), c=(0.35m,0.65m,0.30m).
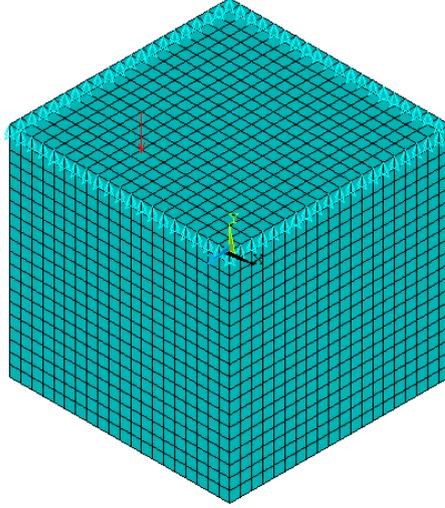
Figure 5.26.: Test Case No. 2: Coupled FE/FE model: Plate backed by a rigid walled cavity.

5.2.1. Computational Results and Discussion

For the solution via the moment-matching approach, 30 Arnoldi vectors were generated using the SISO/SICO Arnoldi process described in the previous section. The noise transfer function (Pressure/Force) at meaurement locations b and c i.e, at (0.75m,0.75m,0.25m) and (0.35m,0.65m,0.30m) inside the fluid domain were specified as outputs for the analysis. For the MOR via Arnoldi approach, three different expansion points have been chosen: $f^1_{exp} = (\omega_E + \omega_B)/4$; $f^2_{exp} = (\omega_E + \omega_B)/2$; $f^3_{exp} = \omega_E$, to analyze the effect of moment matching at different frequencies.

The superimposed noise transfer functions, obtained by ANSYS FE and MOR via Arnoldi for $f^2_{exp} = (\omega_E + \omega_B)/2$ are shown in Figures: [5.27,5.28]. It can be observed that there is no visible difference in the respective noise transfer functions between the two methods. The corresponding local error for all three expansion points and the *true* and *relative* errors are shown in Figures:[5.29,5.30] and Figure:[5.31] respectively. The convergence pattern indicates that to approximate the coupled system

to the required level of accuracy required no more than 15 Arnoldi generated vectors for approximately 1Hz and 30 Arnoldi generated vectors for 300Hz.
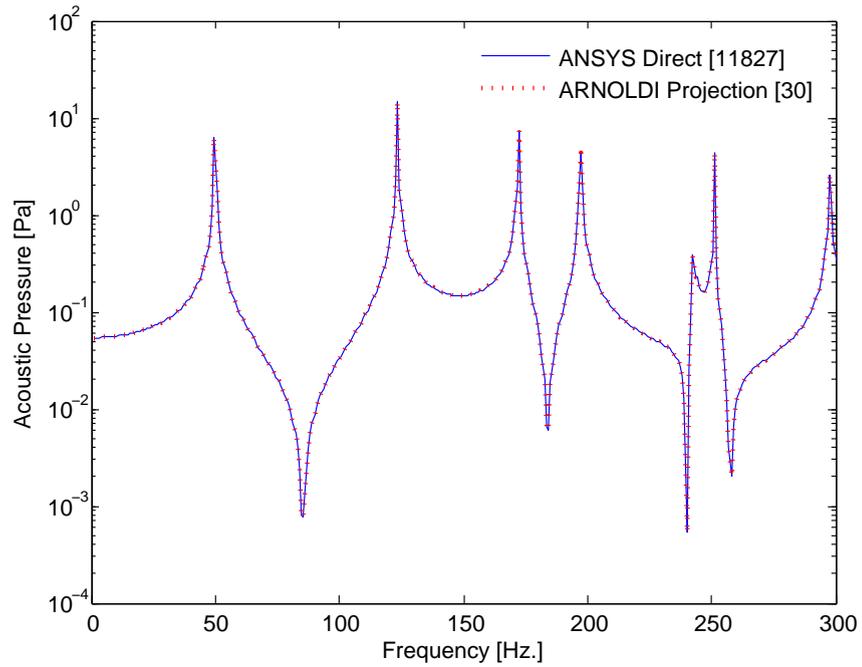
Figure 5.27.: Test Case No. 2: Predicted Noise Transfer Function using direct and moment-matching Arnoldi projection for fluid node at (0.75m,0.75m,0.25m).
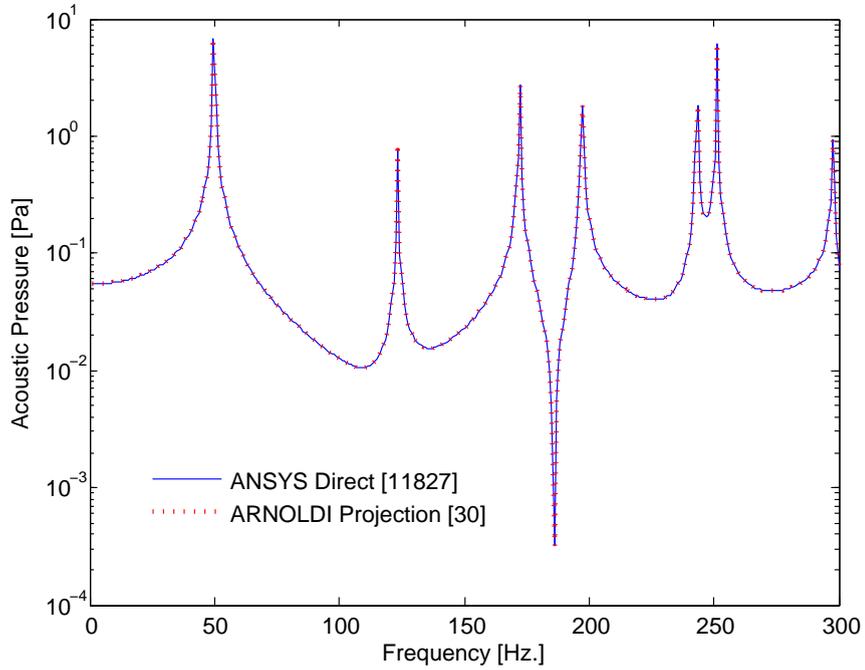
Figure 5.28.: Test Case No. 2: Predicted Noise Transfer Function using direct and moment-matching Arnoldi projection for fluid node at (0.35m,0.65m,0.3m).
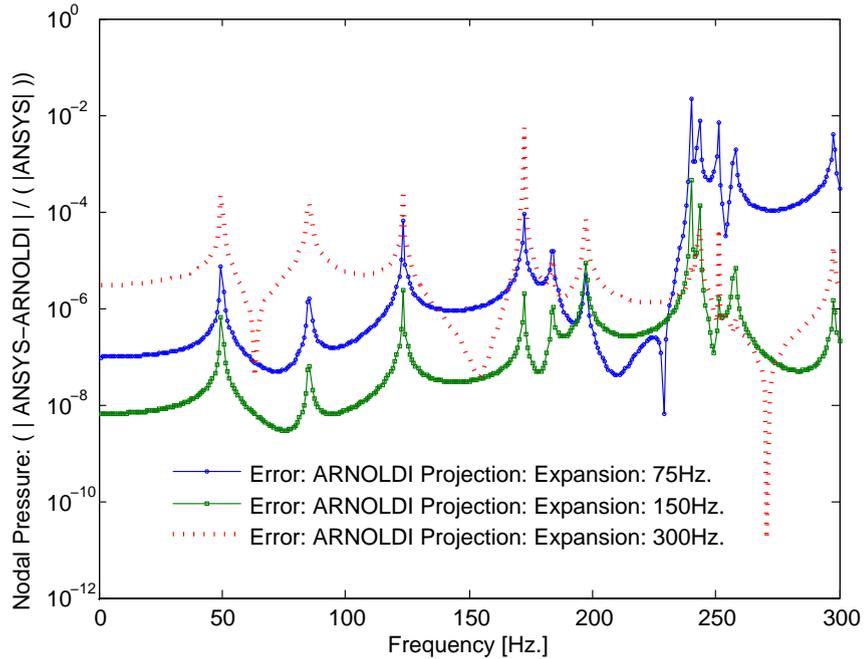
Figure 5.29.: Test Case No. 2: Noise Transfer Function error plot for fluid node at (0.75m,0.75m,0.25m) for f_{exp}=75Hz; f_{exp}=150Hz; f_{exp}=300Hz.
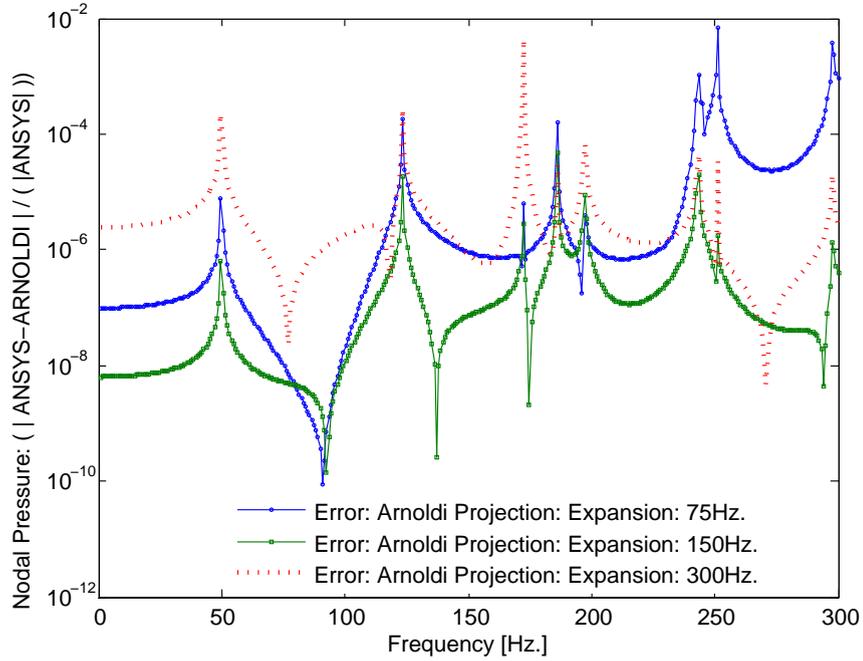
Figure 5.30.: Test Case No. 2: Noise Transfer Function error plot for fluid node at (0.35m,0.65m,0.3m) for f_{exp}=75Hz; f_{exp}=150Hz; f_{exp}=300Hz.
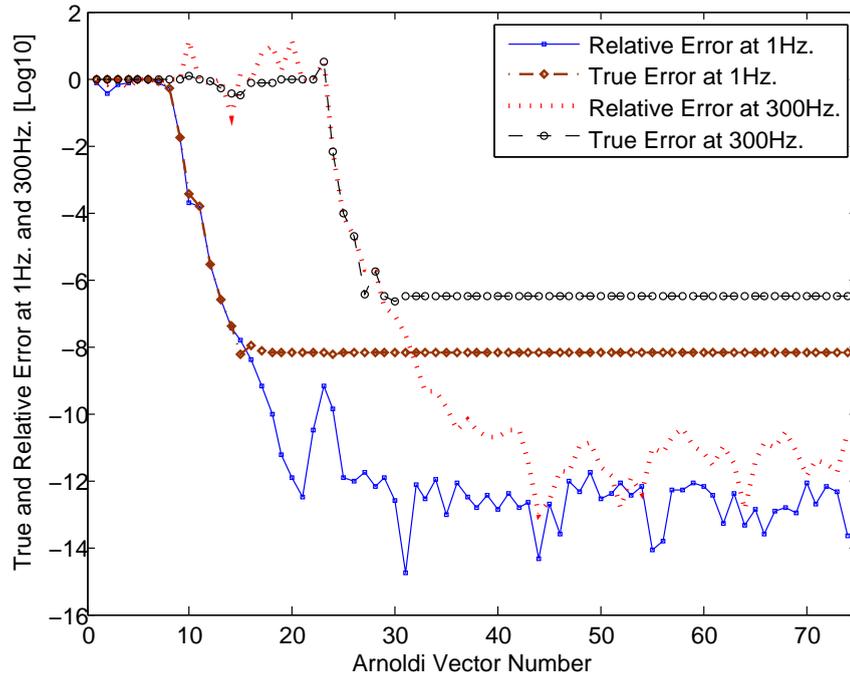

Figure 5.31.: Test Case No. 2: Convergence pattern for Arnoldi vectors at approximately 1Hz and 300Hz.

5.3. Test Case: 2.1: Reciprocity Computation and Comparison with Uncoupled Modal Coupling

The test structure is a 1m × 1m × 0.01m steel plate, backed by a rigid walled cubic cavity of dimensions 1m × 1m × 1m. The mechanical properties of the structure are as follows: Young's Modulus E_s= 200 GPa, mass density ρ_s=7800 kg/m^3 and Poisson's ratio υ=0.3. The cavity is filled with water with the following properties: speed of sound c=343 m/s and mass density ρ_c=1.2 kg/m^3. Four different damping values are chosen for the analysis (a) $\zeta = 0$ (*Undamped*) (b) $\zeta = 0.01$ (c) $\zeta = 0.02$ and (d) $\zeta = 0.03$. A constant amplitude force excitation of 1N, over the frequency range from 0 - 300Hz, was applied at one of the off-center node (0.25m,1m,0.65m) of the structural FE mesh as shown in Figure:[5.26]. Similar to the previous test case, the normal (UY) DOF's belonging to the nodes along the boundary of the aluminium plate are restrained. 350 sub steps were defined for the analysis. A total of 8400 elements were used for the coupled FE model. The Harmonic analysis of the coupled equations were solved using two approaches: (a) the direct method using the AN-SYS FE solver, which in-turn employs the LU decomposition method for all defined sub steps; and (b) MOR via the SISO/SICO Arnoldi algorithm. 30 vectors were generated using the Arnoldi algorithm described in the previous section. The noise transfer function (Pressure/Force) at the center of the box (0.5m,0.5m,0.5m) and (0.75m,0.75m,0.25m), and (0.35m,0.65m,0.30m) inside the fluid domain are specified as outputs for the analysis.

It is well known that when the external excitation of a coupled vibro-acoustic system consist of a mechanical point force (f_j) at a certain location (j) in a certain direction, and an acoustic point source (q_i) at a certain location (i), the following coupled vibro-acoustic reciprocity relationship, originally postulated by Rayleigh (1873) and later confirmed and elaborated by Lyamshev (1959) can be formulated

and applied to coupled structural-acoustic systems for both experimental and computational vibro-acoustic applications (Fahy 2003; Desmet 1998; Cornish 2000; Norris and Rebinsky 2000; Wyckaert et al. 1996):

$$\left|\frac{p_i}{f_j}\right|_{q_i=0} = \left|-\frac{\ddot{x}_j}{q_i}\right|_{f_j=0} \tag{5.1}$$

Where, f_j and p_i correspond to a structural force at location j on the structure and pressure at location i inside a cavity respectively. $\ddot{x}$ and q_i denote the structural acceleration and acoustic volume acceleration confined to the fluid domain. In words, Equation:[5.1] means that the ratio between the acoustical response p_i at location i within the cavity, and a structural force excitation f_j at location j on the structure is equal to the ratio between the acceleration response $\ddot{x}_j$ measured at location j, in the direction of applied force f_j, and an acoustic excitation q_i.

In terms of coupled structural-acoustic modeling, this simply means that the acoustic pressure p_i at location i within the cavity, caused by a unit point force excitation f_j at location j on the structure and the structural acceleration $\ddot{x}_j$ measured at location j, in the direction of applied force f_j, caused by a unit point source acoustic excitation at location i, must have the same amplitudes but opposite phases.

Therefore, to demonstrate the accuracy of the proposed Arnoldi based reduced order modeling technique, the vibro-acoustic reciprocity relation*s* are verified for this test case. Two dynamic transfer functions, namely, the structural accelerence response to unit acoustic excitation (Volume Acceleration) and the acoustic pressure response to a unit structural excitation (Force) for the problem described above is considered. While the unit structural point force location remains the same, the fluid node corresponding to (0.5m,0.5m,0.5m) is chosen for subsequent unit acoustic excitation. To enable this vibro-acoustic reciprocity computation, two different

148

models are set up and solved using the direct approach in ANSYS and MOR via the Arnoldi based projection formulation.

The sparsity plot of the globally assembled higher dimensional stiffness and the mass matrices for ζ=0.01 are shown in Figures:[5.32,5.33] respectively. Here, *nz* represents the number of non-zero elements present in the matrix. It is worth noting that, the higher dimensional matrix is sparse, and the reduced matrix obtained via the projection of Arnoldi vectors results in densely populated system matrices.
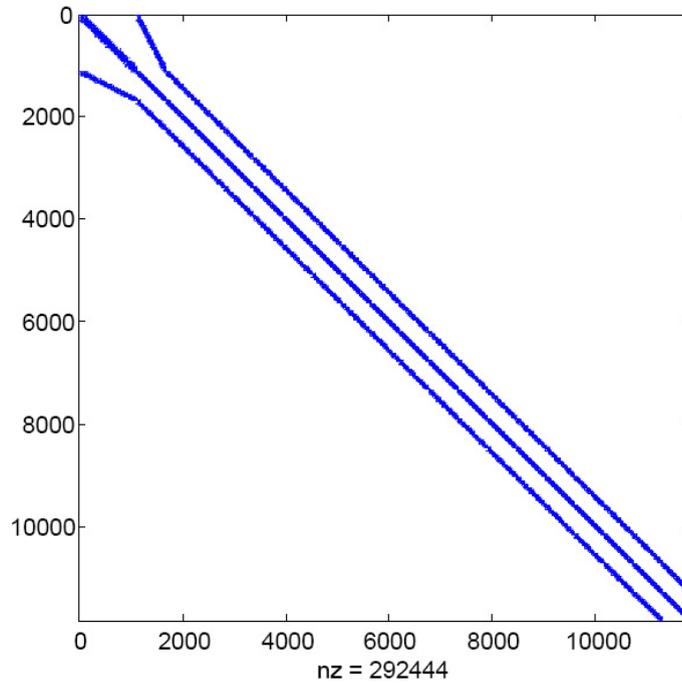
Figure 5.32.: Test Case No. 2.1: Globally Assembled Higher Dimensional Stiffness Matrix Sparsity Plot for ζ=0.01.

In addition to the direct inversion technique, for this test case, the results from an uncoupled modal approach are also utilized for solution accuracy comparison purposes. This well known uncoupled modal approach (or the so called *modal coupling technique*) (Lyon and Maidanik 1962; Fahy 1969; Pope 1971; Dowell et al. 1977), presented also in the book by Fahy (1985) is a popular dimension reduction method
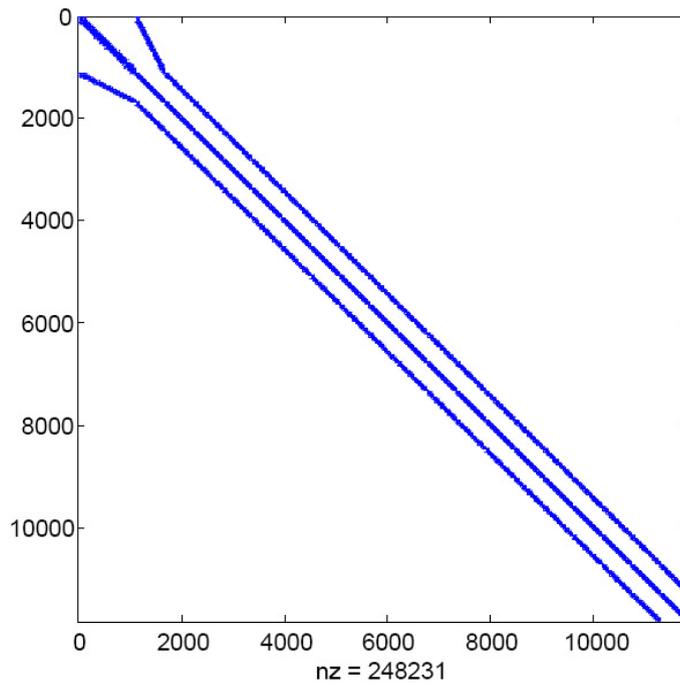
Figure 5.33.: Test Case No. 2.1: Globally Assembled Higher Dimensional Mass Matrix Sparsity Plot for ζ=0.01.

in coupled structural-acoustics. This uses the *in vacuo* modal responses of a structure and hard walled acoustic modal response of a cavity and combines them into a coupled vibro-acoustic response. Therefore, for this test case, a comparison between two reduced order models: ROM via one-sided Arnoldi (OSA) approach and ROM via the well known uncoupled modal coupling are performed[6]. A short discussion of the uncoupled modal approach is given in Appendix:(B) and in Puri et al. (2007).

---

[6]This *modal coupling* part of the work presents results from a collaboration between The University of Adelaide, Australia, who have experience with modal coupling (Cazzolato 1999), and Oxford Brookes University, UK, who have applied Arnoldi based reduced order modeling techniques to fully coupled structural-acoustic analysis and optimization problems (Puri et al. 2006; Puri et al. 2007). Some of the results discussed in this section can also be found in Puri et al. (2007).

5.3.1. Computational Results and Discussion

The reciprocity transfer functions, namely, the structural accelerence over unit acoustic excitation (volume acceleration) and cavity pressure over input force obtained by *moment matching* via the Arnoldi process for $\zeta=0,\zeta=0.01,\zeta=0.02,\zeta=0.03$ are shown in Figures:[5.34,5.35,5.36,5.37]. The noise transfer functions (cavity pressure over input force) corresponding to fluid nodes (0.5m,0.5m,0.5m),(0.75m,0.75m,0.25m) and (0.35m,0.65m,0.30m) obtained by using the direct inversion method in ANSYS and moment matching via the Arnoldi process for $\zeta=0.01,\zeta=0.02$, $\zeta=0.03$ are shown in Figures:[5.38,5.39,5.40] respectively. The corresponding *local error* plots obtained using Equation:[4.93] for the structural and fluid nodes are shown in Figures:[5.41,5.42,5.43,5.44]. The convergence plots shown in Figures:[5.45,5.46,5.47] indicate that a maximum of 30 Arnoldi vectors are required for the solution state convergence.

The computational times required to solve the coupled model via ANSYS direct method for all defined substeps and by employing order reduction via the Arnoldi process are shown in Table:[5.8]. In the case of a structurally damped model, the complex numbers relating to the structural damping are extracted. The higher dimensional model is then read using Mathematica (Wolfram 2003), and order reduction and projection performed via the Arnoldi process. The harmonic analysis and convergence of the reduced system is then performed using LU decomposition in the Mathematica/Matlab (Matlab 2006) environment. The split computational times are shown in Table:[5.9].
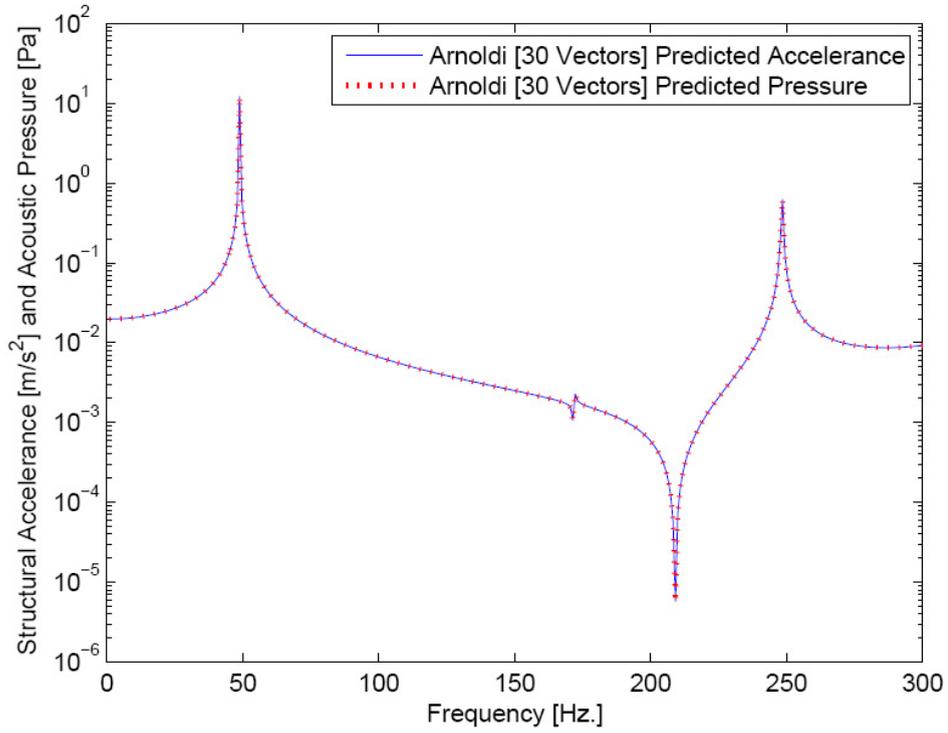
Figure 5.34.: Moment matching Arnoldi projection predicted vibro-acoustic reciprocity transfer functions for structural node at (0.25m,1.0m,0.65m) and fluid node at (0.5m,0.5m,0.5m) for ζ=0.
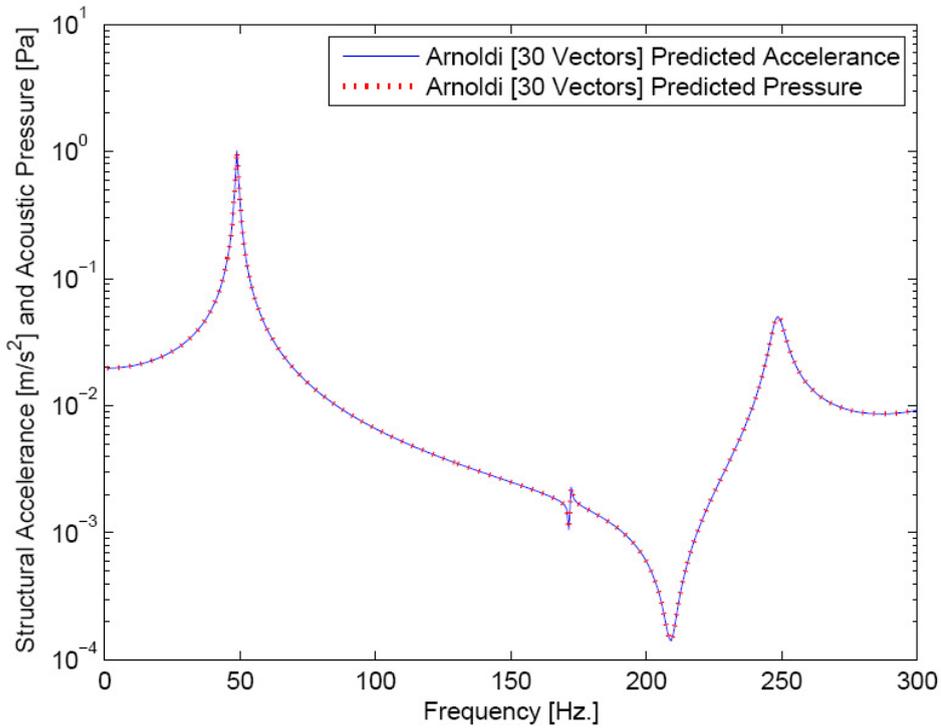
Figure 5.35.: Moment matching Arnoldi projection predicted vibro-acoustic reciprocity transfer functions for structural node at (0.25m,1.0m,0.65m) and fluid node at (0.5m,0.5m,0.5m) for ζ=0.01.
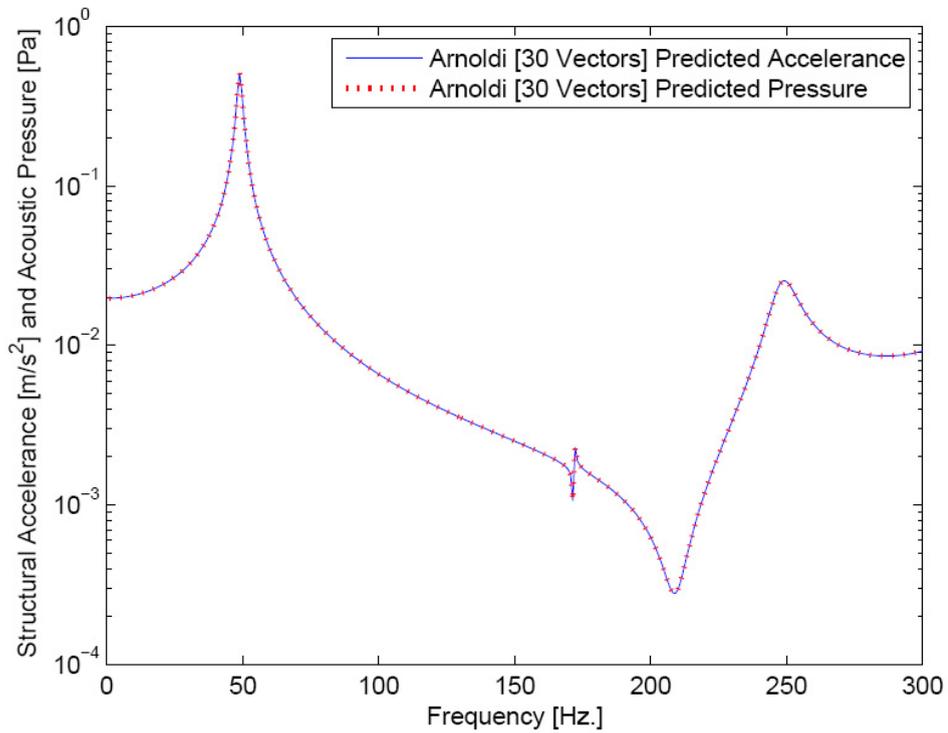
Figure 5.36.: Moment matching Arnoldi projection predicted vibro-acoustic reciprocity transfer functions for structural node at (0.25m,1.0m,0.65m) and fluid node at (0.5m,0.5m,0.5m) for ζ=0.02.
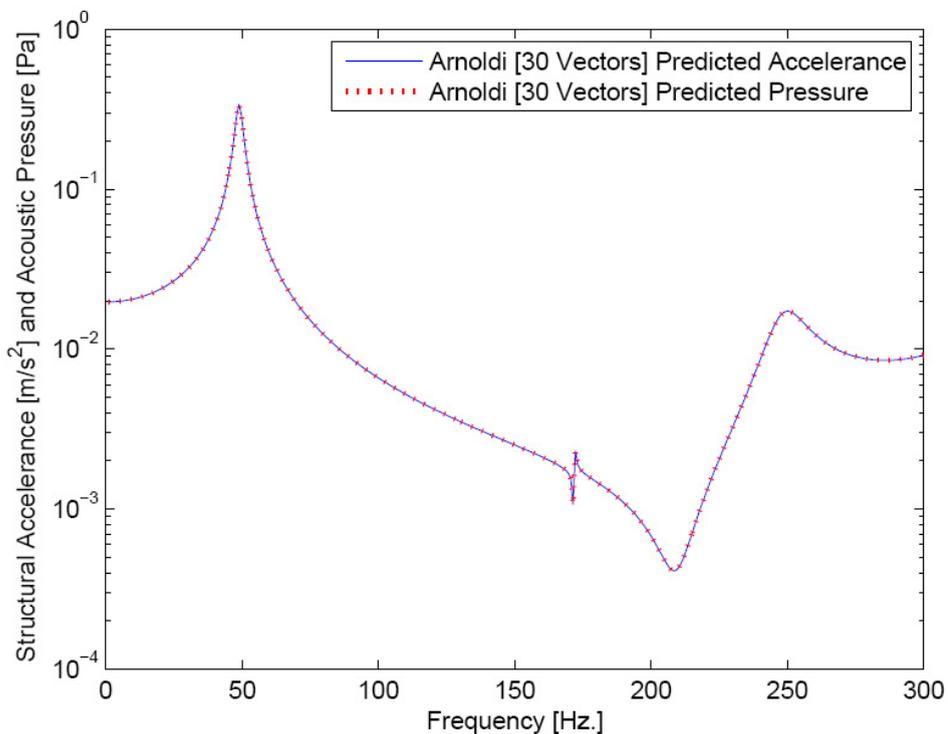

Figure 5.37.: Moment matching Arnoldi projection predicted vibro-acoustic reciprocity transfer functions for structural node at (0.25m,1.0m,0.65m) and fluid node at (0.5m,0.5m,0.5m) for ζ=0.03.
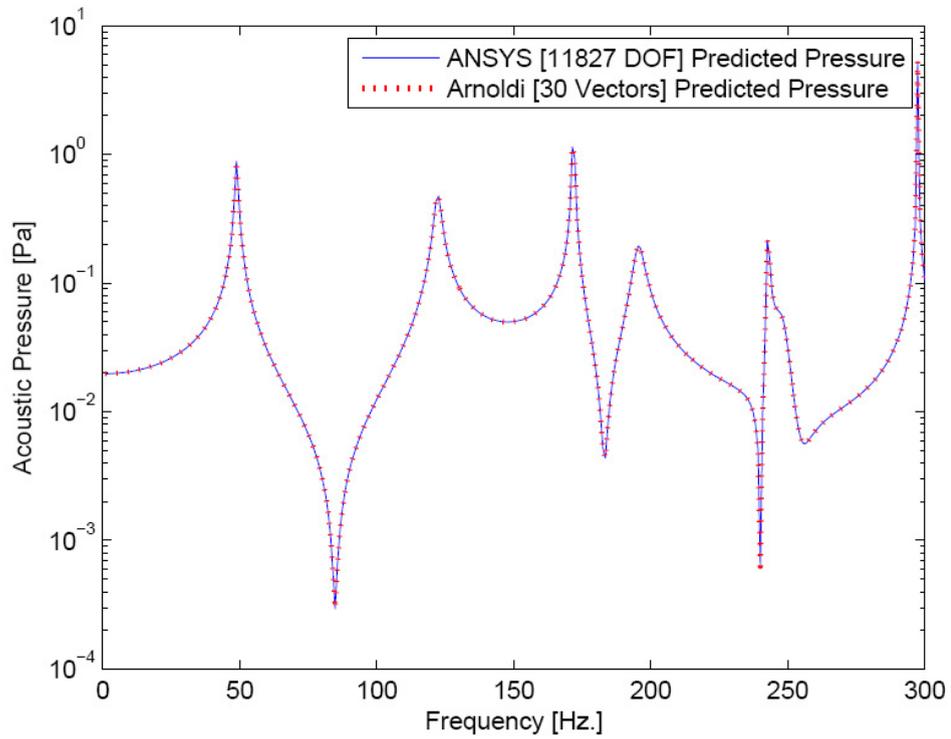
Figure 5.38.: ANSYS and moment matching Arnoldi projection predicted fluid pressure at (0.75m,0.75m,0.25m) for ζ=0.01.
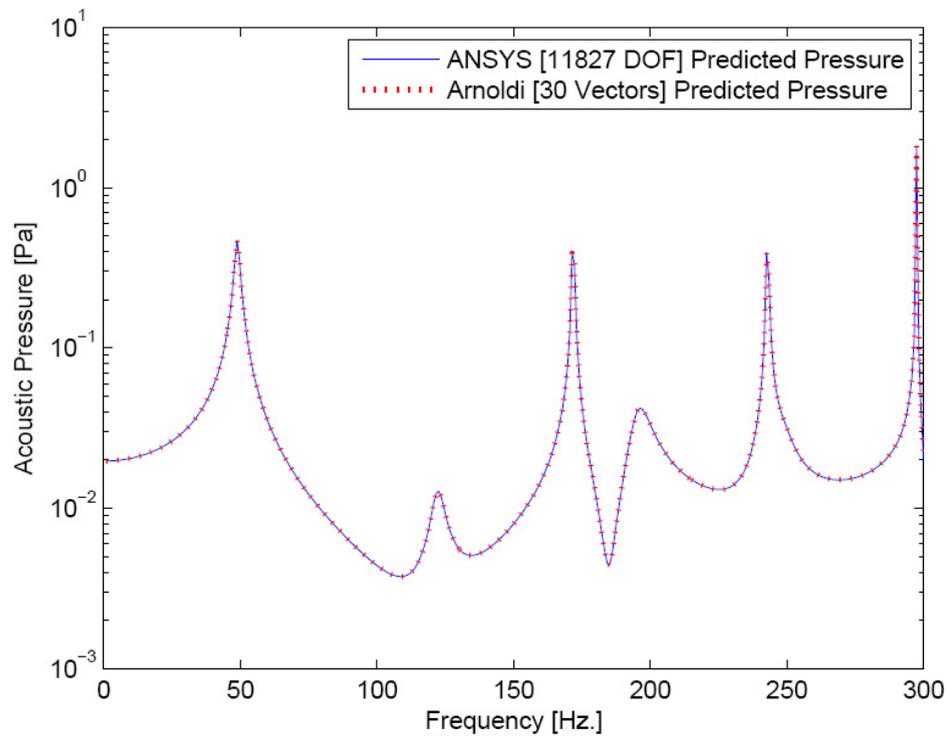
Figure 5.39.: ANSYS and moment matching Arnoldi projection predicted fluid pressure at (0.35m,0.65m,0.30m) for ζ=0.02.
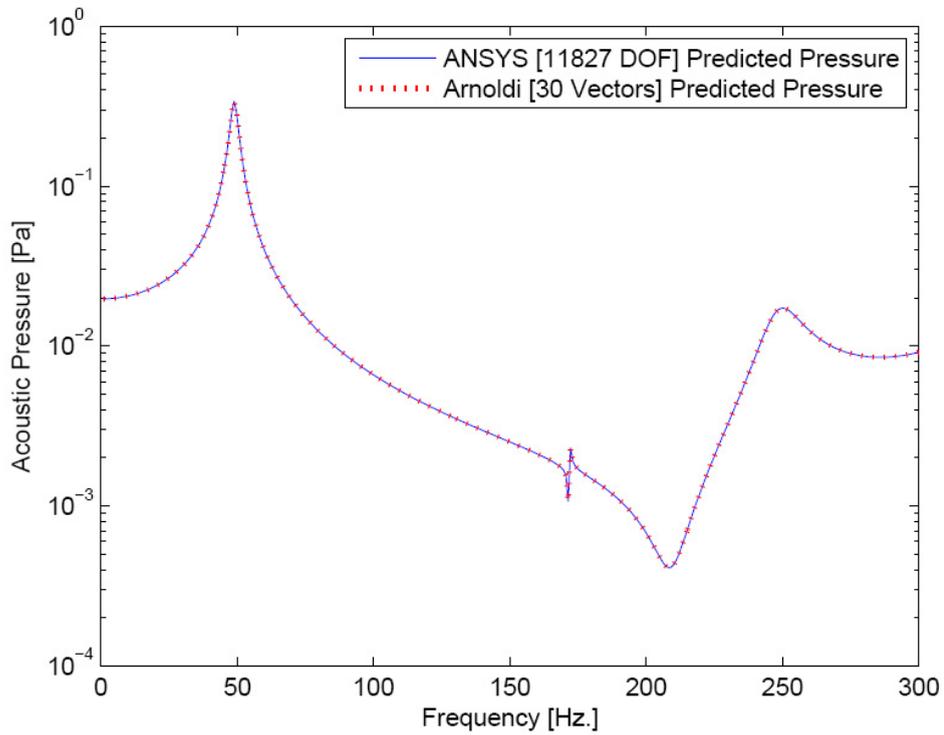
Figure 5.40.: ANSYS and moment matching Arnoldi projection predicted fluid pressure at (0.5m,0.5m,0.5m) for ζ=0.03.
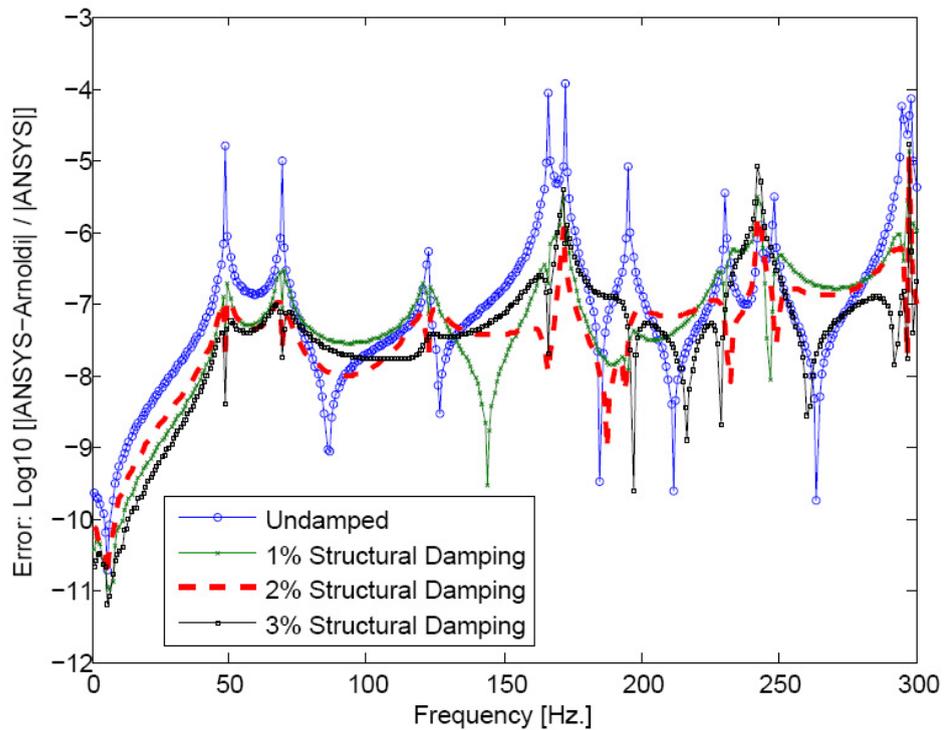
Figure 5.41.: Local Error plot for structural node at (0.25m,1m,0.65m) for ζ=0,0.01,0.02,0.03.
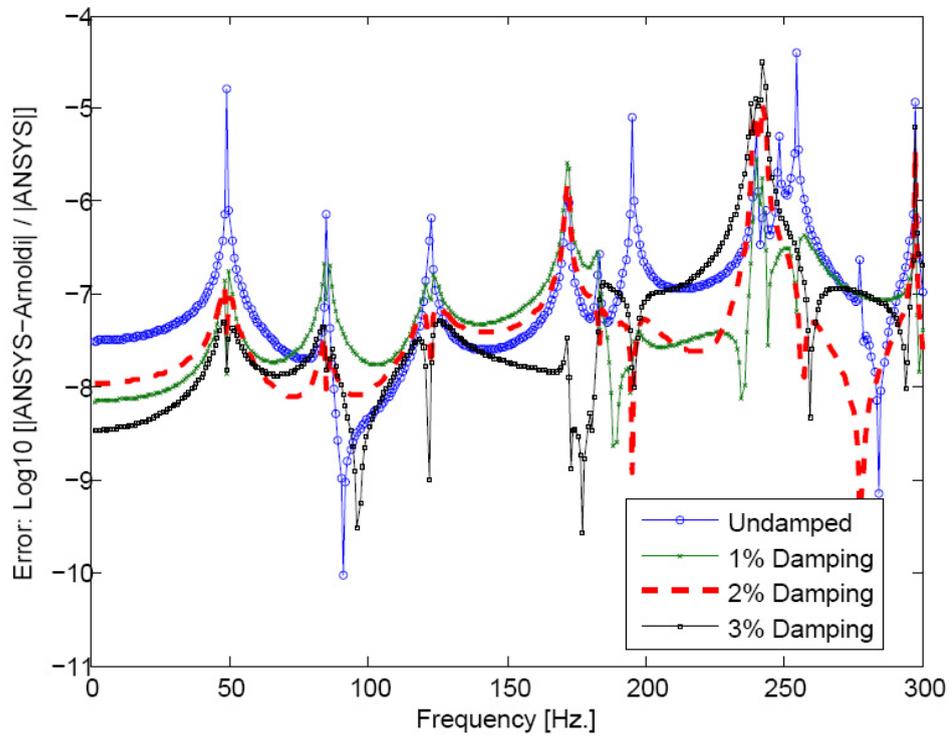
Figure 5.42.: Local Error plot for fluid node at (0.75m,0.75m,0.25m) for ζ=0,0.01,0.02,0.03.
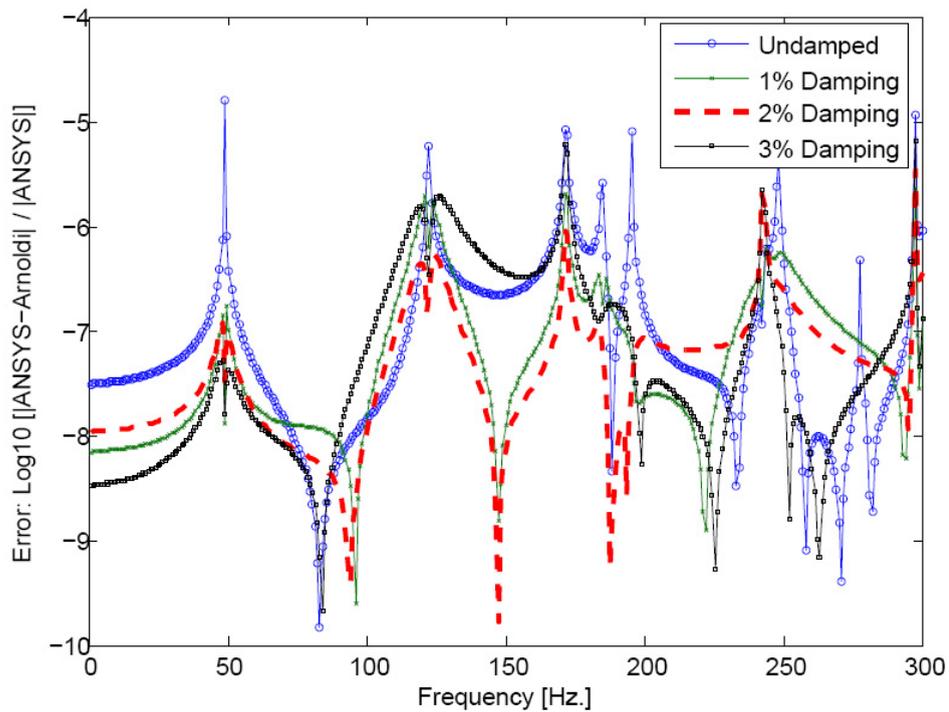
Figure 5.43.: Local Error plot for fluid node at (0.35m,0.65m,0.30m) for ζ=0,0.01,0.02,0.03.
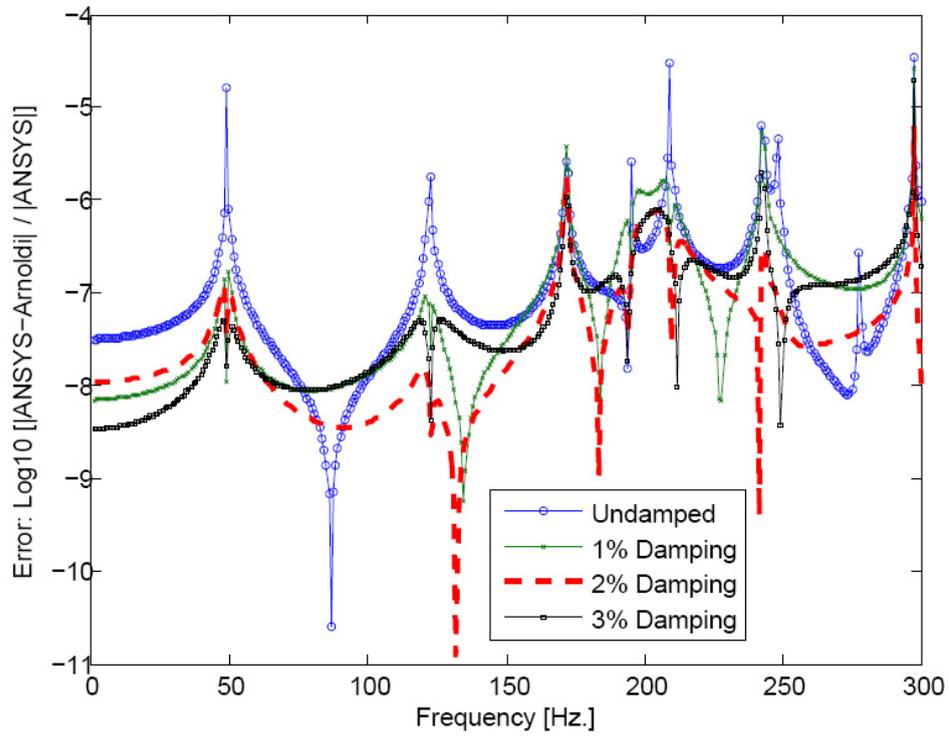
Figure 5.44.: Local Error plot for fluid node at (0.5m,0.5m,0.5m) for ζ=0,0.01,0.02,0.03.
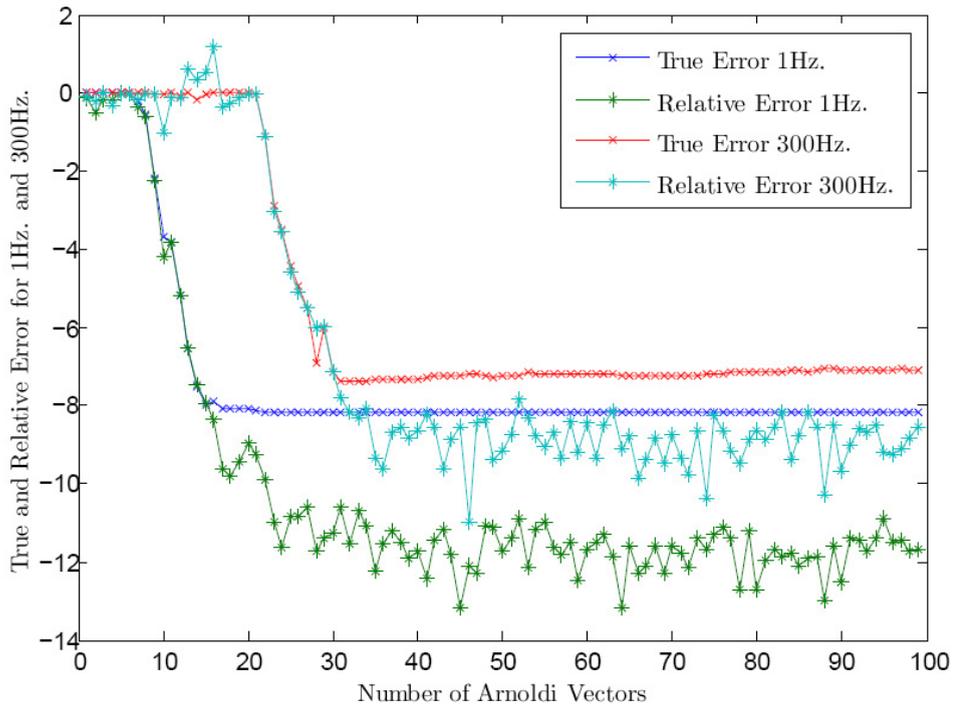
Figure 5.45.: Test Case No. 2.1: Convergence Plot for ζ=0.01.
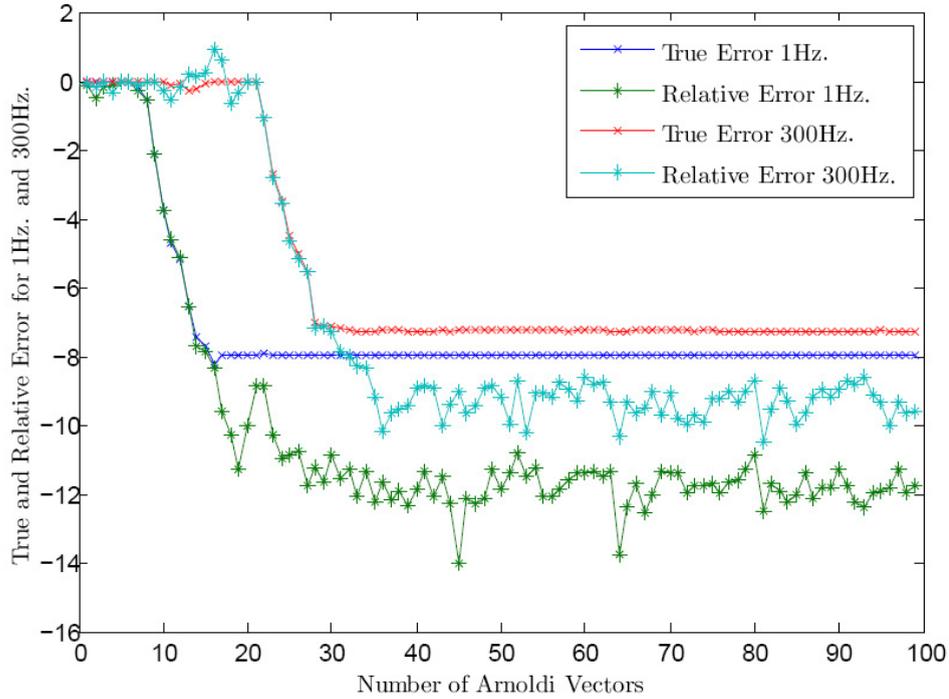
Figure 5.46.: Test Case No. 2.1: Convergence Plot for ζ=0.02.

Table 5.8.: A comparison of computational times for reciprocity test case.

Test Case	ANSYS Direct	ROM via Arnoldi	Time Reduction
$\zeta = 0$	7709 s	322 s	95.82%
$\zeta = 0.01$	7304 s	446 s	93.89%
$\zeta = 0.02$	7057 s	448 s	93.65%
$\zeta = 0.03$	7344 s	474 s	93.54%

A comparison of ROM solutions generated by matching the higher dimensional system moments (around an expansion point) and by truncating and retaining uncoupled structural and acoustic modes in their respective basis are shown in Figures:[5.48,5.49]. The results indicate that the reduced order model generated via the moment matching leads to excellent accuracy over the entire frequency range. The moments in the test case shown are matched at approximately half of the analysis

Table 5.9.: Split Computational Times for reciprocity test case: ROM via Arnoldi.

Test Case	Computational Steps: ROM via Arnoldi	Time
$\zeta = 0$	ANSYS Static Solution (ANSYS)	08 s
	Extract Matrices (ANSYS/*dumpmatrices*)	266 s
	Read Matrices (Mathematica)	04 s
	Vector Computation and Projection (Mathematica)	43 s
	Harmonic Analysis and Convergence (Mathematica/MATLAB)	01 s
	Total: ROM via Arnoldi	**322 s**
$\zeta = 0.01$	ANSYS Static Solution (ANSYS)	07 s
	Extract Matrices (ANSYS/*dumpmatrices*)	267 s
	Read Matrices (Mathematica)	04 s
	Vector Computation and Projection (Mathematica)	167 s
	Harmonic Analysis and Convergence (Mathematica/MATLAB)	01 s
	Total: ROM via Arnoldi	**446 s**
$\zeta = 0.02$	ANSYS Static Solution (ANSYS)	07 s
	Extract Matrices (ANSYS/*dumpmatrices*)	265 s
	Read Matrices (Mathematica)	05 s
	Vector Computation and Projection (Mathematica)	170 s
	Harmonic Analysis and Convergence (Mathematica/MATLAB)	01 s
	Total: ROM via Arnoldi	**448 s**
$\zeta = 0.03$	ANSYS Static Solution (ANSYS)	08 s
	Extract Matrices (ANSYS/*dumpmatrices*)	275 s
	Read Matrices (Mathematica)	05 s
	Vector Computation and Projection (Mathematica)	185 s
	Harmonic Analysis and Convergence (Mathematica/MATLAB)	2 s
	Total: ROM via Arnoldi	**474 s**
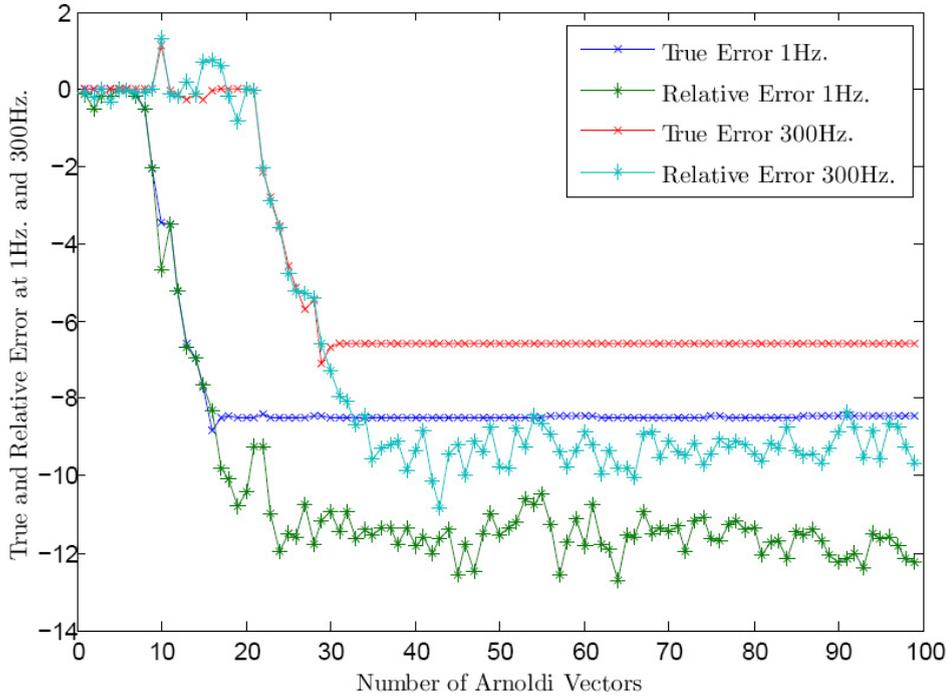
Figure 5.47.: Test Case No. 2.1: Convergence Plot for ζ=0.03.

range. Obviously, if a Taylor series expansion is considered around a higher frequency, a reduced order model could be obtained with better approximation properties around that frequency range. On the other hand, the truncated modal coupling (uncoupled modes) approach, where 34 modes ($1.5 \times \omega_e$) are retained in total, gives reasonably good accuracy at resonance and poor accuracy off resonance, compared with the *direct method*. In the *full* uncoupled modal approach, where 106 modes are retained, leads to better accuracy in comparison with the truncated version. This effect of including more modes in the Modal Coupling method can be seen in Figures:[5.50,5.51]. It can be observed that the accuracy of prediction via the uncoupled modal approach is improved, but it is still not as good as the Arnoldi based reduced order modeling approach. Further, the acoustic uncoupled modal basis has to be substantially increased to achieve the desired accuracy. This phenomenon is similar to the one observed in the benchmark test case (Section:5.1), where a very higher number of modes (up to 4500Hz) were included in the AMLS method in order to achieve desired accuracy. The loss of accuracy due to residues from

truncated modes is well documented for weakly coupled systems (Fahy 1985). The phenomenon seems to occur both in water and air filled cavities. It is worth noting that, for many applications, the contribution of the prediction off resonance may be minor. An interesting comparison is with the case of active control application by Cazzolato (1999). A comparison of error quantities of ROMs obtained via moment matching Arnoldi and uncoupled modal approaches (Truncated and Full) for the undamped and damped test cases are shown in Figures:[5.53, 5.54, 5.55, 5.56]. It can be observed that for some outputs, retaining a higher number of modes in the uncoupled basis does not necessarily improve accuracy for all outputs considered in this test case. For example, in Figure:[5.54], retaining a larger number of modes (Structure + Fluid: 106) results in an increase in maximum error when compared to the ANSYS direct inversion technique. This is because, the prediction around 200Hz (a minor shift) in Figure:[5.50], has not been accurately captured in the uncoupled modal basis method. On the other hand, moment matching Arnoldi approaches seem to accurately capture the coupled dynamics of the system under investigation.
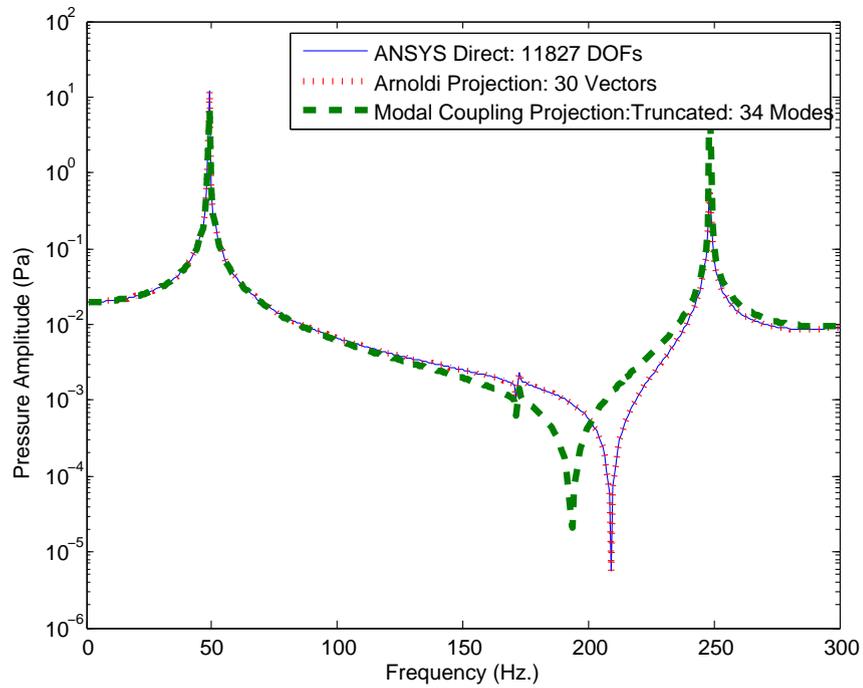
Figure 5.48.: ANSYS direct and truncated uncoupled modes (fluid+structure) projection predicted noise transfer functions for fluid node at (0.5m,0.5m,0.5m) for ζ=0.
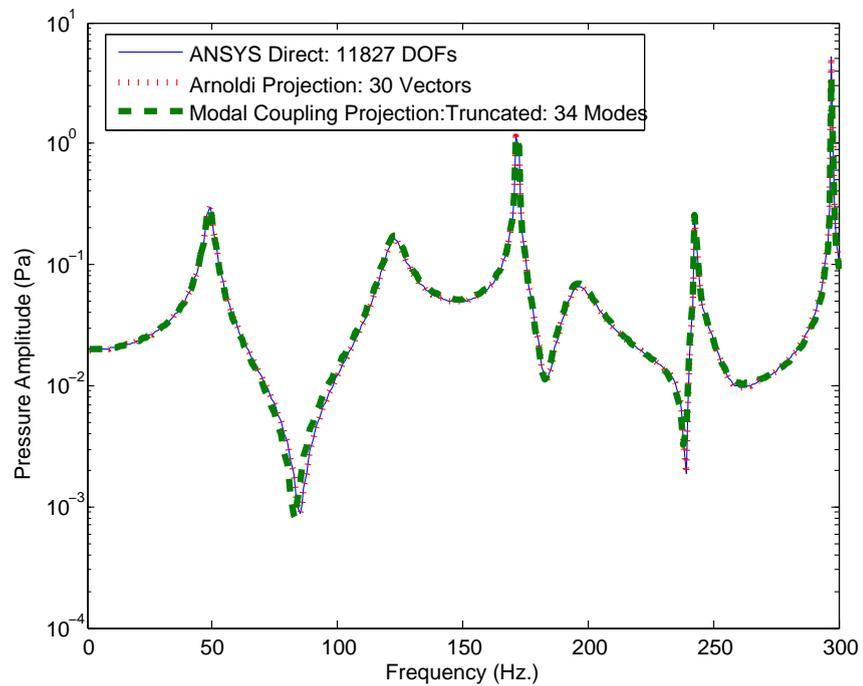
Figure 5.49.: ANSYS direct and truncated uncoupled modes (fluid+structure) projection predicted noise transfer functions for fluid node at (0.75m,0.75m,0.25m) for ζ=0.03.
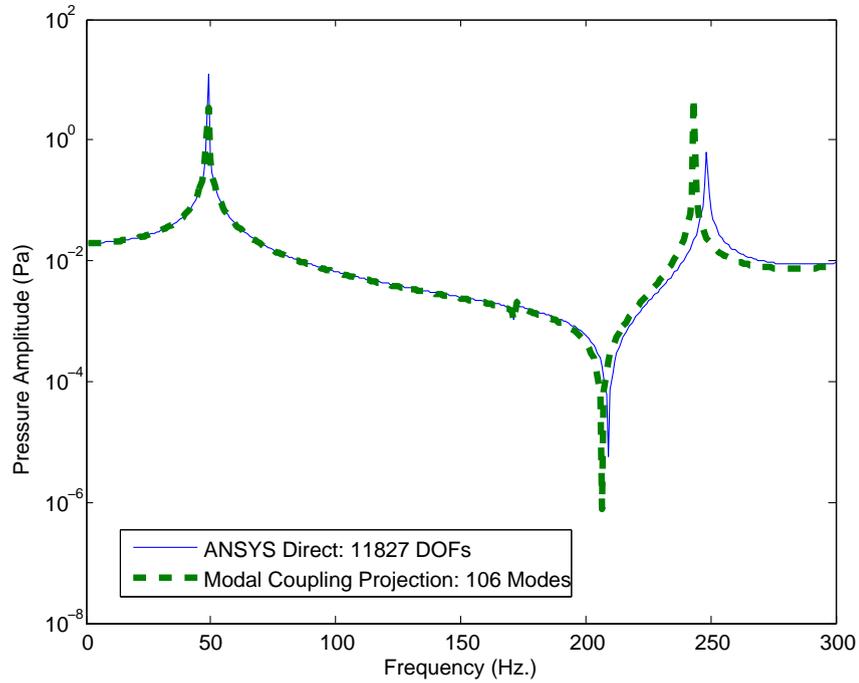
Figure 5.50.: ANSYS direct and uncoupled modes (fluid+structure) projection predicted noise transfer functions for fluid node at (0.5m,0.5m,0.5m) for $\zeta=0$.
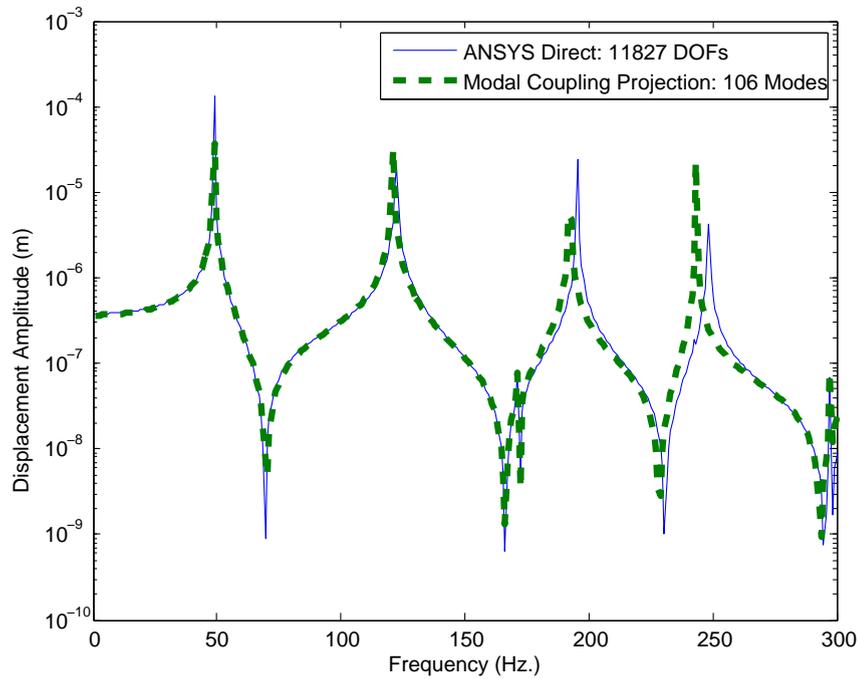
Figure 5.51.: ANSYS direct and uncoupled modes (fluid+structure) projection predicted driving point displacement transfer functions for structural node at (0.25m,1m,0.65m) for $\zeta=0$.
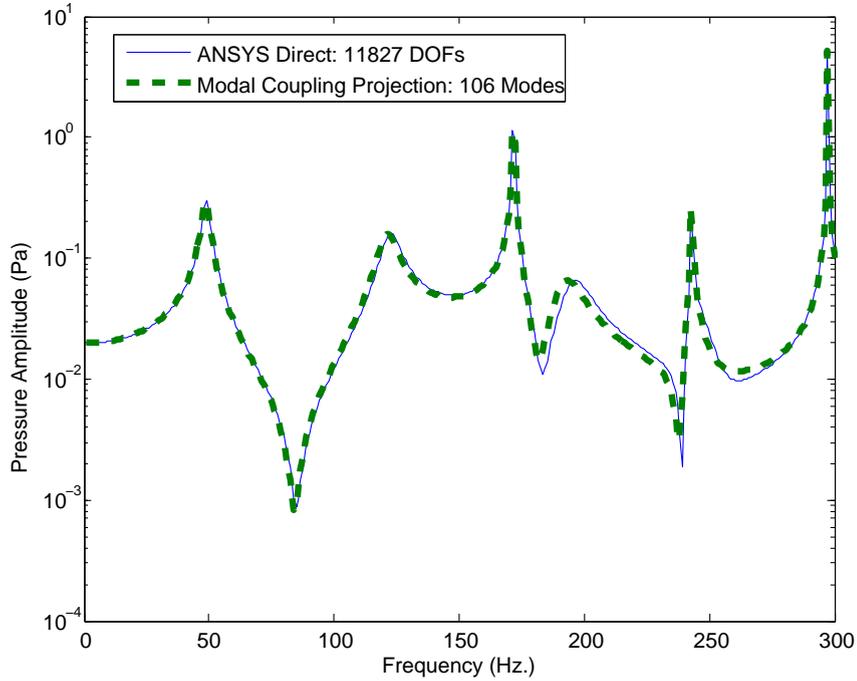
Figure 5.52.: ANSYS direct and uncoupled modes (fluid+structure) projection predicted noise transfer functions for fluid node at (0.75m,0.75m,0.25m) for ζ=0.03.
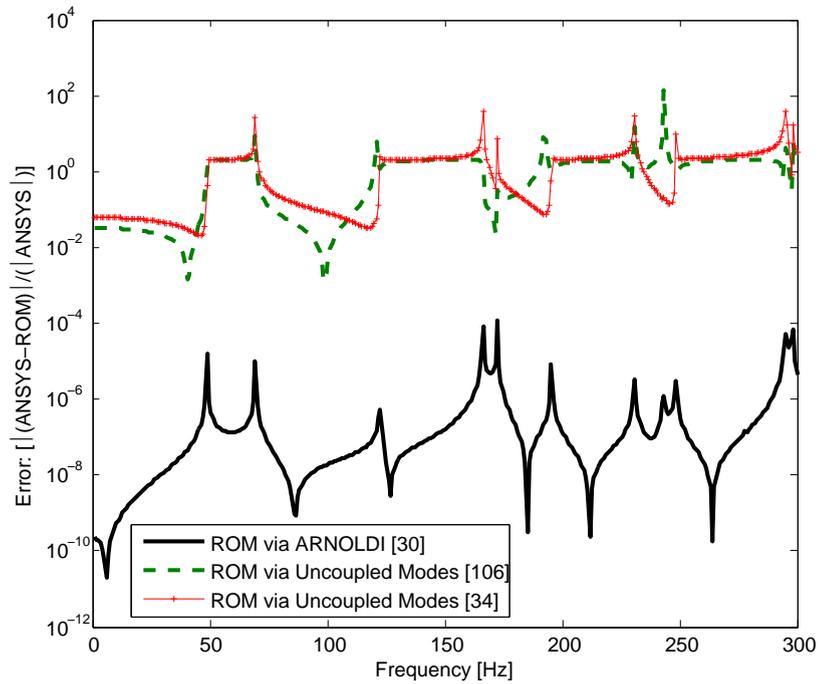
Figure 5.53.: A comparison of error quantities for driving point displacements for structural node at (0.25m,1m,0.65m) obtained using Arnoldi projection, Uncoupled modes approach (Full) and Truncated uncoupled modal approach for ζ=0.
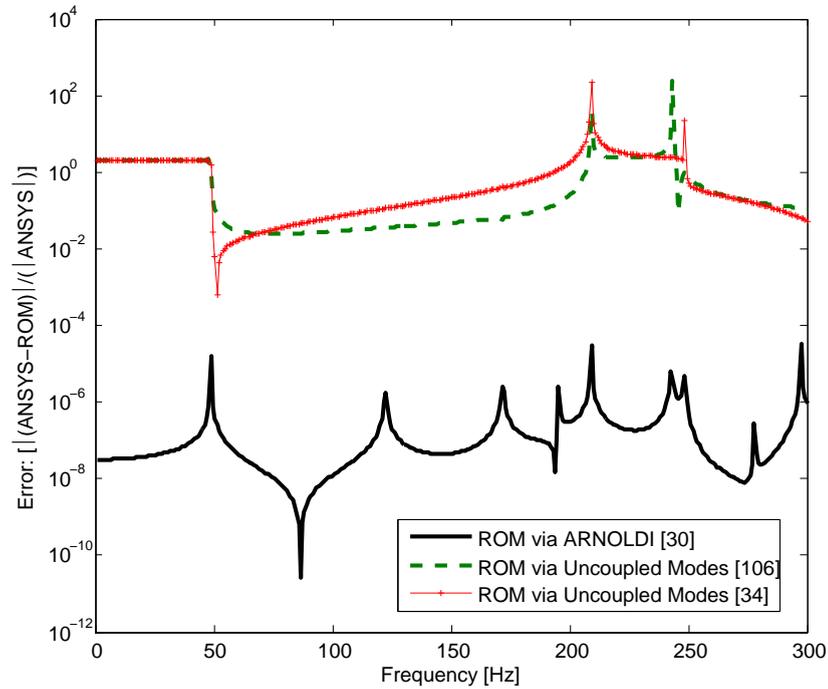
Figure 5.54.: A comparison of error quantities for noise transfer function for fluid node at (0.5m,0.5m,0.5m) obtained using Arnoldi projection, Uncoupled modes approach (Full) and Truncated uncoupled modal approach for ζ=0.
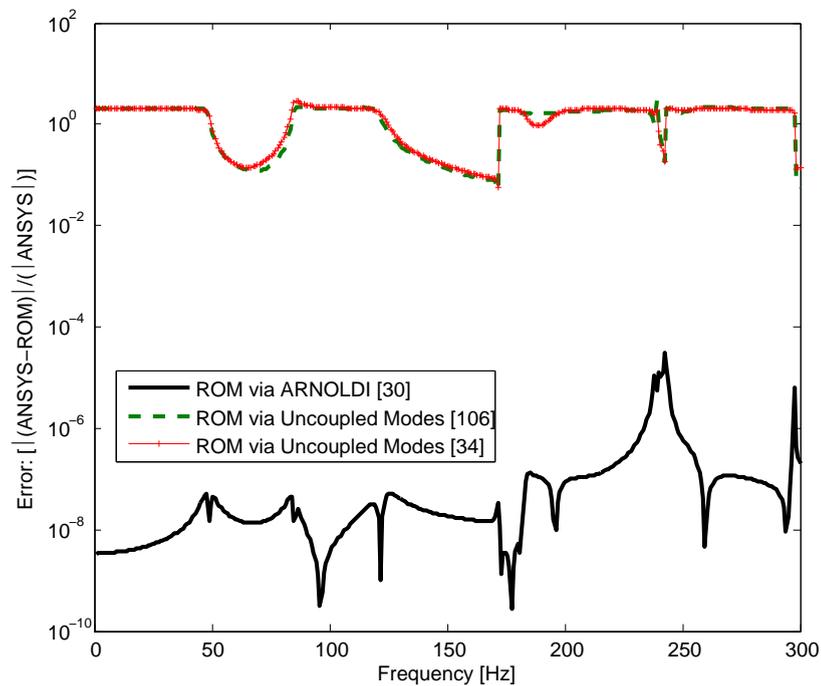
Figure 5.55.: A comparison of error quantities for noise transfer function for fluid node at (0.75m,0.75m,0.25m) obtained using Arnoldi projection, Uncoupled modes approach (Full) and Truncated uncoupled modal approach for ζ=0.03.
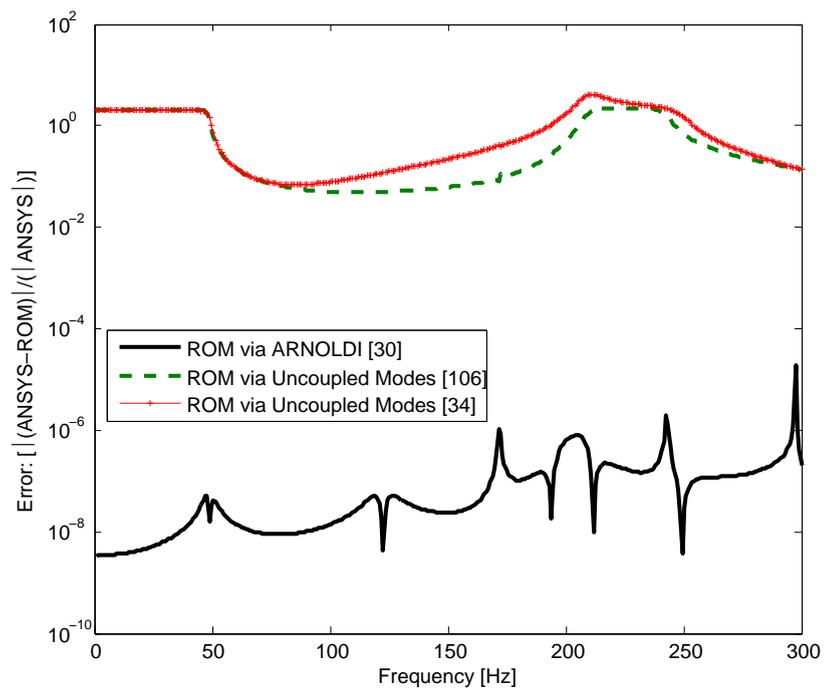
Figure 5.56.: A comparison of error quantities for noise transfer function for fluid node at (0.5m,0.5m,0.5m) obtained using Arnoldi projection, Uncoupled modes approach (Full) and Truncated uncoupled modal approach for ζ=0.03.

5.4. Test Case: 3: 3D Plate backed Rectangular Water Filled Cavity

A plate backed water filled cavity is considered as the third test case to compare the efficiency and accuracy of dimension reduction via the Arnoldi process. This solution method is also compared with a harmonic analysis using the direct LU solution method in ANSYS. The cavity-plate has the following dimensions: 0.35 m long, 0.29 m wide, and 0.14 m deep and 0.0015 m thick aluminium plate. The mechanical properties of the structure are as follows: Young's Modulus E_s= 72 GPa, mass density ρ_s=2700 kg/m^3 and Poisson's ratio υ=0.33. The cavity is filled with water with the following properties: speed of sound c=1500 m/s, mass density ρ_c=1000 kg/m^3. The plate is discretized using 18 × 15 ANSYS SHELL181 elements and the cavity is discretized using 18 × 15 × 4 ANSYS FLUID30 elements. The coupled system was excited using a constant structural point force of 1N over the entire frequency range of 0-600Hz at one of the off-center structural nodes on the simply supported plate. For this test case, the normal (UY) DOF's belonging to the nodes along the boundary of the aluminium plate are restrained. These are shown in Figures:[5.57,5.58]. The desired output quantities considered for this test case are as follows: (a) the structural displacement response at driving point i.e at the unit structural point force location a$_2$=(0.039m,0.14m,0.078m) and (b) fluid pressure close to the center of the rectangular domain at b$_2$=(0.135m,0.07m,0.175m). A description of this test case can also be found in Tournour and Atalla (2000).

It is worth mentioning that the dimension of the resulting coupled FE model for this test case is indeed small - compared to test cases: (1,2 and 2.1). However, from a modal coupling viewpoint, the presence of a higher density fluid results in a very strong coupling between the plate modes and the cavity modes. Indeed, since the modal coupling is proportional to the square root of the bulk modulus of the fluid,

the presence of a heavy fluid results in a very strong coupling between the plate modes and the cavity modes. Roughly speaking, the coupling strength between the fluid and the structural domains is directly proportional to the density of the fluid (Cepkauskas and Stevens 1983; Hong and Kim 1995a; Hong and Kim 1995b). At this point, it is worth mentioning that this is also true for the coupling between the lower plate modes and the higher cavity modes, usually low but drastically increased by the high bulk modulus of the fluid (Tournour and Atalla 2000). Therefore, similar to the benchmark test case, this test case has also been chosen to evaluate the performance of the Arnoldi based projection formulation for *strong coupling*. It is worth mentioning that for industrial NVH applications (e.g. prediction of noise in an automotive or aerospace interior) air is used as the fluid medium, which results in *weak coupling*. That is, there exists a *weak coupling* between the structural modes and the rigid walled cavity modes. An illustration of the reduced accuracy and efficiency of the uncoupled modal approach for this test case[7] can be found in Appendix:(B). The sparsity plots for the resulting higher dimensional coupled stiffness and mass matrices are shown in Figures:[5.59, 5.60].

For the damped case, two different forms of structural damping are considered for this test case: (a) Constant, frequency independent damping, which is frequency independent by definition and (b) Linearly varying, frequency dependent damping. The damping parameters for constant and frequency dependent damping used for this test case are shown in Table:[5.10, 5.11]. The undamped computations described were performed on a Windows XP, Pentium 4, 3GHz, 2GB RAM machine [Me1]. The constantly damped and linearly damped computations described were performed on a Windows XP, Pentium 4, 3.2GHz, 2GB RAM machine [Me2]. The corresponding *bench* calculations are shown in Appendix:(A).

---

[7]Tournour and Atalla (2000) also demonstrated the reduced accuracy and convergence properties for strongly coupled systems.

For the constant damping cases [TC3$_{LD}$, TC3$_{MD}$, TC3$_{HD}$], the fluid fluid pressure at approximately the centre of the rectangular cavity is considered as the output node of interest. For linearly damped test cases [TC3$_{ld}$, TC3$_{md}$, TC3$_{hd}$], the structural driving point displacement is considered as output for the analysis. Similar to test case-1, the frequency dependent damping models results in an explicit participation of [C_{sa}] and the *direct-inversion* technique cannot be avoided. Therefore, for dimension reduction of the higher dimensional system matrices, two different moment matching Arnoldi approaches are investigated: (a) The *linearization* method, where the second order system is converted into an equivalent first order form and the moments are matched via the one sided Arnoldi process (b) The two-sided Second order Arnoldi process (TS-SOAR), which does not need conversion to first order and thus preserves the underlying second order structure for the given problem. The reader is reminded that the *equivalent linearized system* is obtained via Equations: [4.70a, 4.70b]. The sparsity plot obtained using MATLAB for the equivalent linearized system ($\mathbf{D}_{sa}$, $\mathbf{G}_{sa}$) is shown in Figures:[5.61,5.62].

Table 5.10.: Constant Damping values and Expansion point for One sided Arnoldi Process for the water filled rectangular cavity.

Damped Test Cases	Damping Value	Expansion Point
Low Damping [TC3$_{LD}$]	β_j^{ζ}=0.03	300Hz
Medium Damping [TC3$_{MD}$]	β_j^{ζ}=0.05	300Hz
High Damping [TC3$_{HD}$]	β_j^{ζ}=0.10	300Hz

To provide a variation to this test case, the fluid medium of the coupled finite element model is parametricaly modified to air. In this way, the Arnoldi projections are evaluated for weakly coupled systems. For the air filled test case, two boundary
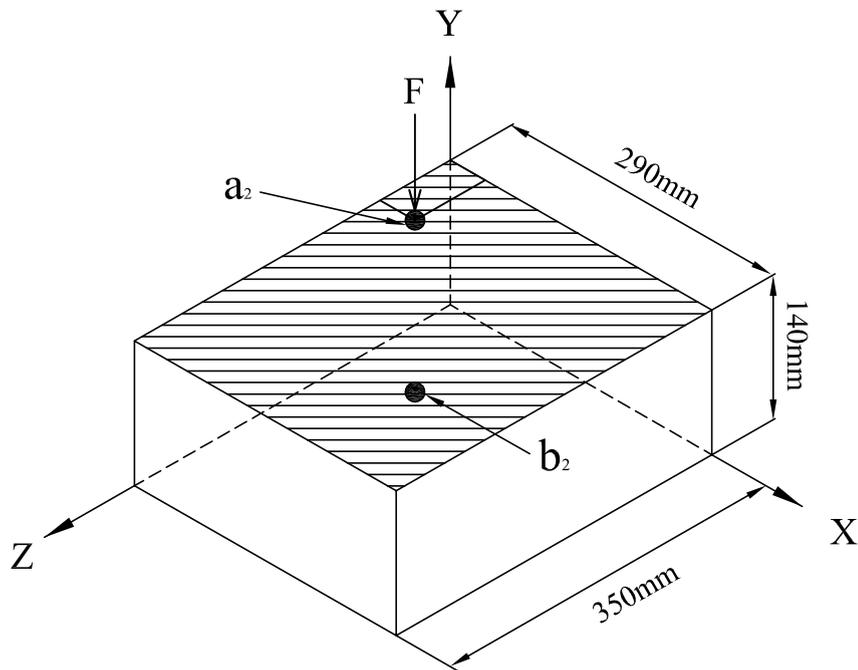
Figure 5.57.: Test Case No. 3: Plate backed rectangular cavity (water filled) system. Excitation location: $a_2 = (0.039m, 0.14m, 0.078m)$; Measurement location(s): $a_2 = (0.039m, 0.14m, 0.078m)$, $b_2 = (0.135m, 0.07m, 0.175m)$.
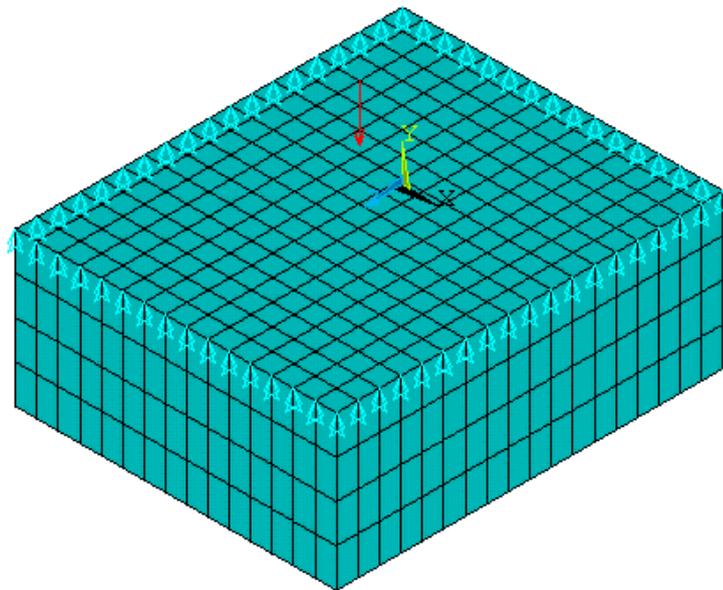
Figure 5.58.: Test Case No. 3: Fully Coupled FE model.
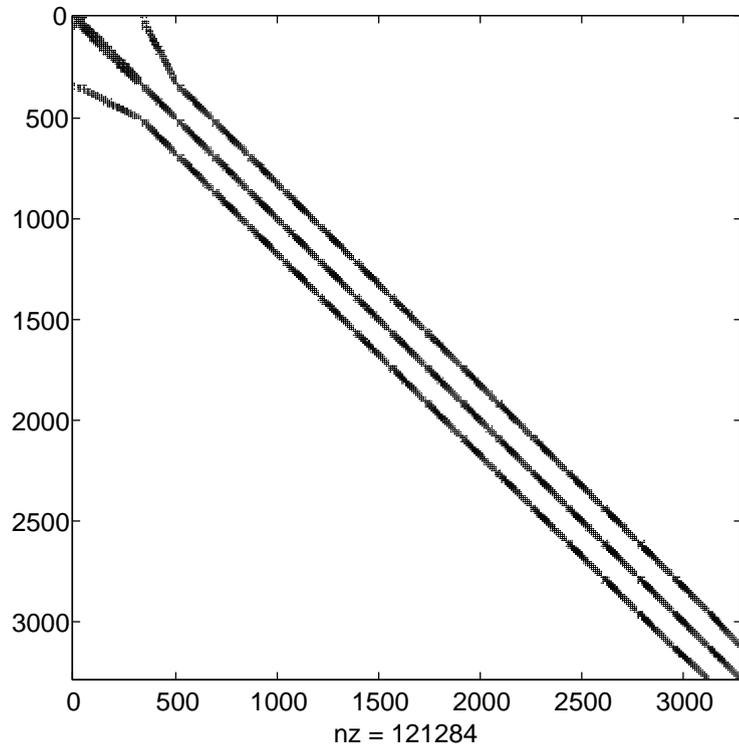
Figure 5.59.: Test Case No. 3: Stiffness Matrix sparsity plot.
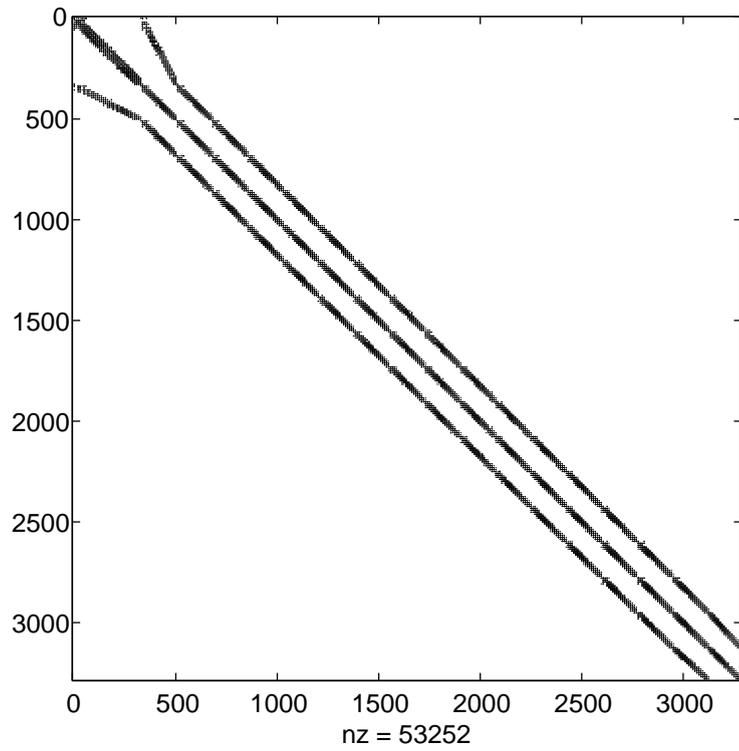
Figure 5.60.: Test Case No. 3: Mass Matrix sparsity plot.
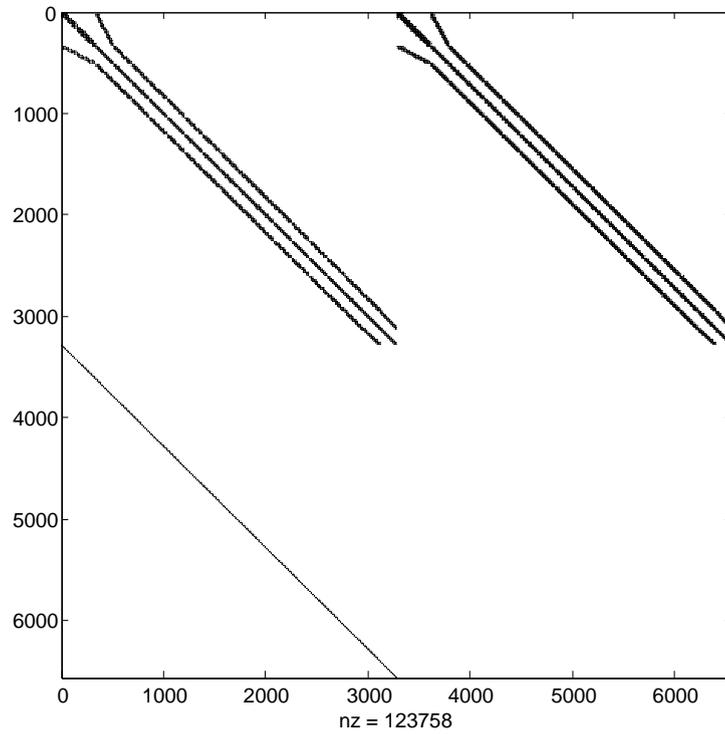
Figure 5.61.: Test Case No. 3: Equivalent Linearized System (Equation:4.70a) $\mathbf{D}_{sa}$ sparsity plot for β_j^m=4.0E-05 [TC3$_{md}$].
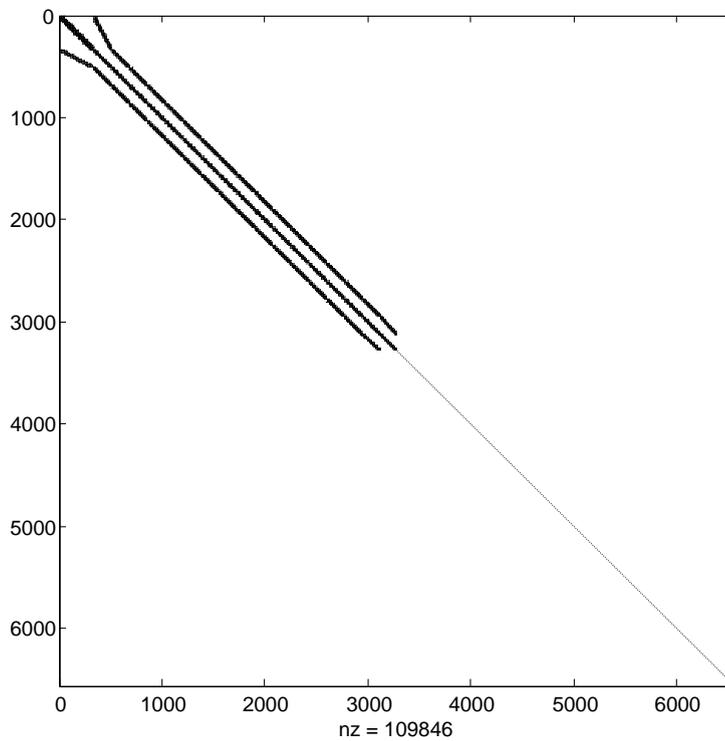
Figure 5.62.: Test Case No. 3: Equivalent Linearized System (Equation:4.70a) $\mathbf{G}_{sa}$ sparsity plot for β_j^m=4.0E-05 [TC3$_{md}$].

Table 5.11.: Frequency Dependent Damping values and Expansion points for Two-Sided Second order Arnoldi Process and One sided Arnoldi (Linearized system) for the water filled rectangular cavity.

Damped Test Cases	Damping Value	Expansion Points for TS-SOAR	Expansion Point for OSA
Low Damping [TC3$_{ld}$]	β_j^m=2.0E-05	300Hz / 300Hz	300Hz
Medium Damping [TC3$_{md}$]	β_m^ζ=4.0E-05	300Hz / 300Hz	300Hz
High Damping [TC3$_{hd}$]	β_m^ζ=6.0E-05	300Hz / 300Hz	300Hz

conditions are investigated: (a) Free-free and (b) fully clamped (all DOF's along the edges of the plate constrained). In addition to this, the free-free test case is acoustically damped, via the use of frequency independent absorption co-efficient (β_{ac}), which directly inserts terms into C_{sa} (ANSYS 2005). A description of the air filled test cases can be found in Table:[5.12].

Table 5.12.: A description of test cases for the air filled rectangular cavity.

B.C's	Damped Test Cases	Damping Value	Expansion Point
Free-Free	[TC3$_{FFa}$]	β_{ac}=0.04	TS-SOAR: 350Hz
Clamped	[TC3$_{CLa}$]	Undamped	TSA: 600Hz

5.4.1. Computational Results and Discussion

For the dimension reduction methods, 50 vectors were generated using the SICO Arnoldi and SISO TS-SOAR algorithm implemented in Mathematica. For the undamped model with an expansion point of 250Hz, the noise transfer function and the structural receptance transfer function (structural displacement over structural input force) and the fluid acoustic transfer function (cavity pressure over structural input force) are shown in Figures:[5.63,5.64]. The corresponding fluid pressure and structural displacement errors are shown in Figure:[5.65]. For the MOR via Arnoldi approach, an expansion point of $f_{exp} = 350Hz$ was used. The convergence plots at 1Hz and 600Hz obtained via Equations:[4.94a,4.94b] are shown in Figure:[5.66]. It can be observed that to approximate the coupled system to the required level of accuracy required no more than 50 Arnoldi generated vectors for both 1Hz and for 600Hz.
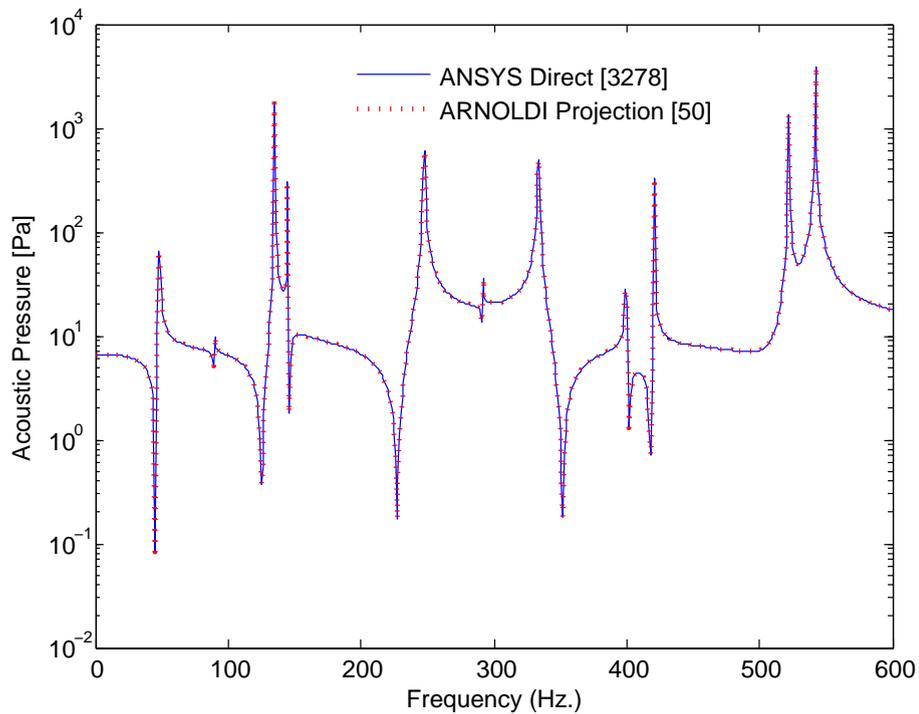
Figure 5.63.: Test Case No. 3: Predicted Fluid Noise Transfer Function (NTF) using direct and moment-matching Arnoldi projection for structural node at (0.135m,0.07m,0.175m).
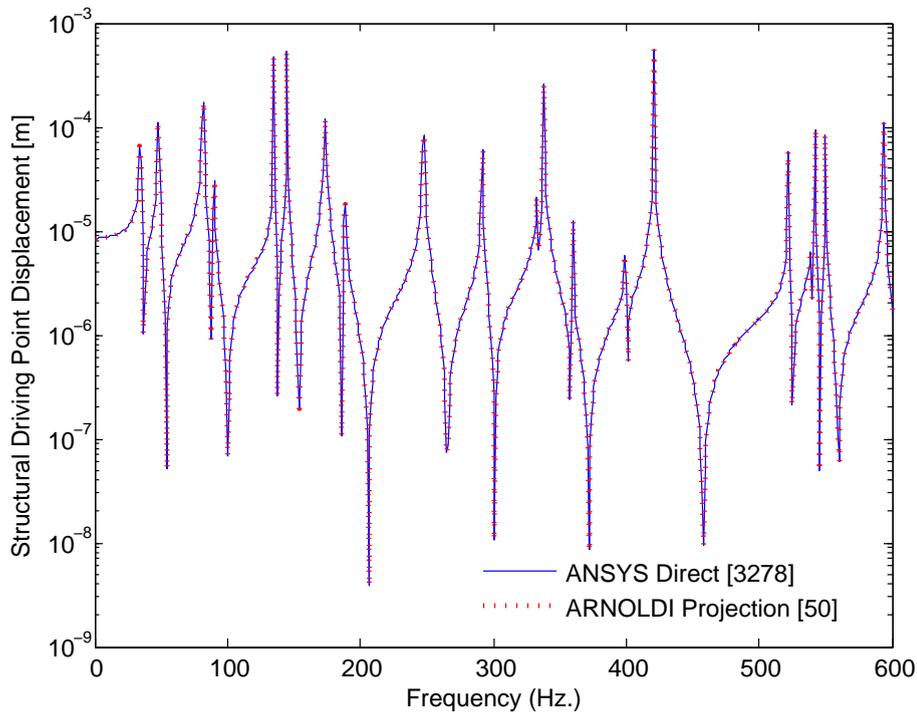
Figure 5.64.: Test Case No. 3: Predicted Structural Displacement Transfer Function (Receptance) using direct and moment-matching Arnoldi projection for fluid node at (0.039m,0.14m,0.078m).

For the constantly damped material models described in Table:[5.10], the structural receptance transfer function and the fluid acoustic noise transfer function are shown in Figures:[5.67, 5.69, 5.71]. The corresponding convergence patterns for $\zeta = 3\%$, $\zeta = 5\%$, $\zeta = 10\%$ are shown in Figures:[5.68, 5.70, 5.72]. Similar to the undamped version of the described test case, it can be observed that to approximate the coupled higher dimensional system to the required level of accuracy required no more than 40 Arnoldi generated vectors for both 1Hz and for 600Hz. At this point, machine precision is reached, accounting for 16 significant digits for the described computation. The error plots obtained for the constantly damped test cases is shown in Figure:[5.73]. Here, it can be observed that, for a given number of Arnoldi generated vectors (50 in this case), the error seems to decrease (relatively) with the addition of increasing damping. Loosely speaking, this phenomenon is due to the fact that in an undamped calculation, the response is not smoothed, making
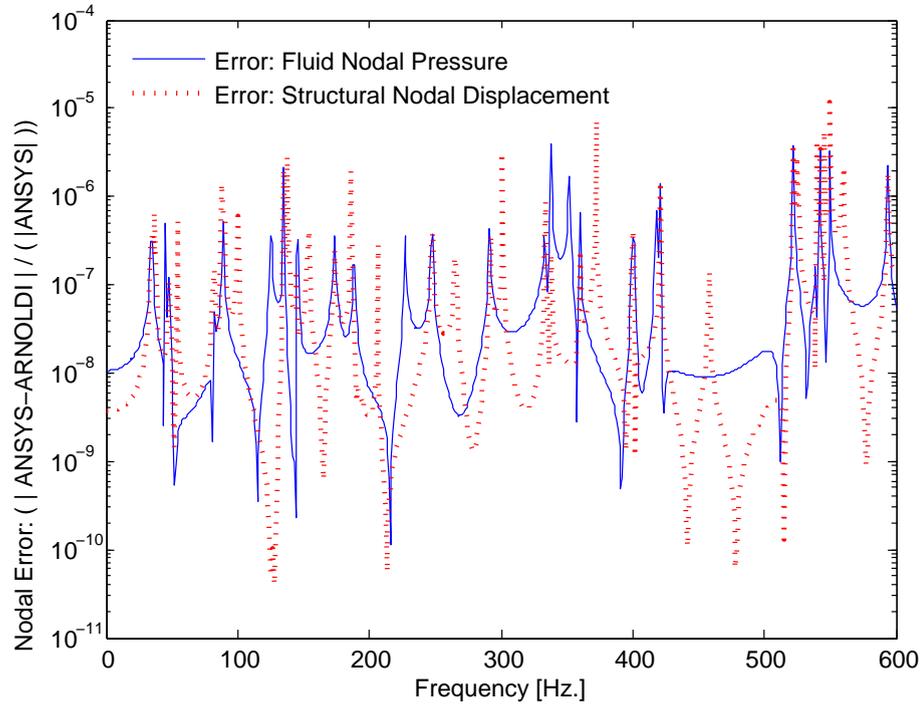
Figure 5.65.: Test Case No. 3: Error Plot for fluid and structural outputs.
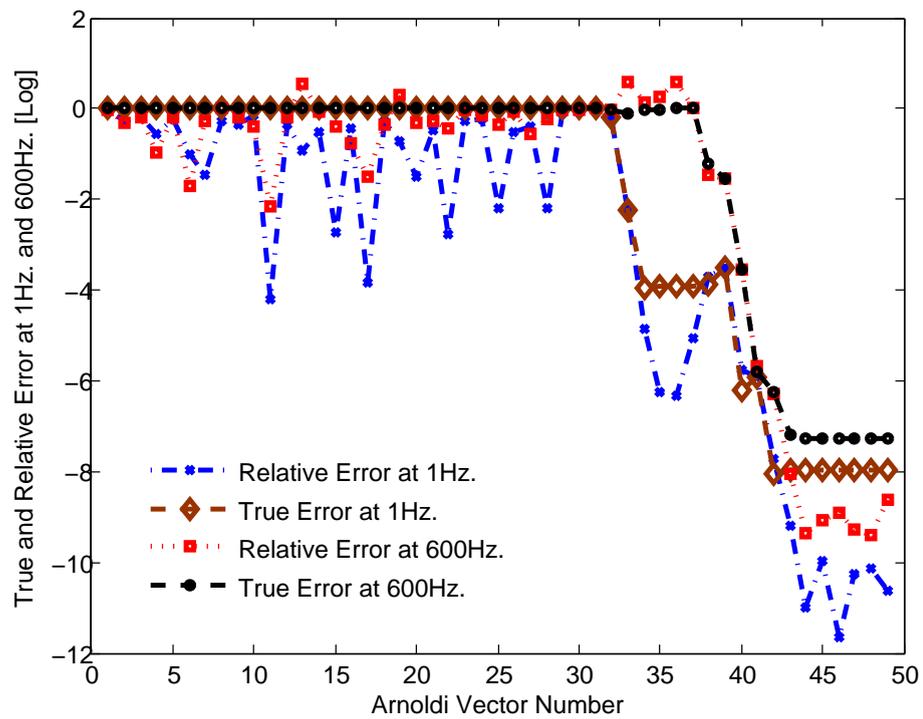
Figure 5.66.: Test Case No. 3: Convergence pattern for Arnoldi vectors at 1Hz and 600Hz.

errors more apparent. Also, in the undamped case, the poles and zeros of the transfer function follow immediately after each other whereas in the damped cases, the transition between them is well smoothed due to the presence of damping.
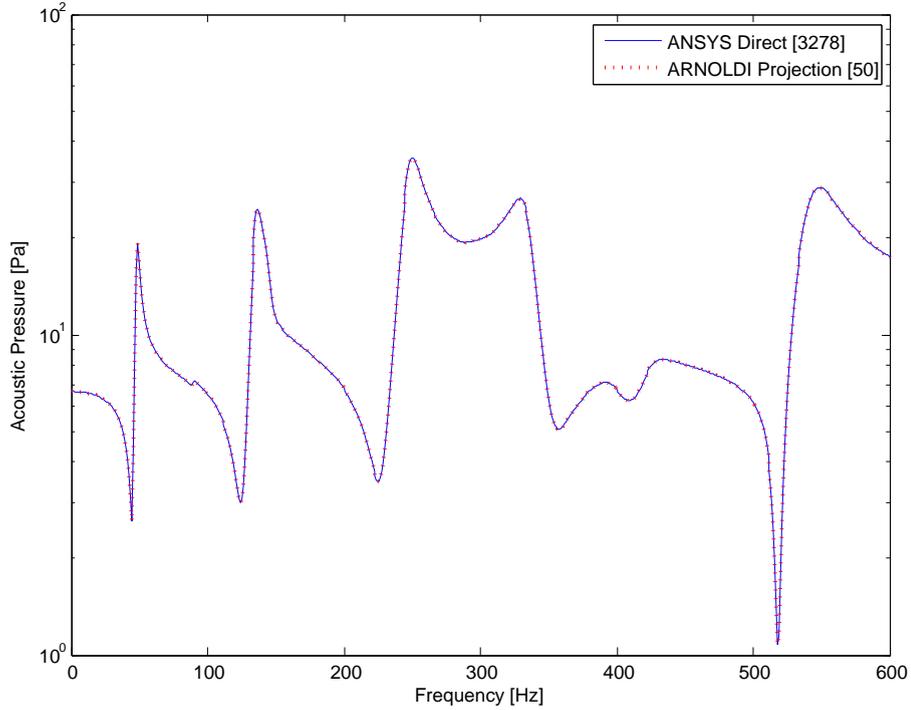
Figure 5.67.: Predicted Fluid Noise Transfer Function using direct and moment-matching Arnoldi (OSA) projection for fluid node at (0.135m,0.07m,0.175m) for ζ=0.03.

For the frequency varying (linearly) damped material models described in Table:[5.11], the structural receptance transfer function obtained using the *linearization* approach and SISO TS-SOAR process are shown in Figures:[5.74, 5.75,5.76]. The error quantities for the ROM obtained using the TS-SOAR process is shown in Figure:[5.77]. It can be observed that there is no visible difference in the transfer functions obtained using both approaches. The corresponding convergence models for the Arnoldi vectors generated via the SISO TS-SOAR and SICO OSA (linearization method) are shown in Figures:[5.81, 5.82,5.83, 5.84, 5.85, 5.86]. In the case where the given higher dimensional system is turned into an equivalent linearized
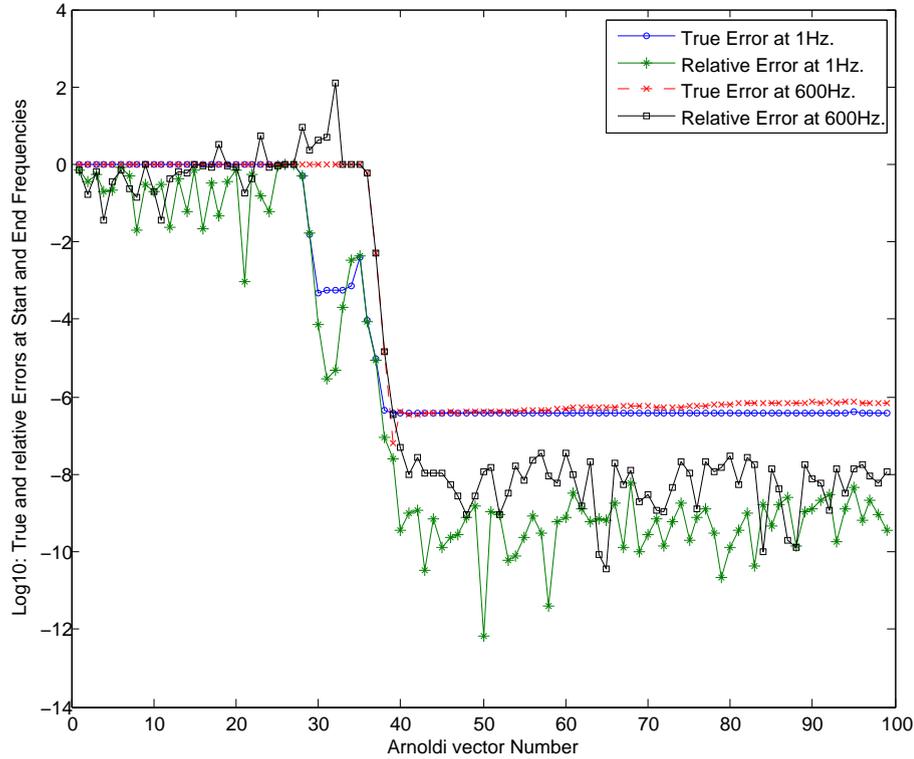
Figure 5.68.: Convergence pattern for moment-matching Arnoldi (OSA) projection at 1Hz and 600Hz for ζ=0.03.

form, 100 Arnoldi (OSA) vectors are required to accurately approximate the system. On the other hand, for the TS-SOAR process, where the system retains its second order structure, only 30 Arnoldi (TS-SOAR) vectors are required to accurately approximate the system. The difference in the number of vectors can be attributed to the fact that in the linearized system, scaling factors are introduced (in the form of identity matrix and sparse zero matrices) to form $\mathbf{D}_{sa}$ and $\mathbf{G}_{sa}$, and therefore, more vectors are required to counter the introduced scaling. At this point, it is worth mentioning that there are different methods to compute the equivalent linearized system. In this thesis, the simplest method for linearization (Equations:4.70a,4.70b)is adopted. For a description of other methods, the reader is referred to Bai (2002), Bai, Meerbergen, and Su (2005), Freund (2001), Freund (2000). A comparison of local error quantities for the ROM obtained via SICO OSA and SISO TS-SOAR for all three damping models are shown in Figures:[5.78, 5.79, 5.80]. It can actu-
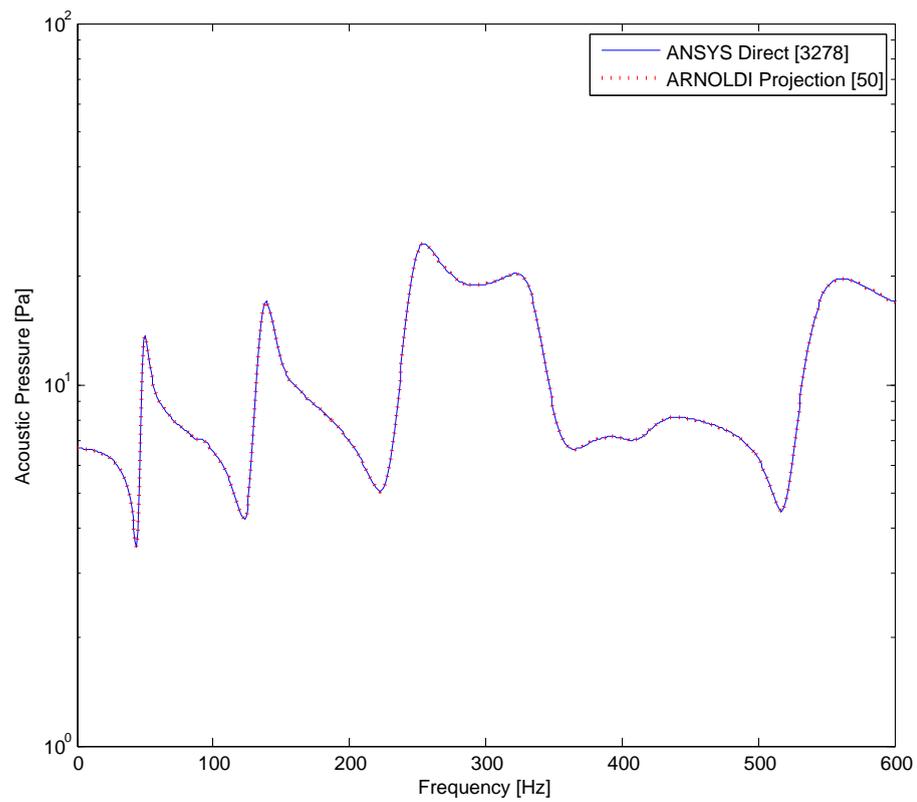
Figure 5.69.: Predicted Fluid Noise Transfer Function using direct and moment-matching Arnoldi (OSA) projection for fluid node at (0.135m,0.07m,0.175m) for ζ=0.05.
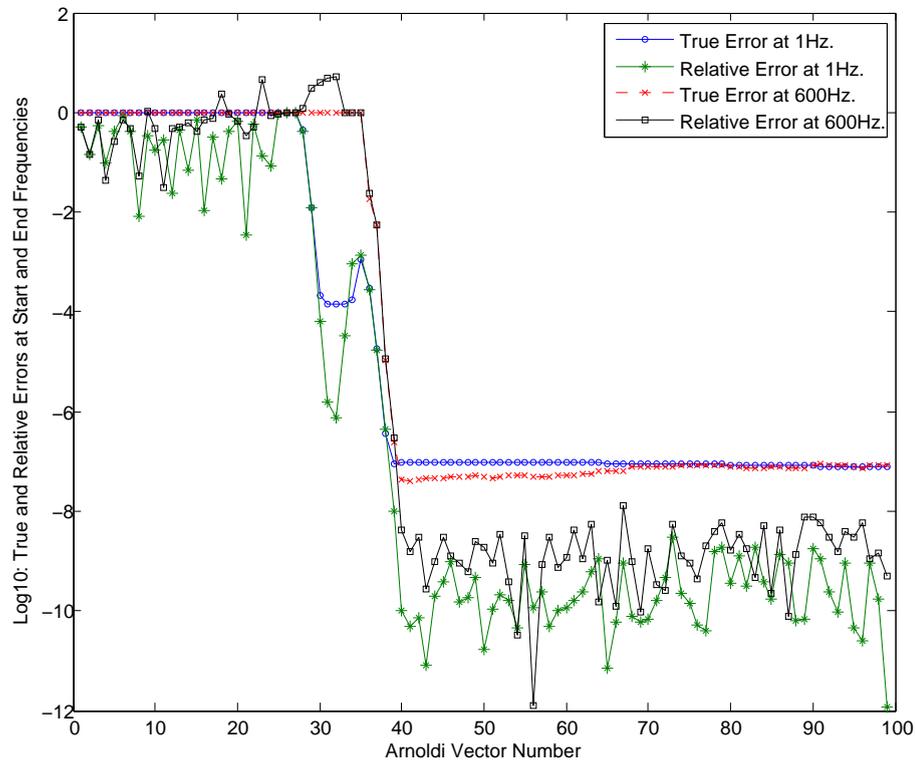
Figure 5.70.: Convergence pattern for moment-matching Arnoldi (OSA) projection at 1Hz and 600Hz for ζ=0.05.
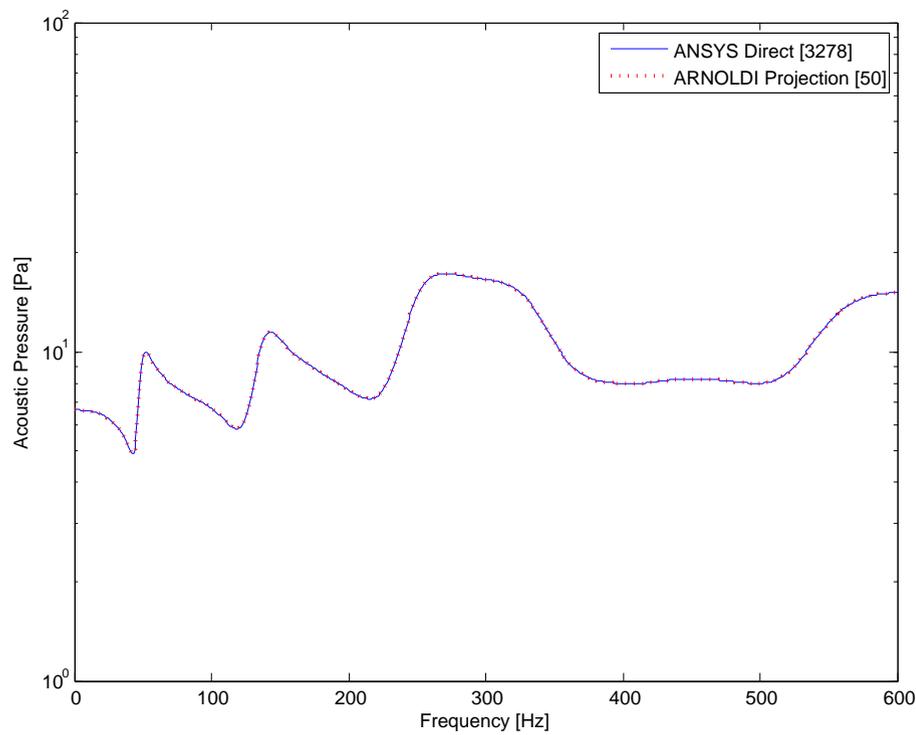
Figure 5.71.: Predicted Fluid Noise Transfer Function using direct and moment-matching Arnoldi (OSA) projection for fluid node at (0.135m,0.07m,0.175m) for ζ=0.10.
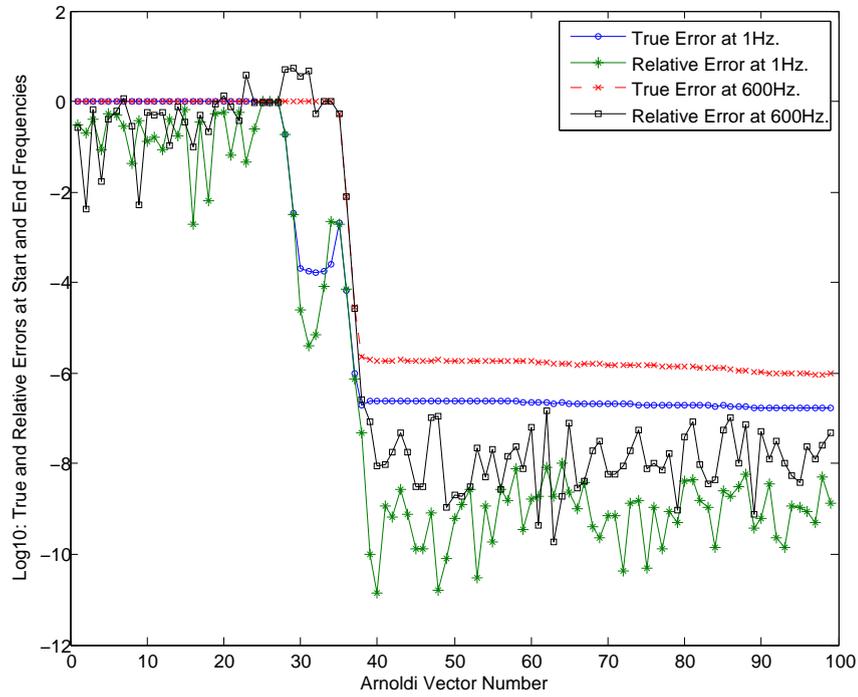
Figure 5.72.: Convergence pattern for moment-matching Arnoldi (OSA) projection at ω=1Hz and ω=600Hz for ζ=0.10.
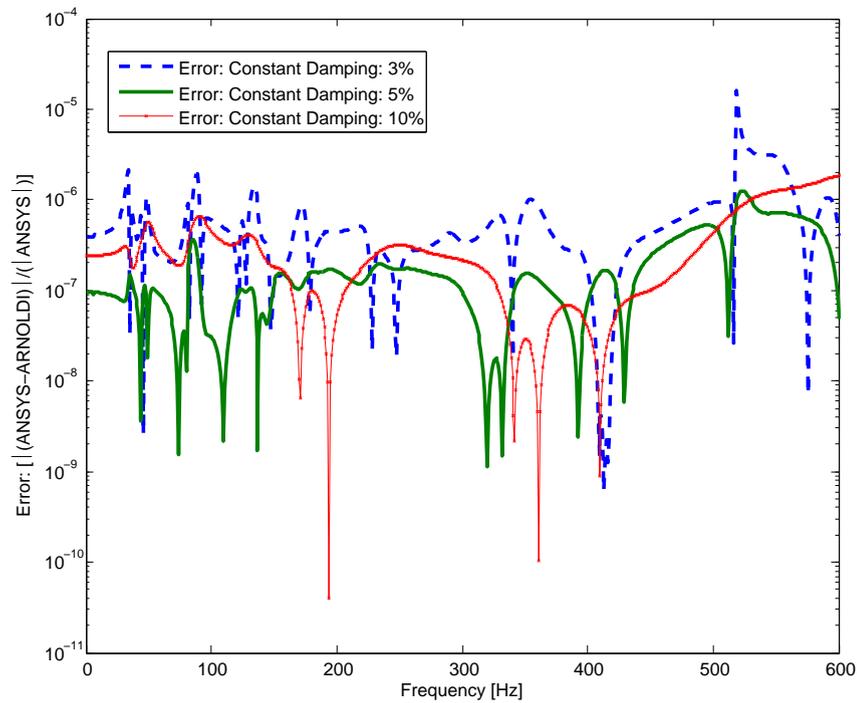
Figure 5.73.: Error plot for fluid grid point at (0.135m,0.07m,0.175m) for damping values: ζ=0.03, ζ=0.05, ζ=0.10.

ally be observed that while the error quantities are very low around the expansion point (where the higher dimensional, second order system matrices are factorized) for the TS-SOAR process, the error quantities in general, are very low throughout the entire frequency range for the linearized ROM. The observation is consistent with all three damping models investigated in this test case. This means that, the higher dimensional linearized model generates a ROM where the errors are the least - compared with the second order retaining TS-SOAR process.
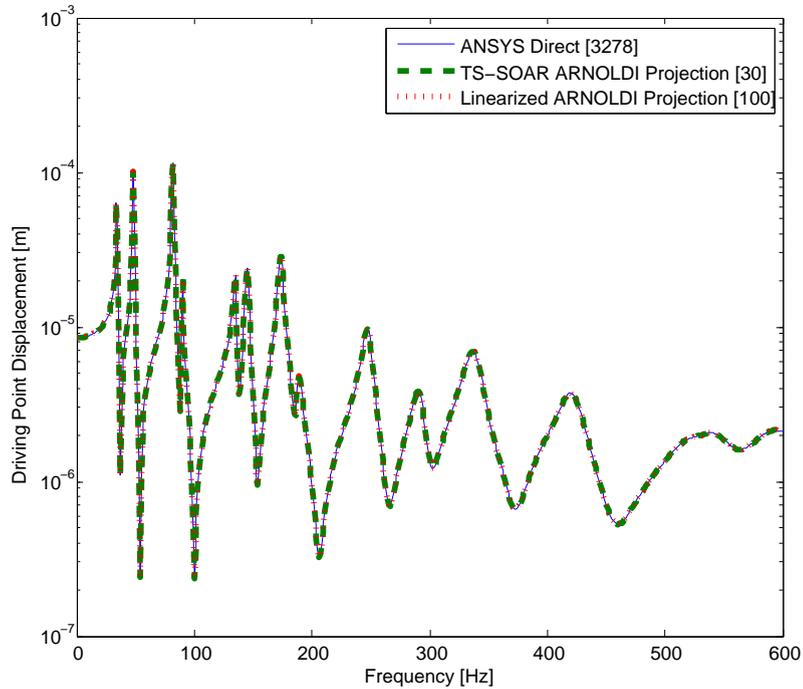
Figure 5.74.: Predicted Driving Point Displacement Transfer Function (Receptance) using direct and moment-matching Linearized Arnoldi and TS-SOAR projection for structural node at (0.039m,0.14m,0.078m) for β_j^m=2.0E-05.
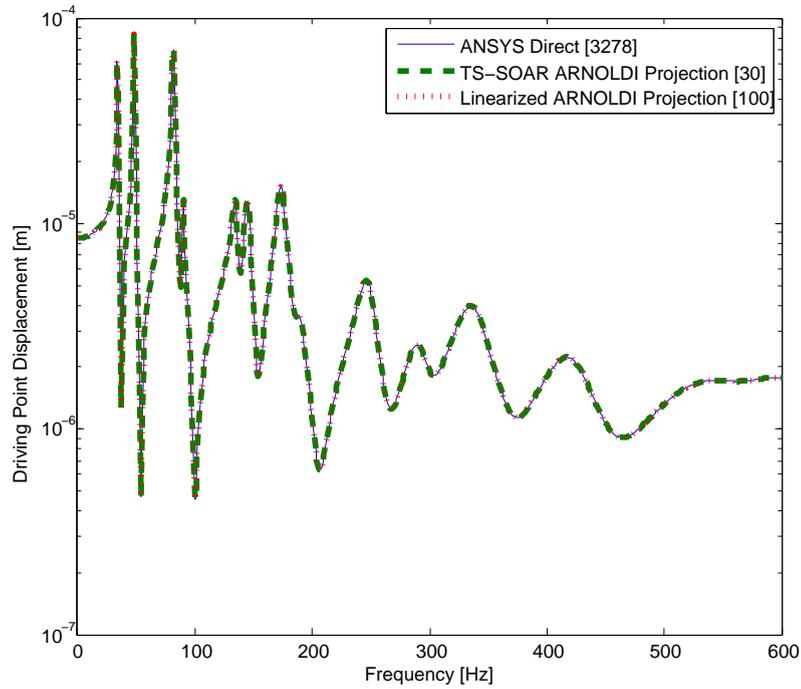
Figure 5.75.: Predicted Driving Point Displacement Transfer Function (Receptance) using direct and moment-matching Linearized Arnoldi and TS-SOAR projection for structural node at (0.039m,0.14m,0.078m) for β_j^m=4.0E-05.
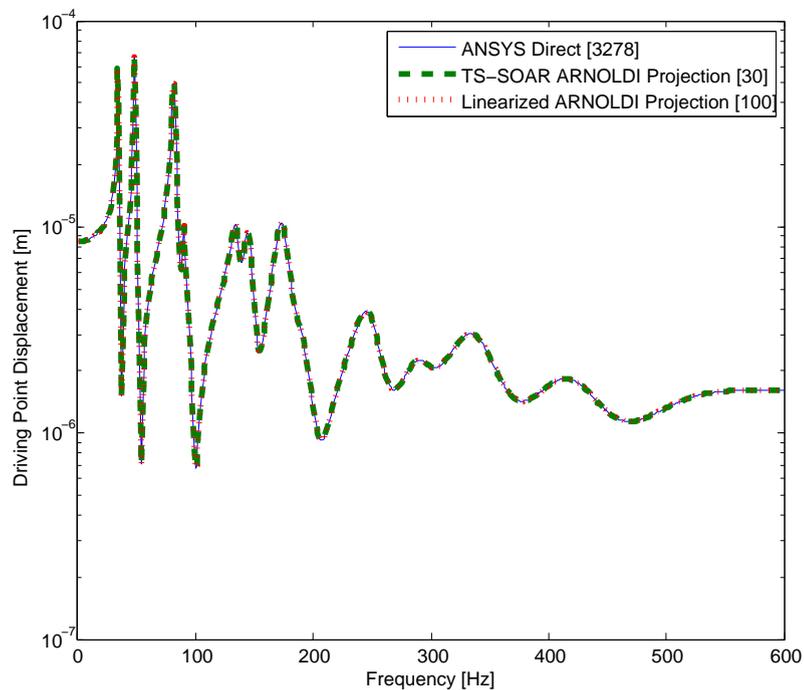
Figure 5.76.: Predicted Driving Point Displacement Transfer Function (Receptance) using direct and moment-matching Linearized Arnoldi and TS-SOAR projection for structural node at (0.039m,0.14m,0.078m) for β_j^m=6.0E-05.
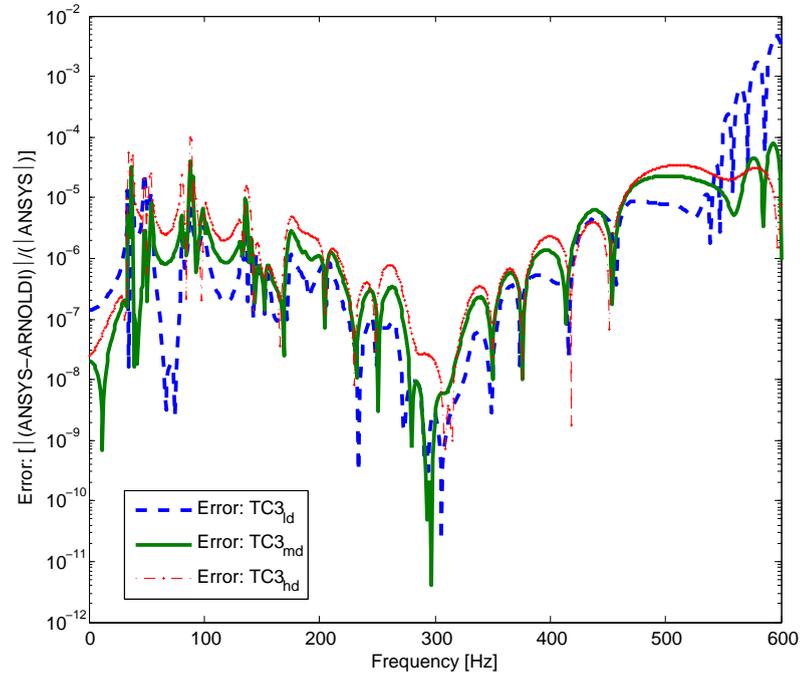
Figure 5.77.: Error plot for Predicted Driving Point Displacement Transfer Function (Receptance) at (0.039m,0.14m,0.078m) for TS-SOAR projection for damping values: β_j^m=2.0E-05 [TC3$_{ld}$], β_j^m=4.0E-05 [TC3$_{md}$], β_j^m=6.0E-05 [TC3$_{hd}$].
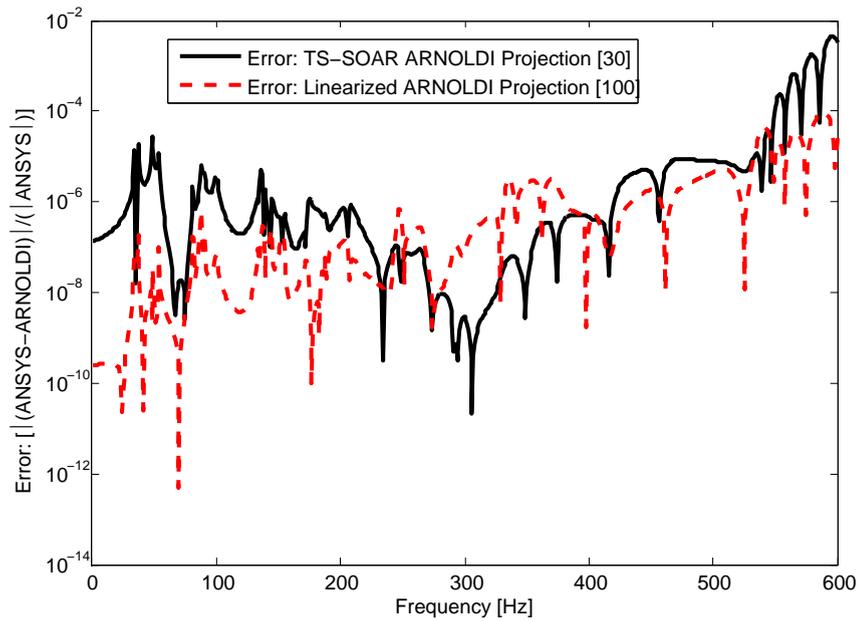
Figure 5.78.: Error plot for Predicted Driving Point Displacement Transfer Function (Receptance) at (0.039m,0.14m,0.078m) for Linearized Arnoldi and TS-SOAR projections with damping value β_j^m=2.0E-05 [TC3$_{ld}$].
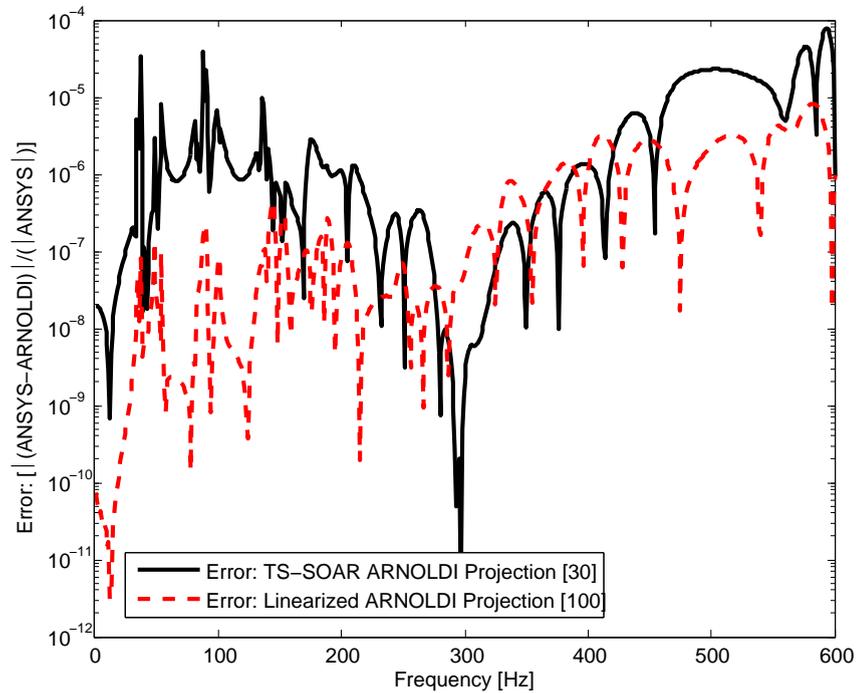
Figure 5.79.: Error plot for Predicted Driving Point Displacement Transfer Function (Receptance) at (0.039m,0.14m,0.078m) for Linearized Arnoldi and TS-SOAR projections with damping value β_j^m=4.0E-05 [TC3$_{md}$].
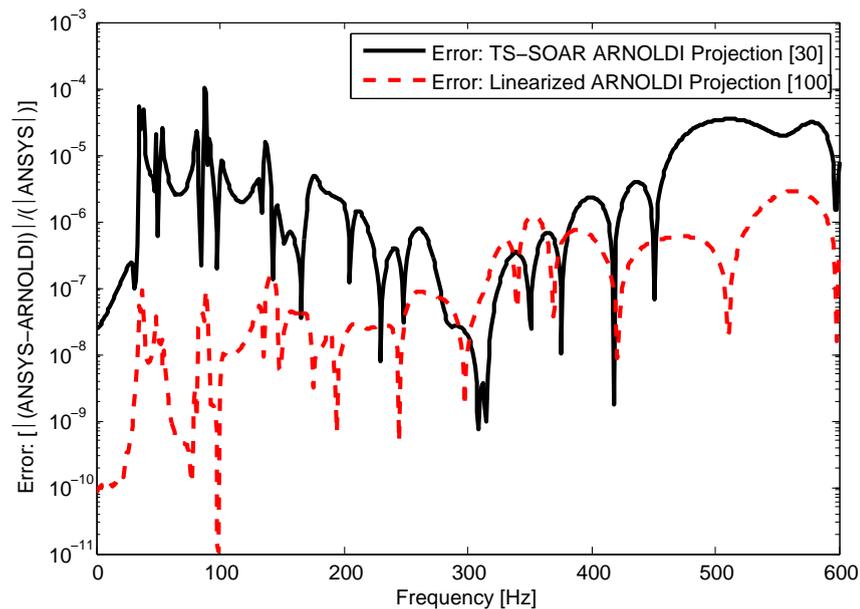
Figure 5.80.: Error plot for Predicted Driving Point Displacement Transfer Function (Receptance) at (0.039m,0.14m,0.078m) for Linearized Arnoldi and TS-SOAR projections with damping value β_j^m=6.0E-05 [TC3$_{hd}$].
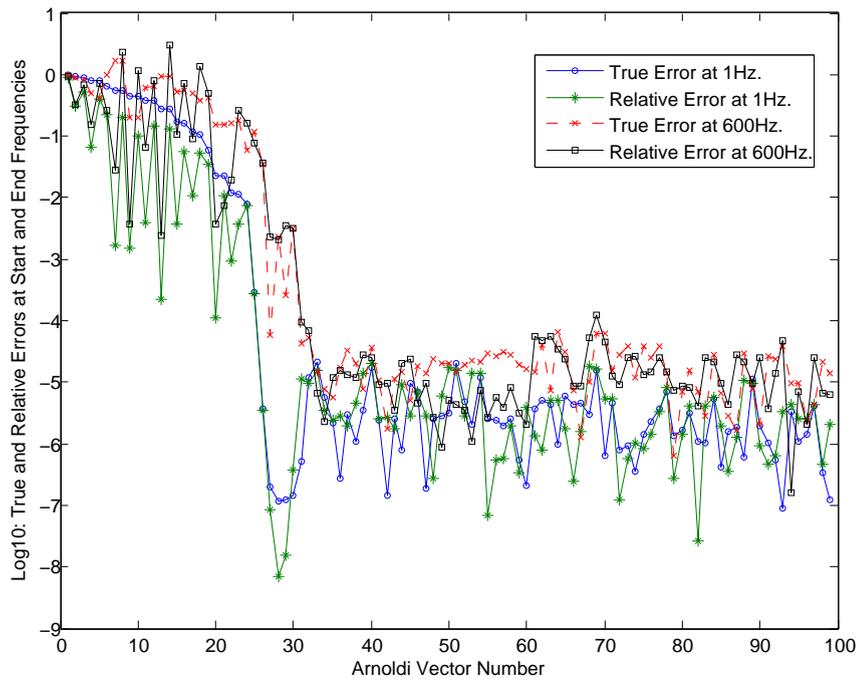
Figure 5.81.: Convergence pattern for moment-matching Arnoldi (TS-SOAR) projection at 1Hz and 600Hz for β_j^m=2.0E-05.
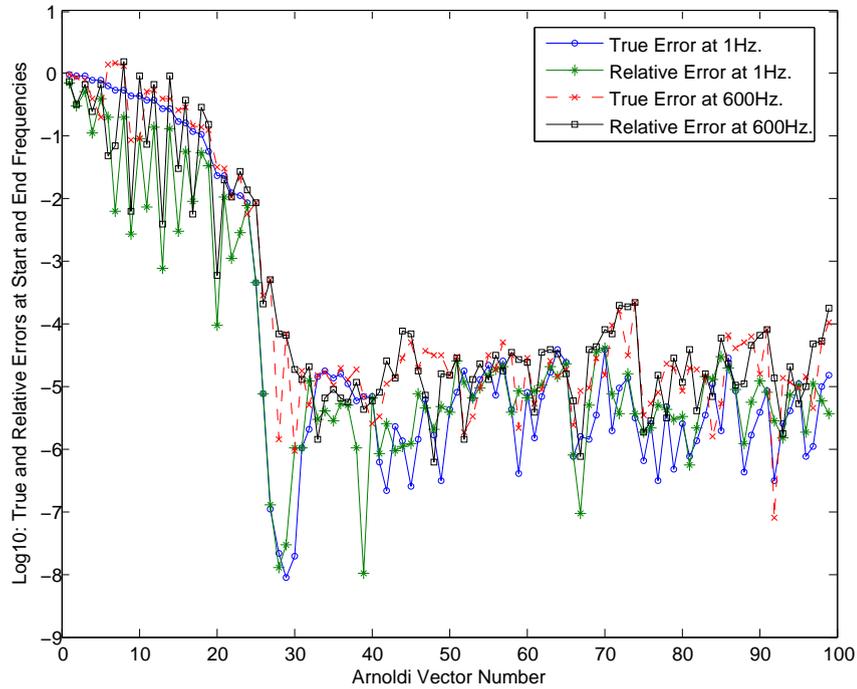
Figure 5.82.: Convergence pattern for moment-matching Arnoldi (TS-SOAR) projection at 1Hz and 600Hz for β_j^m=4.0E-05.

The computational times required to solve the coupled model via ANSYS direct inversion method for the undamped and constantly damped test cases via the One-sided Arnoldi process is shown in Table:[5.13]. For these test cases, the computational time for the ROM is simply the sum of Arnoldi vector generation, projection to second order form and reduced harmonic analysis in the desired frequency band and sub steps. That is, the computational time required to read and write the higher dimensional system matrices are excluded. This is because, in the case of direct implementation of Arnoldi variants in a commercial FE environment, it is easy to continue directly from the globally assembled structural-acoustic matrices thereby alleviating the problem of extracting the assembled matrices. It is worth adding that, similar to Test Case No. 2, the complex numbers relating to the structural damping are extracted. The higher dimensional model is then read using Mathematica (Wolfram 2003), and order reduction and projection performed via the Arnoldi process. The reduced harmonic analysis and convergence of the reduced system is
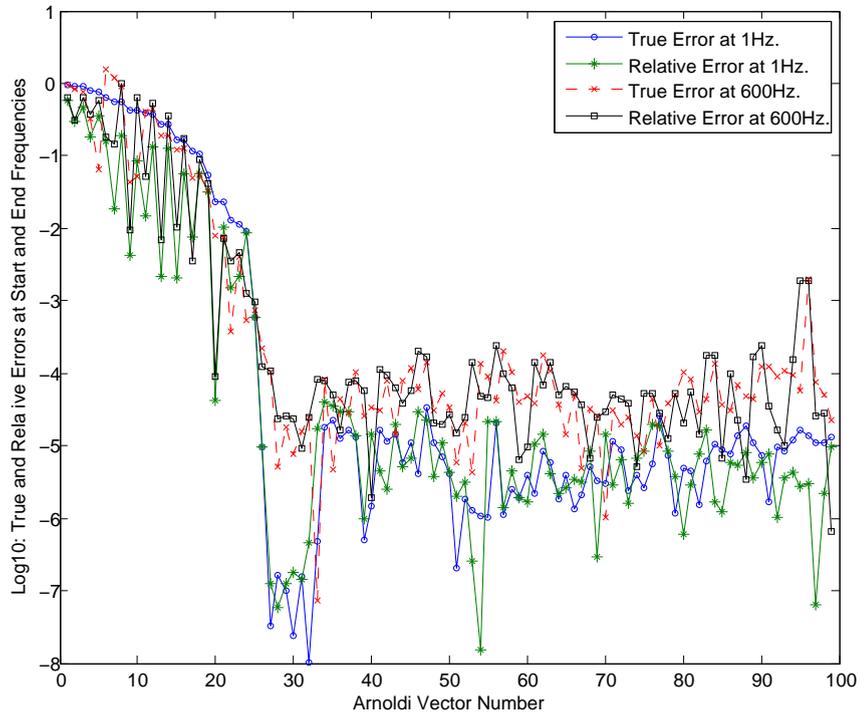
Figure 5.83.: Convergence pattern for moment-matching Arnoldi (TS-SOAR) projection at 1Hz and 600Hz for β_j^m=6.0E-05.
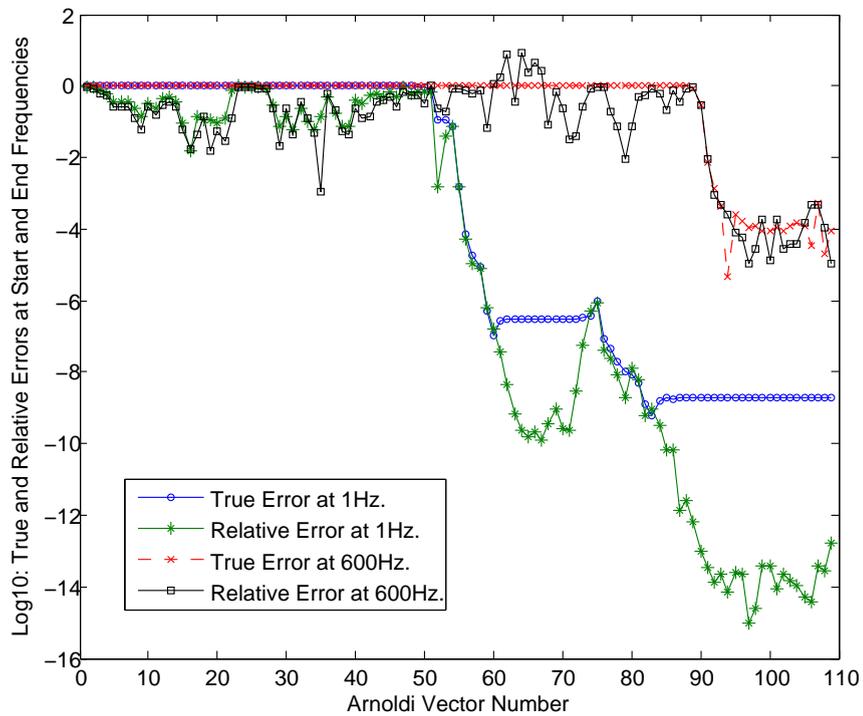
Figure 5.84.: Convergence pattern for moment-matching Linearized Arnoldi projection at 1Hz and 600Hz for β_j^m=2.0E-05.
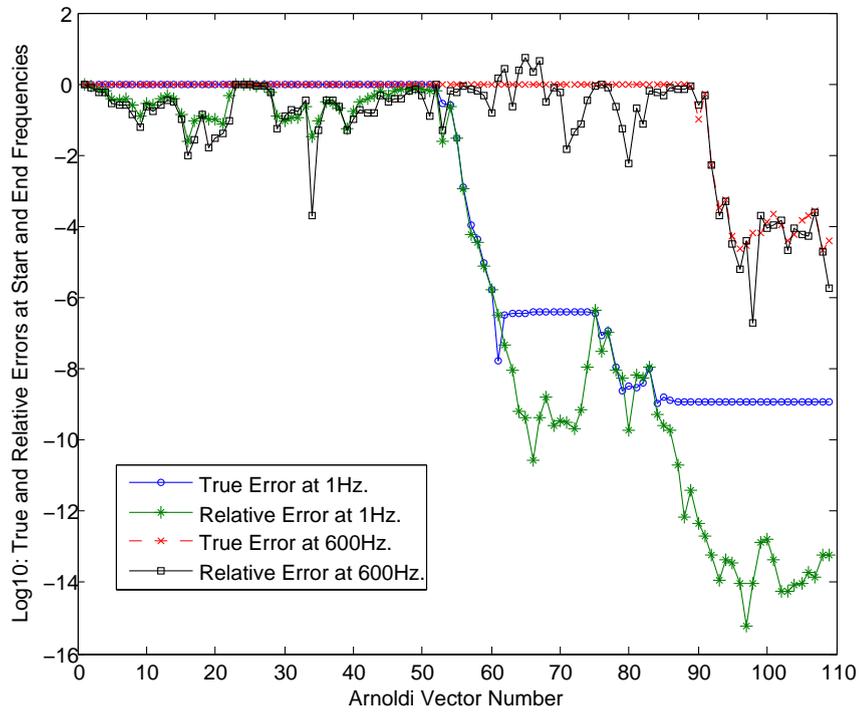
Figure 5.85.: Convergence pattern for moment-matching Linearized Arnoldi projection at 1Hz and 600Hz for β_j^m=4.0E-05.
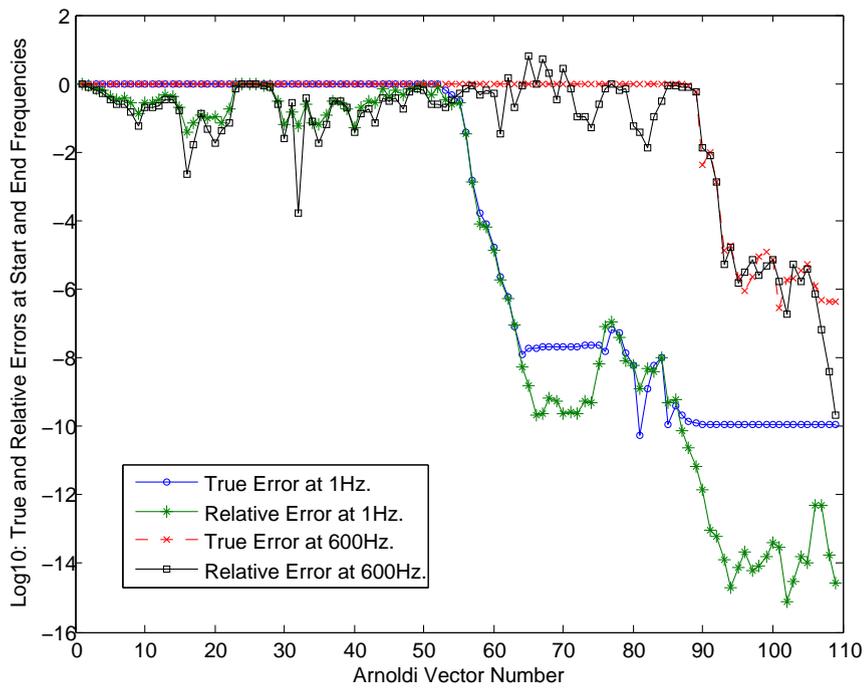
Figure 5.86.: Convergence pattern for moment-matching Linearized Arnoldi projection at 1Hz and 600Hz for β_j^m=6.0E-05.

then performed using LU decomposition in Mathematica/Matlab (Matlab 2006) environment.

Obviously, the resulting accuracy of the linearized approach and second order retaining TS-SOAR process warrants a comparison of computational time for both ROM methods in the case of frequency dependent structural damping. The computational times required to solve the coupled system via the ANSYS direct inversion method and dimension reduction via the linearization Arnoldi (OSA) approach and structure preserving TS-SOAR approach are shown in Table:[5.14].

Similar to the undamped and constantly damped computations, the computational time for the ROM is simply the sum of Arnoldi vector generation, projection to first order (Linearization Arnoldi) / second order form (TS-SOAR) and reduced harmonic analysis in the desired frequency band and substeps. It can be observed that the computational time required by the linearization approach is slightly higher than the structure preserving TS-SOAR process. This is primarily due to the larger size of the fully coupled structural-acoustic system encountered due to the conversion to a first order system of double the dimension. As a result, an LU factorization of the first order system matrices is expensive. It is worth reminding the reader that, in this test case, the order of the higher dimensional system is quite small (3278 states) and the converted state space model (6556 states) is still small thus making an LU factorization of the system matrices possible using standard numerical packages like MATLAB/Mathematica[8]. However, for a large scale system, it is likely that an LU factorization of the converted first order system is not possible due to memory requirements, thus making the linearization approach often not practical. On the other hand, the TS-SOAR process does not require any conversion, and therefore

---

[8]In MATLAB an LU decomposition is performed using the [L,U,P] = lu(A) and subsequently the backslash operator is used to solve the set of linear equations (Matlab 2006). In Mathematica the command LinearSolve[A, b] performs an LU decomposition and the required forward and backward substitution to solve the matrix equation A.x=b (Wolfram 2003).

only requires an LU factorization (around a given expansion point) of the original system matrices.

Table 5.13.: A comparison of computational times for undamped and damped test cases.

Test Case	ANSYS Direct	ROM via Arnoldi	Time Reduction
$\zeta = 0$	2435 s	8.9 s	99.6%
TC3$_{LD}$	1136 s	13.6 s	98.8%
TC3$_{MD}$	915 s	14.2 s	98.4%
TC3$_{HD}$	1579 s	12.9 s	99.1%

Table 5.14.: A comparison of computational times for frequency dependent damping test cases.

Test Case	ANSYS Direct	ROM via Arnoldi [Linearization]	ROM via Arnoldi [TS-SOAR]
TC3$_{ld}$	1803 s	30.2 s (-98.3%)	13.7 s (-99.2%)
TC3$_{md}$	1346 s	23.4 s (-98.3%)	13.8 s (-98.9%)
TC3$_{hd}$	1796 s	20.4 s (-98.8%)	13.5 s (-99.2%)

The undamped noise transfer function for the fluid node, considering air as the fluid medium backed by a fully clamped plate (see Table:[5.12]) is shown in Figure:[5.87]. The prediction error, considering the transfer function states, obtained by ANSYS direct inversion and TSA projection framework is shown in Figure:[5.88]. It can be observed that the transfer functions via the TSA projection framework and direct inversion are identical in terms of pressure amplitudes. Further, the dimension of the ROM in this case is 11. i.e. the ROM matrices: M_{rsa}, K_{rsa} are of dimensions 11×11. For the acoustically damped, free-free plate test case, the TS-SOAR pro-

cess was used to generate the ROM. The resulting noise transfer function and the subsequent local error is shown in Figures:[5.89,5.90]. In this test case, the dimension of the ROM (including C_{rsa}) is 50. Compared to the fully clamped test case with no acoustic damping, an increase in the number of Arnoldi vectors is evident. This increase is primarily due to the boundary conditions of the structure, which in turn influences the noise transfer function. An interesting observation can be made from a modal view-point, that is, since the modal density of a free-free plate tends to be higher than a clamped plate, more Arnoldi vectors are required to accurately capture the low frequency dynamics of the coupled system.

The computational times required for the air filled rectangular cavity test cases, are tabulated in Table:[5.15]. Note that in these test cases, the two-sided Arnoldi variants (TSA and TS-SOAR) are tested for solution accuracy and computational efficiency. The ROM timings include only the time required for the Arnoldi vector generation, projection to second order form and reduced harmonic analysis. The matrix extraction times are excluded due to the reasons mentioned earlier. It can be seen that the computational times via ROM variants is almost negligible, when compared to directly solving the system of equations.

Table 5.15.: A comparison of computational times for undamped and acoustically damped air filled test cases.

Test Case	ANSYS Direct	ROM via Arnoldi	Time Reduction
[TC3$_{FFa}$]	1095 s (100%)	18.5 s (1.68%)	98.31%
[TC3$_{CLa}$]	1551 s (100%)	4.9 s (0.31%)	99.68%
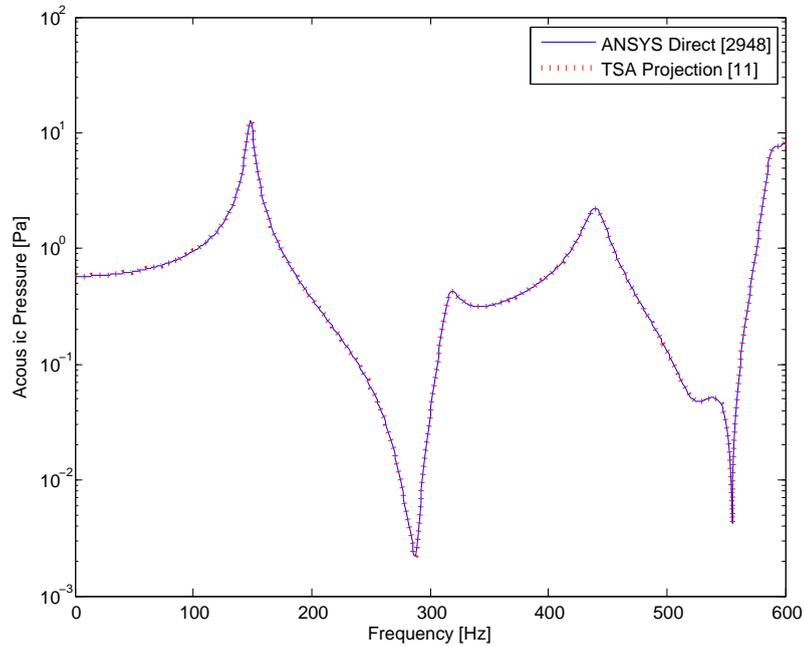
Figure 5.87.: Predicted Noise Transfer Function (NTF) using direct and moment-matching TSA projection for fluid node at (0.135m,0.07m,0.175m) for the air filled, clamped plate model.
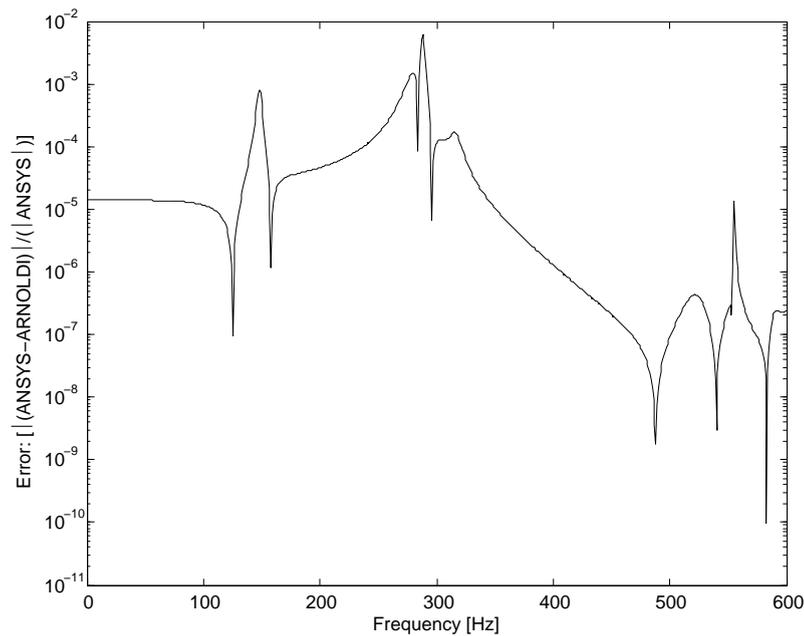
Figure 5.88.: Error plot for ANSYS and TSA predicted Noise Transfer Functions (NTF) for fluid node at (0.135m,0.07m,0.175m).
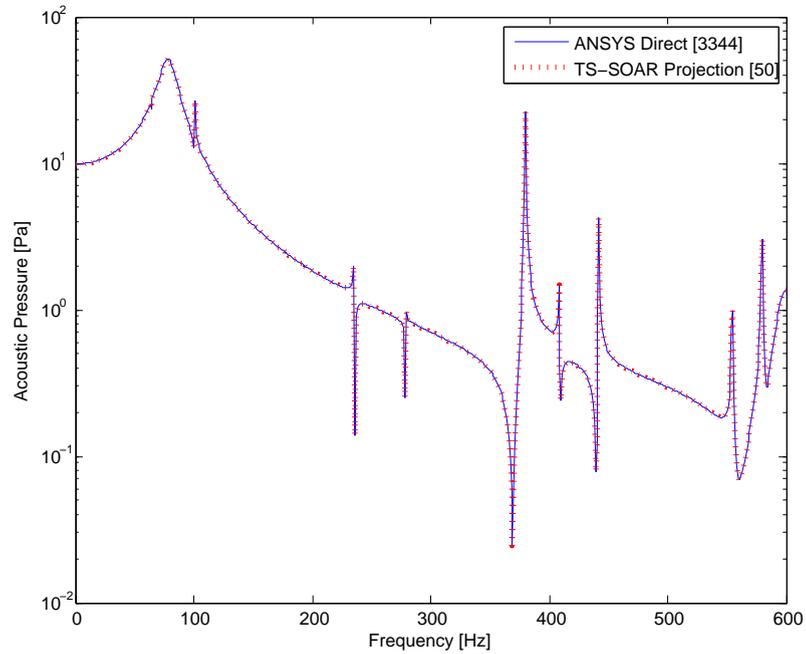
Figure 5.89.: Predicted Noise Transfer Function (NTF) using direct and moment-matching TSA projection for fluid node at (0.135m,0.07m,0.175m) for the air filled, free-free plate model.
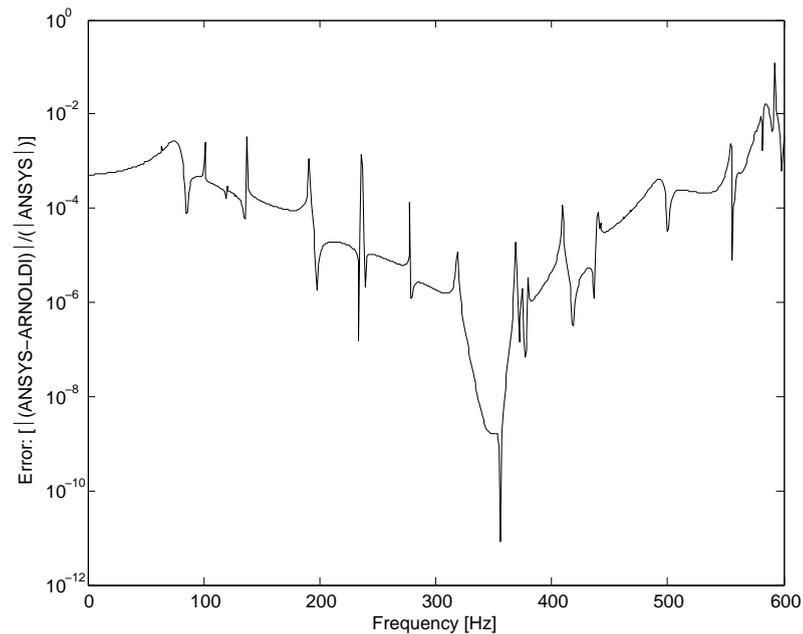
Figure 5.90.: Error plot for ANSYS and TS-SOAR predicted Noise Transfer Functions (NTF) for fluid node at (0.135m,0.07m,0.175m).

5.5. Test Case: 4: Cylinder enclosing an air-filled cavity

A steel cylinder is considered as the fourth test case to test the accuracy and efficiency of the proposed Arnoldi based projection formulations. The cylinder has the following dimensions: 1.01 m long, 0.18256 m radius, and 0.001219 m thick. The steel has the following mechanical properties: Young's modulus E_s= 200 GPa, mass density ρ_s=7800kg/m^3, Poisson's ratio v_s=0.33. The cavity is filled with air having the following properties: speed of sound c=343m/s, mass density ρ_c=1.2kg/m^3. The coupled system is excited using a normal unit point load defined in Figure:[5.91]. A description of this test case can also be found in Tournour and Atalla (2000), Boily and Charron (1999).

The cylinder is discretized using 32 4-node quadrilateral ANSYS SHELL63 along the perimeter and 22 elements along the length. The cavity is discretized using 4-node one DOF pressure elements (ANSYS FLUID30) with 32 mesh divisions along the perimeter, 22 mesh divisions along the length, and 15 mesh divisions along the diameter. Two variations of the test case are considered here: (a) Clamped and (b) Free-Free. The coupled free-free FE/FE discretized model is shown in Figure:[5.92]. The desired output quantities considered for this test case are the fluid nodal pressure values along the central axis of the cylinder. All three forms of damping are considered for this test case: (a) undamped (b) constantly damped and (c) frequency dependent, linearly varying structural damping. A description of the undamped and damped test cases are tabulated in Table:[5.16].

The sparsity plot of the globally assembled higher dimensional stiffness, mass and damping matrices for TC4$_{FD2}$ is shown in Figures:[5.93,5.94, 5.95] respectively. For Test Case: TC4$_{FD2}$ (Table:5.16), two different Arnoldi variants are considered

Table 5.16.: Damping values and Expansion points for One sided Arnoldi and TS-SOAR Process for Test Case No.4 ‡ B.C's: Boundary conditions.

B.C's‡	Damped Test Cases	Damping Value	Expansion Point
Free-Free	Undamped [TC4$_{FF}$]	–	300Hz
Clamped	Undamped [TC4$_{CL}$]	–	600Hz
Clamped	Constant Damping [TC4$_{CD1}$]	β_j^ζ=0.05	550Hz
Clamped	Constant Damping [TC4$_{CD2}$]	β_j^ζ=0.10	550Hz
Clamped	Freq. Dependent [TC4$_{FD1}$]	β_j^m=5.0E-05	600 / 600 Hz
Clamped	Freq. Dependent [TC4$_{FD2}$]	β_j^m=7.0E-05	600 / 600Hz

for dimension reduction: (a) Equivalent linearized system followed by One-Sided Arnoldi (LIN-OSA) reduction and (b) Structure preserving, Two-Sided Second order Arnoldi (TS-SOAR) reduction. The sparsity plot of the equivalent linearized system is shown in Figures:[5.96, 5.97].
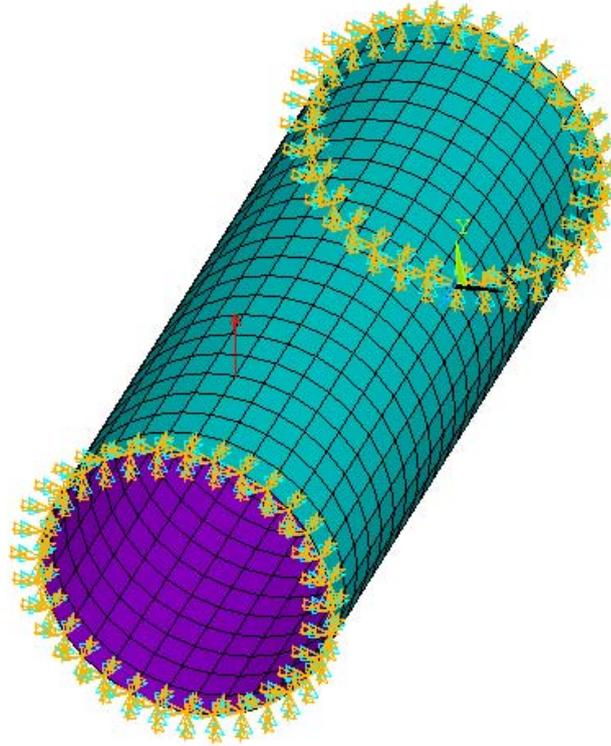
Figure 5.91.: Test Case No. 4: Clamped Cylindrical cavity (air filled) system - Structural Finite Element model. Excitation location: (0.039m,0.14m,0.078m); Measurement location(s): 21 fluid grid points along the central axis of the cylinder.
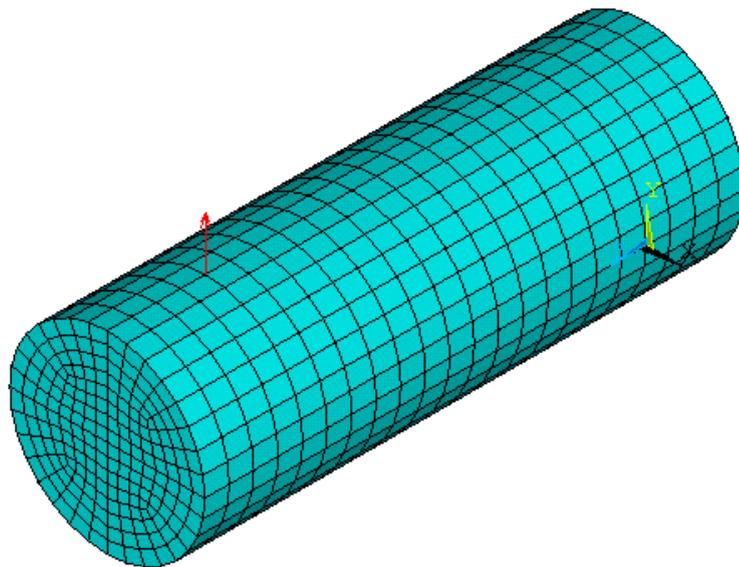
Figure 5.92.: Test Case No. 4: Free-Free Cylindrical cavity (air filled) system: Fully Coupled FE model.
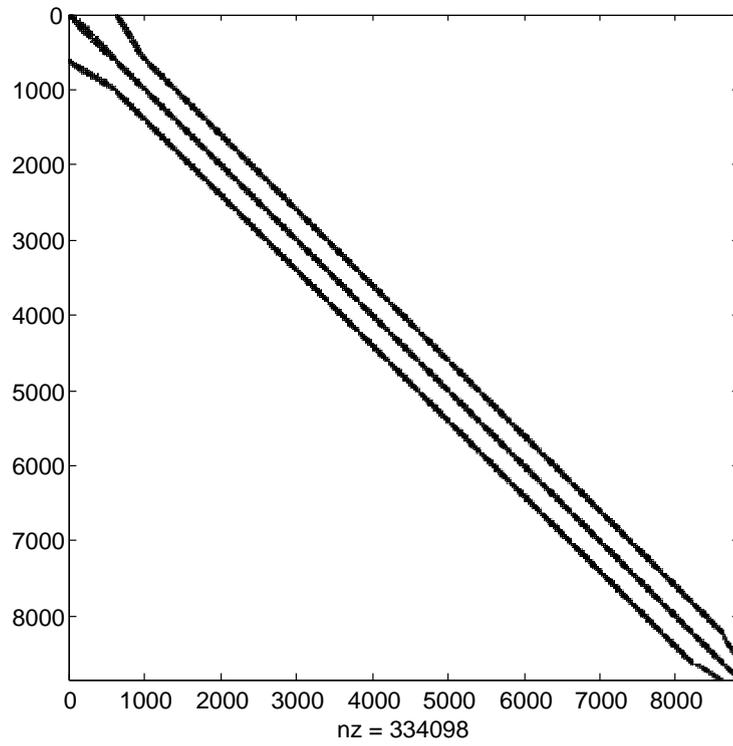
Figure 5.93.: Test Case No. 4: Clamped Cylindrical cavity: Global Stiffness Matrix sparsity plot.
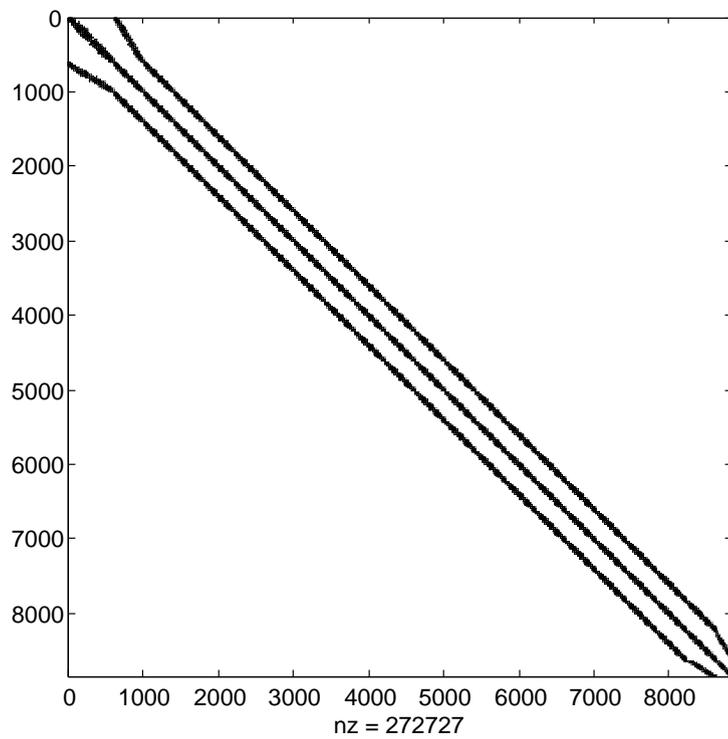
Figure 5.94.: Test Case No. 4: Clamped Cylindrical cavity: Global Mass Matrix sparsity plot.
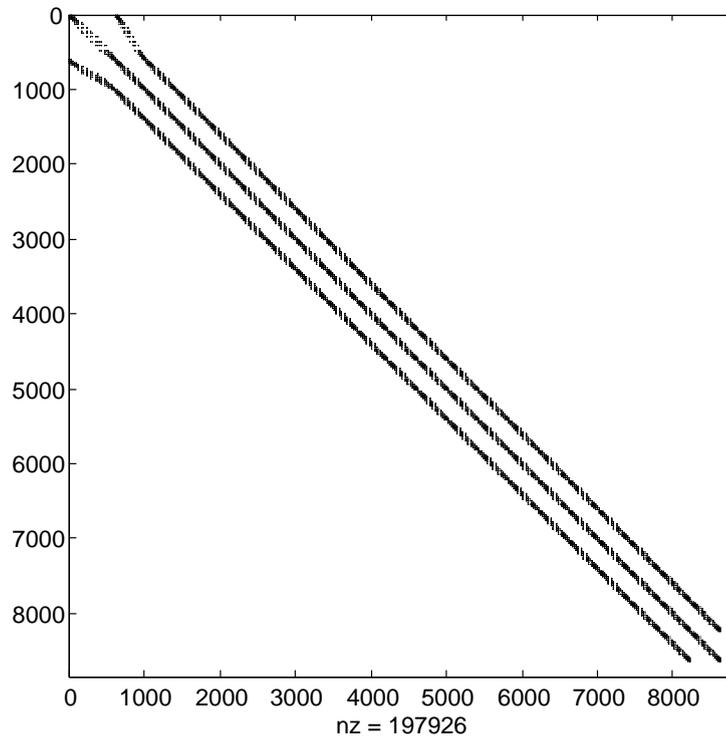
Figure 5.95.: Test Case No. 4: Clamped Cylindrical cavity: Global Damping Matrix sparsity plot
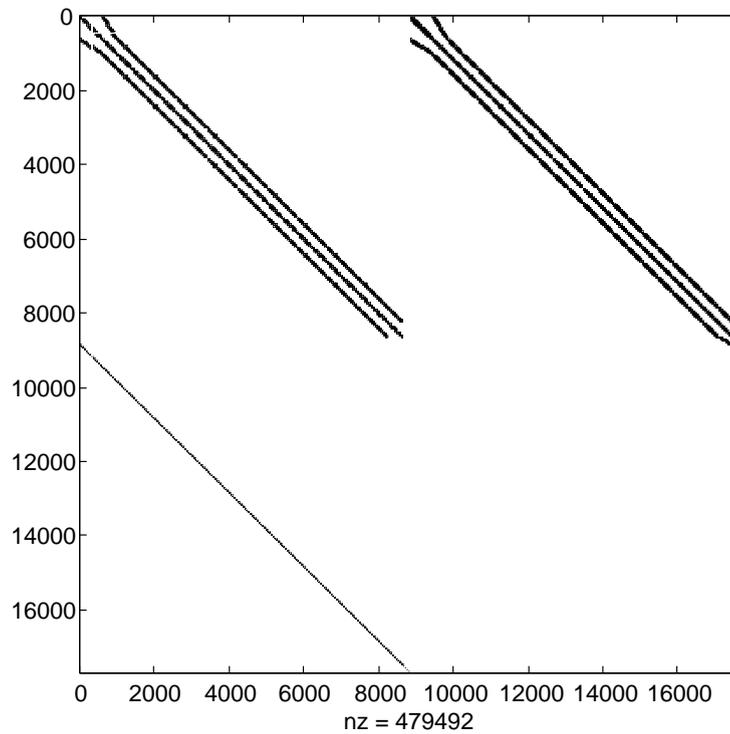
Figure 5.96.: Test Case No. 4: Equivalent Linearized System (Equation:4.70a) $\mathbf{D}_{sa}$ sparsity plot for β_j^m=7.0E-05 [TC4$_{FD2}$].
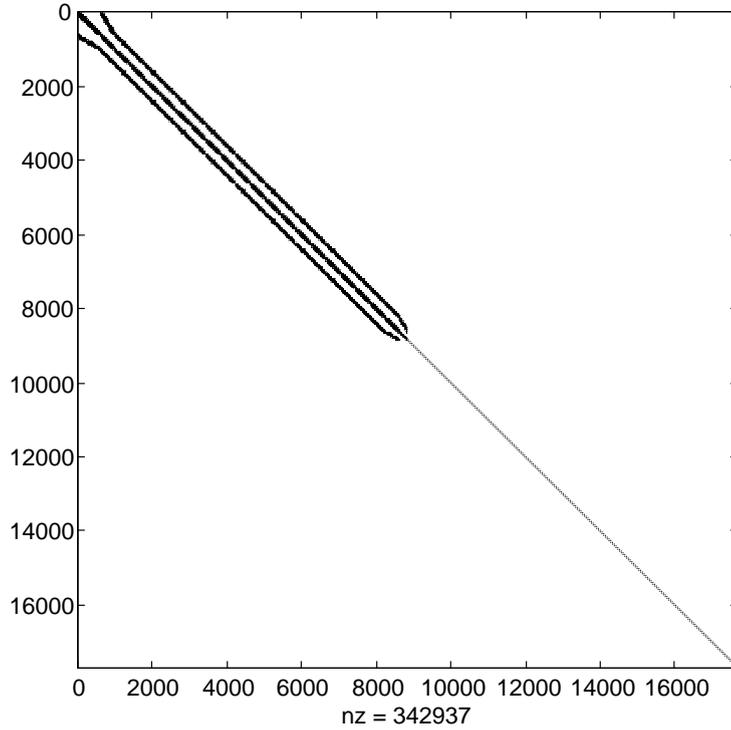
Figure 5.97.: Test Case No. 4: Equivalent Linearized System (Equation:4.70a) $\mathbf{G}_{sa}$ sparsity plot for β_j^m=7.0E-05 [TC4$_{FD2}$].

5.5.1. Computational Results and Discussion

For the undamped test cases described in Table:[5.16], the fluid acoustic noise transfer function (for 21 fluid outputs along the central axis) are shown in Figures:[5.98, 5.101]. It can be seen that there is no visible difference between the RMS averaged (reference pressure: 20E-06 N/m^2) transfer functions (SPL) values, obtained using the direct inversion technique and ROM via Arnoldi. The corresponding local error quantities are shown in Figures:[5.99, 5.102] respectively. The maximum error for the RMS averaged sound pressure values is in the order of 10^{-2}. Considering SPL values, this means that the difference between direct inversion and ROM via Arnoldi computed pressures is almost negligible. The convergence patterns in the plots shown in Figures:[5.100,5.103] suggest that it is not possible to better approximate the solution states by generating more than 100 vectors for the free-free test case and 70 vectors for the clamped test case. The difference in the number of vectors can be attributed to the boundary conditions (from a modal view-point,

more modes are encountered with free-free boundary conditions) and the resulting dimension of the higher dimensional states[9].
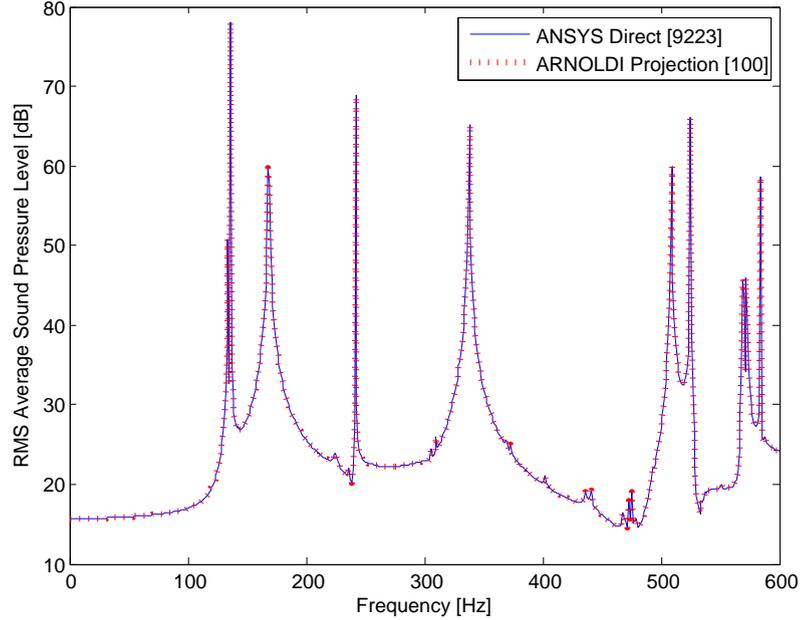
Figure 5.98.: Predicted RMS Averaged Fluid Noise Transfer Function using direct and moment-matching Arnoldi projection utilizing 21 fluid pressure outputs along the central axis of the undamped free-free cylinder [TC4$_{FF}$].

The RMS averaged noise transfer functions for the constantly damped test cases with $\zeta = 0.05$ and $\zeta = 0.10$ are shown in Figures:[5.104, 5.107]. Again, similar to the undamped test case, it can be be observed that there is no visible difference between the transfer functions, and the solution can be said to have converged for the chosen outputs. The local error plots for the corresponding transfer functions in Figures:[5.105, 5.109] indicate that the maximum error is in the order of 10^{-4}. Obviously, the higher accuracy of the damped solutions can be attributed to the fact that the response is well smoothed (when compared with the undamped transfer

---

[9]The free-free model consists of 9223 (fluid+structure) DoFs, the clamped model 8839 (fluid+structure) DoFs. The reduction in DoFs for the same model is due to the introduction of clamped boundary conditions accounted for as zeros in the structural FE model. Therefore, the equations are deleted from the global structural-acoustic model resulting in a lower DoF count.
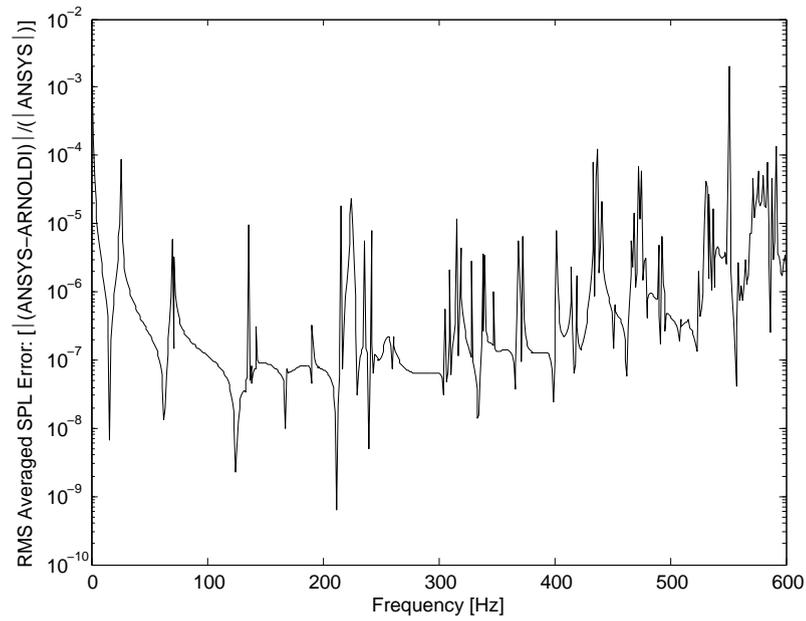
Figure 5.99.: Local RMS Averaged Error Plot utilizing 21 fluid pressure outputs [TC4$_{FF}$].
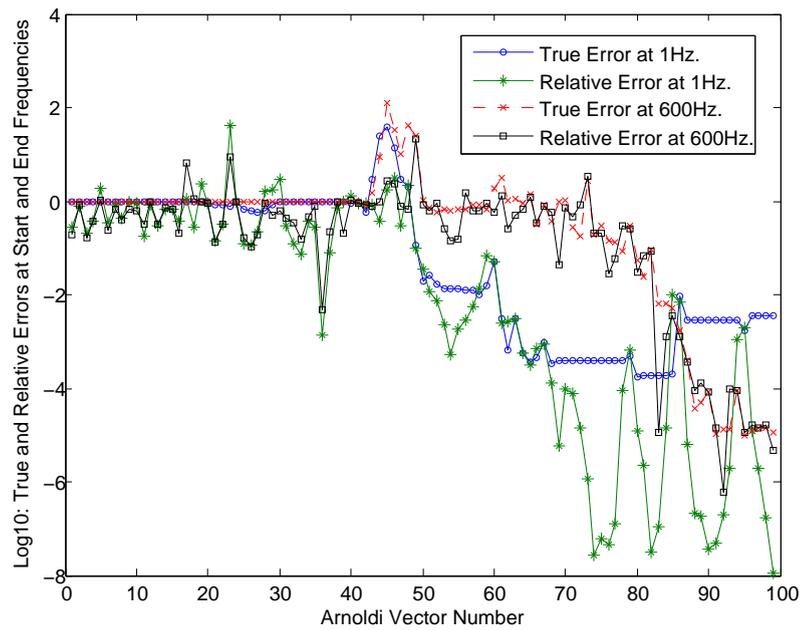
Figure 5.100.: Convergence pattern utilizing 21 fluid pressure outputs [TC4$_{FF}$].
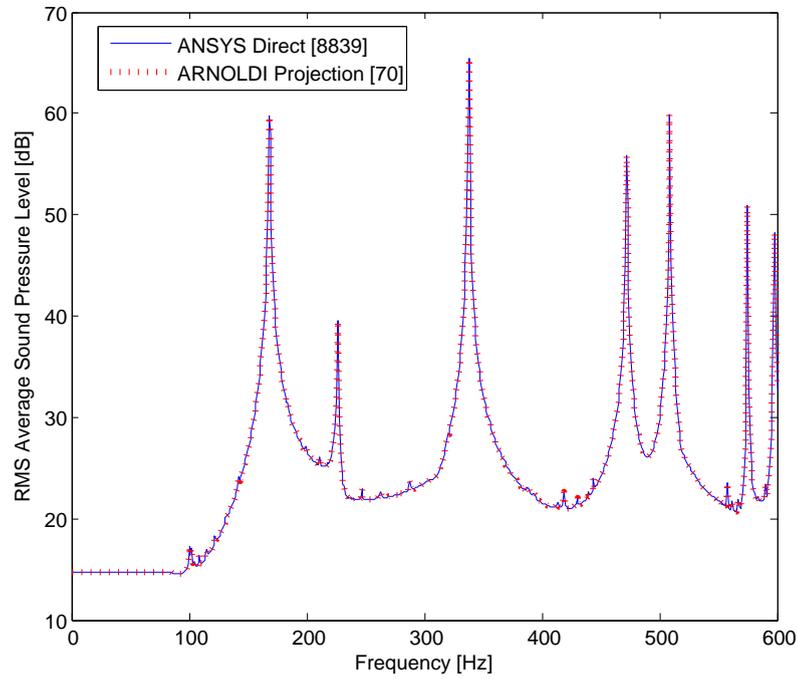
Figure 5.101.: Predicted RMS Averaged Fluid Noise Transfer Function using direct and moment-matching Arnoldi projection utilizing 21 fluid pressure outputs along the central axis of the clamped cylinder model [TC4$_{CL}$].
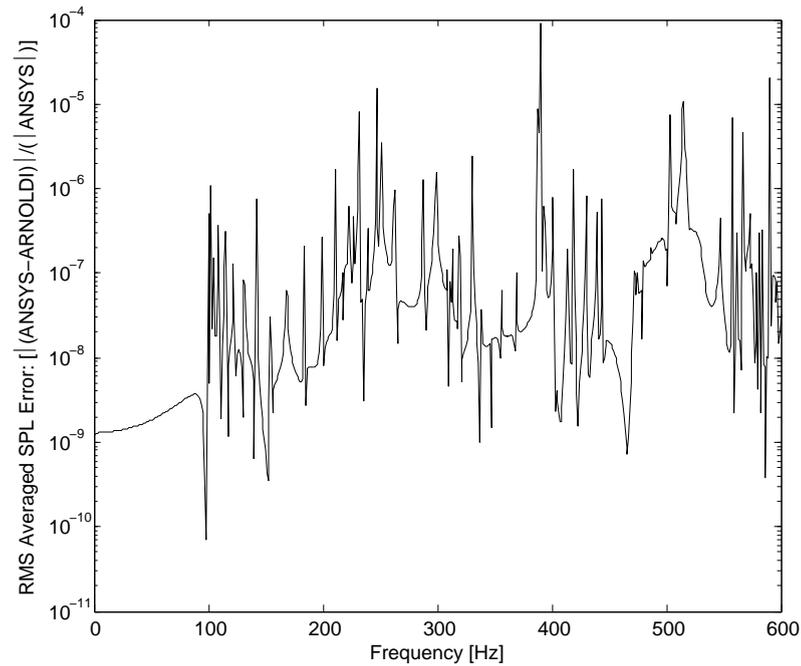
Figure 5.102.: Local RMS Averaged Error Plot utilizing 21 fluid pressure outputs [TC4$_{CL}$].
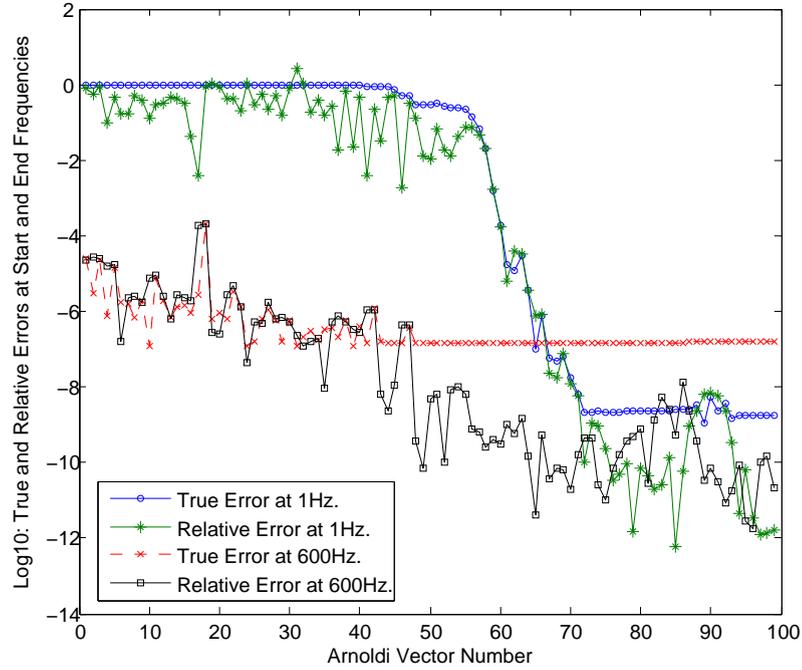
Figure 5.103.: Convergence pattern for 21 fluid pressure outputs [TC4$_{CL}$].

functions) in the case of a damped model. From a moment-matching viewpoint, the higher accuracy could mean that the original higher dimensional model is stable. This would mean that a damped structural-acoustic model is more stable than an undamped model. Additionally, from the convergence plots shown in Figures:[5.106, 5.108] indicate that to achieve convergence, a reduced order model of 60 is required. Therefore 60 Arnoldi vectors were generated for this test case.

For the frequency dependent damping models, the SISO Two-Sided Second Order Arnoldi (TS-SOAR) and the first order based linearization (with OSA) framework are investigated to generate the reduced order models. For the frequency dependent damping model [TC4$_{FD1}$], with β_j^m=5.0E-05, the noise transfer function at the center of the cylinder is shown in Figure:[5.110]. The local error plot (Figure:5.111) and the convergence pattern (Figure:5.112) shows that no accuracy is lost by generating the ROM via TS-SOAR approach and that no more than 40 Arnoldi generated
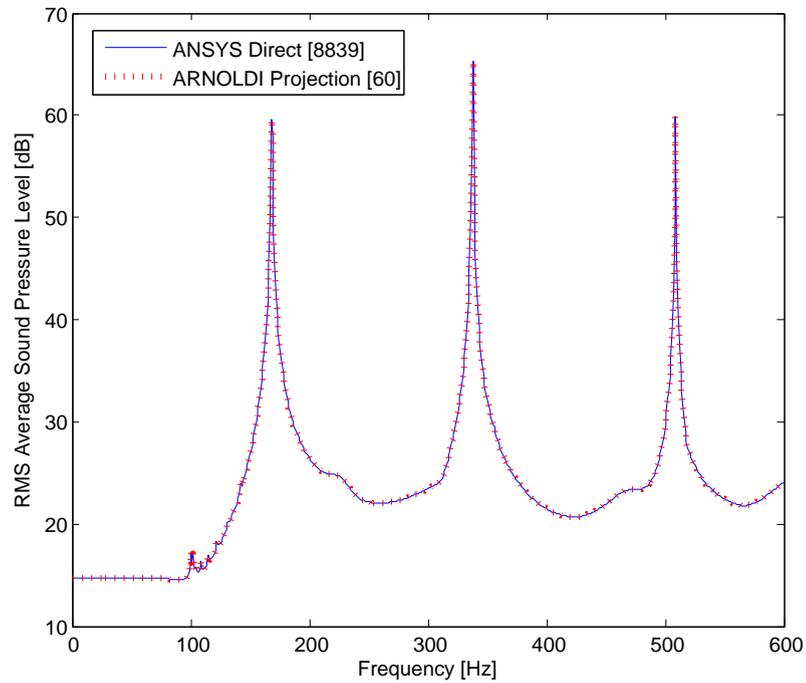
Figure 5.104.: Predicted RMS Averaged Fluid Noise Transfer Function using direct and moment-matching Arnoldi projection utilizing 21 fluid pressure outputs along the central axis of the clamped cylinder model [TC4$_{CD1}$] with ζ=0.05.
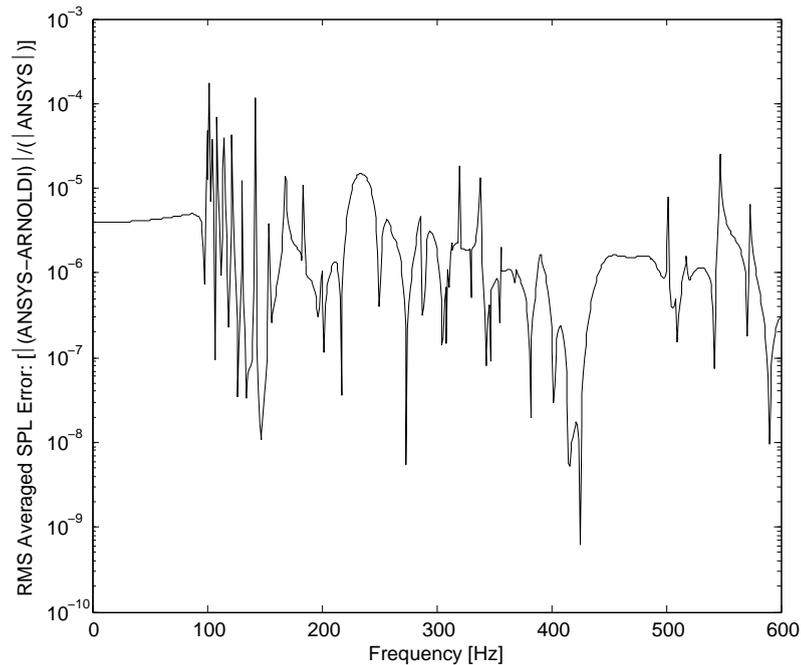
Figure 5.105.: Local RMS Averaged Error Plot utilizing 21 fluid pressure outputs for ζ=0.05.
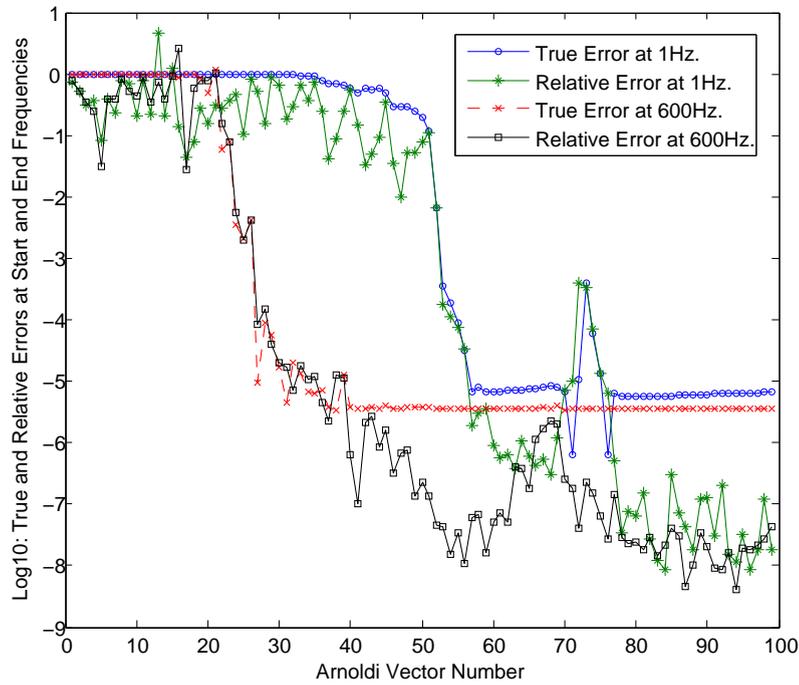
Figure 5.106.: Convergence pattern for moment-matching Arnoldi (OSA) projection at 1Hz and 600Hz for ζ=0.05.
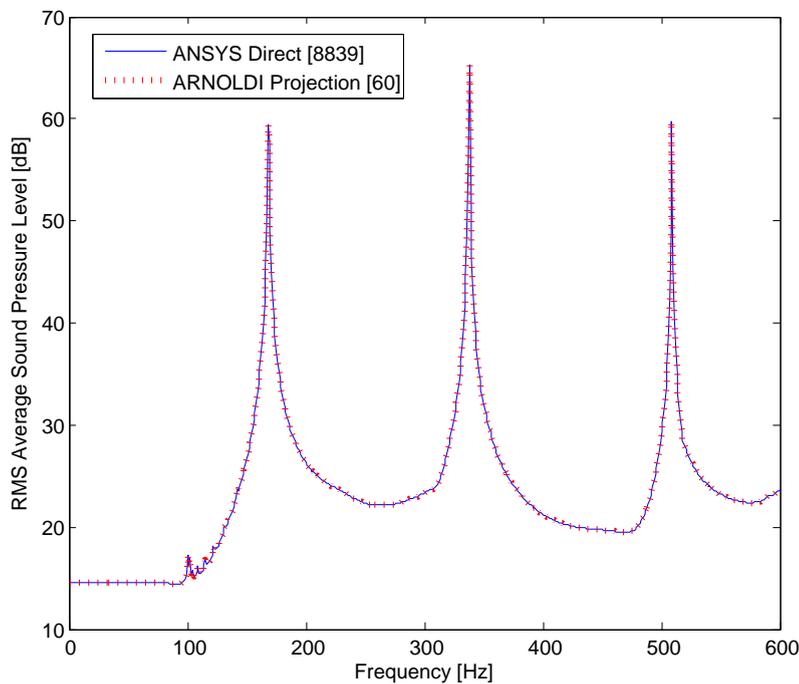
Figure 5.107.: Predicted RMS Averaged Fluid Noise Transfer Function using direct and moment-matching Arnoldi projection utilizing 21 fluid pressure outputs along the central axis of the clamped cylinder model [TC4$_{CD2}$] with ζ=0.10.
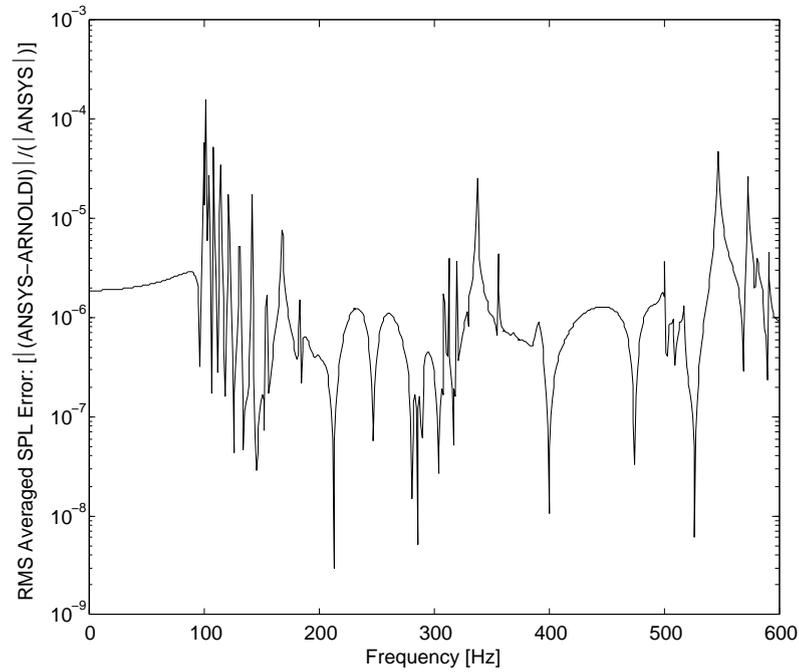
Figure 5.108.: Local RMS Averaged Error Plot utilizing 21 fluid pressure outputs for ζ=0.10.
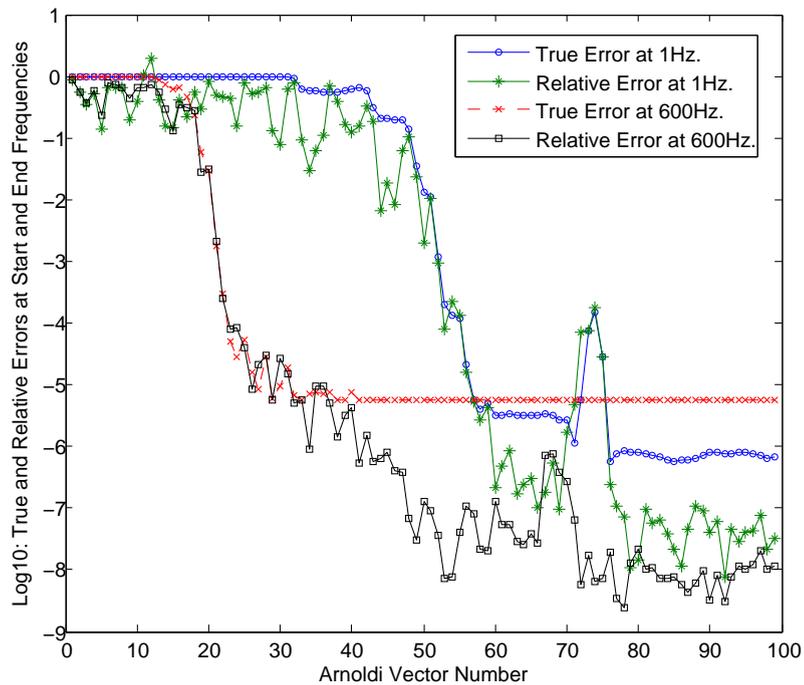
Figure 5.109.: Convergence pattern for moment-matching Arnoldi (OSA) projection at 1Hz and 600Hz for ζ=0.10.

vectors (for each subspace) are required for the solution state to be considered converged. For the structural acoustic model with β_j^m=7.0E-05, [TC4$_{FD2}$], it can be observed from Figure:[5.113] that both the linearization (with OSA) and TS-SOAR projection framework generate accurate reduced order models. However, to achieve convergence, the first order transformed model requires 200 Arnoldi generated vectors, as shown in Figure:[5.115], (due to the introduced scaling to a first order system), whereas, for the TS-SOAR framework, a ROM of dimension 40 seems to be adequate for the considered output. For the linearization approach, an expansion point of 600Hz ($2 \times \pi \times 600$) has been chosen for the analysis. The local error quantities shown in Figure:[5.114], although not directly visible in their respective transfer functions (and thus negligible), indicate that the linearized Arnoldi approach gives a higher degree of accuracy over the entire frequency range. On the other hand, the TS-SOAR approach generates a ROM with higher accuracy around the chosen expansion point (600Hz).

The computational times required to solve the higher dimensional problem via direct and Arnoldi based dimension reduction techniques are shown in Table:[5.17]. The time required for ROM via Arnoldi is a combination of the time required to generate the Arnoldi vectors, project the system to second order form and perform a harmonic analysis on the reduced order model. It is worth mentioning that the time required to generate and extract the relevant structural acoustic database files (Rudnyi and Korvink 2006) (similar to Table: 5.9) is excluded. For the test case described in this section, the time required for matrix extraction is around 112 seconds. It can be observed that the computational times are very consistent with different versions of the test cases. The linearization approach (for Test Case: TC4$_{FD2}$) results in a drop of computational efficiency (by around 3%) due to the increased dimension of the equivalent system (see Figures:5.96, 5.97) and the fact that more Arnoldi vectors
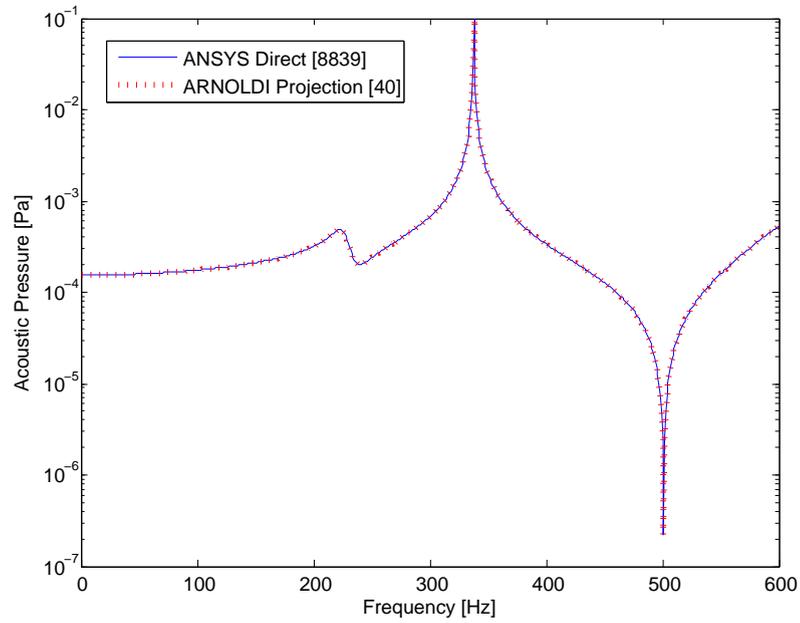
Figure 5.110.: Predicted Noise Transfer Function (NTF) using direct and moment-matching TS-SOAR projection for fluid node at the center of the cylindrical cavity model $[\text{TC4}_{FD1}]$ with β_j^m=5.0E-05.
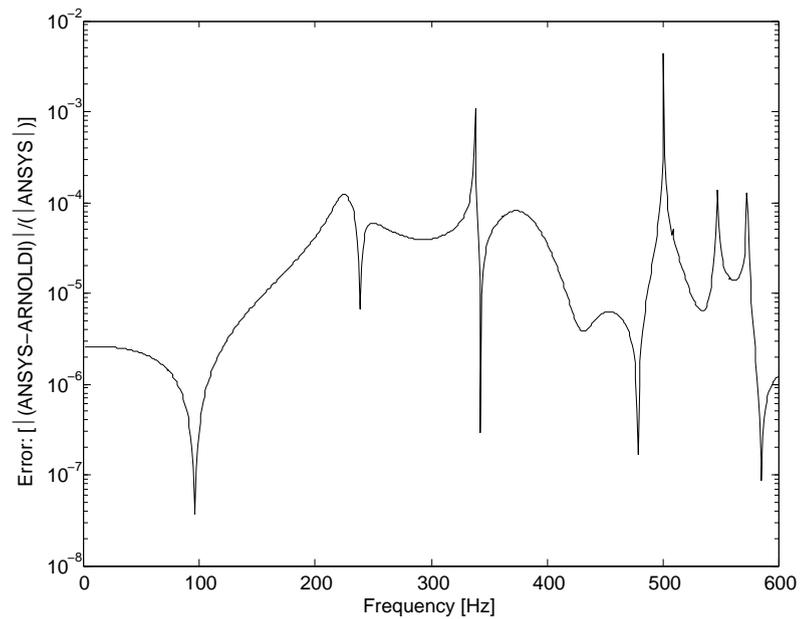
Figure 5.111.: Local Error Plot for fluid node at the center of the cylindrical cavity with β_j^m=5.0E-05.
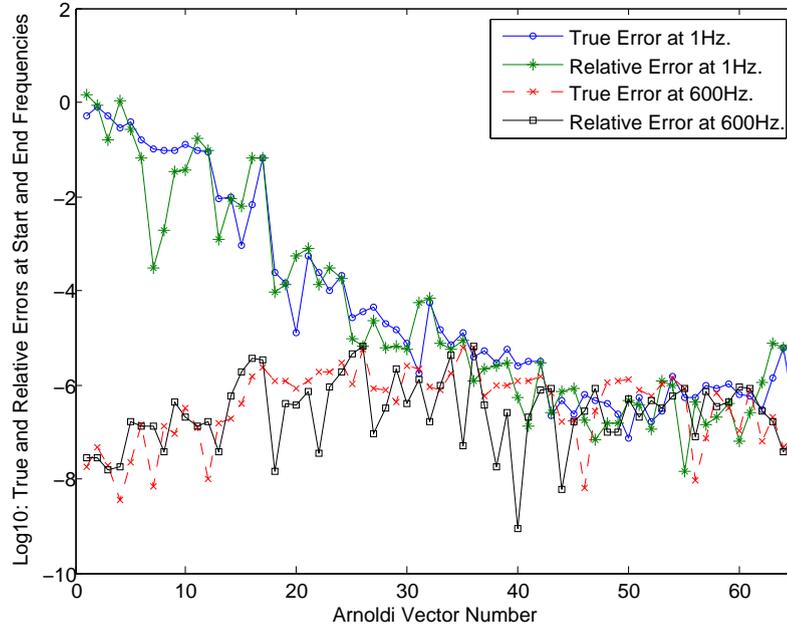
Figure 5.112.: Convergence plot for fluid node at the center of the cylindrical cavity with β_j^m=5.0E-05.
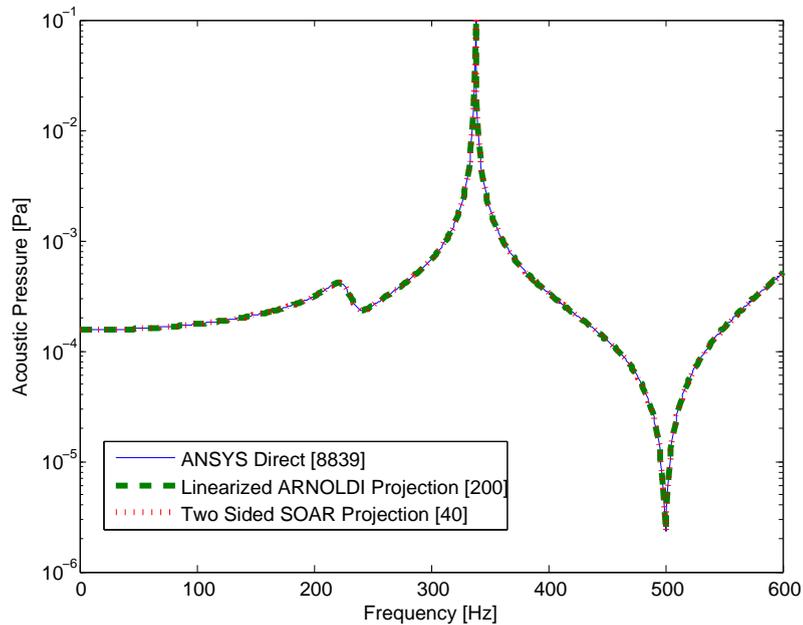
Figure 5.113.: Predicted Noise Transfer Function (NTF) using direct and moment-matching Linearized Arnoldi (OSA) and TS-SOAR projection for fluid node at the center of the cylindrical cavity model [TC4$_{FD2}$] with β_j^m=7.0E-05.
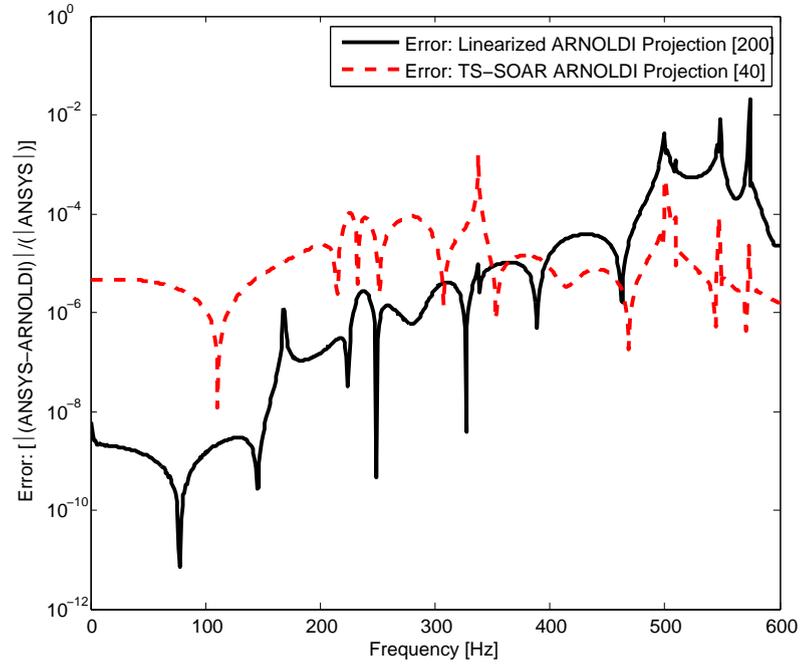
Figure 5.114.: Local Error quantities for ROMs generated via moment-matching Linearized OSA Arnoldi and TS-SOAR projection for fluid node at the center of the cylinder with β_j^m=7.0E-05.
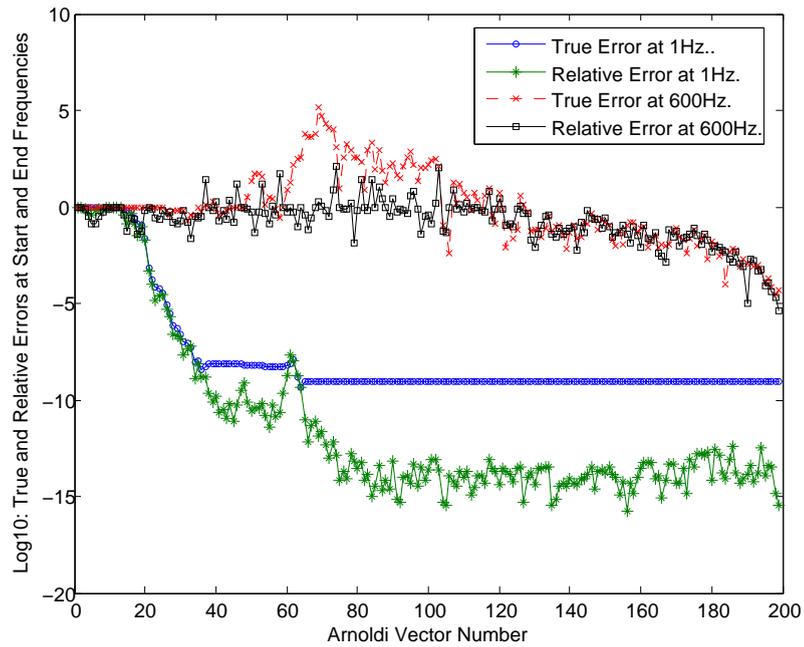
Figure 5.115.: Convergence plot for moment-matching Linearized Arnoldi (OSA) for fluid node at the center of the cylinder with β_j^m=7.0E-05.

were required to achieve convergence of the solution state.

As mentioned before, this test case has also been utilized to study accuracy and convergence properties of the uncoupled modal superposition method in (Boily and Charron 1999; Tournour and Atalla 2000). Note that Boily and Charron (1999) also investigated the same cylindrical cavity with free-free boundary conditions. The authors in their work demonstrated that even using 572 structural modes (using more than one-quarter of the total number of degrees of freedom DOF) of their structural model, the modal superposition technique did not reach convergence. The work concluded that almost every structural mode should be retained in the modal basis, which is often not possible for large models. Additionally, they concluded that the 1.2 (or even 2) $\times \omega_E$ criterion is not a reliable criterion for the problem at hand. Tournour and Atalla (2000) investigated the same cylindrical cavity model with rigid caps clamped at its ends. The authors of the work concluded that since the rigid walled cavity mode and several elastic modes are almost orthogonal to the structural modes, they can never be captured using the standard uncoupled modal synthesis (coupling) technique (i.e. without taking into account the effect of *dropped* modes via the application of pseudostatic correction factors). Indeed, there is no guarantee that the computed modes included for the mode superposition via a modal analysis would be enough (in other words, will participate in the dynamic response) for the time/harmonic response analysis, and often an approximate guess of modes within the $1.5 - 2n$ range are computed for projection, n being end frequency (Wilson et al. 1982; Boily and Charron 1999; Tournour and Atalla 2000).

Tournour and Atalla (2000) investigated the cylinder with rigid caps clamped at its ends and applied pseudostatic corrections to the uncoupled modal basis method to attain convergence. The computational times described in Tournour and Atalla (2000) are compared with the Arnoldi approaches in Table:[5.18]. Although no ex-

plicit machine specifications were included in the published paper, it can be observed that the solution times for the direct inversion technique are nearly the same (6420 sec. - 90.4%), (7100 - 100%) and therefore can be used as guide to compare solution times with Arnoldi approaches[10]. When compared to the uncoupled modal basis approach (with pseudostatic corrections), Arnoldi approaches seem to increase the reduction in solution times by around 6%. This is of course, including the time required to extract the higher dimensional structural acoustic system (156.9 sec). Assuming that the computational time consists of simply generating the required Arnoldi vectors, projection to second order form and a reduced harmonic analysis (total of 74.1 sec), the reduction in solution times is around 9%.

Table 5.17.: A comparison of computational times for undamped and damped test cases.

Test Case	ANSYS Direct	ROM via Arnoldi	Time Reduction
$[TC4_{FF}]$	3988 s	16.4 s	99.5%
$[TC4_{CL}]$	3608 s	16 s	99.5%
$[TC4_{CD1}]$	7100 s	74 s	98.9%
$[TC4_{CD2}]$	7119 s	76.1 s	98.9%
$[TC4_{FD1}]$	4201 s	95.1 s	97.7%
$[TC4_{FD2}]$	4719 s	88.2 s	98.1%
Linearization		160.5 s	96.5%

---

[10]Note that in this thesis, for this test case, a frequency sweep (for FRF computation) is executed over the frequency range of 0-600Hz, whereas, in Tournour and Atalla (2000) the frequency range for FRF computation is 0-500Hz.

Table 5.18.: A comparison of computational times with uncoupled modal superposition [§] (Tournour and Atalla 2000).

Test Case	Direct	ROM	Time Reduction
Cylindrical Cavity	6420 s	587 s [MSP]	90.85%
Model[§]	[5988 DOF]	617 s [MSP+Corrections]	90.38%
[TC4$_{CD1}$]	7100 s	231 s (74.1 s) [Arnoldi]	96.74%
	[8839 DOF]		(98.9%)

5.6. Test Case: 5: Demonstrator Structure

A simplified vehicle structure, made up of simple beams and plates was generated to provide a more complex test case for the solution of fully coupled undamped systems using MOR based on the Arnoldi algorithm. This solution method was also compared with a harmonic analysis using the direct LU solution method in ANSYS. The FE structural model was divided into seven areas. Two of these areas, which corresponded to the vehicle roof, and front firewall, were meshed using four noded quadrilateral shell elements (ANSYS SHELL181), with six degrees of freedom (UX,UY,UZ,ROTX,ROTY,ROTZ) at each node. The structural model is shown in Figure:[5.117].

The mechanical properties of the structural elements are as follows: Young's Modulus E_s= 200 GPa, mass density ρ_s=7800kg/m^3 and Poisson's ratio υ_s=0.33. The enclosed cavity is filled with air with the following properties: speed of sound c=343m/s and mass density $\rho_c = 1.2 kg/m^3$. A total of 692 structural elements - a combination of beam and shell elements, were found to be sufficient to capture the dynamic behavior of the structural model. In this simplified model, the joints were assumed to be rigid. The acoustic model was modeled using eight noded acoustic brick elements (ANSYS FLUID30), with one pressure degree of freedom at each node. The coupled model is shown in Figure:[5.118]. The structural and acoustic model were coupled using the ANSYS Fluid Structure Interaction (FSI) flag, which in turn creates the *wetted surface* carrying the additional pressure DOF for nodes on the specified fluid-structure interface. Faces other than the roof and the firewall were assumed to be fully reflective i.e. rigid walls. The panel thickness range from 1.75-2mm. The coupled model was excited using a constant structural point force of 1N over the entire frequency range of 0-300Hz at one of the nodes on the front structural member as shown in Figures:[5.116,5.117, 5.118]. In this case study, the beams

have been ignored for the coupled model i.e. the *wetted surface* was not created for the elements belonging to the faces of the beam. The output nodes considered for this test case was representative of front left driver's ear location (0.332m, 0.38m, 0.249m) and at (0.766m, 0.452m, 0.249m). The dimension of the coupled higher dimensional system is 10264.

Table 5.19.: Damping values and Expansion points for One sided Arnoldi Process for Test Case No.5

Test Cases	Damping Value	Expansion Point
Undamped [TC5$_{UD}$]	–	75Hz, 150Hz and 300Hz
Constant Damping [TC5$_{CD}$]	ζ=0.04	300Hz
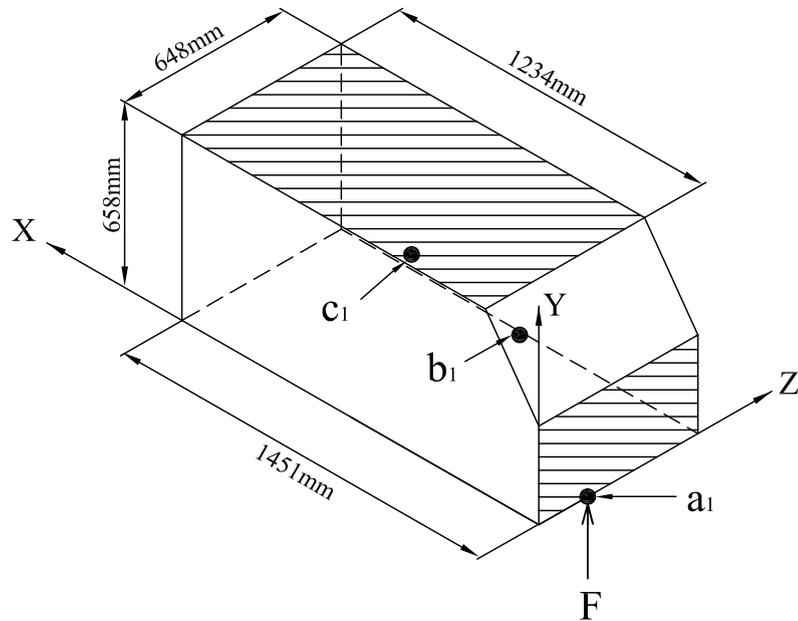
Figure 5.116.: Test Case No. 5: Beam-Plate model structure. Excitation location: $a_1 = (0, 0, 0.2m)$; Measurement location(s): $b_1 = (0.332m, 0.38m, 0.249m)$, $c_1 = (0.766m, 0.452m, 0.249m)$.
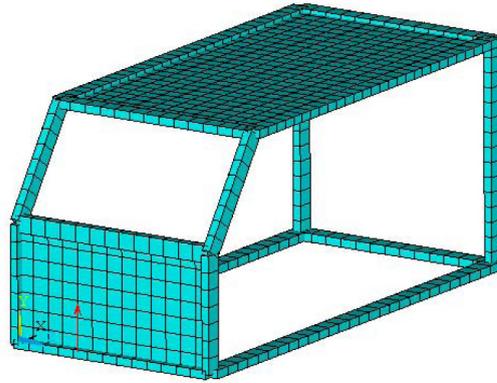
Figure 5.117.: Test Case No. 5: Structural FE Model.
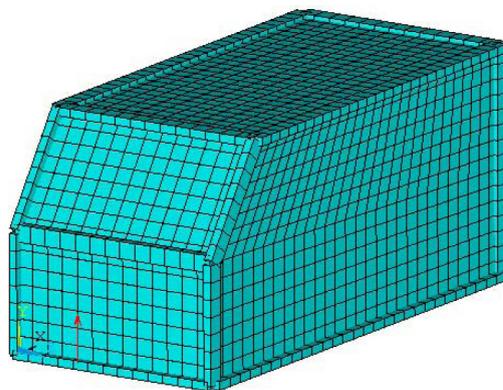
Figure 5.118.: Test Case No. 5: Fully coupled structural-acoustic FE Model.

5.6.1. Computational Results and Discussion

For the undamped test case,[TC5$_{UD}$], 150 vectors were generated using the SISO / SICO Arnoldi algorithm implemented in Mathematica. The noise transfer functions at the fluid nodes representative of the drivers ear location (0.33m,0.38m,0.24m) and at (0.76m,0.45m,0.24m) are shown in Figures:[5.119, 5.120]. Similar to other test cases shown in this thesis, it can be observed that there is no visible difference in the noise transfer functions obtained via the direct inversion method and the Arnoldi based projection formulation. For the MOR via Arnoldi approach, again, three different expansion points have been chosen: f_{exp}^1=75Hz; f_{exp}^2=150Hz; f_{exp}^3=300Hz. The corresponding local error for all three expansion points and the *true, relative* errors are shown in Figures:[5.121,5.122] and Figure:[5.123] respectively. In this case, The convergence pattern indicates that to approximate the coupled system to the required level of accuracy required no more than 115 Arnoldi generated vectors at approximately 1Hz and 130 Arnoldi generated vectors for 300Hz.
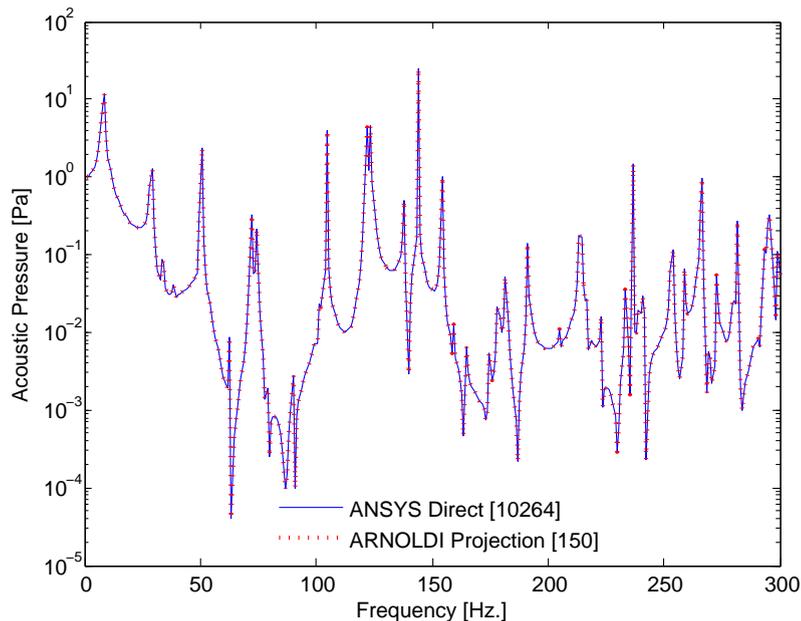
Figure 5.119.: Test Case No. 5: Predicted Noise Transfer Function using direct and moment-matching Arnoldi projection for fluid node at (0.332m,0.38m,0.249m).
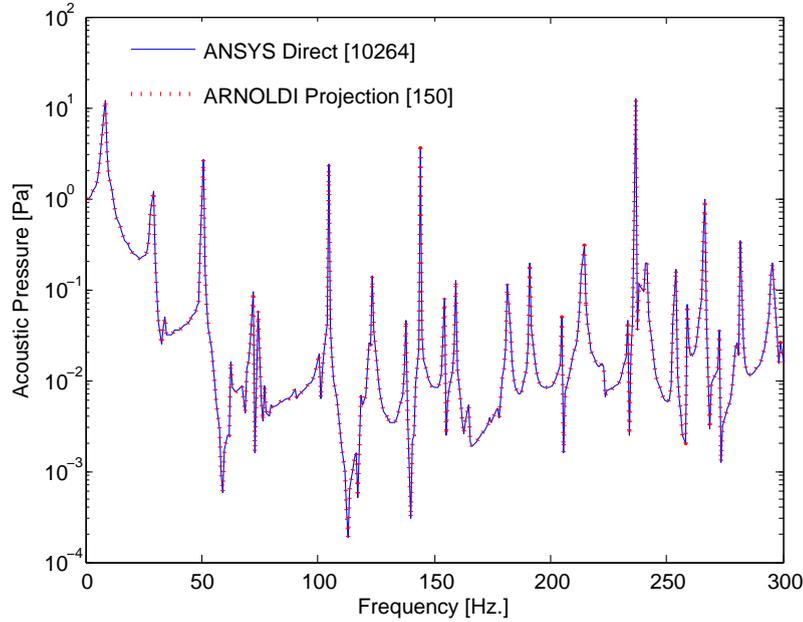
Figure 5.120.: Test Case No. 5: Predicted Noise Transfer Function using direct and moment-matching Arnoldi projection for fluid node at (0.766m,0.452m,0.249m).

For the constantly damped test case, [TC5$_{CD}$], the convergence pattern in Figure:[5.126] indicate that around 120 Arnoldi vectors are required for the solution states to converge. The RMS averaged noise transfer functions at the fluid nodal grid locations representative of the drivers ear location (0.33m,0.38m,0.24m), (0.76m,0.45m,0.24m) and at (0.86m,0.45m,0.29m) is shown in Figures:[5.124]. It can be observed that there is no visible difference in the RMS averaged noise transfer functions obtained via the direct inversion method and the Arnoldi based projection formulation. For the MOR via Arnoldi approach, the coupled higher dimensional system was factorized at 300Hz The corresponding local error for the damped test case is shown in Figure:[5.125]. Similar to the observation from the other test cases shown in this work, it can be observed that the errors for the constantly damped test cases are lower than the undamped test cases. Further, fewer number of Arnoldi vectors seem to be required to achieve convergence when compared to the undamped problem.
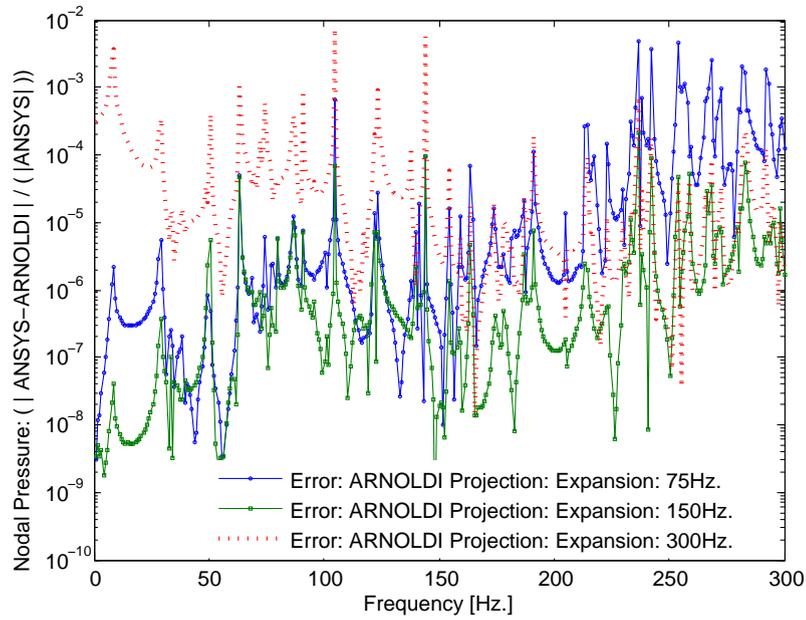
Figure 5.121.: Test Case No. 5: Noise Transfer Function error plot for fluid node at (0.33m,0.38m,0.24m) for f_{exp}^1=75Hz; f_{exp}^2=150Hz; f_{exp}^3=300Hz.
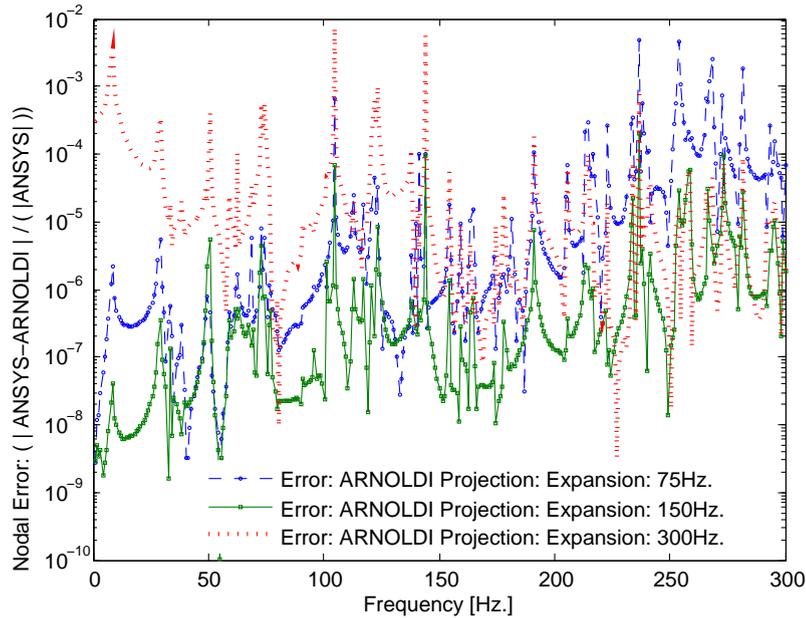
Figure 5.122.: Test Case No. 5: Noise Transfer Function error plot for fluid node at (0.76m,0.45m,0.24m) for f_{exp}^1=75Hz; f_{exp}^2=150Hz; f_{exp}^3=300Hz.
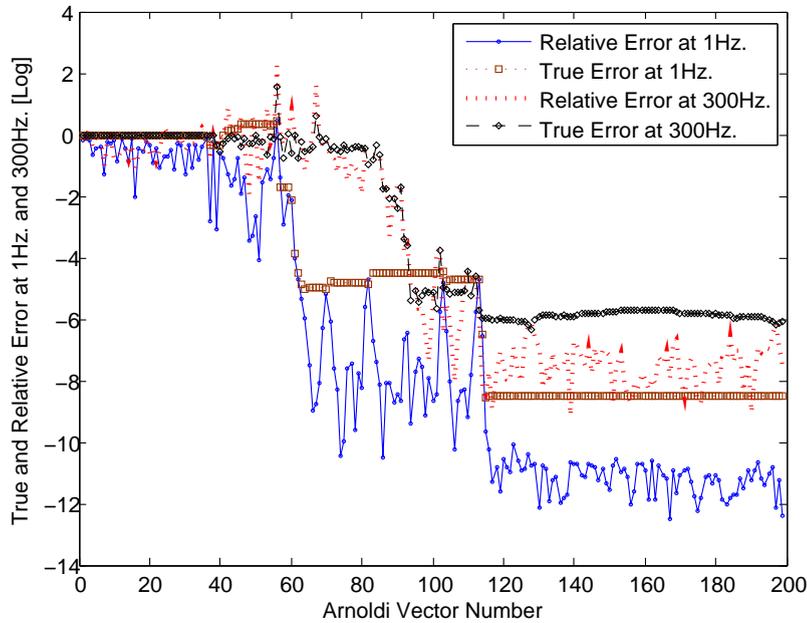
Figure 5.123.: Test Case No. 5: Convergence pattern for Arnoldi vectors (f^2_{exp}=150Hz) at approximately 1Hz and 300Hz.

The computational times required to compute an automatic ROM via Arnoldi (with an expansion point of 300Hz) is shown in Table:[5.20]. all computations are driven by MATLAB. Note that the matrix extraction times are added to the calculation. The total cost of generating the required Arnoldi vectors, projection and reduced harmonic analysis are shown in brackets. When compared to the direct inversion technique, it can be seen that the reduced order model gives a significant reduction in computational time (94.47% and 88.27%) for both test cases. If the higher dimensional matrix extraction times are excluded (as would be the case in a commercial FE environment), the time reduction increases to 99.03% and 94.05% for the undamped and damped computations respectively. The computations described in this section were performed on [Me2].
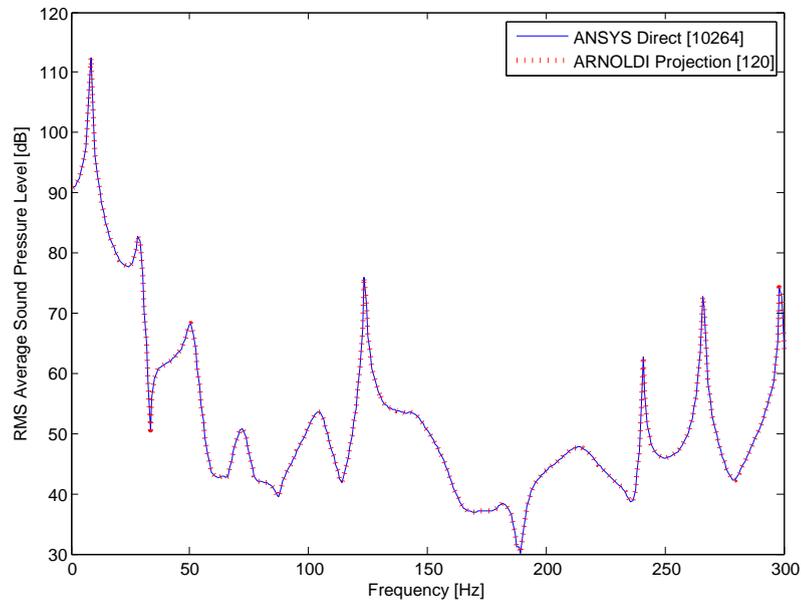
Figure 5.124.: Test Case No. 5: RMS averaged Noise Transfer Function for fluid nodes at (0.766m,0.452m,0.249m), (0.33m,0.38m,0.24m), (0.86m,0.45m,0.29m).
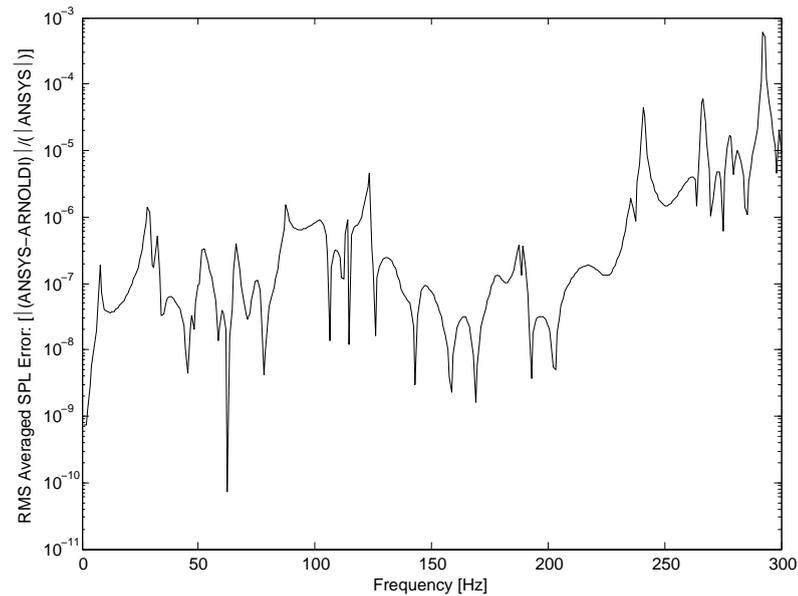
Figure 5.125.: Test Case No. 5: RMS averaged Noise Transfer Function error plot for fluid nodes at (0.766m,0.452m,0.249m), (0.33m,0.38m,0.24m), (0.86m,0.45m,0.29m).
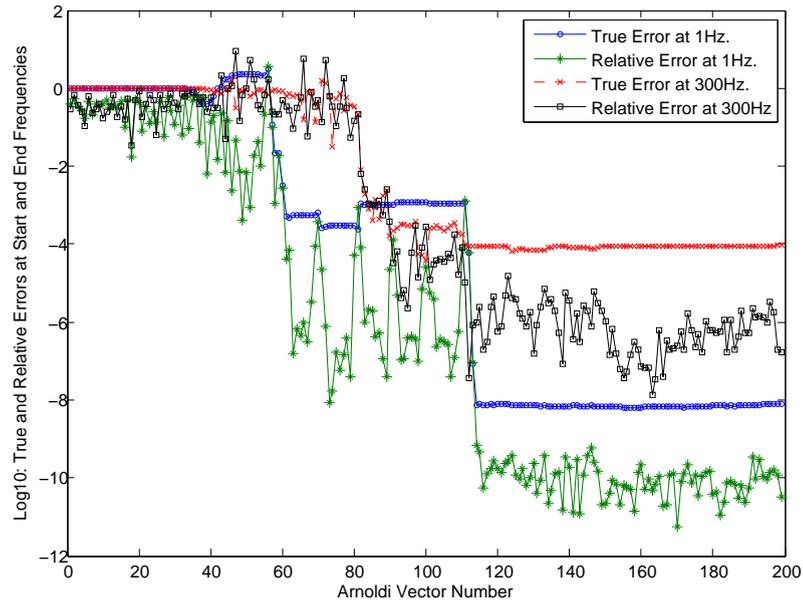
Figure 5.126.: Test Case No. 5: Convergence plot for Arnoldi vectors at approximately 1Hz and 300Hz.

Table 5.20.: A comparison of computational times for undamped and damped Test Case No. 5.

Test Case	Direct	ROM	Time Reduction
Undamped [TC5$_{UD}$]	1905 s	105.3 s (18.3s)	94.47%
			(99.03%)
Constant Damping [TC5$_{CD}$]	1581 s	185.3 s (94 s)	88.27%
			(94.05%)

5.7. Test Case: 6: Demonstrator Structure: Adhesive Bonded Joint

It is well known that the modeling of joints, gaps and sealants in a vehicle or an aerospace FE model leads to better vibro-acoustic prediction accuracy over the entire frequency range. However, one of the major challenges facing CAE modeling of joints is also to efficiently balance the requirement for accuracy with the need for maintaining reasonable vehicle FE model sizes and computer run time (DTI 2004). Therefore, in this test case, an adhesive bonded panel-frame structure is considered to validate the accuracy of Arnoldi based projection formulations. The model is a detailed coupled FE/FE model of the *demonstrator structure*, which was built to test different modeling techniques. For this test case, one of these areas, which corresponded to the vehicle roof, was meshed using four noded quadrilateral shell elements (ANSYS SHELL181), with six degrees of freedom at each node. The roof panel is bonded to the beams, using SOLID45 elements the *solid-shell* macro modeling approach (Durodola et al. 1999; Aruleswaran 2001):

$$\tilde{t}_{FEA} = \frac{\sum \tilde{t}_{plates}}{2} + \tilde{t}_{adh} \tag{5.2a}$$

$$\tilde{E}_{FEA} = \frac{\tilde{E}_{adh}}{\tilde{t}_{adh}} \times \tilde{t}_{FEA} \tag{5.2b}$$

where, $\tilde{t}_{FEA}$, is the modified bond line thickness for the structural finite-element model, $\tilde{t}_{plates}$ are the thickness of the adherents, $\tilde{t}_{adh}$ is the actual thickness of the adhesive bond, $\tilde{E}_{FEA}$ is the modified modulus[11] value for the structural finite-element model and $\tilde{E}_{adh}$ is the actual modulus value of the adhesive.

The mechanical properties of the structural elements are as follows: Young's

---

[11]Note that both static and dynamic modulus could be used in the structural finite element model for the adhesive (Aruleswaran 2001).

Modulus E_s= 200 GPa, mass density ρ_s=7800 kg/m^3 and Poisson's ratio υ=0.33. The enclosed cavity is filled with air with the following properties: speed of sound c=343m/s, mass density ρ_c=1.2kg/m^3. Two different adhesives, Epoxy Betamate 5318-4 and Polybutadiene Terostat 3218F are considered for analysis. The mechanical properties of the adhesives, obtained from tensile tests and Dynamic Mechanical Thermal Analysis (DMTA) of small scale adhesive samples are shown in Table:[5.21]. Note that the modulus and bond line thickness are modified for use in the structural part of the coupled finite element models as per Equations:[5.2a,5.2b]. The distribution of elements in the finite element coupled model areas follows: 4472 structural (4258 SHELL 181 and 214 SOLID45 for the adhesive bond) elements, 740 acoustic interface elements (FLUID30) along the fluid-structure interface and 32742 acoustic elements (FLUID30) not in contact with the structure. The coupled model was excited using a unit point force excitation at (x, y, z)=(1.45m,0, 0.15m). The structural and the coupled model are shown in Figures:[5.127,5.128]. The fluid node at (x, y, z)=(0.9m,0.5m,0.08m) is considered as the output for the coupled analysis. A description of the test models considered for the coupled analysis are described in Table:[5.22]. Note that for models TC6$_{BM}$ and TC6$_{TT}$, in addition to an overall structural damping ratio, specific material damping is also specified for adhesive (structural) elements.

5.7.1. Computational Results and Discussion

For the constantly damped test cases: TC6$_{BM}$ and TC6$_{TT}$, the two-sided Arnoldi (TSA) process was chosen to test the accuracy of Krylov subspace based moment matching techniques. Note that these two models carry a frequency independent damping for the adhesive materials in addition to a constant structural damping of 3%. i.e. local damping exists in addition to overall structural damping. The
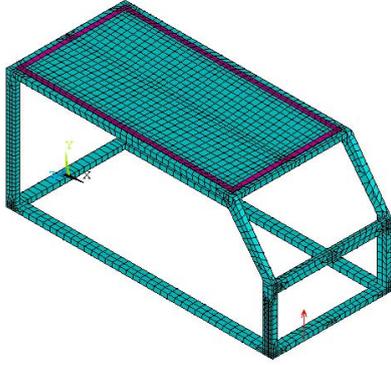
Figure 5.127.: Test Case No. 6: Structural model with adhesive bond (pink elements).
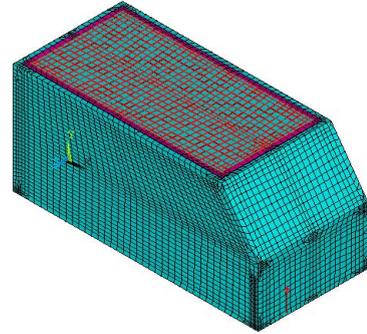
Figure 5.128.: Test Case No. 6: Coupled Structural-Acoustic model.

Table 5.21.: Dynamic material properties of the adhesives (averaged at 20-30 degrees, f=90Hz) considered for the vibro-acoustic analysis (Aruleswaran 2001).

Adhesive	Density [Kg/m^3]	Thickness [mm]	Modulus [Gpa]	Loss Factor [η]
Epoxy Betamate 5318-4 TC6$_{BM}$	1380	0.51	1.44	0.0559
Polybutadiene Terostat 3218F TC6$_{TT}$,TC6$_{Tac}$	1500	0.51	0.0142	0.5319

Table 5.22.: Damping values and Expansion points for Two sided Arnoldi Processes (TSA, TS-SOAR) for Test Case No. 6.

Test Cases	Damping Value	Expansion Point
[TC6$_{BM}$]	η=0.0559, ζ=0.03	TSA: 150Hz
[TC6$_{TT}$]	η=0.5319, ζ=0.03	TSA: 150Hz
[TC6$_{Tac}$]	β_{ac}=0.1	TS-SOAR: 150Hz

resulting coupled structural-acoustic models are of dimension is 62,354. The number of equations are indeed very large and a LU factorization of this system cannot be performed[12] on a 32 bit environment using standard numerical packages such as MATLAB and Mathematica. However, since the test case aims to validate simply the accuracy of the projection formulations, the results presented here arise from computations carried out using Mathematica on a 64 bit environment.

The noise transfer function for the specified fluid output at $(x, y, z) = (0.9\text{m}, 0.5\text{m}, 0.08\text{m})$ for both adhesive models (TC6_{BM}, TC6_{TT}) are shown in Figure: [5.129]. The local error quantities in the frequency domain are shown in Figure:[5.130]. The corresponding convergence plots for the start and end frequencies considered for the coupled analysis are shown in Figures:[5.131,5.132]. The convergence plots indicate that a dimension of 90 for the ROM yields very good approximation properties. Indeed, the comparison between an ANSYS direct inversion and TSA projections show that the transfer functions are identical[13]. From an engineering viewpoint, the noise transfer functions obtained by modeling the Betamate and Terostat adhesives, demonstrate that using a low modulus adhesive with higher damping value yields a slightly better acoustic response for the chosen node. The amplitude of pressure close to the fluid resonance peak at 120Hz have decreased by the use of a higher damping adhesive. Similar lower pressure amplitudes are apparent around 170-225Hz and 280-300Hz frequency bands. The sparsity plots for the higher dimensional coupled system matrices (Figures:C.1,C.2,C.3), and a comparison of the noise transfer functions (Figures:C.4,C.5) with the direct inversion technique can be found in Appendix:(C). Note that the importance of choosing a particular node for characterizing the interior acoustic behavior evaluation is often questioned in literature (Marburg 2002a), but it is also the most common form

---

[12]An attempt to LU factorize K_{sa} for this test case in MATLAB fails due to memory requirements on a 32 bit environment. This well known drawback is associated with the scalability issues of such commercially available packages like Matlab or Mathematica.

[13]This can be observed from Figures:[C.4,C.5] in Appendix:(C).

for objective function evaluations in vibro-acoustic optimization studies (Marburg 2002a; Marburg et al. 1997; Marburg 2002b).
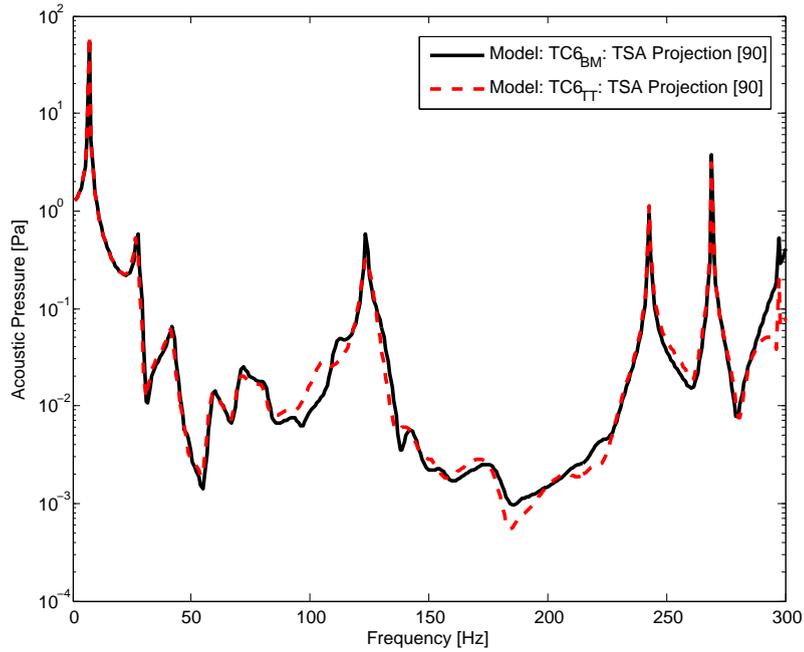

Figure 5.129.: Test Case No. 6: Predicted Noise Transfer Function using direct and moment-matching Two Sided Arnoldi projection for fluid node at (0.9m,0.5m,0.08m) for adhesively bonded coupled models [TC6$_{BM}$] and [TC6$_{TT}$].

The noise transfer functions obtained by direct inversion and structure preserving TS-SOAR process for the acoustically damped model [TC6$_{Tac}$] is shown in Figure:[5.133]. The corresponding local error quantities and the convergence models in the frequency domain for the start and end frequencies are shown in Figures:[5.134, 5.135]. The convergence plots indicate that around 70 vectors are enough for the solution state to converge. Once again, it can be observed that no accuracy is lost by employing structure preserving moment matching formulations. Note that in this test case, no structural damping was specified. This was carried out in order to validate the proposed techniques on coupled structural-acoustic models that yield transfer functions of a mixed nature. Since the model is only acoustically damped,
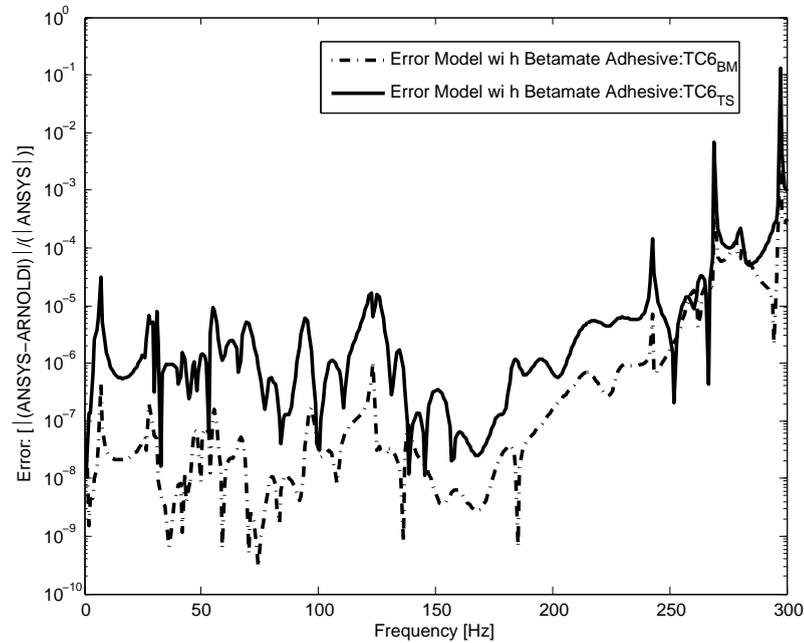
Figure 5.130.: Test Case No. 6: Noise Transfer Function error plot for fluid node at (0.9m,0.5m,0.08m) for adhesively bonded coupled models [TC6$_{BM}$] and [TC6$_{TT}$].
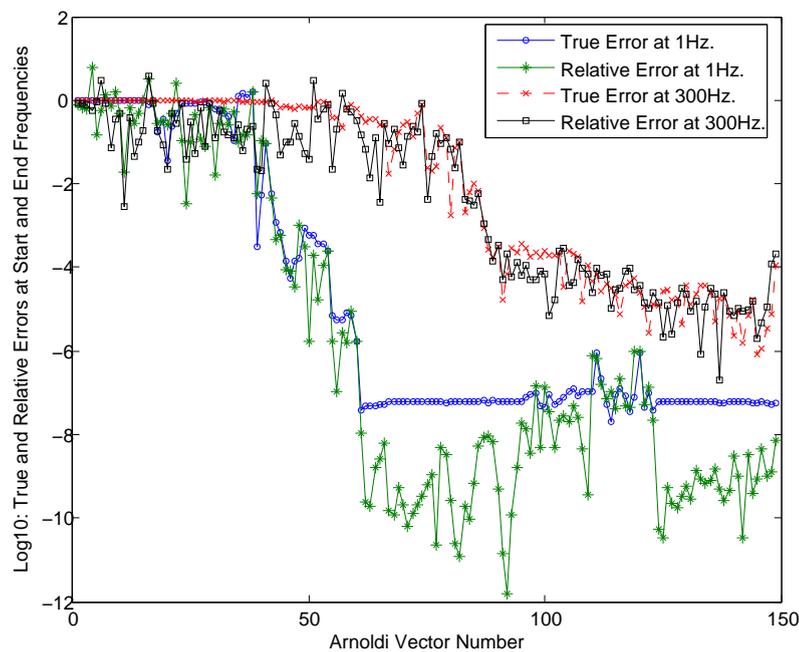
Figure 5.131.: Test Case No. 6: Convergence plot for Arnoldi vectors at approximately 1Hz and 300Hz for the coupled model with Betamate adhesive [TC6$_{BM}$].
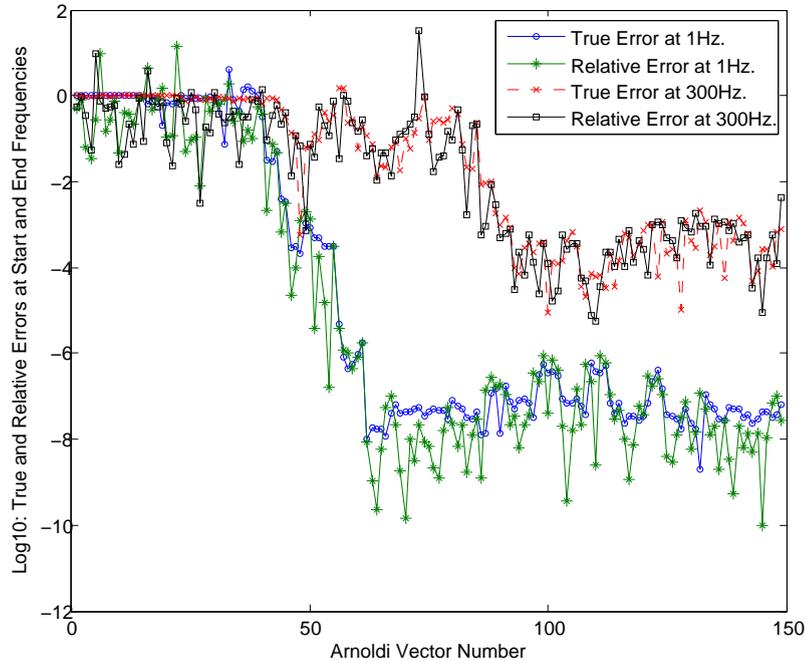
Figure 5.132.: Test Case No. 6: Convergence plot for Arnoldi vectors at approximately 1Hz and 300Hz for the coupled model with Terostat adhesive [TC6$_{TT}$].

most structural peaks would remain *undamped* (the test case is weakly coupled), whereas reduction in pressure amplitudes can be expected at frequencies close to the acoustic resonant frequencies. This phenomenon is shown for this test case [TC6$_{Tac}$], by comparing the noise transfer function from an undamped and acoustically damped computation in Appendix:(C).

As mentioned earlier, since an LU factor could not be computed (in Mathematica or Matlab) using [Me1],[Me3], the computations described in this test case were carried out on [Me4], Intel Xeon 3.80GHz, 64bit, 10GB RAM machine with 64bit Mathematica and Matlab. It is worth reminding the reader that in the case of an uncoupled or a coupled modal analysis for modal type projections, the memory requirements for a given model is higher with modal projections than with the direct inversion method. On the other hand, the memory requirements for the direct inversion method is much smaller but however requires longer solution times. Therefore,

in a modern computing environment, speed and not memory is the limiting factor on the computation of coupled responses (with small sub-steps) in the time or frequency domain (PADT 2006).
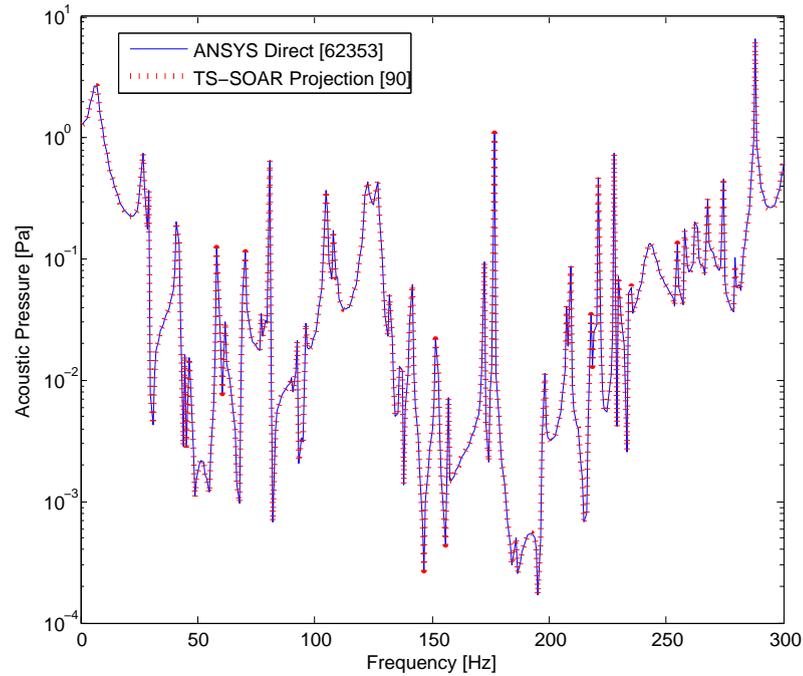
Figure 5.133.: Test Case No. 6: Predicted Noise Transfer Function using direct and moment-matching Two Sided Second order Arnoldi (TS-SOAR) projection for fluid node at (0.9m,0.5m,0.08m) with constant acoustic damping [TC6$_{Tac}$].
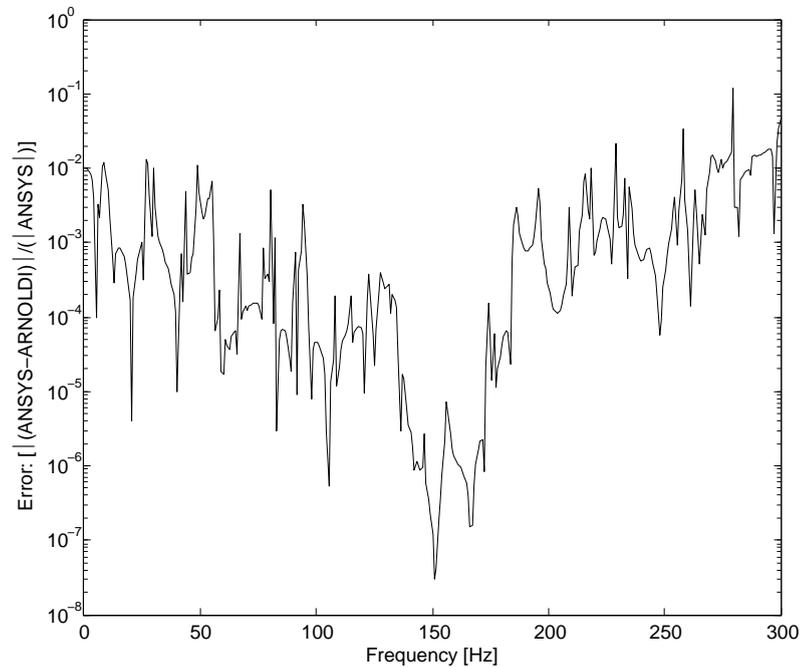
Figure 5.134.: Test Case No. 6: Noise Transfer Function error plot for structural acoustic model [TC6$_{Tac}$].
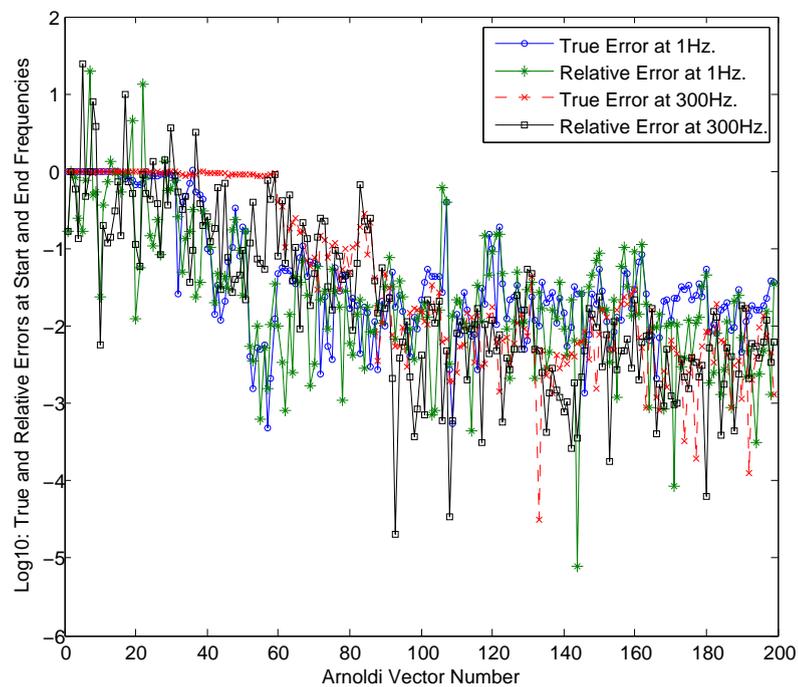
Figure 5.135.: Test Case No. 6: Convergence plot for Arnoldi vectors at approximately 1Hz and 300Hz for Terostat adhesive with constant acoustic damping [TC6$_{Tac}$].

6. Structural Acoustic Optimization via Krylov Subspace Techniques

It is clear from existing literatures (Belegundu et al. 1994; Marburg 2002a; Fernholz and Robinson 1998; Niyogi et al. 2000) that in order to improve the acoustic characteristics of a vehicle or a aerospace cabin interior, numerical optimization is often employed. Since there exists two forms of solution (coupled and uncoupled), it is often left to the engineer to decide on the approach best suited to the problem under investigation. As mentioned earlier, however, a *one-way* coupled scheme via the FEM/FEM or FEM/BEM type *chained approach* analysis ignores the fluid loading on the structure, which is often the cause of cavity boom at low frequencies. In addition to this, there is often a degree of uncertainty in classifying a structural acoustic system (such as an automotive or an aerospace interior) as weakly or strongly coupled (Desmet 1998; Bregant et al. 2005). Therefore, a fully coupled analysis is often preferred in many vehicle/aerospace applications, but the computational effort required to directly solve Equation:[3.42] restricts its subsequent use.

Over the recent years, different novel materials have been developed to control noise and vibration in vehicles and commercial aircraft. In particular, fiber reinforced composites have generated significant interest in the development of structural materials due to their low density, high stiffness and excellent damping characteristics. However, the coupled structural-acoustic problem is complicated if the flexible

structural portion are built of thin laminated composite plates since they interact with the acoustic field in their own strange manners (Niyogi et al. 2000). Additionally, the orthotropic nature of such fiber reinforced composite materials implies that the directional stiffness depends on the orientation of fibers. Such flexibility can often be exploited to tailor the material to obtain the required structural acoustic performance (Fernholz and Robinson 1998). In this work, the feasibility of reducing interior noise levels through optimal lamination angles of a composite plate structure via dimension reduction is demonstrated.

6.1. Strategy for Design Optimization

Obviously, in order to asses the suitability of a particular design, vibro-acoustic analysis is performed. Evaluation of the objective function via the most accurate direct inversion method is expensive. If a modal basis is used to compute the objective function, it is well known that sacrifices in accuracy and damping have to be made. Aside from these computational complications, it is also desirable to retrieve efficiently, using as few as possible function evaluations, the desired vibro-acoustic behavior (e.g. decreased sound pressures or structural displacements at certain points in the acoustic or the structural domain) of the system under investigation. This may be achieved, for example, by direct optimization of the objective function using gradient based optimization algorithms, which essentially fall under two categories: (a) *forward* finite difference scheme and (b) *central* finite difference schemes. Once the gradient is known, methods such as feasible directions (known as steepest descent) can be applied to update the vector of design variables. In the line-search algorithm, the updated vector of design variables, λ_{k+1}, is evaluated as follows (Haftka and Gurdal 1992):

$$\lambda_{k+1} = \lambda_k + \sigma d \tag{6.1}$$

where, σ represents the step-size, and d represents the gradient. These schemes, although straightforward to implement, suffer from inefficiencies when there are a large number of design variables to be optimized and inaccuracies when sensitivities are calculated near resonant frequencies (Salagame et al. 1995). In addition to this, a small enough step size should be chosen, since the sensitivities strongly depend on the specified step size. Therefore, the lack of accurate gradient information, convergence into local optimum hampers the effectiveness of the gradient based optimization approach. It is worth noting that, to speed up the sensitivity computations, the adjoint variable method could be utilized. For detailed mathematical derivations for non-symmetric matrices and applications of the adjoint variable method for structural-acoustic optimization, the reader is referred to Choi (2004), Dong and Kim (2003), Kim et al. (2004), Kim et al. (2003). Marburg (2002a) acknowledged the fact that random searches had to be carried out at different stages of a first order gradient based vibro-acoustic optimization (available within ANSYS), in order for the optimizer to escape local minima. It is therefore beneficial to apply *gradient-free* global search methods, such as genetic algorithms and pattern search, besides the gradient based optimization algorithms. In general, the aim of such gradient-free algorithms is to somehow exhaust the design space.

Mathematically speaking, two different optimization problems can be stated, as follows:

(A) ***Baseline* Formulation:**

$$Find \ a \ vector \ of \ design \ variables : \theta = (\theta_1, \theta_2, \theta_3 .... \theta_n) \tag{6.2}$$

$$which \ minimizes \ the \ objective \ function : f(\theta),$$

$$subject \ to \ lower \ and \ upper \ bounds : \theta_i^{lower} \leq \theta_i \leq \theta_i^{upper} \tag{6.3}$$

where, the objective function $f(\theta)$ is the absolute pressure at any given location(s) and the lower and upper bounds on the design variables are given by θ_i^{lower} and θ_i^{upper}.

(B) *Structural Weight* Constraint Formulation:

$$Find \ a \ vector \ of \ design \ variables : \theta = (\theta_1, \theta_2, \theta_3....\theta_n) \tag{6.4}$$

$$which \ minimizes \ the \ objective \ function : f(\theta),$$

$$subject \ to \ lower \ and \ upper \ bounds : \theta_i^{lower} \leq \theta_i \leq \theta_i^{upper} \tag{6.5}$$

$$subject \ to \ constraint : \left(1 - \frac{W_{initial}}{W_{feasible}}\right) \leq 0 \tag{6.6}$$

where, the constraint function can be written as given by Equation:[6.6], such that the structural weight does not exceed a user specified value. The constraint is essentially fulfilled when the weight of the new design, obtained by the optimizer does not exceed the initial structural mass. Such a formulation is often utilized when the thickness of the structural model is formulated as an additional design variable. Similar to the weight formulation, an alternate variation of the formulation could be proposed, where the pressure values at various location can be set not to exceed a specified value. Mathematically speaking, Equation:[6.6] can be modified as:

$$Subject \ to \ constraint : \left(1 - \frac{SPL_{rms \ initial}}{SPL_{rms \ feasible}}\right) \leq 0 \tag{6.7}$$

where, a constraint function can be written as given by Equation:[6.7], such that the sound pressure values do not exceed a user specified value at certain grid locations in the fluid domain. For example, an optimization could be performed, where the objective function is to minimize sound pressure level at a *drivers* ear location, whilst specifying an acoustic constraint such that the pressure values at the *passengers* ear location do not exceed a user specified or the initial values. However, such

a formulation assumes that the sound field of the original design is well known, and target frequency bands have been identified, where pressure levels are desired to be reduced. Obviously, a natural question is also to include the constraint calculation location to the objective function, thereby minimizing pressure values at both locations.

It is worth reminding the reader that instead of minimizing the total mass of the structural model, an alternate formulation can be proposed, where the objective function takes the form of minimization of structural mass, whilst fulfilling certain acoustic pressure constraints. In such a case, the objective of the design modification is primarily to minimize structural mass and therefore is not considered for the current study.

Since the noise levels are quantified in terms of the noise transfer function at discrete nodal locations, some form of averaging is essential to arrive at a single objective function value for the entire frequency range. If a simple average is utilized, then no distinction is made between the peaks and the troughs of the transfer function. However, it is well known that the peaks of the transfer function occur at discrete frequencies, which are often sought to be reduced. Another possibility is to simply minimize the maximum response of the original design. Numerous possibilities exist to formulate the objective function, and their effectiveness depends on the nature of the coupled problem. For the optimization problem stated above, the objective function is formulated as (Marburg 2002b; Marburg and Hardtke 2002):

$$f_\theta = \breve{f}_\theta^{\frac{1}{n}} \tag{6.8a}$$

$$\breve{f}_\theta = \frac{1}{\omega_{max} - \omega_{min}} \int_{\omega_{min}}^{\omega_{max}} \vartheta\{p_l(\omega)\}d\omega \tag{6.8b}$$

$$\vartheta\{p_l\} = \begin{bmatrix} (p_l - p_{ref})^n & p_l > p_{ref} \\ 0 & p_l \leq p_{ref} \end{bmatrix} \tag{6.8c}$$

where, the function ϑ is a weighting function applied to the nodal sound pressure level (SPL) value, $\{p_l(\omega)\}$. It can be seen that the weighting function depends on reference pressure, p_{ref}.

At this point, note that any value of p_{ref} can be used and is used as a control parameter to take into account the peaks of a noise transfer function . For $n = 2$, this formulation of objective function, given by Equation:[6.8a] results in a frequency averaged root mean square value. This ensures that the higher peaks of the noise transfer function are given more importance, avoiding deep valleys as compensations for high peaks during the optimization process (Marburg 2002a). For $n = 1$, the formulation results in a mean value, where p_{ref} controls the values to the taken into account for optimization.

It was demonstrated in Section:[5], that moment matching techniques provide an excellent alternative to other known methods for fully coupled structural-acoustic analysis. Therefore, the reduced order modeling technique outlined in Section:[4] is incorporated into the optimization process to speed up simulation time, while maintaining the accuracy of the nodal sound pressure values. A general framework of optimization via dimension reduction is given in Figure:[6.1]. In contrast to traditional methods such as direct inversion or modal superposition via uncoupled or coupled modes, the work computes the desired objective function via moment matching techniques. In some sense, since this is the first application of moment matching methods to optimization, various known configurations are checked for accuracy via the direct method available within ANSYS. Note also that since it is the lamination angles which this study seeks to optimize, and thus the material properties of the composite structure, the reduced order model must be regenerated at each iteration

involving a change in the lamination angle.

Each function evaluation in the optimization loop consists of the following fully automated steps: First, a solid model is generated from a 2D profile of the demonstrator structure. A fluid volume mesh followed by a structural surface mesh is then generated, and the *two-way* coupling between the fluid and structural domains are enforced using the ANSYS FSI flag. Appropriate boundary conditions and loads are applied, which in this case are *rigid walls* for fluid elements not in contact with the structure and unit point force at structural node*(s)* of interest. Next, the matrices $[K_{sa}], [M_{sa}], [F_{sa}], [L_{sa}]$ are extracted and order reduction is performed via the Arnoldi process to match sufficient number of moments of the coupled system matrices. A harmonic analysis is then carried out in the desired frequency range using the reduced system matrices $[K_{rsa}], [M_{rsa}], [F_{rsa}], [L_{rsa}]$. The RMS SPL at *driver's ear location* is computed according to Equation:[6.8a] as a part of the post-processing step. It is worth mentioning that the entire optimization loop was driven by MATLAB using simple input/output text files to read and write function values.

The optimization is carried out using MATLAB GAPS Toolbox (Matlab 2006) where function calls are made to Mesh Adaptive Direct Search (MADS) algorithm. In what follows, an outline of the MADS algorithm and its advantages over GPS discussed.
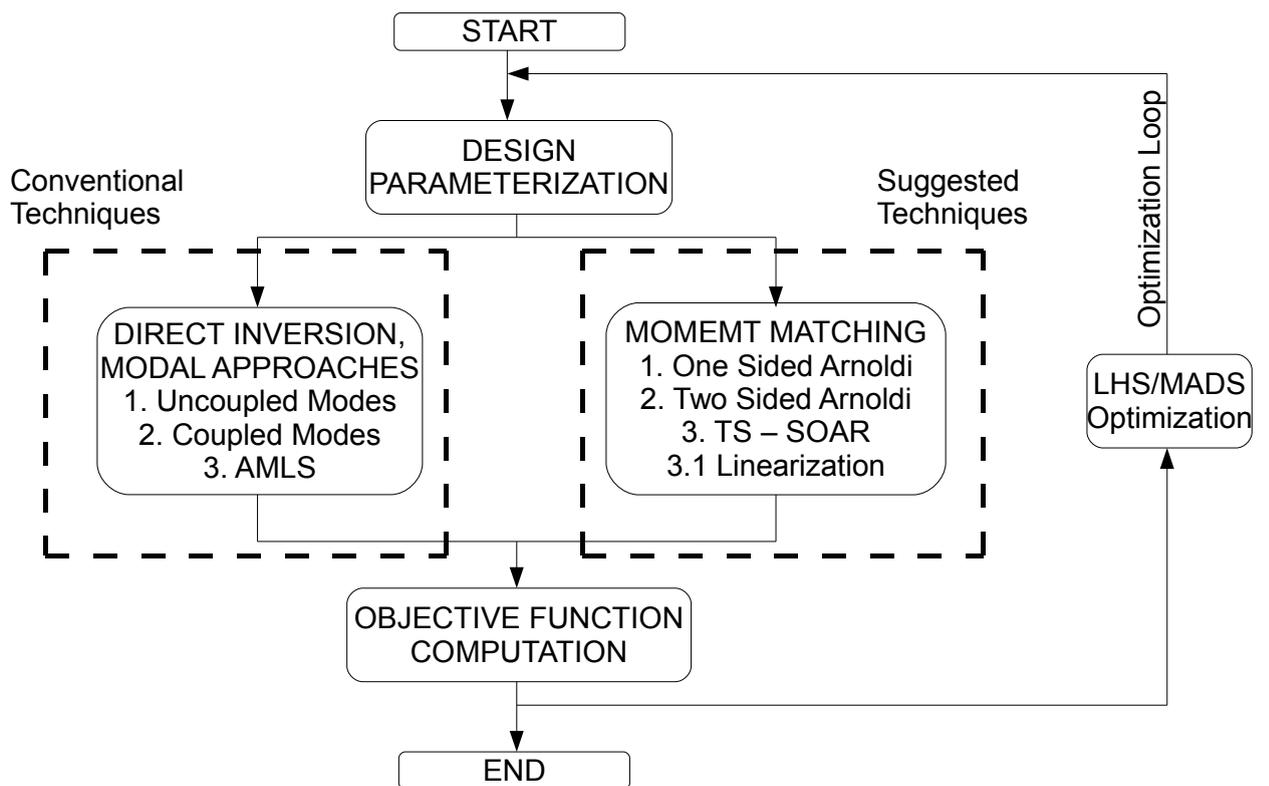
Figure 6.1.: General framework for vibro-acoustic optimization via conventional and suggested techniques.

6.2. LHS / Mesh Adaptive Direct Search Algorithm

In terms of optimization methods for computing the *best* design variables, the generalized pattern search (GPS) methods offer the advantage of a flexible framework for problems with no available gradient information. At the same time, they also provide strict mathematical convergence properties for the expensive function. The convergence of pattern search methods has been studied extensively by Torczon (1997), Audet and J. E. Dennis (2002), Audet and J. E. Dennis (2004). Convergence properties and results for optimization problems with bound, linear and nonlinear constraints have been derived by Lewis and Torczon (1999), Lewis and Torczon (2000), Lewis and Torczon (2002). However, one of the key drawbacks of the GPS algorithm is that local exploration of the space of variables is restricted to a finite number of fixed directions (called poll directions), which could result in slow convergence. The recently proposed mesh adaptive direct search (MADS) method (Audet and J. E. Dennis 2006), overcomes this restriction by generating a dense set of local polling directions. MADS is an iterative class of derivative free, frame based algorithms, specifically designed for non-smooth optimization problems, and in general can be seen as an extension to the GPS algorithm. A successful application of MADS for aeroacoustic noise optimization can be found in Marsden (2004).

Each iteration of MADS is divided into two steps, SEARCH and POLL. The SEARCH step allows the evaluation of the objective function at a finite set of points. Any search strategy can be used, including none, in which case the SEARCH is said to be empty. A lot of flexibility is available within this SEARCH step and is free of rules except for the fact that the trial points must lie within the *search* space and are finite. The set of trial points considered for function evaluation is called a *mesh*, and is governed by the mesh parameter Δ_k^m. If SEARCH fails to find an improved point, then POLL is executed, and if the POLL step also does not succeed, then

the mesh is refined. When a SEARCH step fails to improve the objective function value, a POLL step is invoked, before terminating the current iteration. The key difference between GPS and MADS lies in this POLL step. In addition to the mesh size parameter Δ_k^m, a poll size parameter Δ_k^p is defined to ensure that the local exploration of the design variable space is not restricted to a finite set of directions (Marsden et al. 2004). In this way, at every iteration, the mesh size parameter Δ_k^m is always much smaller than the poll size parameter. Therefore, when a POLL is successful, the mesh decreases gradually when compared to the GPS algorithm. The set of trial points considered during the POLL step is called a *frame*. The frame is constructed using the current design point, called the *frame center* and the mesh, poll size parameters, Δ_k^p and Δ_k^m to obtain a positive set of directions (stored in columns of the *direction* matrix), where each column represent the set of search directions. Simple examples of MADS polling construction for $n + 1$ and $2n$ basis[1] can be found in Marsden (2004), Matlab (2006).

As a result of the POLL step, design variables neighboring the current best design variable on the mesh are evaluated. This guarantees the convergence of MADS. Depending on the result of the POLL step, i.e. successful or unsuccessful, the mesh resolution is decreased or increased. Note that by refining the mesh, it is possible to obtain a dense set of polling directions which in turn means that as the mesh becomes infinitely fine, one approaches to be able to poll (i.e. generate design points and compute objective function) in any desired direction. If the POLL step generated an improvement of the objective function, then a SEARCH step is performed on the current mesh with updated Δ_{k+1}^m and Δ_{k+1}^p. Otherwise, the current design variable is said to be the *local minimizer* on the current mesh. It is worth mentioning that the mesh is in fact conceptual and is never actually constructed. An outline of the general MADS algorithm is shown in Figure:[6.2]. For a detailed dis-

---

[1]Here, n is the number of POLL directions.

cussion of convergence analysis and employing rules to compute *frame* and mesh refinement, the reader is referred to Audet and J. E. Dennis (2006), Abramson and Audet (2006).

The first step in the optimization is to choose a set of initial data. Latin hypercube sampling (LHS), introduced by McKay et al. (1979), is commonly used to find a well distributed set of initial data in the parameter space, thus ensuring that each input variable has all portions of its range represented in the chosen data set. To choose a sample set of m vectors in the parameter space, each dimension is divided into m subintervals, and a point within each subinterval is selected (this is often done by randomly sampling from a uniform distribution over the subinterval). The sample set is then obtained by randomly grouping these points to form vectors. Consequently, for each dimension, each interval appears exactly once in the set. Once the initial data set $x_1, \ldots, x_m$ has been chosen, the cost function $f(\theta)$ is evaluated at these points.

LHS offers flexible design sizes n (number of scenarios simulated) for any number of simulation inputs, k. Given a value for n, a LHS is typically constructed as follows (Kleijnen 2005):

(a) First LHS divides each input range into n intervals of equal (or chosen) length, numbered from 1 to n.

(b) Next, LHS places these integers $1, \ldots, n$ such that each integer appears exactly once in each row and each column of the design.

(c) Within each cell of the design in the table, the exact input value may be sampled uniformly or randomly.

(d) The values are then scaled to fit the boundary of the design variables[2].

---

[2]In MATLAB, the command: lhsdesign(n,p,'maximin') generates a latin hypercube sample X

Generally speaking, LHS assumes that an adequate meta-model is more complicated than a low- order polynomials which are assumed by classic designs such as fractional factorials (Kleijnen 2005). LHS, however, does not assume a specific meta-model or simulation model. Instead, LHS focuses on the design space formed by the k dimensional unit cube defined by the k standardized simulation inputs, given by:

$$0 \leq d_{i;j} \geq 1 \tag{6.9}$$

where, $i = 1, \ldots n$ and $j = 1, \ldots k$. Therefore, the approach can be seen as a *one-shot*, space-filling design. For a description of the algorithm used to generate LHS design points and a review of associated software implementation, the reader is referred to Koehler and Owen (1996), Giunta (2002), Giunta et al. (2003).

In order to avoid getting trapped in a local minima, in this work, we chose to evaluate initial trial points in the first iteration of MADS using 100 runs from sample points generated using Latin Hypercube Sampling (McKay et al. 1979), with a criterion of maximizing the minimum distance between design variables. The best design variable thus obtained, is then passed on to MADS. Note that it is only in the first iteration of the SEARCH step a LHS is required.

---

containing n values on each of p variables with a maximin criterion. For each column, the n values are randomly distributed with one from each interval $(0, 1/n), (1/n, 2/n), ..., (1-1/n, 1)$, and they are randomly permuted.

[1] **Initialization:** Let $x_0 \in \Omega$. Search space, feasible region $\Omega = \Re^n$. Define mesh

size and poll size parameters. $\Delta_0^p \geq \Delta_0^m > 0$. Set iteration counter $k \longleftarrow 0$.

[2] **SEARCH and POLL step:** Perform SEARCH and POLL (including *dynamic*

ordering) steps until an improved mesh point is found on the mesh.

[2.1] **Optional SEARCH:** Evaluate function f_θ on a finite subset of trial points

on the mesh. Any **SEARCH** strategy is valid - including none.

[2.2] **Local POLL:** Evaluate cost function f_θ on computed *frame* using Δ_k^m, Δ_k^p

and the positive spanning $n + 1$ or $2n$ set.

[3] **Parameter Update:** Update mesh size Δ_{k+1}^m and poll size Δ_{k+1}^p, Set $k \longleftarrow k + 1$

and return to SEARCH and POLL steps.

Figure 6.2.: Algorithm:6: A general MADS algorithm (Audet and J. E. Dennis 2006)

6.3. Test Case: Scale Model Structure

A scale model structure is considered as the test case for fully coupled, vibro-acoustic optimization. One boundary surface of an acoustic cavity consists of a flat rectangular plate with fully clamped boundaries, while all other cavity boundary surfaces are perfectly rigid. The acoustic cavity is comprised in the volume of an enclosing rectangular prism. A cross section of the volume geometry is shown in Figure:[6.3]. The cross section has the following co-ordinate (x, y, z) values: A=(0,0,0), B=(1.5,0,0), C=(1.5,0.75,0), D=(1.25,1,0), E=(0.5,1,0), F=(0,0.5,0). The extrusion for the cross section to form the rectangular prism is 0.5m. The air in the cavity has an ambient fluid density ρ_f =1.225 kg/m3 and a speed of sound c=340 m/s. The coupled vibro-acoustic system is excited by a time-harmonic mechanical point force F, applied at location (x_f, y_f, z_f)=(0.66,1.0,0.35) on the plate, in the direction normal to the plate. The edges of the plate along the boundary of the rectangle are clamped. The output fluid node for the analysis is located at (x_o, y_o, z_0)=(0.65,0.74,0.25). A description of a similar test case can also be found in Desmet (1998).
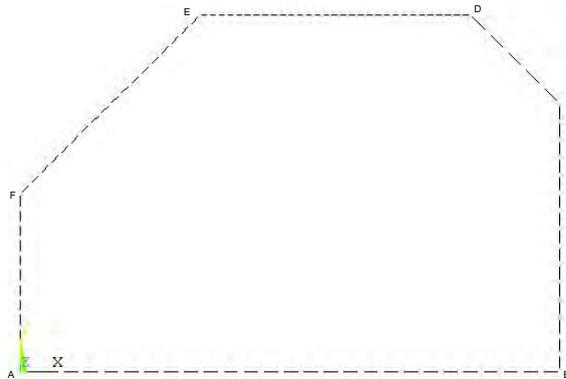
Figure 6.3.: 2-D cross section of the rectangular prism considered for the coupled structural acoustic optimization.

The first candidate material for the fully clamped plate is a glass fiber reinforcement in the form of uni-directional fabric (Owens-Corning - Standard E-Glass Fiberglass) and epoxy resin (Ciba Geigy XR-1553) with catalyst addition (HY - 956) as

matrix for the composite material. The second material is a Polypropylene glass composite, developed within the scope of this project (EPSRC - Faraday Advance 2003), is made up of continuous unidirectional glass reinforced polypropylene prepregs, produced by melt impregnation, in lay-ups for thermoplastic composite structures. The following figures are manufacturers provisional figures for Polypropylene / Glass with a 60% glass content by weight (35% by volume)[3].

A total of 310 structural elements - SHELL181, and 7310 acoustic fluid elements (including 330 interface elements) were used for the coupled model. SHELL181 is a 4-node shell element with six degrees of freedom at each node: translations in the global x, y, and z directions, and rotations about the x, y, and z-axes. The accuracy in modeling composite shells via SHELL181 is governed by the first order shear deformation theory (usually referred to as Mindlin-Reissner shell theory or FSDT) (ANSYS 2005; Bathe 1995). It is worth noting that for the composite elements, an alternate cartesian co-ordinate system is chosen and invoked, in order to align the strongest fiber along the length of the plate. The acoustic model is modeled using eight noded acoustic brick elements (ANSYS FLUID30), with one pressure degree of freedom at each node. The coupled model is shown in Figure:[6.4]. The structural and acoustic model were coupled using the ANSYS Fluid Structure Interaction (FSI) flag, which in turn creates the *wetted surface* with nodes on a fluid-structure interface having both displacement and pressure degrees of freedom (ANSYS 2005). Faces other than the roof and the firewall were assumed to be fully reflective i.e. rigid walls. The resulting dimension of the coupled vibro-acoustic system via the Cragg's u/p formulation is 10,266.

---

[3]Measurements based on 8 ply (4 mm) test specimens.
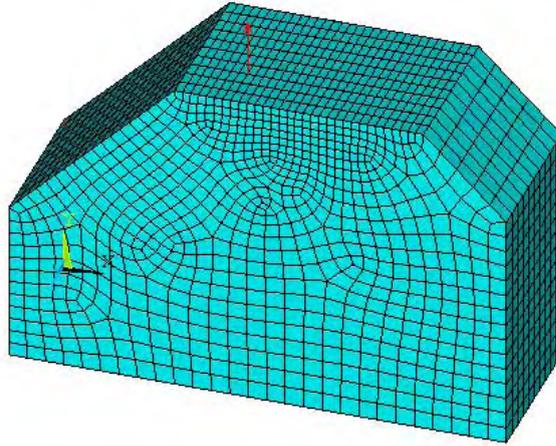
Figure 6.4.: Coupled Structural-Acoustic model for vibro-acoustic optimization.

6.3.1. Computational Results and Discussion: Four design variables.

In this section results are presented for the E-Glass Fiber composite (Table:6.1) with a wall thickness of 4mm, with 4 layers of equal thickness. In the four parameter results presented here, the allowable range of θ is $0 < \theta < 180$. Therefore, the value of θ determines the stacking sequence and thus the material properties and corresponding stiffness of the constrained structural plate. Here, values beyond 90 degrees indicates a stacking arrangement in the negative direction. The results for the LHS/MADS optimization are summarized in Table:[6.2]. Results are presented and compared for the LHS/MADS sequence with varying sample sizes for the LHS generation. A p_{ref} value of 60dB is used for this current study. An initial stacking sequence of $[0/0/0/0]_{sym}$ is specified for the optimization. The steps in the LHS/MADS method are briefly reviewed below:

[a]Initial LHS sample size is chosen (50, 100 and 150 for this case).

[b]Evaluate the function values for all LHS designs via moment matching, One Sided Arnoldi.

[c]Pass best design variable (with the least objective function value) to MADS

248

Table 6.1.: Material properties and thickness of candidate composite materials (E-Glass Fiber and PP Glass Fiber) for structural acoustic optimization.

Material Property	E-Glass Fiber Composite	PP Glass Fiber Composite
ρ [Kg/m^3]	1780	1480
E_{11} [Gpa]	44.8	28
E_{22} [Gpa]	11.27	4
E_{33} [Gpa]	11.27	4
G_{12} [Gpa]	4.86	1.39
G_{13} [Gpa]	4.86	1.39
G_{23} [Gpa]	4.45	1.40
ν_{12}, ν_{13}, ν_{23}	0.28, 0.28, 0.20	0.40, 0.39, 0.62
ζ	4%	4%
Thickness [mm]	4 and 2.1	3.8

via function call.

[d]SEARCH and POLL MADS steps till hard (in MADS, this is *mesh* convergence) or soft convergence is achieved.

[e]Add data points to cache of known points (to avoid repeated evaluation) and go back to [a]

Iterations continue in this manner until the objective function value converges to give the final stacking sequence.

The results presented in Table:[6.2] indicate that a general decrease in objective function values is apparent for all three LHS sample sizes (followed by MADS) investigated in this test case. A larger sample size seems to give results with a larger

number of total function evaluations and least objective function value. This could be attributed to the fact that, when an LHS sample size of 150 is used, the design points are more thoroughly distributed in the design space, leading to POLL steps closer to the global minimum. Figures:[6.5, 6.6, 6.7] show the variations in function value and mesh size per iteration. The decrease (or the *break*) in the mesh size can be seen as the local minimas of the RMS weighted objective function value obtained from the structral-acoustic noise transfer function. In terms of the composite stacking sequences, it can be seen that the composite material is no longer symmetrical in terms of lamination angles after optimization. From an initial lay up of $[0/0/0/0]_{sym}$ the lamination angles move towards a lay up of $[67/44/120/56]$. Note that the face sheets of both the inner layers tend to be moving towards a more cross ply orientation of $[44/120]$, whereas the outer layer of the composite material tend to be moving towards a more even orientation $[67/56]$.

Figure:[6.8] compares the sound pressure level before and after optimization. It can be seen that the optimized design variables result in a significant reduction in SPL values across the entire frequency range. Sound pressure levels near fluid resonant frequencies $\approx$122Hz, $\approx$178Hz have decreased by around 35dB and 45dB respectively. In addition to this, the structurally damped resonant peak causing fluid excitation at 60Hz has now been *shifted* to a lower pressure amplitude peak at around 90Hz during the optimization process. This result can be attributed to shifting of modes during the optimization process. Such a shift in noise-emitting modes is due to the change in stiffness of the structure (and therefore the natural frequencies), as an effect of a change in lamination angles of the composite structure (Niyogi et al. 2000).

Note that the analysis was performed over a frequency band of 0-200Hz at 1Hz increments and a p_{ref} value of 60dB was specified for the analysis. Typically, for au-

tomotive NVH studies, this frequency range corresponds to the *low-frequency* range. If a mid/higher frequency model is to be considered, more number of elements should be utilized in the coupled model generation to take into account the spatial variation at higher frequencies (Desmet 1998). For this test case, the computational times required for the optimization via ROM is 460 minutes. This corresponds to 2.2 minutes per design. From a computational viewpoint, this result indicates that a significant reduction is computational time could possibly be achieved by modeling the coupled vibro-acoustic system as as input-output problem, without sacrificing solution accuracy. A cross check validation of the optimized design variables with the direct inversion method can be found in Appendix:(D).

Table 6.2.: Optimization results for E-Glass Fiber composite with thickness of 4mm with 4 layers. [†] Number of function evaluations

LHS Search[†]	MADS[†]	Stacking Sequence	Objective Function
50	100	[74/0/35/40]	3.67 *(19.79 for* $[0/0]_{sym}$*)*
100	76	[42/31/176/76]	3.63 *(19.79 for* $[0/0]_{sym}$*)*
150	50	[67/44/120/56]	2.67 *(19.79 for* $[0/0]_{sym}$*)*
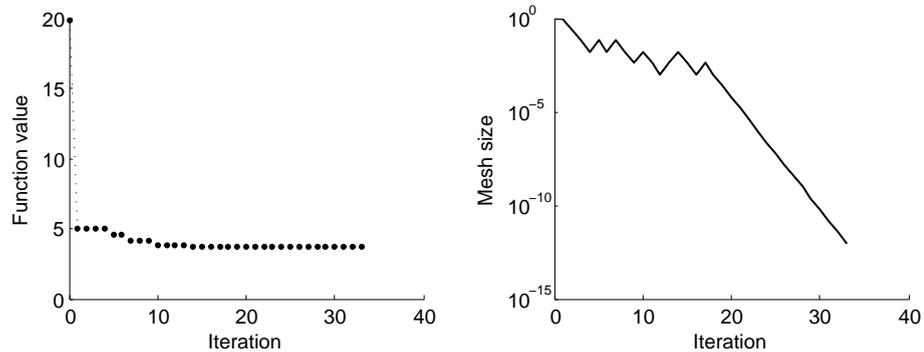
Figure 6.5.: Change in RMS objective function value (*left*) and mesh size (*right*) during optimization with initial 50 samples from LHS and starting stacking sequence $[0/0]_{sym}$
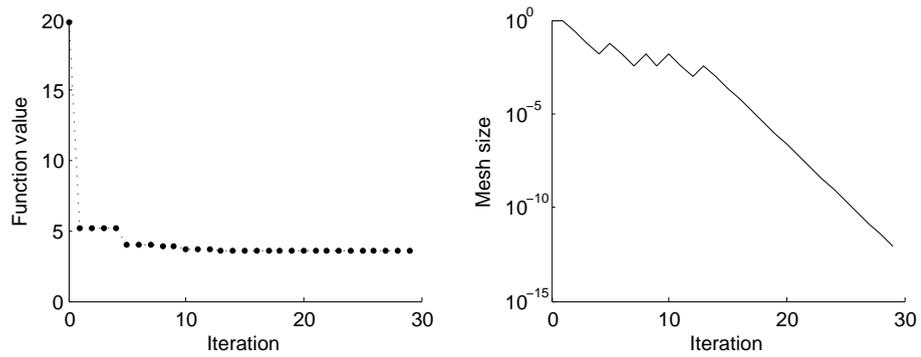
Figure 6.6.: Change in RMS objective function value (*left*) and mesh size (*right*) during optimization with initial 100 samples from LHS and starting stacking sequence $[0/0]_{sym}$
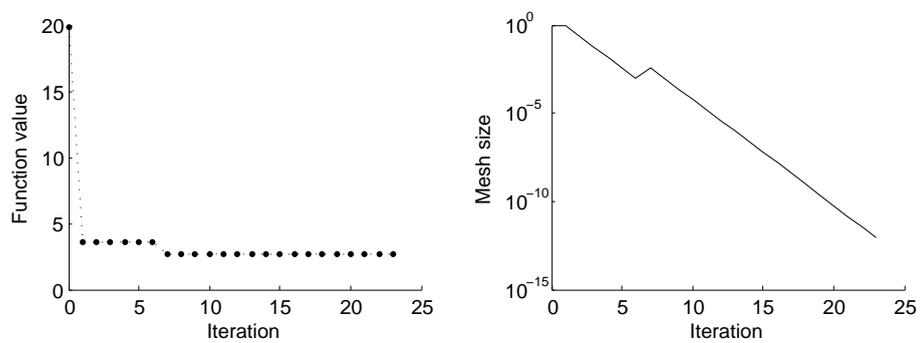
Figure 6.7.: Change in RMS objective function value (*left*) and mesh size (*right*) during optimization with initial 150 samples from LHS and starting stacking sequence $[0/0]_{sym}$
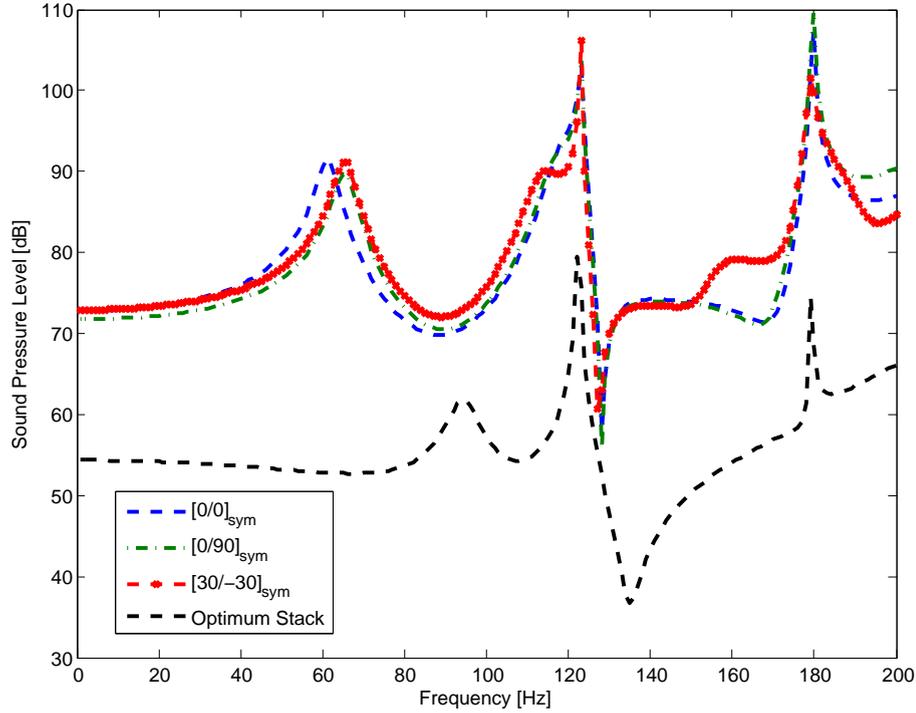
Figure 6.8.: A comparison of Arnoldi predicted fluid pressure for composite stacking sequences: $[0/0]_{sym}$, $[0/90]_{sym}$, $[30/-30]_{sym}$ and optimum stacking sequence $[67/44/120/56]$ obtained by LHS/MADS optimization.

6.3.2. Computational Results and Discussion: Eight design variables.

In this section results are presented for the E-Glass Fiber and PP Glass Fiber composite (Table:6.1) with a wall thickness of 2.1mm, (8 layers) for the E-Glass Fiber composite and 3.8mm (8 layers) for the PP Glass composite. Similar to the four parameter results presented earlier, the allowable range of θ is $0 \leq \theta \leq 180$. A reference pressure value of 60dB was enforced for the vibro-acoustic optimization.

The results for LHS/MADS sequential optimization with 150 LHS samples for the E-Glass Fiber composite are tabulated in Table:[6.3]. The objective function value has decreased from 28.9 for a $[0/0/0/0]_{sym}$ lay up to 4.96 for an unsymmetric lay up of $[153/68/70/64/32/31/37/45]$. Once again, the LHS/MADS optimizer has converged to a design with face sheets of the outer layer of the composite material

(E-Glass Fiber) with a cross-ply orientation (153/45). Meanwhile, the (3/3) inner lamination angles seem to be shifted by around 30 degrees with respect to each other. Figure:[6.10] compares the sound pressure level before and after optimization. A general decrease in SPL levels for the considered fluid output is apparent over the entire frequency range. An illustration of the optimized lamination angles for the considered composite material is shown in Figure:[6.11]. In this case, sound pressure levels near fluid resonant frequencies $\approx$122Hz, $\approx$178Hz have decreased by around 40dB and 20dB (when compared to a $[30/-30/30/-30]_{sym}$ configuration) respectively. Note that the coupled resonance peak at 178Hz is slightly *shifted* in comparison with other configurations. In addition to this, four structurally damped resonant peaks ($\approx$30Hz, $\approx$50Hz, $\approx$75Hz $\approx$145Hz for $[30/-30/30/-30]_{sym}$ configuration) causing the nodal fluid excitation no longer seem to appear in the transfer function of the optimized lay up. Similar to results encountered in four parameter test case, this result can be attributed to shifting of modes (due to the change in the structural stiffness) during the optimization process. This phenomenon is well documented (Fernholz and Robinson 1998; Niyogi et al. 2000).

All optimizations were performed on a stand alone Pentium 4, 3.2GHz, 2Gb RAM machine [Me2]. Figure:[6.9] shows the variations in function value and mesh size as the optimization progressed. In terms of computational efficiency, the search performed with initial 150 LHS samples takes longer to attain mesh convergence. Figure:[6.9] indicates that there are numerous local minimas encountered by the optimizer. This could possibly explain the reason for the very high number of function evaluations (648 objective function evaluations) needed for this test case.

The results for LHS/MADS sequential optimization with initial 50, 100 and 150 LHS samples for the PP Glass Fiber composite are tabulated in Table:[6.4]. The objective function value has dropped from 27.71 for a $[0/0/0/0]_{sym}$ lay up to 12.61

Table 6.3.: Optimization results for E-Glass Fiber composite with thickness of 2.1mm with 8 layers.[†] Number of function evaluations

LHS Search[†]	MADS[†]	Stacking Sequence	Objective Function
150	498	[153/68/70/64/ 32/31/37/45]	4.96 *(28.9 for* $[0/0/0/0]_{sym}$*)*
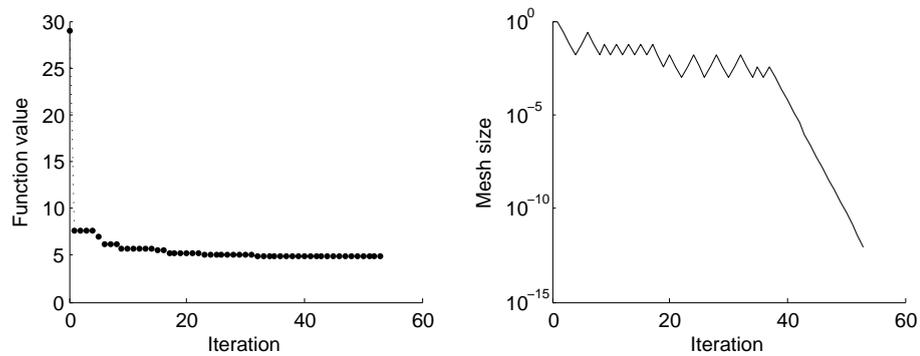
Figure 6.9.: Change in RMS objective function value (*left*) and mesh size (*right*) during optimization with initial 150 samples from LHS and with a starting stacking sequence $[0/0/0/0]_{sym}$ for E-Glass fiber composite.
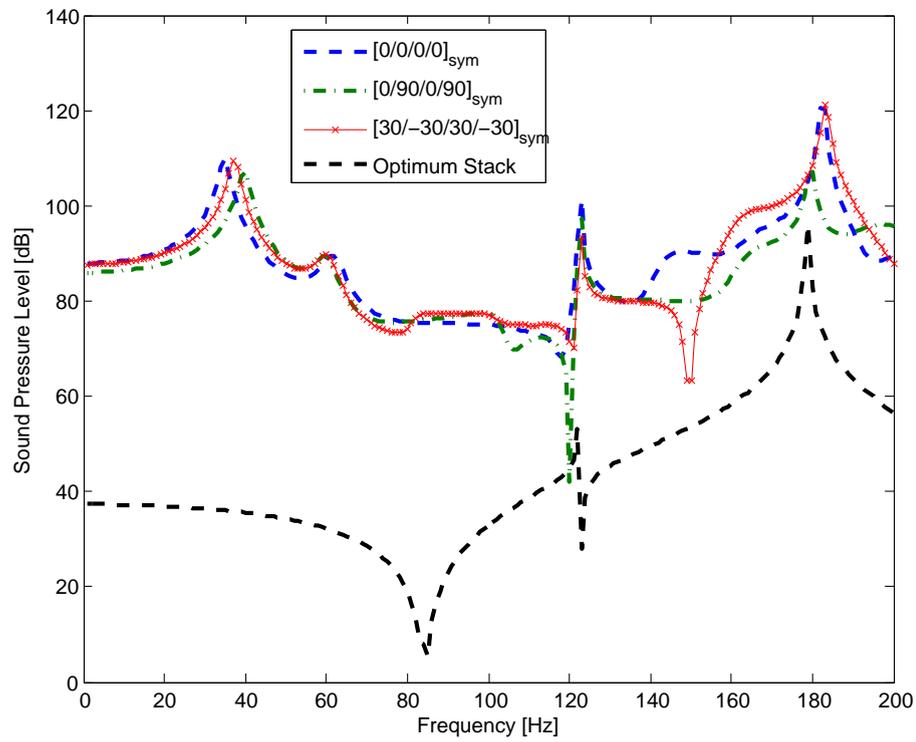
Figure 6.10.: A comparison of Arnoldi predicted fluid pressure for composite stacking sequences: $[0/0/0/0]_{sym}$, $[0/90/0/90]_{sym}$, $[30/-30/30/-30]_{sym}$ and optimum stacking sequence $[153/68/70/64/32/31/37/45]$ obtained by LHS/MADS optimization.
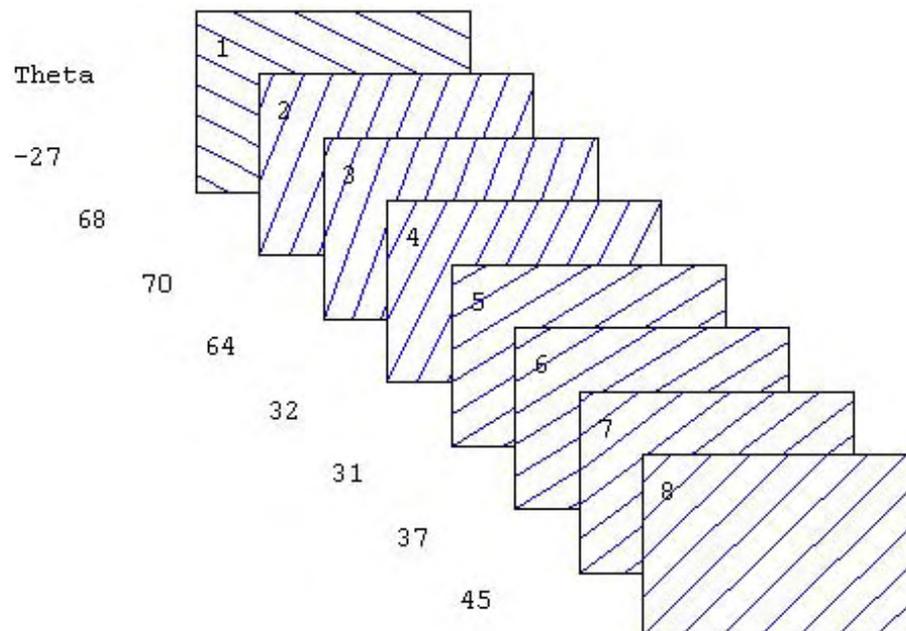
Figure 6.11.: Layer plot of optimum stacking sequence for E-Glass Fiber composite with wall thickness of 2.1mm with 8 layers.

for an unsymmetric lay up of [166/6/59/18/53/31/17/59]. Once again, it can be observed that the face sheets of the outer most layers of the composite material (PP Glass Fiber) tend to be moving towards a cross-ply orientation (166/59). A comparison of SPL values before and after optimization is shown in Figure:[6.15]. Generally speaking, a significant decrease in the amplitudes of pressure values can be observed over the entire frequency range. Note that the peak at around 85Hz observed in the other lay up configurations, has now been split into two peaks at ≈70Hz and ≈90Hz with much lower pressure amplitudes. On the other hand, in the frequency range of 120-150Hz, the *optimum* stacking sequence results in higher peak pressures when compared to say the $[0/0/0/0]_{sym}$ configuration. This result can be primarily attributed to the fact that: (a) the value of p_{ref} used in this study was 60dB and (b) the optimization was considered over the entire frequency band of 0-200Hz in 1Hz increments. The successful design simply meets both the above criterions and as a result does not focus on a particular frequency band. A cross check validation of the optimized design variables with the direct inversion method can be found in Appendix:(D).

Figures:[6.12,6.13, 6.14] show the variation in mesh size and objective function value during the optimization process with the considered LHS sample sizes. For the PP Glass composite material properties with the least RMS SPL value, a total of 427 function evaluations were required to achieve mesh convergence. Note that the test case is essentially a *single-component* model with an enforced p_{ref} value of 60dB. Obviously, if a similar composite material is used on a partial surface of a real-life structure such as an automotive BIW, and an optimization performed, the results would be very different (in terms of lamination angles). This is primarily because in this test case, the structural modes are controlled by the composite plate alone, whilst, in a real life structure, the global (and other local) modes would also play a major role in the noise transfer function. Additionally, it is worth mentioning

that the optimization considered only one fluid output to compute the objective function. Therefore, it is very much possible that the optimized lay up results in higher SPL values around other fluid grid locations. Apparently, at this moment, there is no literature addressing this particular issue in vibro-acoustic optimization (Marburg 2002a). However, since this work aims to demonstrate the feasibility of reducing SPL levels by tailoring the lamination angles (via Arnoldi ROM projections), a comparison with other possible objective function formulations becomes out of the scope of this current study.

Table 6.4.: Optimization results for PP Glass Fiber composite with thickness of 3.8mm with 8 layers. [†]Number of function evaluations.

LHS Search[†]	MADS[†]	Stacking Sequence	Objective Function
50	200	[159/69/83/150 95/106/161/175]	14.62 *(27.71 for $[0/0/0/0]_{sym}$)*
100	334	[62/153/88/120/ 101/159/0/178]	13.94 *(27.71 for $[0/0/0/0]_{sym}$)*
150	277	[166/6/59/18/ 52/31/17/59]	12.61 *(27.71 for $[0/0/0/0]_{sym}$)*
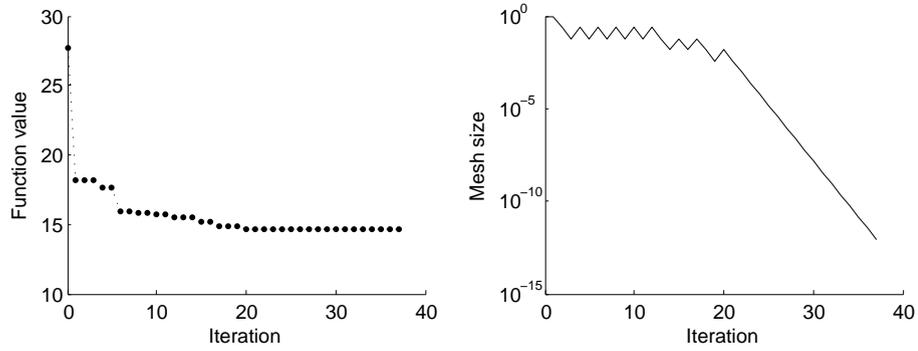
Figure 6.12.: Change in RMS objective function value (*left*) and mesh size (*right*) during optimization with initial 50 samples from LHS and with a starting stacking sequence $[0/0/0/0]_{sym}$ for PP-Glass fiber composite.
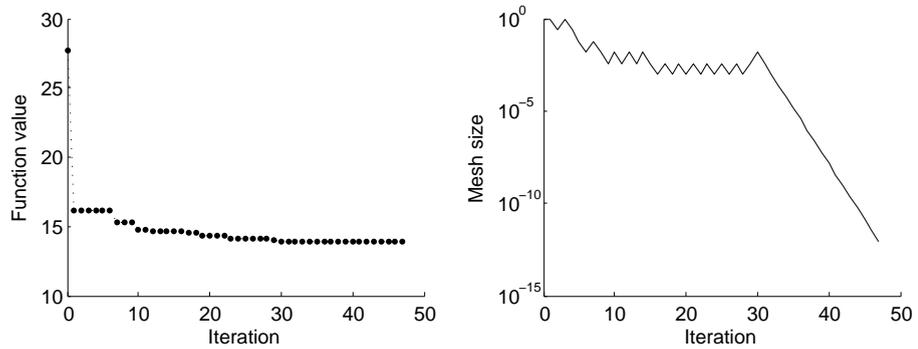
Figure 6.13.: Change in RMS objective function value (*left*) and mesh size (*right*) during optimization with initial 100 samples from LHS and with a starting stacking sequence $[0/0/0/0]_{sym}$ for PP-Glass fiber composite.
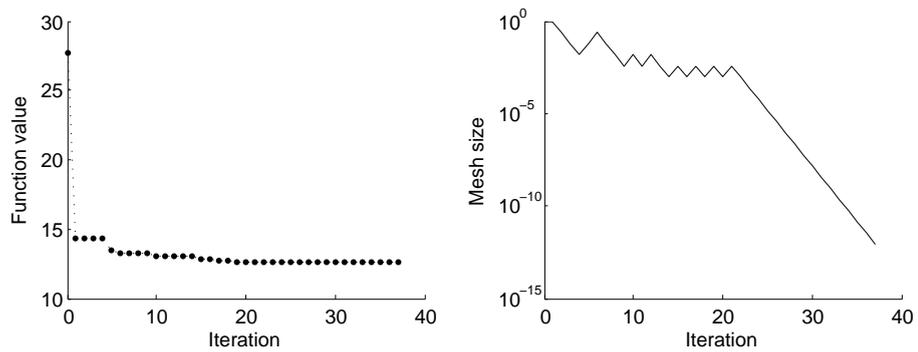
Figure 6.14.: Change in RMS objective function value (*left*) and mesh size (*right*) during optimization with initial 150 samples from LHS and with a starting stacking sequence $[0/0/0/0]_{sym}$ for PP-Glass fiber composite.
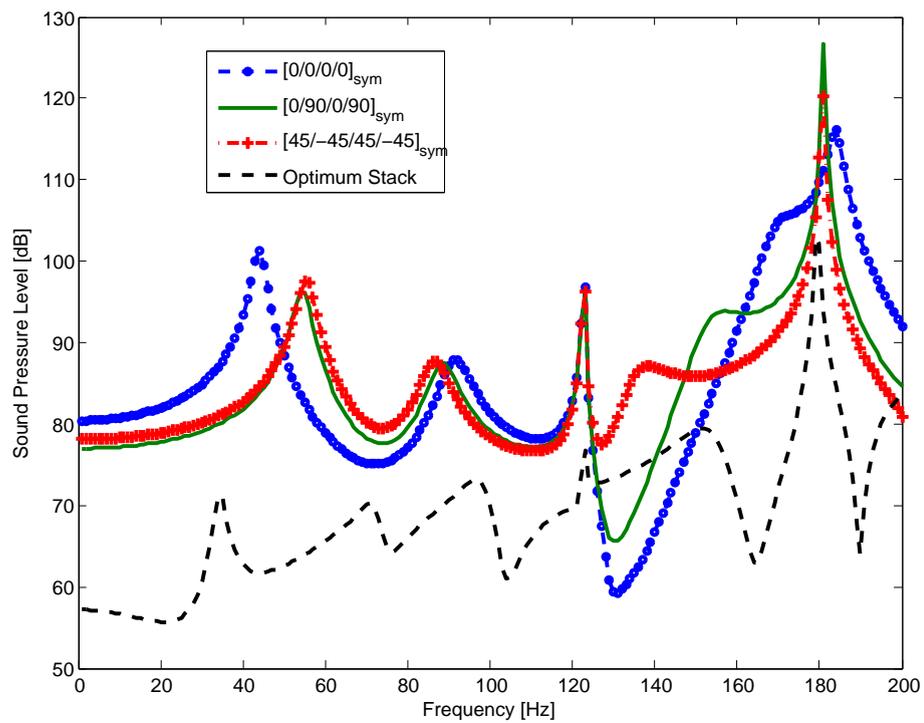
Figure 6.15.: A comparison of Arnoldi predicted fluid pressure for composite (PP-Glass) stacking sequences: $[0/0/0/0]_{sym}$, $[0/90/0/90]_{sym}$, $[30/\text{-}30/30/\text{-}30]_{sym}$ and optimum stacking sequence $[166/6/59/18/52/31/17/59]_{sym}$ obtained by LHS/MADS optimization.

7. Conclusions and Recommendations

In this thesis, it was shown that the vibro-acoustic coupled model can be formulated as an input output problem, where the main goal is to accurately represent the the two-way coupled interaction between the fluid and the structural domains under investigation. Although finite element methods (via direct inversion or modal superposition) can provide models with the desired level of accuracy, they are generally of very high order and are therefore not suitable for design sensitivity or vibro-acoustic optimization studies. Moreover, if a dense fluid is utilized for the cavity (e.g. water), it is well known that uncoupled modal superposition suffers from lack of reliable criterions for *kept-modes* for projection to a lower dimension eigen vectors space in the case of strongly coupled problems. In the case of *weakly coupled* problems, there exists a problem of computing a large number of acoustic modes for inclusion into the acoustic modal base due to the violation of the continuity condition along the fluid-structure interface. Therefore, an engineer needs to take into account the fluid medium (and thus any associated correction factors), before proceeding to predict pressures in the fluid domain. In addition to this, for real life structures such as an automotive or an aircraft interior, manufacturing tolerances and material property uncertainty, often requires repeated simulations. In this way, the material properties and manufacturing tolerances (e.g. shell thickness) are *back calculated* for a given model. The work demonstrated that lower order vibro-acoustic models can

be directly obtained by systematic dimension reduction of a higher order coupled models. The resulting models seem to exactly replicate the input output behavior of the higher dimensional model over a wide range of frequencies. The reduction can be performed based on the specific problem at hand such that the important dynamics of the coupled system are accurately captured.

Reduced order, fully coupled structural acoustic models have been developed for linear, 2-D and 3-D interior acoustic problems utilizing Cragg's displacement/pressure (u/p) formulation. In Chapter:[5], the proposed reduction methods were applied to fully coupled structural-acoustic systems of low, medium and high orders and the computational results discussed. The results clearly show that very good approximation properties can be obtained by matching the low frequency moments of the *weakly* (or) *strongly* coupled vibro-acoustic systems. For the undamped and constantly damped test cases, it was shown that One sided Arnoldi (OSA) and Two-Sided Arnoldi (TSA) were very effective for dimension reduction of the higher dimensional system. Further, it was demonstrated that by matching more number of moments ($2q$ in two-sided methods as opposed to q in one sided methods), a ROM could be generated with a higher degree of accuracy. For the linearly damped test cases, the Two-Sided Second Order Arnoldi (TS-SOAR), which generates candidate vectors (for projection) belonging to the induced second order Krylov subspaces, was shown to generate a ROM with excellent accuracy and computational efficiency. This method directly utilizes the coupled damping matrix C_{sa} in the dimension reduction process. Note that the SOAR procedure can also be used to solve the quadratic eigenvalue problem (Bai and Su 2005b). When compared to the linearization state space approach, the TS-SOAR process preserves the underlying second order structure of the coupled problem. Dimension reduction has been demonstrated for both structural and acoustic excitation via the well known reciprocity computation of the displacement and pressure dynamic transfer functions. The number of states (in the

generalized co-ordinates) required by dimension reduction via Arnoldi based Krylov subspace techniques was shown to be typically of a much lower order compared to the original higher dimensional model. For the test cases investigated in this work, the number of states required by direct projection to accurately capture the coupled dynamics is summarized in Table:[7.1].

Structural damping is considered in this work in two different forms: constant damping and linearly dependent (frequency) damping models. These damping models are typically of the kind currently used in industrial NVH studies. It was shown that constant damping can be incorporated into the dimension reduction process, by applying the standard one-sided and two-sided Arnoldi algorithm(s) to the higher dimensional, complex, structural-acoustic system. For a coupled system with linearly dependent structural damping or constant acoustic damping (in the form of boundary admittance coefficient), the Two-Sided, Second order Arnoldi process (TS-SOAR) and dimension reduction by equivalent state space transformation techniques have been demonstrated. The TS-SOAR process, essentially eliminates the need for a LU factorization of the coupled system of double the dimension generated by transformation to first-order. Additionally, the underlying second order structure of the original problem is preserved. In terms of accuracy, dimension reduction of damped models was shown to be more accurate than undamped systems - compared to the direct inversion technique. Generally speaking, an important observation can be made from this work: It is very much possible to generate *structure preserving*, *moment matching*, ROMs for an interior, fully coupled, undamped and damped, structural-acoustic analysis.

A comparison of commonly employed solution strategies for fully coupled fluid-structure analysis is presented in Table:7.2[1]. In essence, it can be seen that the

---

[1]The table makes a comparison between moment matching Arnoldi and ABAQUS implemented Coupled Lanczos (CL) and the AMLS version of the CMS procedure.

Table 7.1.: A comparison between the number of higher dimensional and lower dimensional states for dimension reduction via Arnoldi based Krylov subspace techniques. TC7§ Optimization test case.

Test Case	Higher Dimensional States (DOFs)	Lower Dimensional States (DOFs)	Reduction Factor
TC1	23,412	100	× 234
TC2	11,827	30	× 394
TC2.1	11,827	30	× 394
TC3	3,278	50	× 66
TC4	9223	100	× 92
TC5	10,264	150	× 68
TC6	62,353	90	× 693
TC7§	10,266	25	× 411

moment matching techniques do not pass through the eigen-solution and therefore do not rely on the number of kept modes for projection. Alternatively, an LU factorization is a strict requirement for Arnoldi based moment matching techniques. Throughout this work, it was assumed that an LU factor of the higher dimensional system matrices at any desired expansion point is available. Indeed, in the numerical examples presented in Chapter:[5], it was demonstrated that this LU factor was available for a wide range of expansion points.

Obviously, one could envisage a number of extensions that could be applied to the reduced order models obtained by matching some of the *low frequency moments* outlined in this research. The reader is also referred to *Markov parameter* matching, where, essentially, the first few Markov parameters (or the so called *high-frequency moments*) are matched and a structure-preserving reduced order model constructed (Chahlaoui et al. 2005; Salimbahrami 2005). Provided that an underlying FE/FE code is available for coupled matrix extraction, a direct application of the moment matching framework (and its variants) is possible to the velocity potential formulation, the displacement formulation for the fluid or any other mathematically valid fluid/structure coupled formulation. These higher dimensional formulations could also account for porous material behavior. Note that moment matching for damped systems involving an explicit participation of $[C_{sa}]$ was also demonstrated via the state-space, first order based transformation technique. There exists coupled vibro-acoustic applications, where state space modeling is also employed for active noise control (Lane and Griffin 2001; Oliveira et al. 2006; Auweraer et al. 2006) and the straightforward Arnoldi based projection formulations discussed in this thesis could possibly be applied to these coupled systems. Further, it could be possible to start with a basis of eigen modes, and then to use the Krylov-subspace based moment matching methods to enhance this basis in order to improve the accuracy in the pre-defined spectrum (Lehner and Eberhard 2006; Lehner and Eberhard 2007). Other

Table 7.2.: A comparison of fully coupled fluid-structure analysis formulations. (Puri et al. 2007)

Method	Uncoupled Modal Projection	Coupled Modal Projection	Moment Matching Arnoldi Projection
Basis vector computation	Solve Uncoupled Eigen Problem $\mathcal{O}(N_f^3 + N_s^3)$	Solve Coupled Eigen Problem $\mathcal{O}((N_f + N_s)^3)$	One LU of [A] and Matrix/Vector dot $\mathcal{O}(2q^2N + 2qN_{nz})$
Treatment of full Coupling	Projected after Eigensolution	Intrinsic	Intrinsic
Reduced model matrix properties (Undamped)	Full Damping (Everstine) Diagonal mass, stiffness matrices	Diagonal mass, stiffness matrices	Full mass, stiffness matrices
Reduced model matrix properties (Damped)	Full Damping	Full Damping	Full Damping

possible Krylov subspace based reduction approaches include SVD-Krylov (Antoulas 2003) and the newly developed Fourier based model reduction processes (Willcox and Megretski 2005; Gugercin and Willcox 2008).

In terms of algorithm development, it is worth noting that an implicitly restarted Arnoldi process (Lehoucq 1995; Sorensen 1995; Antoulas 2003) could be invoked, which essentially, saves memory and increases the efficiency of the Arnoldi process. Generally speaking, after a few initial iterates, the Arnoldi process is interrupted, and the current approximation the associated residual is computed. These then become the starting matrices and vectors for the new recursion that is executed for at most m iterations. Thus the main advantage of a restarted Arnoldi scheme is that at most k iterations of the Arnoldi method are carried out, so that both computational costs and memory allocations per cycle are under user control (Simoncini and Szyld 2007). Note that the SOAR scheme was only recently developed, and a restart of SOAR is still an open research question (Meerbergen 2007a).

The Q-Arnoldi version of the Arnoldi algorithm could possibly also be utilized to reduce second order damped systems. Q-Arnoldi is, in fact, developed for the eigenvalue problem. It does preserve the structure to some extent. In comparison with the SOAR method, the Q-Arnoldi scheme can compute a Schur factorization for the quadratic eigenvalue problem (QEP) which SOAR cannot achieve. For a description of Q,W schemes of the Arnoldi process, the reader is referred to Meerbergen (2007b), Bai et al. (2005). However, in comparison with the SOAR process, in the Q-Arnoldi process, the complete second order structure of the underlying problem might not be preserved. It is easy to see that the two-sided Arnoldi processes can be efficiently parallelized (Grimme 1997), allowing for simultaneous evaluation of Arnoldi vectors for the given subspaces. In this way, further reduction in computational times can be achieved. Since the Arnoldi iteration is closely connected with solving linear sys-

tems[2] (Simoncini and Szyld 2007), computing a few eigenvalues (Sorensen 1995; Bai and Su 2005b) and moment matching based dimension reduction (Bai et al. 2005), today, active research is ongoing within the mathematical and computational sciences community to improve the computational efficiency properties of the Arnoldi method e.g. see Yang (1998). Although not verified in this thesis, it could easily turn out that any modified version of the Arnoldi iteration could be utilized to generate a reduced order model for the fully coupled structural-acoustic case.

Throughout this thesis, a non-zero, real expansion point was chosen for matrix factorization. Another interesting approach, which expands the system matrices at complex expansion point*s* (Antoulas and Sorensen 2001; Grimme 1997) could provide useful insights for establishing an automatic search criteria for factorization. In this work, the primary aim was to accurately represent the input-output behavior (in the form of system *transfer function*) of the coupled system. Since the Arnoldi vectors generated effectively span the same subspace as the eigen vectors (Willcox 2000), it could further be possible to obtain the eigen values directly from the reduced system. However, for a coupled structural-acoustic case, to the authors knowledge, no existing work compares the eigen values and eigen vectors obtained from the higher dimensional interior, structural-acoustic model and the lower dimensional model obtained directly by moment matching. For an initial state space LTI transformed model for the prediction of natural frequencies and mode shapes of fluid loaded plates, the reader is referred to Li and Li (2006a), Li and Li (2006b). Here, the modal parameters by recasting the original system (including the frequency dependent acoustic damping matrix) into a generalized eigenvalue problem (GEP). It is worth reminding the reader that recasting a second order system to a state-space form, doubles the dimension of the resulting system. Additionally, the physical sig-

---

[2]In fact, the use of the Krylov subspaces in iterative methods for linear systems (for structural-acoustic applications see: Malhotra et al. (1997), Freund and Malhotra (1997)) is counted among the "Top 10" algorithmic ideas of the 20th century.

nificance of the higher dimensional coupled system matrices are lost. Note that the reduced order model generated via moment matching, can also be utilized for a time-domain simulation of the coupled system. Although in this work, no explicit test cases were generated for a time domain simulation, various engineering examples exist (Willcox 2000; Lassaux 2002; Salimbahrami 2005), where successful simulation of the ROM in the time domain were performed.

A constrained composite plate - rectangular prism cavity system was modeled and the lamination angles of the composite structure, assuming one flexible wall, were optimized to demonstrate the feasibility of reducing interior noise levels through optimal lamination angles. A point force simulating the structure borne noise was applied to the model. Optimization of the lamination angles was performed over a frequency range of $0 \longrightarrow 200$Hz at 1Hz increments. One observation location (approximately at the *drivers ear* location) in the fluid domain was used to define a RMS weighted objective function value for the optimization problem. The proposed optimization framework incorporated dimension reduction via Krylov subspace techniques to save computational time whilst preserving the accuracy of the state variables (pressures) inside the fluid domain. The optimized design variables were cross validated for accuracy in comparison with the direct inversion technique. It was demonstrated that it is very efficient and straightforward to incorporate such structure preserving, moment matching techniques in a NVH design cycle to save computational time, without sacrificing the accuracy of the computed objective function under investigation.

Typically, for automotive NVH applications, gradient based methods are often utilized to compute sensitivities of the design variables. Although it is well known that the transfer function is multi-modal, the use of *evolutionary* algorithms such as Genetic algorithm (GA) are considered to be time consuming (Marburg 2002a).

Therefore, in this work, a tailored version of MADS has been utilized for the optimization of the coupled structural-acoustic problem. This approach was chosen to give flexibility in controlling the number of function evaluations required and remove the requirement of choosing a good starting design vector. The optimization method incorporated a LHS search and a new polling method (in the form of MADS) for the coupled structural-acoustic optimization problem. It was also demonstrated that the initial LHS search is vital to successful optimization. The four parameter and eight parameter results show that the optimizer always seem to converge to a non-symmetric lay-up for the composite plate. In terms of the optimized noise transfer function, both mode-shifting and peak-splitting phenomenons were observed.

In terms of coupled vibro-acoustic optimization, it is worth mentioning that incorporating constraints can be done with ease in an LHS/MADS environment e.g. the filter approach (Marsden 2004), use of Lagrange multipliers (Matlab 2006). A straight forward extension can also be made be simply applying the yes/no criterion for constraints (Marsden 2004). In terms of future optimization work, the use of surrogates for vibro-acoustic optimization is worth investigation. Surrogates (such as Kirring) fit well among with pattern search methods. This is because of the inherent flexibility of MADS, because they can be separated into a SEARCH step, which offers the user flexibility to incorporate any search strategy, and a POLL step which provides the basis for proof of convergence. Another possible approach could be a Genetic algorithm (GA) /MADS sequence, where the results from a GA search are passed to MADS. For an application of such a 2-stage hybrid algorithm (using a stochastic genetic algorithm for stage 1 followed by a deterministic pattern search algorithm for stage 2) for locating heavy atoms in biological applications, the reader is referred to Payne and Eppstein (2005).

The optimization work described in this thesis did not explicitly consider any ef-

fects of stacking sequence (symmetry, balancing) on the structural integrity of the structure. Obviously, these effects cannot be ignored by any manufacturer and in general, automotive and aerospace designers place structural integrity higher up in priority than acoustic comfort. For example, all automotive manufacturers acknowledge the effect of the choice of joining technologies on NVH characteristics, but it is not seen as a primary influence on design strategies (DTI 2004). However, note that the constrained optimization framework described in Section:[6], allows for such an evaluation of structural integrity. Precisely speaking, in Equations:[6.4→ 6.6], additional structural constraints (like stresses or maximum deflection of shells) can be enforced, requiring a single component or global model static analysis. In such a case, it is worth noting that the computational time would increase.

A. Machine Specifications

Table:[A.1] lists the MATLAB bench timings[1] on V7.1.

Table A.1.: Bench timings for machines used for validating structural-acoustic analysis via Krylov subspace based projection techniques.

Machine	LU	FFT	ODE	Sparse	2-D	3-D
[Me1]	0.5061	0.9194	0.4626	1.1400	1.0569	1.4666
[Me2]	0.2417	0.3262	0.3177	0.5275	0.6747	0.4828
[Me3]	0.3438	0.3688	0.2859	0.4906	0.4106	0.5890
[Me4]	0.1947	0.2888	0.1842	0.4570	0.3939	0.7202

---

[1]In general, the lower the values are, the better.

B. Uncoupled Modal Coupling Theory

Fahy (1985) describes equations for the coupled structural-acoustic response of a system in terms of the summation of structural and acoustic mode shapes. The structural displacement is described in terms of a summation over the *in vacuo* normal modes as follows:

$$w(\mathbf{r}_s) = \sum_{p=1}^{\infty} w_p \, \phi_p(\mathbf{r}_s) \tag{B.1}$$

where ϕ_p is the mode shape of the pth structural mode, $\mathbf{r}_s$ is an arbitrary location on the surface of the structure, and w_p is the modal participation factor of the pth mode. Note that the time dependent term $e^{j\omega t}$ has been removed from this equation and others in this section to simplify the analysis.

The acoustic pressure is described in terms of a summation of the acoustic modes of the fluid volume with rigid boundaries as:

$$p(\mathbf{r}) = \sum_{n=0}^{\infty} p_n \, \psi_n(\mathbf{r}) \tag{B.2}$$

where ψ_n is the acoustic mode shape of the nth mode, $\mathbf{r}$ is an arbitrary location within the volume of fluid, and p_n is the modal participation factor of the nth mode. Note that the $n = 0$ mode is the acoustic bulk compression mode of the cavity that must be included in the summation.

The equation for the coupled response of the structure is given by (Fahy 1985):

$$\ddot{w}_p + \omega_p^2 \, w_p = \frac{S}{\Lambda_p} \sum_n p_n C_{np} + \frac{F_p}{\Lambda_p} \tag{B.3}$$

where ω_p are the structural resonance frequencies, Λ_p are the modal masses, F_p are the modal forces applied to the structure, S is the surface area of the structure, and C_{np} is the dimensionless coupling coefficient given by the integral of the product of the structural (ϕ_p) and acoustic (ψ_n) mode shape functions over the surface of the structure, given by:

$$C_{np} = \frac{1}{S} \int_S \psi_n(\mathbf{r}_s) \, \phi_p(\mathbf{r}_s) \, dS \tag{B.4}$$

The equation for the coupled response of the fluid is given by: (Fahy 1985)

$$\ddot{p}_n + \omega_n^2 \, p_n = -\left(\frac{\rho_0 c^2 S}{\Lambda_n} \right) \sum_p \ddot{w}_p C_{np} + \left(\frac{\rho_0 c^2}{\Lambda_n} \right) \dot{Q}_n \tag{B.5}$$

where, ω_n are the resonance frequencies of the cavity, ρ_0 is the density of the fluid, c is the speed of sound in the fluid, Λ_n is the modal volume, and Q_n is the source strength with units of volume velocity (hence $\dot{Q}_n$ has units of volume acceleration). The *in vacuo* structural and hard walled acoustic modes are calculated using the commercial finite element package ANSYS, and N_s structural and N_a acoustics modes are retained.

The equations for the fully coupled vibro-acoustic system, can be formed into a matrix equation using Equations: [B.3,B.4,B.5] as follows:

$$\begin{bmatrix} \mathbf{A} & -S \, \mathbf{C} \\ -S \, \omega^2 \, \mathbf{C}^\mathrm{T} & \mathbf{B} \end{bmatrix} \begin{bmatrix} \mathbf{w}_p \\ \mathbf{p}_n \end{bmatrix} = \begin{bmatrix} \mathbf{F}_p \\ \dot{\mathbf{Q}}_n \end{bmatrix} \tag{B.6}$$

where $\mathbf{A}$ is a $(N_{\mathrm{s}} \times N_{\mathrm{s}})$ diagonal matrix with elements $A_{pp} = \Lambda_p(\omega_p^2 - \omega^2)$ and $\mathbf{B}$ is a $(N_{\mathrm{a}} \times N_{\mathrm{a}})$ diagonal matrix with elements $B_{nn} = \Lambda_n/\rho_0 c^2 \left(\omega_n^2 - \omega^2\right)$. The off diagonal elements account for the cross coupling between structure and fluid, where $\mathbf{C}$ is a $(N_{\mathrm{s}} \times N_{\mathrm{a}})$ matrix with individual entries given by the elements of C_{np}. This matrix can be solved by matrix inversion techniques to find the coupled modal participation factors, and hence the coupled response of both the structure and cavity. Damping can easily be added on a modal basis (Fahy 1985; Cazzolato 1999).

The modal coupling technique, although well suited for *weakly coupled* systems, is not sufficiently accurate when the structural and acoustic subsystems are *strongly coupled*. An illustration of the reduced accuracy and efficiency of the uncoupled modal approach for *strongly coupled* problems can also be found in Tournour and Atalla (2000), Boily and Charron (1999). As a check, to demonstrate this fact for this work, consider the undamped, simply supported plate-cavity system in Test Case No.3 (Section:5.4). A comparison between the direct inversion method and uncoupled modal coupling for the structural and fluid response locations are shown in Figures:[B.1,B.2]. For the uncoupled modal coupling, the acoustic modal analysis for kept modes was driven till 20,000Hz (well above the common $2 \times f_{max}$ criterion). It can be observed that in spite of retaining a large number of acoustic modes, the modal coupling method does not attain convergence.
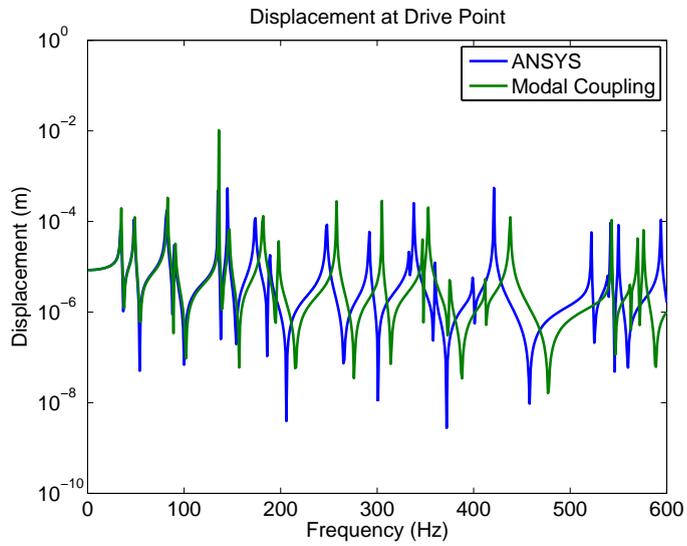
Figure B.1.: Test Case No. 3: Predicted driving point structural displacement transfer function (receptance) using direct and uncoupled modal coupling projection.
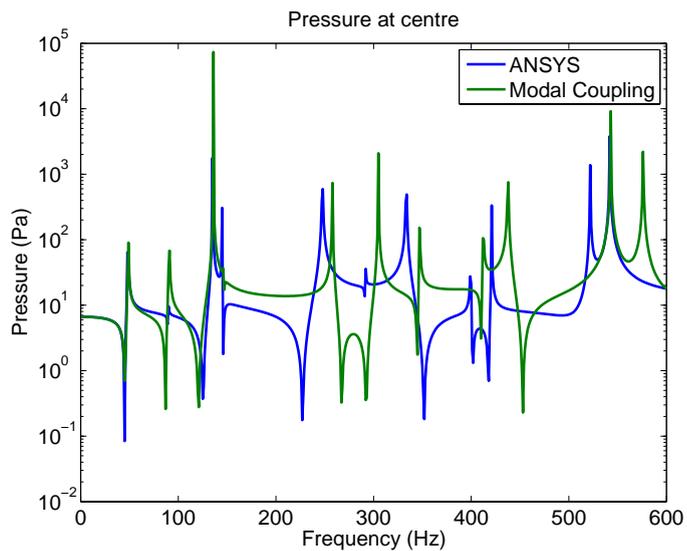
Figure B.2.: Test Case No. 3: Predicted Fluid Noise Transfer Function using direct and uncoupled modal coupling projection for fluid node at the center of the acoustic domain.

C. Test Case No. 6

The sparsity plot for the coupled mass, stiffness and damping matrices are shown in Figures:[C.1,C.2,C.3]. A comparison between the noise transfer functions obtained by direct inversion and TSA projections for the coupled models: $TC6_{BM}$,$TC6_{TT}$, are shown in Figures:[C.4,C.5]. A comparison of direct inversion predicted noise transfer function at fluid node $(0.9m, 0.5m, 0.08m)$ for undamped and constant acoustically damped model $[TC6_{Tac}]$ is shown in Figure:[C.6]. It can be clearly observed that most of the structural peaks do not differ in terms of pressure amplitudes, whereas, coupled peaks close to the acoustic resonance frequencies at $\approx$122Hz, $\approx$240Hz and $\approx$265Hz have decreased due to the addition of constant acoustic damping in the form of boundary admittance coefficients.
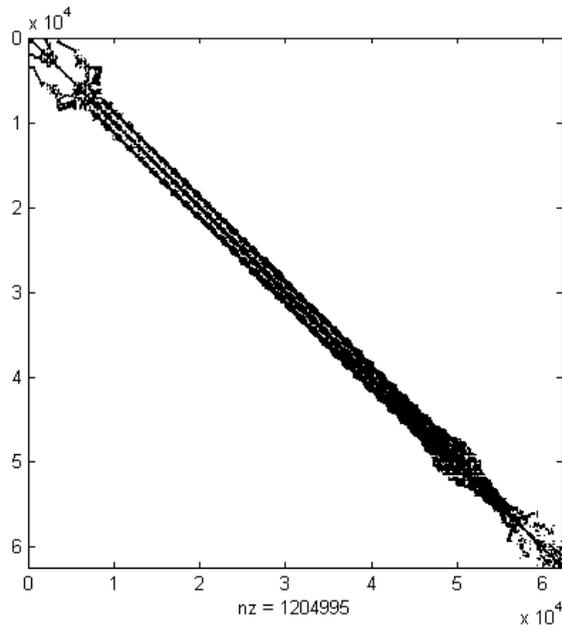
Figure C.1.: Test Case No. 6: Sparsity plot for coupled Stiffness Matrix.
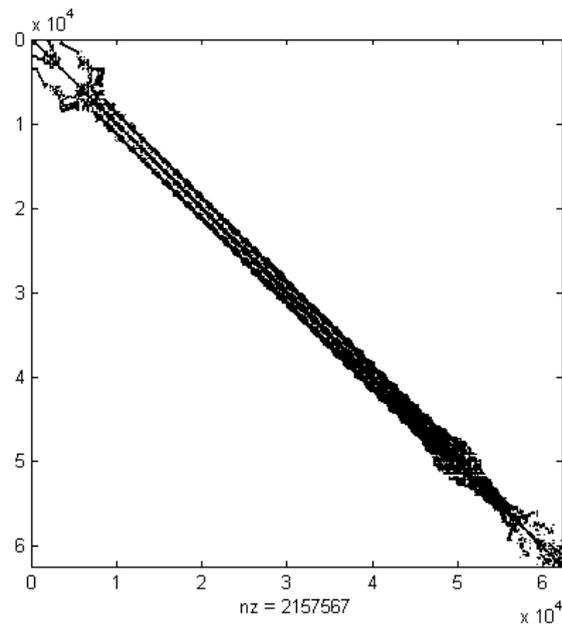
Figure C.2.: Test Case No. 6: Sparsity plot for coupled Mass Matrix.
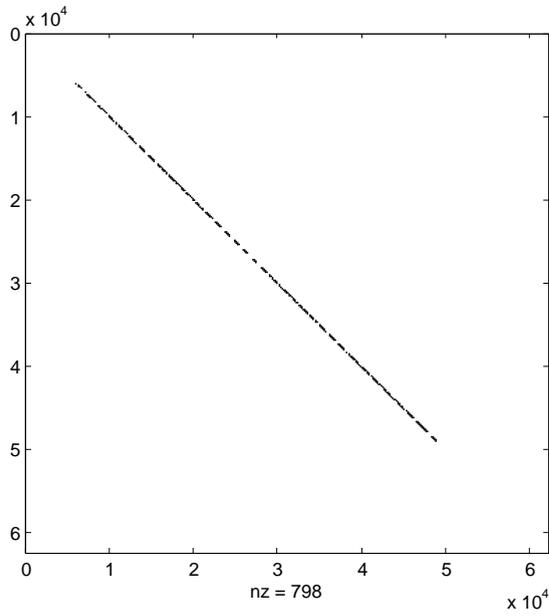
Figure C.3.: Test Case No. 6: Sparsity plot for coupled Damping matrix.
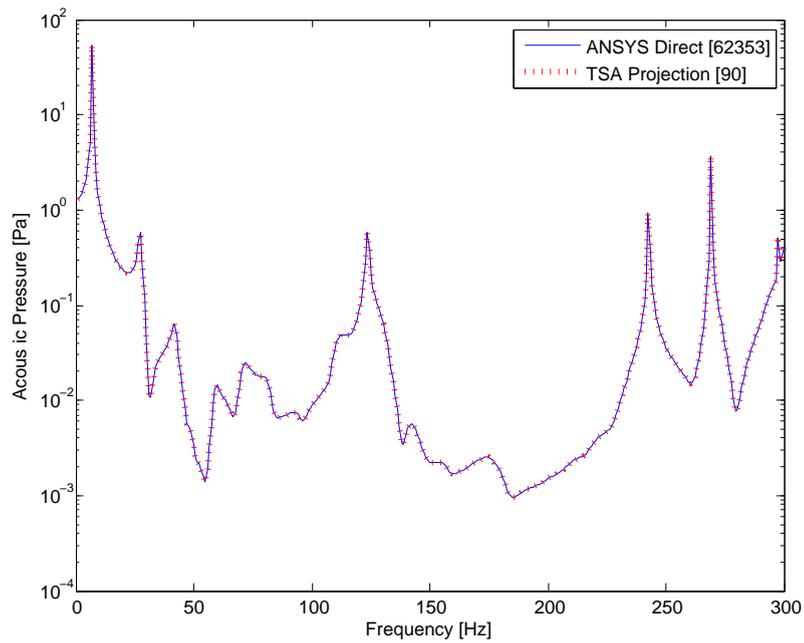
Figure C.4.: Test Case No. 6: ANSYS and TSA projection predicted Noise Transfer Function at fluid node (0.9m,0.5m,0.08m) for model TC6$_{BM}$.
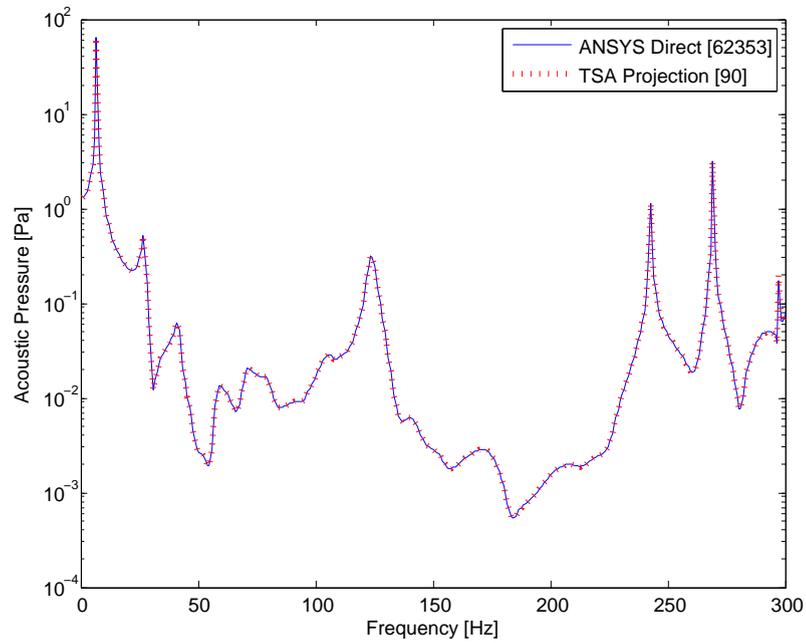
Figure C.5.: Test Case No. 6: ANSYS and TSA projection predicted Noise Transfer Function at fluid node (0.9m,0.5m,0.08m) for model TC6$_{TT}$.
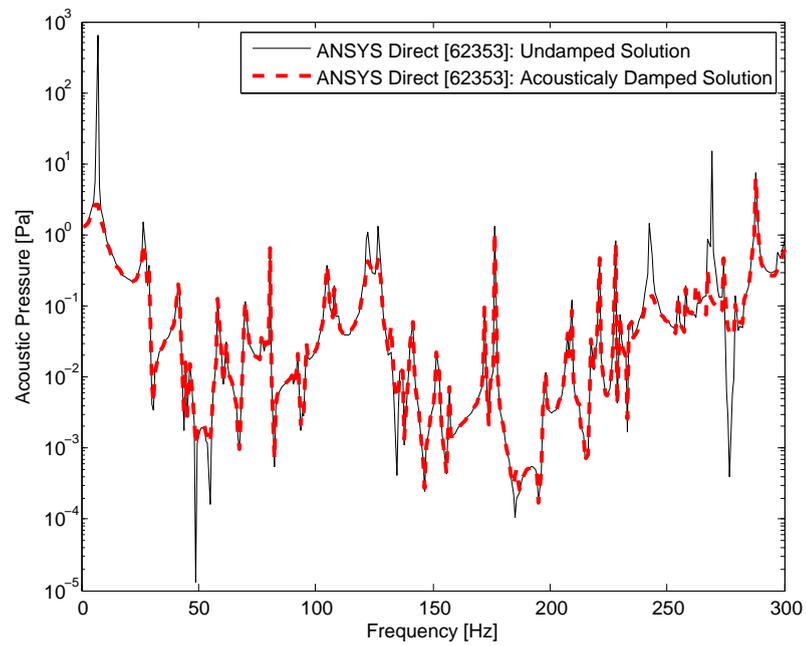
Figure C.6.: Test Case No. 6: A comparison of direct inversion predicted noise transfer at fluid node (0.9m,0.5m,0.08m) for undamped and constant acoustically damped model [TC6$_{Tac}$].

D. Optimization Test case

Since the optimization utilizes One-sided Arnoldi (OSA) process for dimension reduction, the resulting optimized design variables are a consequence of function calls to Arnoldi. Therefore, in order to cross validate the final design variable, an accuracy comparison is made with the direct inversion technique. The resulting noise transfer functions for the 4 layer E-Glass fibre composite is shown in Figure:[D.1]. For the 8 layer E-Glass fibre and PP Glass fibre composites, the *optimized* noise transfer function are compared in Figures:[D.2, D.3]. It can be observed that no accuracy is lost by generating ROMs via moment matching based procedures.
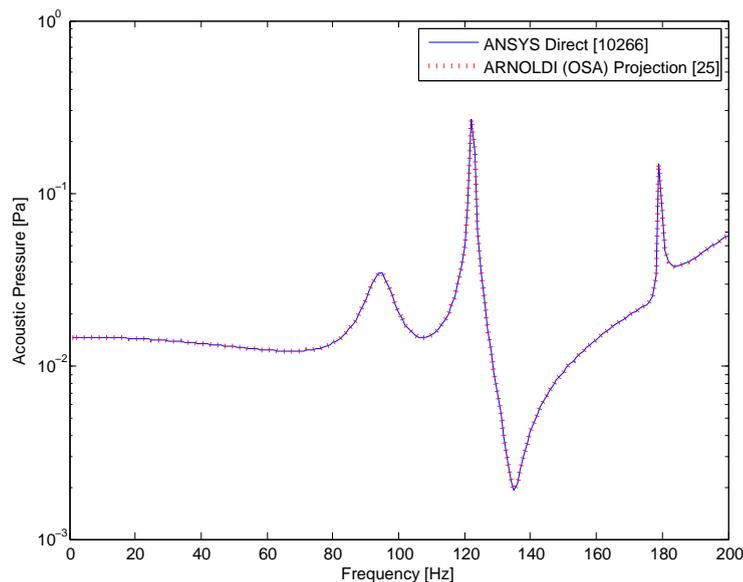
Figure D.1.: A comparison of noise transfer function obtained by ANSYS direct and One-sided Arnoldi (OSA) projection for optimized 4 layer stacking sequence.
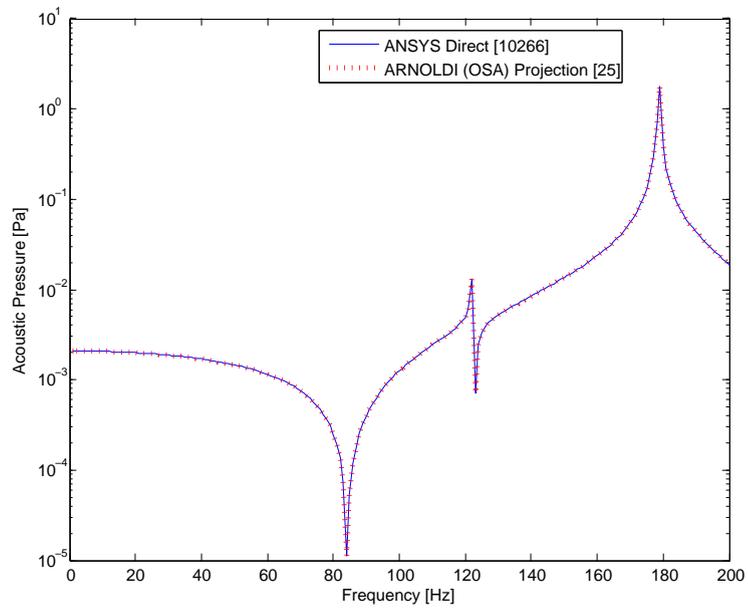
Figure D.2.: A comparison of noise transfer function obtained by ANSYS direct and One-sided Arnoldi (OSA) projection for optimized 8 layer stacking sequence (with material E-Glass Fiber composite).
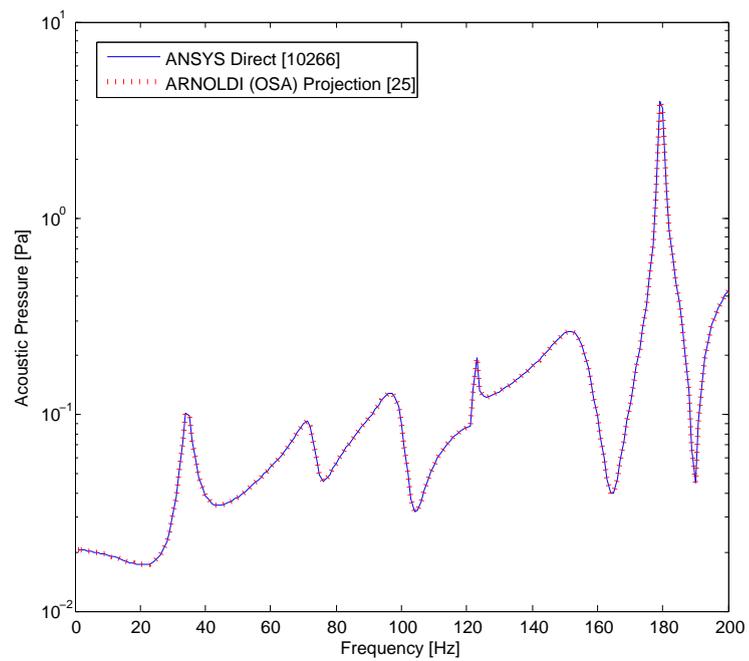
Figure D.3.: A comparison of noise transfer function obtained by ANSYS direct and One-sided Arnoldi (OSA) projection for optimized 8 layer stacking sequence (with material PP-Glass Fiber composite).

E. Sample Computational Files

In this section, the procedure to run a systematic model reduction for the fully coupled, structural-acoustic model, [TC3$_{FFa}$] from Test Case No.3 (Table:5.12). It is assumed that ANSYS, Mathematica and MATLAB is available to drive the following computations. The user directory is the working directory and the home directories are the default installation directories of MATLAB and Mathematica. The files listed in this section are available in the attached DVD.

[S1]. Run higher dimensional model: As a start point, the higher dimensional model is solved via the direct method in ANSYS for results comparison with the proposed Arnoldi based projection formulations. Place contents of the folder FolderTC3FF to the user directory. For convenience, it is recommended to run the model file (Model.txt), and the subsequent post-processing files (harmres1tModel.txt,harmres2tModel.txt) in the ANSYS batch mode[1]. The list of generated files are listed in file StepS1.txt.

[S2]. Extract files and assemble second order system: Extract contents of zip file (DM.zip) to the user working directory[2]. The following steps should be executed to extract the higher dimensional M_{sa}, K_{sa} and C_{sa} and assemble the

---

[1]Throughout this thesis, all ANSYS computations were performed in batch mode (from MATLAB) for timing comparison.

[2]The zip file contains a compiled version of the open source C++ code *dumpmatrices* (Rudnyi and Korvink 2006) which is also used in this test case (in conjunction with the WRFULL command in ANSYS) to extract and write the higher dimensional system matrices in Matrix Market format. The DLL libraries from the ANSYS distribution were required to compile the programs.

system outside ANSYS. First, run file ComplexHDmatrices.txt in ANSYS. Next, Run file: extractfiles.bat externally[3]from MATLAB. Now, modify the first line of all *.B files as follows: [3278 2 1] $\longrightarrow$ [3278 1 1]. This is because in this test case, the coupled system is excited using only one input vector. Run AssembleModelMb.bat followed[4] by copyfiles.bat from MATLAB . The list of generated files are listed in file StepS2.txt.

[S3]. Perform Arnoldi vector computation and projections: In this step, dimension reduction is performed via the Krylov Subspace based TS-SOAR process. This is then followed by projections and reduced harmonic simulation. To achieve this computation, the file ArnoldiCompsMb.bat needs to be run via MATLAB[5]. Note that in this test case, an expansion point of f_{exp} =350Hz is used for the analysis[6]. The list of generated files in this step are shown in lists file StepS3.txt.

[S4]. Plot results and local error: Run file MatTransfer.m followed by file Diff-Files.m to compute local error and compare ANSYS direct and TS-SOAR projection approaches. Comp.pdf, Diff.pdf are the output files with comparison and local error plots. The list of generated files in this step are shown in lists file StepS4.txt. Additionally, for generation of first order systems, the file FirstOrderSpy.txt needs to be run in MATLAB with the Read* and ReadFo* files in the user working directory. Second order sparsity pattern can be analyzed using Spy.txt file by running in MATLAB.

---

[3]External files can be run in MATLAB via the (!) command. Place file AssembleModelMa.txt in the Mathematica home directory and MATLAB file AssembleModelMb.bat in the user directory.

[4]Note that all files needs changing in terms of working directory and Mathematica/Matlab home directories. An example of the syntax is given in each file.

[5]Place file ArnoldiCompsMa.txt in the Mathematica home directory and MATLAB file ArnoldiCompsMb.bat in the user directory.

[6]Note that the following parameters need to be modified (in file ArnoldiCompsMa.txt) accordingly for a change in expansion points: osexpansionforM,osexpansionforE,tsexpansionforM,tsexpansionforE in the module SecOrderTSSOAR in the file SecOrder.m.

References

ABAQUS (2005). *V6.5 Theory and Benchmark Manual.* http://www.simulia.com/; Accessed on: 01/02/2005.

Abramson, M. A. and C. Audet (2006). Convergence of Mesh Adaptive Direct Search to second-order stationary points. *SIAM Journal on Optimization 17*(2), 606–619.

Ali, A., C. Rajakumar, and S. Yunus (1995). Advances in acoustic eigenvalue analysis using boundary element method. *Computers and Structures 56*(1), 837–847.

ANSYS (2005). *V10 Theory Manual.* http://www.ansys.com; Accessed on: 06/12/2005.

Antoulas, A. and D. Sorensen (2001). Approximation of large-scale dynamical systems: An overview. *International Journal of Applied Mathematics and Computer Science 11*(1), 1093–1121.

Antoulas, A. C. (2003). *Approximation of large-scale dynamical systems* (1st ed.). ISBN: 0-89871-529-6: Society for Industrial and Applied Mathematics.

Arnoldi, W. (1951). The principle of minimized iterations in the solution of the matrix eigenvalue problem. *Quarterly Journal of Applied Mathematics 9*, 17–29.

REFERENCES

Aruleswaran, A. (2001). *Dynamic Behaviour of Adhesive Bonded Sub-assemblies for Automotive Vehicle Structures*. Ph. D. thesis, Department of Mechanical Engineering, Oxford Brookes University, UK.

Atalla, N. and R. J. Bernhard (1994). Review of numerical solutions for low frequency structural-acoustic problems. *Applied Acoustics 43*(5), 271–294.

Audet, C. and J. J. E. Dennis (2002). Analysis of Generalized Pattern Searches. *SIAM Journal on Optimization 13*(3), 889–903.

Audet, C. and J. J. E. Dennis (2004). A pattern search filter method for nonlinear programming without derivatives. *SIAM Journal on Optimization 14*(4), 980–1010.

Audet, C. and J. J. E. Dennis (2006). Mesh Adaptive Direct Search algorithms for constrained optimization. *SIAM Journal on Optimization 17*(1), 188–217.

Auweraer, H. V., L. P. Oliveira, M. D. Silva, S. Herold, J. Mohring, and A. Deraemaeker (2006). A virtual prototyping approach to the design of smart structures applications. In *Proceedings of the International Conference on Noise and Vibration Engineering ISMA2006, Leuven, Belgium*, Volume 1, pp. 273–284.

Bai, Z., P. Feldmann, and R. W. Freund (1997). Stable and passive reduced-order models based on partial Padé approximation via the Lanczos process. *Numerical Analysis Manuscript No. 97–3–10*(Available online from http://cm.bell-labs.com/cs/doc/97; Accessed on: 03/05/2004).

Bai, Z. J. (2002). Krylov subspace techniques for reduced order modeling of large scale dynamical systems. *Applied Numerical Mathematics 43*, 9–44.

Bai, Z. J., K. Meerbergen, and Y. Su (2005). Arnoldi methods for structure preserving dimension reduction of second-order dynamical systems. *Dimension Reduction of Large-Scale Systems, Lecture Notes in Computer Science and Engineering 45*, 173–189.

REFERENCES

Bai, Z. J. and Y. Su (2005a). Dimension reduction of large-scale second-order dynamical systems via a Second-Order Arnoldi method. *SIAM Journal on Scientific Computing 26*(5), 1692 – 1709.

Bai, Z. J. and Y. Su (2005b). SOAR: A Second-order Arnoldi method for the solution of the quadratic eigenvalue problem. *SIAM Journal on Matrix Analysis and Applications 26*(3), 640–659.

Bathe, K., C. Nitikitpaiboon, and X. Wang (1995). A mixed displacement-based finite element formulation for acoustic fluid-structure interaction. *Computers and Structures: Nonlinear Finite Element Analysis and ADINA Proceedings of the 10th ADINA Conference 56*(2-3), 225–237.

Bathe, K. J. (1995). *Finite Element Procedures* (1st ed.). ISBN 0-13-301458-4: Prentice-Hall, Englewood Cliffs.

Bechtold, T., E. B. Rudnyi, and J. G. Korvink (2005a). Dynamic electro-thermal simulations of microsystem-A review. *Journal of Micromechanics and Microengineering, Institute of Physics publications 15*, R17–R31.

Bechtold, T., E. B. Rudnyi, and J. G. Korvink (2005b). Error indicators for fully automatic extraction of heat-transfer macromodels for MEMS. *Journal of Micromechanics and Microengineering 15*(3), 430–440.

Belegundu, A. D., R. R. Salagame, and G. H. Koopmann (1994). A general optimization strategy for sound power minimization. *Structural and Multidisciplinary Optimization 8*(2-3), 113–119.

Bennighof, J. K. (1999). Vibroacoustic frequency sweep analysis using automated multi-level substructuring. In *40th AIAA/ASME/ASCE/AHS/ASC Structures, Structural Dynamics, and Materials Conference, Collection of Technical Papers, St. Louis, MO, USA*, Volume 1, pp. 1–06.

Bennighof, J. K., M. Kaplan, M. Muller, and M. Kim (2000). Meeting the NVH computational challenge: Automated Multi-level Substructuring. In *Proceed-*

ings of the International Modal Analysis Conference XVIII,(IMAC18), San Antonio, USA,, Volume 1, pp. 909–915.

Boily, S. and F. Charron (1999). The vibroacoustic response of a cylindrical shell structure with viscoelastic and poroelastic materials. *Journal of Applied Acoustics 58*(2), 131–152.

Bouillard, P. and F. Ihlenburg (1999). Error estimation and adaptivity for the finite element method in acoustics: 2D and 3D applications. *Computer Methods in Applied Mechanics and Engineering 176*(17), 147–163.

Brebbia, C., J. Telles, and L. Wrobel (1984). *Boundary Element Techniques: Theory and Applications in Engineering* (1st ed.). Springer Verlag.

Bregant, L., G. Miccoli, and M. Seppi (2005). Construction machinery cab vibroacoustic analysis and optimisation. In *Proceedings of the NAFEMS 2005 World Congress, St Julians, Malta*, pp. 01–14.

Buehrle, R., G. Gibbs, J. Klos, and M. Mazur (2003). Modeling and validation of damped plexiglas windows for noise control. In *44th AIAA/ASME/ASCE/AHS/ASC Structures, Structural Dynamics and Materials Conference, Norfolk, Virginia, USA*, Volume 109, pp. 1069–1075.

Buehrle, R., F. W. Grosveld, and J. H. Robinson (2001). Structural and acoustic numerical modeling of a curved composite honeycomb panel. In *In the 7th AIAA/CEAS Aeroacoustics Conference and Exhibit, Maastricht, The Netherlands*, Volume 2, pp. 1–17.

Campbell, B. (1993). Structural-acoustic analysis for the prediction of body acoustic sensitivities. *Proceedings of the SAE Noise and Vibration Conference, USA 931327*, 472–483.

Cazzolato, B. (1999). *Sensing systems for active control of sound transmission into cavities.* Ph. D. thesis, The University of Adelaide, Adelaide, Australia.

Cepkauskas, M. M. and J. A. Stevens (1983). Fluid-structure interaction via boundary operator method. *Journal of Sound Vibration 90*, 229–236.

Chahlaoui, Y., K. Gallivan, A. Vandendorpe, and P. Van Dooren (2005). Model reduction of second order systems: Model reduction of dynamical systems. *Eds. P. Benner, LNCSE 45, Springer Verlag*, 379–392.

Chiprout, E. and M. S. Nakhla (1994). *Asymptotic Waveform Evaluation and Moment Matching for Interconnect Analysis*. Norwell, MA, USA: Kluwer Academic Publishers.

Choi, K.K.and Kim, N. (2004). *Structural Sensitivity Analysis and Optimization* (1st ed.). Springer.

Cipolla, J. L. (2006). Dassault Systemés Simulia Corporation, USA, Private Communication.

Cockrell, C. R. and F. B. Beck (1996). Asymptotic waveform evaluation (AWE) technique for frequency domain electromagnetic analysis. *NASA Technical Memorandum: NASA Langley Research Center, Hampton, Virginia 110292*, 131–152.

Cornish, R. (2000). A novel approach to optimizing and stabilizing interior noise quality in vehicles. *Proceedings of the Institution of Mechanical Engineers, Part D: Journal of Automobile Engineering 214*(1), 685–692.

Coyette, J. and Y. Dubois-Perlerin (1994). An efficient coupling procedure for handling large size interior structural-acoustic problems. *Proceedings of the International Conference on Noise and Vibration Engineering ISMA19, Leuven, Belgium 11*, 729–738.

Coyette, J. and K. Fyfe (1990). An improved formulation for acoustic eigenmode extraction from boundary element models. *Journal of Vibration and Acoustics 112*(1), 392–397.

Craggs, A. (1969). The transient response of coupled acousto-mechanical systems. *NASA Contractor Report CR1421*, 1–82.

Craggs, A. (1971). The transient response of a coupled plate-acoustic system using plate and acoustic finite elements. *Journal of Sound and Vibration 15*, 509–528.

Craggs, A. (1972). The use of simple three dimensional acoustic finite elements for determining the natural modes and frequencies of complex shaped enclousures. *Journal of Sound and Vibration 23*(3), 331–339.

Craggs, A. (1973). An acoustic finite element approach for studying boundary flexibility and sound transmission between irregular enclosures. *Journal of Sound and Vibration 30*, 343–357.

Craig, R. R. (2000). Coupling of substructures for dynamic analyses - an overview. In *Proceedings of the AIAA/ASME/ASCE/AHS/ASC Structures, Structural Dynamics, and Materials Conference and Exhibit, Atlanta, GA, USA*, pp. 01–12.

Crane, S. P., K. A. Cunefare, S. P. Engelstad, and E. A. Powell (1997). Comparison of design optimization formulations for minimization of noise transmission in a cylinder. *Journal of Aircraft Engineering and Aerospace Technology 34*(2), 236–243.

Davidson, P. (2004). *Structural-Acoustic Analysis: Finite Element Modelling and Reduction Methods*. Ph. D. thesis, Division of Structural Mechanics, LTH, Lund University, Sweden.

Desmet, W. (1998). *A wave based prediction technique for coupled vibro-acoustic analysis*. Ph. D. thesis, Department of Mechanical Engineering, Katholieke Universiteit Leuven, Belgium.

Desmet, W. and D. Vandepitte (2002). Mid-frequency vibro-acoustic modelling:

Challenges and potential solutions. In *Proceedings of the ISMA'2002 International Conference on Noise and Vibration Engineering*, Volume 2, pp. 835–862.

Desmet, W. and D. Vandepitte (2005). Advanced Numerical Acoustics: The Finite Element Method. *Course notes ISAAC 2005: Advanced Numerical Acoustics*, 01–208.

Dong, J. and N. H. Kim (2003). Design optimization for structural-acoustic problems using FEA-BEA with adjoint variable method. In *Proceedings of the 44th AIAA/ASME/ASCE/AHS Structures, Structural Dynamics, and Materials Conference, Gainesville, FL, USA*, pp. 527–533.

Dowell, E. H., G. F. Gorman III , and D. A. Smith (1977). Acoustoelasticity: General theory, acoustic natural modes and forced response to sinusoidal excitation, including comparisons with experiment. *Journal of Sound and Vibration 52*(4), 519–542.

DTI, R. (2004). Hybridmat 2: Strategies in the joining of hybrid materials in automotive structures. *Report - GLOBAL WATCH MISSION Available Online: http://www.faraday-advance.net/content/news/34.pdf; ; Accessed on: 21/04/2006*, 1–68.

Durodola, J., S. Steidler, and A. Beevers (1999). Modelling of adhesive bonded joints in vehicle substructures. In *Proceedings of the 3rd Internation Conference on Materials for Lean Weight Vehicles, U.K*, pp. 32–42.

Engelstad , S. P., K. A. Cunefare, S. Crane, and E. A. Powell (1995). Optimization strategies for minimum interior noise and weight using FEM/BEM. In *Proceedings of the 1995 National Conference on Noise Control Engineering: Progress in Noise Control for Industry, Newport Beach, CA, USA*, Volume 1, pp. 1205–1208.

EPSRC - Faraday Advance (2003). Design and fabrication of low NVH multi material automotive vehicle structures. *Engineering and Physical Sciences Research*

Council (EPSRC) GR/S27245/(01), 2003–2006.

Estorff, O. V. (2003). Computational Methods in Acoustics. *Course Notes - Technische Universitat Hamburg-Harburg, Germany.*

Everstine, G. C. (1981). A symmetric potential formulation for fluid structure interactions. *Journal of Sound and Vibration 79*, 157–160.

Fahy, F. (1969). Vibration of containing structures by sound in the contained fluid. *Journal of Sound and Vibration 10*(3), 490–512.

Fahy, F. (1985). *Sound and structural vibration: radiation, transmission, and response* (1st ed.). ISBN-10: 0122476719: Academic Press, London.

Fahy, F. J. (2000). *Foundations of Engineering Acoustics* (1st ed.). ISBN-10: 0-12247-665-4: Academic Press.

Fahy, F. J. (2003). Some applications of the reciprocity principle in experimental vibroacoustics. *Acoustical Physics 49*(2), 217–229.

Fahy, F. J. and A. D. Mohammed (1992). A study of uncertainty in applications of SEA to coupled beam and plate systems, Part I: Computational experiments. *Journal of Sound and Vibration 158*, 45–67.

Feldmann, P. and R. Freund (1995). Efficient linear circuit analysis by Padé approximation via the Lanczos process. *IEEE Transactions on Computer-Aided Design of Integrated circuits and Systems 1*, 639–649.

Feng, G. C. and L. Kiefling (1976). Fluid Structure Finite element Vibrational Analysis. *Journal of Aircraft Engineering and Aerospace Technology 14*(6), 199–203.

Fernholz, C. M. and J. H. Robinson (1998). Influence of lamination angles on the interior noise levels of an aircraft. *NASA Langley Technical Report 98-10250*, 1–52.

Freund, R. and M. Malhotra (1997). A block QMR algorithm for non-hermitian

linear systems with multiple right-hand sides. *Linear Algebra and Its Applications 254*(1), 119–157.

Freund, R. W. (2000). Krylov subspace methods for reduced order modeling in circuit simulation. *Journal of Applied Mathematics 123*, 395–421.

Freund, R. W. (2001). Model reduction methods based on Krylov subspaces. *Numerical Analysis 03-4-01 Accessed Online: : http://cm.bell-labs.com/cs/doc/03*, 1–53.

Freund, R. W. and M. H. Gutknecht (1994). An implementation of the look-ahead Lanczos algorithm for non-Hermitian matrices. *Journal of Scientific Computing 15*, 313–337.

Gallivan, K., E. Grimme, and P. Van Dooren (1994). Asymptotic Waveform Evaluation via a Lanczos Method. *Applied Mathematica Letters 5*(7), 75–80.

Gao, W., X. Li, C. Yang, and Z. Bai (2005). Implementation and evaluation of an algebraic sub-structuring method for sparse eigenvalue problems. In *Technical report, Lawrence Berkeley National Lab, Berkeley, CA*, pp. 01–25.

Giunta, A. A. (2002). Use of data sampling, surrogate models, and numerical optimization in engineering design. In *40th AIAA Aerospace Sciences Meeting and Exhibit, Reno, NV, USA*, Volume 1, pp. 01–12.

Giunta, A. A., M. Wojtkiewicz, and M. Eldred (2003). Overview of modern design of experiments methods for computational simulations. In *41st AIAA Aerospace Sciences Meeting and Exhibit, Reno, Nevada, USA*, Volume 1, pp. 01–17.

Grimme, E. (1997). *Krylov Projection Methods for Model Reduction.* Ph. D. thesis, Dept. of Electrical Engineering, University of Illinois at Urbana Champaign, USA.

Gugercin, S. and K. Willcox (2008). Brief paper: Krylov projection framework for

fourier model reduction. *Automatica 44*(1), 209–215.

Haftka, R. T. and Z. Gurdal (1992). *Elements of Structural Optimization* (3rd ed.). ISBN-13: 978-0792315056: Springer.

Harari, I. and D. Avraham (1997). Higher order finite elements for acoustic problems. *Journal of Computational Acoustics 5*(1), 33–51.

Harari, I. and J. Hughes (1992). A cost comparison of boundary element and finite element methods for problems of time-harmonic acoustics. *Computer Methods in Applied Mechanics and Engineering 97*, 77–102.

Henderson, B., C. Gerhart, S. Lane, and E. Jensen (2003). Vibro-acoustic launch protection experiment. *Journal of the Acoustical Society of America 114*(3), 2384–2392.

Herrin, D. W., F. Martinus, T. W. Wu, and A. F. Seybert (2003). A new look at the high frequency Boundary Element and Rayleigh Integral approximations. *Proceedings of the SAE 2003 Noise and Vibration Conference and Exhibition, May 2003, Grand Traverse, MI, USA, Session: Vibro-Acoustic Analysis (Part 1 of 2) 2003/01/1451*(01), 01–07.

Hong, K. L. and J. Kim (1995a). Analysis of free vibration of structural-acoustic coupled systems, part I: Development and verification of the procedure. *Journal of Sound and Vibration 188*(8), 561–575.

Hong, K. L. and J. Kim (1995b). Analysis of free vibration of structural-acoustic coupled systems, part II: Two and three dimensional examples. *Journal of Sound and Vibration 188*(4), 577–600.

Hopkins, C. (2002). Statistical energy analysis of coupled plate systems with low modal density and low modal overlap. *Journal of sound and vibration 251*(2), 193–214.

Howard, C. Q., R. Morgans, C. H. Hansen, and A. Zander (2006). Optimization

of vibro-acoustic absorbers inside the payload bay of a launch vehicle using a parallel genetic algorithm and a distributed network. *Journal of Noise Control Engineering 53*(6), 256–267.

Ihlenburg, F. and I. Babuska (1995). Finite element solution of the Helmholtz equation with high wave number Part I: The 'h' version of the FEM. *Computers and Mathematics with Applications 30*(1), 9–37.

Ihlenburg, F. and I. Babuska (1997). Finite element solution of the Helmholtz equation with high wave number Part II: The 'h-p' version of the FEM. *SIAM Journal on Numerical Analysis 34*(1), 315–358.

Jayachandran, V. and M. W. Bonilha (2003). A hybrid SEA/modal technique for modeling structural-acoustic interior noise in rotorcraft. *Journal of the Acoustical Society of America 113*, 1448–1454.

Jha, S. K. and R. J. Priede (1972). Origin of low frequency noise in motor cars. In *14th FISITA Conference, USA*, pp. 46.

Kang, S. W., J. M. Lee, and S. H. Kim (2000). Structural acoustic coupling analysis of the vehicle passenger car compartment with the roof air-gap and trim boundary. *Journal of Vibration and Acoustics 122*(3), 149–162.

Keane, A. J. and W. Price (1997). *Statistical Energy Analysis: An Overview, with Applications in Structural Dynamics.* (1st ed.). ISBN-10: 0521551757: Cambridge University Press.

Kim, N., K. K. Choi, J. Dong, and C. Pierre (2004). Design optimization of structural-acoustic problems using FEM-BEM. *ASME Journal of Mechanical Design 126*(3), 527–533.

Kim, N. H., J. Dong, K. K. Choi, N. Vlahopoulos, Z.-D. Ma, M. P. Castanier, and C. Pierre (2003, June). Design sensitivity analysis for sequential structural-acoustic problems. *Journal of Sound and Vibration 263*, 569–591.

REFERENCES

Kim, S., J. Lee, and M. Sung (1999). Structural acoustic modal coupling analysis and application to noise reduction in a vehicle passenger compartment. *Journal of Sound and Vibration 225*(5), 989–999.

Kim, S. H. and J. M. Lee (1995). A practical method for noise reduction in a vehicle passenger compartment. *Journal of Vibration and Acoustics, ASME 120*(1), 199–205.

Kim, S. H., J. M. Lee, and M. H. Sung (1999). Structural acoustic modal coupling analysis to noise reduction in a vehicle passenger compartment. *Journal of Sound and Vibration 225*(5), 989–999.

Kleijnen, J. P. C. (2005, July). An overview of the design and analysis of simulation experiments for sensitivity analysis. *European Journal of Operational Research 127*(2), 287–300. available at http://ideas.repec.org/a/eee/ejores/v164y2005i2p287-300.html.

Koehler, J. R. and A. B. Owen (1996). Computer experiments. In S. Ghosh and C. R. Rao (Eds.), *Handbook of Statistics*, Volume 13, pp. 261–308.

Kompella, M. S. and R. J. Bernhard (1993). Measurement of the statistical variation of structural–acoustic characteristics of automotive vehicles. In *SAE NVH COnference, USA*, Volume 931272.

Kopuz, S. and N. Lalor (1995). Analysis of interior acoustic fields using the finite element method and boundary element method. *Applied Acoustics 45*(1), 193–210.

Krois, M., K. Dilger, S. Bohm, and S. Koch (2003). Use of compliant adhesive layers in direct glazing of road vehicles for improved sound attenuation. *International Journal of Adhesion and Adhesives 23*(5), 413–425.

Kroop, A. and I. Heiserer (2003). Efficient broadband vibro-acoustic analysis of passenger car bodies using an FE-based component mode synthesis approach. *Journal of Computational Acoustics 11*, 139–157.

Krylov, A. (1931). On the numerical solution of the equation by which the frequency of small oscillations is determined in technical problems. *Izv. Akad. Nauk SSSR Ser. Fiz.Mat. 4*, 491–539.

Lalor, L. and H. H. Priebsch (2007). The prediction of low and mid-frequency internal road vehicle noise: A literature survey. In *Proceedings of the I MECH E Part D Journal of Automobile Engineering*, Volume 221, pp. 377–384. Professional Engineering Publishing.

Lamancusa, J. S. and H. A. Eschenauer (1994). Design optimization methods for rectangular panels with minimal sound radiation. *AIAA Journal 32*, 472–479.

Lampe, J. and H. Voss (2005). Second Order Arnoldi: Reduction application to some engineering problems. *Proceedings of the XVI-th Summer School on Software and Algorithms of Numerical Mathematics, Srni, 2005. Report 93, Arbeitsbereich Mathematik, TU Hamburg-Harburg.*(Available Online: http://www.tu-harburg.de/mat/SCHRIFTEN/rep/rep93.pdf; Accessed on: 14/09/2006), 153 –173.

Lanczos, C. (1950). An iteration method for the solution of the eigenvalue problem of linear differential and integral operators. *Journal Research of the National Bureau of Standards 45*(4), 255–282.

Lane, S. A. and S. Griffin (2001). Active structural acoustic control of a launch vehicle fairing using monolithic piezoceramic actuators. *Journal of Intelligent Material Systems and Structures 12*(12), 795–806.

Langley, R. S. and P. Bremner (1999). A hybrid method for the vibration analysis of complex structural-acoustic systems. *Journal of the Acoustical Society of America 105*, 1657–1671.

Lassaux, G. (2002). High-Fidelity reduced-order aerodynamic models: Application to active control of engine inlets. Master's thesis, Department of Aeronautics and Astronautics, Massachusetts Institute of Technology, USA.

Lee, D. H., W. S. Hwang, and M. E. Kim (2000). Booming noise analysis in a passenger car using a hybrid-integrated approach. *Proceedings of the Society of Automotive Engineers 109*(6), 1069–1075.

Lehner, M. and P. Eberhard (2006). On the use of moment matching to build reduced order models in flexible multibody dynamics. *Multibody System Dynamics 16*, 191–211.

Lehner, M. and P. Eberhard (2007). A two-step approach for model reduction in flexible multibody dynamics. *Multibody System Dynamics 17*, 157–176.

Lehoucq, R. B. (1995). *Analysis and Implementation of an Implicitly Restarted Iteration.* Ph. D. thesis, Dept. of Computational and Applied Mathematics, Rice University, USA.

Leslie, D. and D. Doelle (1972). *Environmental Acoustics* (2 ed.). London: McGraw-Hill Inc.

Lewis, R. M. and V. Torczon (1999). Pattern search algorithms for bound constrained minimization. *SIAM Journal on Optimization 9*(4), 1082–1099.

Lewis, R. M. and V. Torczon (2000). Pattern search methods for linearly constrained minimization. *SIAM Journal on Optimization 10*(3), 917–941.

Lewis, R. M. and V. Torczon (2002). A globally convergent Augmented Lagrangian Pattern Search algorithm for optimization with general constraints and simple bounds. *SIAM Journal on Optimization 12*(4), 1075–1089.

Li, X. and S. Li (2006a). Modal parameter estimation for fluid-loaded structures from reduced order models. *Proceedings of the International Conference on Noise and Vibration Engineering ISMA2006, Leuven, Belgium 1*(1), 95–124.

Li, X. and S. Li (2006b). Modal parameter estimation for fluid-loaded structures from reduced order models. *The Journal of the Acoustical Society of America 120*(4), 1996–2003.

Luo, J. H. and H. Gea (1997). Modal sensitivity analysis of coupled acoustic structural systems. *Journal of Vibration and Acoustics 119*, 545–550.

Lyamshev, L. M. (1959). A question in connection with the principle of reciprocity in acoustics. *Soviet Physics Doklady 5*(4), 431.

Lyon, R. and G. Maidanik (1962). Power flow between linearly coupled oscillators. *Journal of the Acoustical Society of America 34*(5), 623–639.

Lyon, R. H. and R. DeJong (1995). *Theory and Application of Statistical Energy Analysis.* (1st ed.). ISBN-10: 0750691115: R.H. Lyon Corp.

Ma, Z. D. and I. Hagiwara (1991). Improved mode–superposition technique for modal frequency response analysis of coupled acoustic–structural systems. *AIAA Journal 29*, 1720–1726.

Magahlaes, M. D. C. and N. S. Ferguson (2003). Acoustic-structural analysis using the component mode synthesis method. *Applied Acoustics 64*, 1049–1067.

Magahlaes, M. D. C. and N. S. Ferguson (2005). The development of a component mode synthesis (cms) model for three dimensional fluid-structure interaction. *Journal of the Acoustical Society of America 118*(6), 3679–3691.

Malhotra, M., R. Freund, and P. Pinsky (1997). Iterative solution of multiple radiation and scattering problems in structural acoustics using a block quasi-minimal residual algorithm. *Computer Methods in Applied Mechanics and Engineering 146*(1), 173–196.

Malhotra, M. and P. M. Pinsky (2000). Efficient computation of multi-frequency far-field solutions of the Helmholtz equation using Padé approximation. *Journal of Computational Acoustics 6*(1), 223–240.

Marberg, H. and I. M. Miasa (2002). Application and validation of SEA-modelling of a car-like space frame covered with various lightweight panels. Master's thesis, Division of Applied Acoustics, Chalmers University of Technology, Sweden.

Marburg, S. (2002a). Developments in structural-acoustic optimization for passive noise control. *Archives of the Computational Methods in Engineering 9*(4), 291–370.

Marburg, S. (2002b). A general concept for design modification of shell meshes in structural-acoustic optimization: Part I: Formulation of the concept. *Finite Elements in Analysis and Design 38*(8), 725–735.

Marburg, S., H. J. Beer, J. Gier, H. J. Hardtke, R. Rennert, and F. Perret (2002). Experimental verification of structural-acoustic modelling and design optimization. *Journal of Sound and Vibration 252*(4), 591–615.

Marburg, S. and H. J. Hardtke (2002). A general concept for design modification of shell meshes in structural-acoustic optimization: Part II: Application to a floor panel in sedan interior noise problems. *Finite Elements in Analysis and Design 38*(8), 737–754.

Marburg, S., H. J. Hardtke, and H. Jurgen (2003). Investigation and optimization of a spare wheel well to reduce vehicle interior noise. *Journal of Computational Acoustics 11*(3), 425–449.

Marburg, S., H. J. Hardtke, R. Schmidt, and D. Pawandenat (1997). Application of the concept of acoustic influence coefficients for the optimization of a vehicle roof. *Engineering Analysis with Boundary Elements 20*(4), 305–310.

Marsden, A. (2004). *Aerodynamic noise control by optimal shape design.* Ph. D. thesis, Department of Mechanical Engineering, Stanford University, USA.

Marsden, A., M. Wang, J. Dennis, and P. Moin (2004). Suppression of vortex-shedding noise via derivative free optimization. *Physics of Fluids 16*(10), L83–L86.

Maruyama, S., A. Hasegawa, and Y. Hyoudou (1999). Interior noise analysis based on acoustic excitation tests at low-frequency range. *Proceedings of the SAE Noise and Vibration Conference, USA 01*(1999-01-1806).

Mathur, G., C. L. Chin, M. A. Simpson, and J. T. Lee (2001). Structural acoustic prediction and interior noise control technology. *NASA Langley Technical Report 2001-211247*, 01–48.

Matlab (2006). *Matlab Manual V7.0.4.* http://www.matlab.com; Accessed on: 12/03/2006.

McKay, M., W. Conover, and R. Beckman (1979). A comparison of three methods for selecting values of input variables in the analysis of output from a computer code. *Technometrics 21*, 239–245.

Meerbergen, K. (2007a). KU Lueven, Belgium, Private Communication.

Meerbergen, K. (2007b). The Quadratic Arnoldi method for the solution of the quadratic eigenvalue problem. *Internal Report TW490, KU Leuven, Belgium*, 1–22.

Meirovitch, L. (1980). *Computational Methods in Structural Dynamics* (1st ed.). ISBN-10: 9028605800: Springer.

METIS (2005). *Karypis Labs: Metis.* http://glaros.dtc.umn.edu/gkhome/metis/metis; Accessed on: 20/05/2004.

Meyer, C. D. (2000). *Matrix analysis and applied linear algebra* (1st ed.). ISBN: 0-89871-454-0: Society for Industrial and Applied Mathematics.

Morand, H. and R. Ohayon (1979). Substructure variational analysis of the vibrations of coupled fluid structure systems. *International Journal for Numerical Methods in Engineering 14*(4), 741–755.

Morand, H. and R. Ohayon (1995). *Fluid Structure Interaction* (1st ed.). ISBN-13: 978-0471944591: John Wiley and Sons Ltd.

Morrey, D. and F. R. Whear (1995). An experimental investigation of the noise and vibration generated in vehicle structures. *Machine Vibration 4*(1), 84–91.

Morrey, D. and R. Whear (1996). Prediction of interior noise levels in a passenger

car compartment. *Journal of the Acoustical Society of America 100*, 2596–2601.

Mottershead, J. E. and M. I. Friswell (1993). Model updating in structural dynamics: A survey. *Journal of Sound and Vibration 167*(2), 347–375.

MSC/NASTRAN (2005). *MSC/NASTRAN Theory Manual.* http://www.mscsoftware.com/; Accessed on: 27/1/2005.

Naghshineh, K., G. H. Koopmann, and A. D. Belegundu (2002). Material tailoring of structures to achieve a minimum radiation condition. *Journal of Acoustical Society of America 92*(2), 841–855.

NASA (June 21 - 1996). Nasa technical standard: Payload vibroacoustic test criteria. *NASA Report Server NASA-STD-7001*, 01–24.

Nefske, D. J. and H. Sung (1985). Vehicle interior acoustic design using finite element methods. *International Journal of Vehicle Design 6*(1), 24–39.

Nefske, D. J., J. A. Wolf , and L. J. Howell (1982). Structural-Acoustic finite element analysis of the automobile passenger compartment: A review of current practice. *Journal of Sound and Vibration 80*(2), 247–266.

Niyogi, A. G., M. K. Laha, and P. Sinha (2000). A coupled FE/BE analysis of acoustic cavities confined inside laminated composite enclosures. *Journal of Aircraft Engineering and Aerospace Technology 72*(4), 345–357.

Norris, A. and D. Rebinsky (2000). Acoustic reciprocity for fluid-strcuture problems. *Journal of Acoustical Society of America 94*(1), 1714–1716.

Ohayon, R. (2004). Reduced models for fluid–structure interaction problems. *International Journal of Numerical Methods in Engineering 60*, 139–152.

Ohayon, R. and C. Soize (1998). *Structural Acoustics and Vibration* (1st ed.). ISBN-13: 978-0125249454: Academic Press.

Oliveira, L. P., A. Deraemaeker, J. Mohring, H. V. Auweraer, P. Sas, and

W. Desmet (2006). A CAE modeling approach for the analysis of vibroacoustic systems with distributed ASAC control. In *Proceedings of the International Conference on Noise and Vibration Engineering ISMA2006, Leuven, Belgium*, pp. 321–335.

Olson, L. G. and K. J. Bathe (1985). Analysis of fluid structure interactions: A direct symmetric coupled formulation based on fluid velocity potential. *Computers and Structures 21* (1-2), 21–32.

Orzechowski , J. M. and A. E. Landmann (1994). Effect of constrained layer stiffness on performance of damping tile materials using finite element modeling with Rayleigh Integral. *Proceedings of the 1994 National Conference on Noise Control Engineering: Progress in Noise Control for Industry, USA 1* (1), 627–632.

PADT (2006). The Focus: A publication for ANSYS users from PADT Inc. http://www.padtinc.com/epubs/focus/default.asp ; Accessed on: 22/08/2007.

Pal, C. and I. Hagiwara (1993). Dynamic analysis of a coupled structural-acoustic problem: Simulatneous multi-modal reduction of vehicle interior noise level by combined optimization. *Finite Elements in Engineering and Design 14*, 21–32.

Patil, A. R. and M. J. Crocker (2000). Prediction and optimization of radiated sound power and radiation efficiency of vibrating structures using FEM. *SAE 2000 World Congress, Session: Noise and Vibration, Detroit, MI, USA 1*, 01–08.

Payne, J. L. and M. J. Eppstein (2005). A hybrid genetic algorithm with pattern search for finding heavy atoms in protein crystals. In *GECCO '05: Proceedings of the 2005 conference on Genetic and evolutionary computation*, New York, NY, USA, pp. 377–384. ACM.

Peng, C., D. Morrey, and P. Sanders (1996). Low-frequency impedance measurement using the two-microphone tube technique. *Journal of Acoustical Society*

of America 100, 2810–2820.

Petyt, M., J. Lea, and G. H. Koopmann (1976). A finite element method for determining the acoustic modes of irregular shaped cavities. *Journal of Sound and Vibration 45*, 495–502.

Pierre, R. L. and G. H. Koopmann (1995). A design method for minimizing the sound power radiated from plates by adding optimally sized, discrete masses. *Journal of Mechanical Design, American Society of Mechanical Engineers 117*(1), 243–251.

Pillage, L. T., X. Huang, and R. A. Rohrer (1989). AWEsim: asymptotic waveform evaluation for timing analysis. In *DAC '89: Proceedings of the 26th ACM/IEEE conference on Design automation*, New York, NY, USA, pp. 634–637. ACM.

Pirk, R., W. Desmet, B. Pluymers, P. Sas, and L. C. S. Goes (2002). Vibro-acoustic analysis of the Brazilian Vehicle Satellite Launcher fairing. In *Proceedings of the ISMA'2002 International Conference on Noise and Vibration Engineering, KU Leuven, Belgium*, pp. 2075–2085.

Plunt, J. (1993). On the use and misuse of statistical energy analysis for vehicle interior noise. In *Proceedings of the SAE NVH Conference, USA*, pp. 931301.

Pluymers, B. (2006). *Wave based modelling methods for steady state vibro-acoustics*. Ph. D. thesis, Department of Mechanical Engineering, Katholieke Universiteit Leuven, Belgium.

Pope, L. (1971). On the transmission of sound through finite closed shells: Statistical energy analysis, modal coupling, and non-resonant transmission. *Journal of the Acoustical Society of America 50*(3), 1004–1018.

Press, W., S. A. Teukolsky, W. T. Vetterling , and B. P. Flannery (2002). *Numerical Recipes in C++: The Art of Scientific Computing* (2nd ed.). ISBN-10: 0521750334: Cambridge University Press.

Pretlove, A. J. (1966). Forced vibrations of a rectangular panel backed by a closed rectangular cavity. *Journal of Sound and Vibration 3*, 252–261.

Priebsch, H. H., I. Hauer, H. Fellner, G. Polt, and F. Brandl (2001). Numerical simulation of vehicle interior noise up to 250Hz. In *Proceedings of the Styrian Noise, Vibration and Harshness Congress, Austria*, pp. 149–162.

Puri, R., D. Morrey, A. Bell, J. F. Durodola, E. B. Rudnyi, and J. G. Korvink (2006). Krylov Subspace techniques for low frequency structural-acoustic analysis and optimization. In *INCE Conference Proceedings*, Volume 115, pp. 3843–3852.

Puri, R. S., D. Morrey, and J. L. Cipolla (2007). A comparison between One-sided and Two-sided Arnoldi based model order reduction techniques for fully coupled structural acoustic analysis. In *153rd Meeting of the Acoustical Society of America, The Journal of Acoustical Society of America*, Volume 121.

Puri, R. S., D. Morrey, J. F. Durodola, R. C. Morgans, and C. Q. Howard (2007). A comparison of structural-acoustic coupled Reduced Order Models (ROMS): Modal coupling and Implicit moment matching via Arnoldi. In *14th International Congress on Sound and Vibration (ICSV14)*, pp. 1–8.

Rabbiolo, G., R. J. Bernhard, and F. A. Milner (2004). Definition of a high-frequency threshold for plates and acoustical spaces. *Journal of Sound and Vibration*, 647–667.

Ratzlaff, C. L., N. Gopal, and L. T. Pillage (1991). RICE: Rapid interconnect circuit evaluator. In *DAC '91: Proceedings of the 28th conference on ACM/IEEE design automation*, New York, NY, USA, pp. 555–560. ACM.

Rayleigh, L. (1873). Some general theorms relating to vibrations. *Proceedings of the London Mathematical Society 4*, 357–368.

Reid, J. (1970). On the method of conjugate gradients for the solution of large sparse systems of linear equations. *In Large sparse sets of linear equations,*

Proc. Conf., St. Catherine's College, Oxford 4, 231—-254.

Rudnyi, E. B. and J. Korvink (2006). Model order reduction for large scale engineering models developed in ANSYS. *Lecture Notes in Computer Science and Engineering 3732*, 349–356.

Saad, Y. (1981). Krylov subspace methods for solving large unsymmetric linear systems. *Mathematics of Computation 37*(155), 105–126.

Salagame, R. R., A. Belegundu, and G. H. Koopman (1995). Analytical sensitivity of acoustic power radiated from plates. *Journal of Vibration and Acoustics 117*, 43–48.

Salimbahrami, B. (2005). *Structure Preserving Order Reduction of Large Scale Second Order Models*. Ph. D. thesis, Department of Electrical Engineering, Technische Universitaet Muenchen, Germany.

Salimbahrami, B., B. Lohmann, T. Bechtold, and J. Korvink (2005). A two-sided Arnoldi algorithm with stopping criterion and MIMO selection procedure. *Mathematical and Computer Modelling of Dynamical Systems 11*(1), 79–93.

Schenck, H. (1968). Improved integral formulation for acoustic radiation problems. *Journal of the Acoustical Society of America 44*(1), 41–58.

Seybert, A., T. Wu, and W. Li (1993). A coupled FEM/BEM for fluid structure interaction using Ritz vectors and Eigenvectors. *Journal of Vibration and Acoustics* (115), 152–158.

Seybert, A. F. and D. W. Herrin (1999). The prediction of sound radiation from real structures. *Proceedings of the Sixth International Congress on Sound and Vibration (ICSV6) 1*(01), 33–42.

Shorter, P. J. (1998). *Combining Finite Elements and Statistical Energy Analysis*. Ph. D. thesis, Dept. of Mechanical Engineering, University of Auckland, New

Zealand.

Simoncini, V. and D. B. Szyld (2007). Recent computational developments in Krylov subspace methods for linear systems. *Numerical Linear Algebra with Applications 14*, 01–59.

Soize, C., A. Desanti, and J. M. David (1992). Numerical methods in elastoacoustics for low and medium frequency ranges. *La Recherche Aerospatiale*, 25–44.

Sorensen, D. C. (1995). Implicitly restarted Arnoldi/Lanczos methods for large scale eigenvalue calculations. In D. E. Keyes, A. Sameh, and V. Venkatakrishnan (Eds.), *Parallel Numerical Algorithms: Proceedings of an ICASE/LaRC Workshop,Hampton, VA,USA*, Volume 13, pp. 261–308.

Stammberger, M. and H. Voss (2007). Automated multi-level substructuring for a fluid-solid vibration problem. *Proceedings of ENUMATH07. Report 117, Arbeitsbereich Mathematik, TU Hamburg-Harburg.*(http://www.tu-harburg.de/ins/forschung/rep/rep117.pdf; Accessed on: 02/10/2007), 01 – 08.

Stepanishen, P. and D. L. Cox (2000). Structural-acoustic analysis of an internally fluid-loaded spherical shell: Comparison of analytical and finite element modeling results. *NUWC Technical Memorandum, Newport, Rhode Island* (00-118).

Stryczek, R., A. Kroop, and S. Wegner (2004). Vibro-acoustic computations in the mid-frequency range: efficiency, evaluation and validation. In *Proceedings of the International Conference on Noise and Vibration Engineering ISMA2004, Leuven, Belgium*, pp. 1603–1612.

Su, T. J. and R. Craig (1991a). Krylov model reduction algorithm for undamped structural dynamics systems. *AIAA Journal of Guidance and Control Dynamics 14*(6), 1311–1313.

Su, T. J. and R. Craig (1991b). Model reduction and control of flexible structures using Krylov vectors. *AIAA Journal of Guidance and Control Dynamics 14*(2),

260–267.

Sung, H. and D. J. Nefske (1986). Component mode synthesis of a vehicle structural-acoustic system model. *AIAA Journal 26*(6), 1021–1026.

Sung, S. H. and D. J. Nefske (1999). Development and experimental evaluation of a vehicle structural-acoustic trimmed-body model. In *Proceedings of the SAE Noise and Vibration Conference, USA*, pp. 472–483.

Sysnoise (2004). *V5.5 Theory Manual.* http://www.lmsintl.com; Accessed on: 11/08/2004.

Thompson, L. L. (2006). A review of finite-element methods for time-harmonic acoustics. *Journal of the Acoustical Society of America 119*(3), 1315–1330.

Torczon, V. (1997). On the convergence of pattern search algorithms. *SIAM Journal on Optimization 7*(1), 1–25.

Tournour, M. and N. Atalla (2000). Pseudostatic corrections for the forced vibroacoustic response of a structure-cavity system. *Journal of Acoustical Society of America 107*(5), 2379–2386.

Wagner, M. and M. Malhotra (2003). A Krylov subspace projection method for simultaneous solution of Helmholtz problems at multiple frequencies. *Computer Methods In Applied Mechanics And Engineering 192*(41-42), 4609–4640.

Wagner, M., P. Pinsky, and A. Oberai (2003). Application of Padé via Lanczos approximations for efficient multifrequency solution of Helmholtz problems. *Journal of the Acoustical Society of America 113*(1), 313–319.

Wallace, C. E. (1972). Radiation resistance of a rectangular plate. *Acoustical Society of America 51*(1), 946–952.

Wang, X. (1998). On a mode superposition method for fluid-structure interaction problems. In *Proceedings of ASME Symposium on Dynamics, Acoustics and Simulations, USA*, pp. 01–06.

REFERENCES

Wang, X. and K. Bathe (1997). Displacement/pressure based mixed finite element formulations for acoustic fluid structure interaction problems. *International Journal for Numerical Methods in engineering 40*, 2001–2017.

Wentzel, R. and E. Green (1997). Assessing headliner and roof assembly acoustics. *Transcations of the Society of Automotive Engineers 106*(2), 2730–2741.

Whear, R. and D. Morrey (1996). A technique for experimental acoustic modal analysis. In *Proceedings of the Institution of Mechanical Engineers*, Volume 210, pp. 143–151.

Willcox, K. (2000). *Reduced-Order Aerodynamic Models for Aeroelastic Control of Turbomachines*. Ph. D. thesis, Department of Aeronautics and Astronautics, Massachusetts Institute of Technology, USA.

Willcox, K. and A. Megretski (2005). Fourier series for accurate, stable, reduced-order models in large-scale linear applications. *SIAM Journal of Scientific Computing 26*(3), 944–962.

Willcox, K., J. Peraire, and J. White (2002). An Arnoldi approach for generation of reduced-order models for turbomachinery. *Computers and Fluids 31*(03), 369–389.

Wilson, E. L., M. W. Yuan, and D. J. M. (1982). Dynamic analysis by direct superposition of Ritz vectors. *Internation Journal of Earthquake Engineering and Structural Dynamics 19*, 813–821.

Wodtke, H. W. and J. S. Lamancusa (1998). Sound power minimization of circular plates through damping layer placement. *Journal of Sound and Vibration 215*(5), 1145–1163.

Wolf, Jr., J. A. (1977). Modal synthesis for combined structural-acoustic systems. *AIAA Journal 15*, 743–745.

Wolfram (2003). *Mathematica V5.0.* http://www.wolfram.com; Accessed on:

23/06/2005.

Wood, L. A. and C. A. Joachim (1984). Variability of interior noise levels in passenger cars. In *IMechE conference on Vehicle Noise and Vibration, U.K*, Volume C136, pp. 197–206.

Wyckaert, K., F. Augusztinovicz, and P. Sas (1996). Vibro-acoustical modal analysis: reciprocity, model symmetry and model validity. *Journal of Acoustical Society of America 100*(05), 3172–3181.

Yang, C. (1998). *Accelerating the Arnoldi Iteration – Theory and Practice*. Ph. D. thesis, Department of Computational and Applied Mathematics, Rice University, USA.

Yang, C. (2005). Solving large-scale eigenvalue problems in SciDAC applications. In *Journal of Physics, Conference Series*, Number 16, pp. 425–434.

Yang, C., W. Gao, Z. Bai, X. S. Li, L.-Q. Lee, P. Husbands, and E. Ng (2005). An algebraic substructuring method for large-scale eigenvalue calculation. *SIAM Journal of Scientific Computing 27*(3), 873–892.

Yap, F. F. and J. Woodhouse (1996). Investigation of damping effects on statistical energy analysis of coupled structures. *Journal of Sound and Vibration 197*, 351–371.

Zienkiewicz, O. and R. Newton (1969). Coupled vibrations of a structure submerged in a compressible fluid. *Proceedings of the International Symposium on Finite Element Techniques,Stuttgart,Germany 15*, 1–09.